PGSE-NMR and SANS studies of the interaction of model polymer therapeutics with mucin

Paola Occhipinti

Ph.D. 2011

Welsh School of Pharmacy
Cardiff University
Cardiff
CF10 3NB
UK.

UMI Number: U584629

UMI U584629

Declaration

This work has not previously been accepted in substance for any degree and is not concurrently submitted in candidature for any degree.

Signed _(signature)_ (Candidate)   Date 14/3/11

Statement 1

This thesis is being submitted in partial fulfillment of the requirements for the degree of PhD.

Signed _(signature)_ (Candidate)   Date 14/3/11

Statement 2

This thesis is the result of my own independent work/investigation, except where otherwise stated.

Other sources are acknowledged by explicit references.

Signed _(signature)_ (Candidate)   Date 14/3/11

Statement 3

I hereby give consent for my thesis, if accepted, to be available for photocopying and for inter-library loan, and for the title and summary to be made available to outside organisations.

Signed _(signature)_ (Candidate)   Date 14/3/11

To my family

"May the wind always be at your back and the sun upon your face.
And may the wings of destiny carry you aloft to dance with the stars."

Quoted from the movie 'Blow' (2001)

Abstract

The effective uptake/absorption of macromolecules through the body involves several processes: one of these is the transport of the molecule through the mucus layer. The mucus layer is a complex mixture of biological components. Among them, mucin is the molecule that mainly contributes to the gel properties of the layer. Therefore, an *in-vitro* mucin gel can mimic, to a first approximation, the *in-vivo* physico-chemical properties of the mucus.

Therapeutic agents are often conjugated to polymers which behave as drug carriers to improve the tissue targeting specificity of the therapeutic molecule. Therefore, the understanding of the permeability of polymers through mucin solutions is fundamental in the construction of polymer-based drug delivery systems for therapeutics which can be adsorbed through the airways and the gastrointestinal tract. Furthermore, in the case of respiratory disorders such as cystic fibrosis (CF), the mucus can represent a real barrier for the therapeutics' access. The mobility through, and interactions with, mucin solutions of non-ionic/cationic/anionic polymers with different structures (from linear to dendritic) were studied by pulsed-gradient spin-echo nuclear magnetic resonance (PGSE-NMR) and small-angle neutron scattering (SANS). The interaction of non-ionic polymers were limited and related to the steric hindrance of the mucin networks. On the contrary, charged polymers such as polyamidoamines (PAMAM) dendrimers exhibited a pH-dependent interaction with the mucin molecules. At physiological pH, strong binding with mucin molecules was observed for positively charged polymers.

PEGylation is a widely used modification of molecules, proteins and drug delivery systems by covalently attaching one or more polyethylene glycol (PEG) chains: in fact, PEG-modification can reduce the toxicity, increase the half-life of drug delivery systems by enhancing their body resistance and reducing the plasma clearance. PEGylation of positively charged PAMAM dendrimers reduced their adhesive interaction with the mucin molecules, improving greatly the diffusion of these polymers in mucin solutions. After being PEGylated, PEG-PAMAM conjugates can be positively considered as model drug carriers.

Although mucin is the main component in mucus, a more complex and realistic mucus system was studied by SANS. Mucin solutions were enriched with extra components present in mucus, such as phospholipids and serum albumin. Hydrophobic lipid-mucin and protein-mucin interactions were observed. However, the adhesion of mucus components with mucin should be positively considered for the understanding of the mucus as a protective barrier and in the improvement of any treatment for the reinforcement of the mucosal barrier.

Die Slowly

He who becomes slave of habit,
repeating the same paths every day,
he who never changes brands,
does not risk to wear a new colour
and does not talk to whom he doesn't know,
dies slowly.

He who avoids a passion,
he who prefers black on white
and dotted "i" to a whirlwind of emotions,
the kind that make your eyes glimmer,
that turn a yawn into a smile,
that make the heart pound in front of the stumbling and the feelings,
dies slowly.

He who does not overthrow the table when he is unhappy at work,
he who does not risk the certain for the uncertain to follow a dream,
he who does not allow himself at least once in his life,
to flee from sensible advice,
dies slowly.

He who does not travel, he who does not read,
he who does not listen to music,
he who does not find grace in himself,
dies slowly.

He who destroys his self-esteem,
he who does not accept somebody's help,
dies slowly.

He who spends his days complaining of his bad luck
or of the incessant rain,
dies slowly.

He who abandons a project before starting it,
who does not ask about a subject he does not know
or who does not answer when being asked about something he knows,
dies slowly.

Let's avoid death in small doses,
remembering always that to be alive requires an effort by far greater than
the simple fact of breathing.

Only a burning patience will lead to the attainment of a splendid
happiness.

Martha Medeiros

Publications

Occhipinti P. et al., PGSE-NMR and SANS studies of the interaction of model polymer therapeutics with mucin, *Biomacromolecules*, **2010**, 11, 120-125.

Occhipinti P. and Griffiths P. C., Quantifying diffusion in mucosal systems by pulsed-gradient spin-echo NMR, *Advanced Drug Delivery Reviews*, **2008**, 60, 1570-1582.

Contributions to conferences

"M4 Colloids Symposium" (10th July 2007, Bath, UK; 10th July 2008, Bath, UK; 23rd July 2009, Cardiff, UK). Organizing Committee.

"European Student Colloid Conference 2009", 15th-18th July 2009, Almeria, Spain.
Talk: **Occhipinti P.**; 'Small-angle neutron scattering and NMR studies of the mucosal barrier'.

"Cardiff Easter Conference 2009", 31st March-1st April 2009, Cardiff, UK.
Prize winner for the best talk: **Occhipinti P.**; 'Small-angle neutron scattering and NMR studies of the mucosal barrier'.

"2nd European Summer School in Nanomedicine", 12th-16th June 2009, Lisbon, Portugal.
Poster: **Occhipinti P.**, Gumbleton M., Griffiths P. C.; 'The use of PGSE-NMR and SANS to probe the solution interaction of synthetic polymers with mucin'.

"7th International Symposium on Polymer Therapeutics: From Laboratory to Clinical Practice", 26th-28th May 2008, Valencia, Spain.
Poster: **Occhipinti P.**, Gumbleton M., Griffiths P. C.; 'Interactions of synthetic polymers with mucin solutions: a study using pulsed-gradient spin-echo NMR (PGSE-NMR) and small-angle neutron scattering (SANS)'.

"M4 Colloids Symposium", 10th July 2007, Bath, UK.
Talk: **Occhipinti P.**; 'Quantifying the diffusion of polymers through mucin'.

"Gregynog Young Chemists Symposium", 21st-22nd June 2007, Gregynog, UK.
Talk: **Occhipinti P.**; 'Quantifying the diffusion of polymeric drug carriers through mucin'.

"1st European Science Foundation Summer School in Nanomedicine", 10th-15th June 2007, Cardiff, UK.
Poster: **Occhipinti P.**, Gumbleton M., Griffiths P. C.; 'Quantifying the diffusion of polymers through mucin'.

Table of Contents

Chapter 1.   Introduction

<u>Context</u>

The transport of macromolecular drugs and colloidal drug carriers *in-vivo* requires overcoming major biological barriers between the site of initial administration and its action at the target site within the body. Non-injectable routes of administration will have to overcome either a mucosal epithelial surface or cross the epidermis of the skin. However, to access the mucosal cell surface the influence of a bio-gel, the mucus layer, which coats the exposed mucosal epithelial surfaces of the respiratory and intestinal tracts needs to be considered to ensure adequate bioavailability of the therapeutic.

The mucus is a thick and viscous gel which provides protective and lubricative functions between the external environment and the cellular components of the epithelial layer. Despite its biological role, the mucus will, for some molecules, represent a potential barrier for the absorption/transport of macromolecules, for example genes, proteins and polymeric drug delivery systems. Furthermore, in some respiratory disorders such as cystic fibrosis, the mucus viscosity can be so great as to almost totally hinder access of corrective gene delivery systems to the underlying epithelium. An understanding of the mobility and/or binding of macromolecules in mucosal systems is fundamental in the development of macromolecule drug delivery systems.

In this chapter, a general introduction to the composition of mucus and its physico-chemical characteristics is first given. An analysis of the different architectures of macromolecules such as polymers seen as drug delivery carriers is then presented. Finally, a section is dedicated to the studies already performed on the transport of macromolecules through mucus layer and, consequently, to the aims of this thesis.

1.1. The mucus gel and the mucin

1.1.1. The mucus gel

The mucus gel layer is a highly hydrated protein gel which covers several epithelial surfaces for example the gastrointestinal, pulmonary, oral, nasal and urogenital tracts. Its function and composition differs depending on the site of secretion, but a general and fundamental role of the mucus is to protect the mucosal tissues from dehydration, mechanical stress, foreign particles – *i.e.*, harmful microorganism, toxic substances. Therefore, the mucus coating can represent a potential barrier to the efficient delivery of therapeutics to the epithelium and beyond [1-4].

The thickness of the mucus layer depends on its location and it ranges, for example, from 7-70 μm in the airways [5, 6], 50-500 μm in the stomach [2, 7] and 15-150 μm in the colon [8-11]. The thickness of the mucus combined with its inherent viscoelasticity are important factors which affect the pharmacokinetics of therapeutic agents [12, 13]. This situation is exacerbated by the presence of any disease, such as cystic fibrosis (CF) that results in a reduced hydration of mucus and an increase in its viscosity [14], and ulcerative colitis (UC) where the mucus layer is extremely thin, almost nonexistent [15].

1.1.1.1. Composition of mucus

Mucus is essentially a water-rich bio-gel, the main components being water (~ 95%) [16, 17], glycoproteins and lipids (0.5-5%), mineral salts (0.5-1%) and free proteins (1%) [18, 19]. An estimation of the proportion of each type of molecules within mucus is given in Table 1.1.

Constituents	Wt% of total weight	Wt% of dry mass
Water	~ 95	
Mucins		5
Lipids	5	37
Proteins		39
DNA		6

Table 1.1 *Composition of pig gastric mucus* [18, 19].

The composition differs slightly depending on the site of secretion (*e.g.*, ocular mucus: protein 29 % w/w [of dry solids], carbohydrate 53 % w/w, lipid 12 % w/w; submaxillary gland mucus: protein 31 % w/w, carbohydrate 58 % w/w, lipid 11 % w/w)[18], the physiological role of the mucus layer and the presence of any disease. Apart from water, the main component of mucus is the glycoprotein mucin – with an approximate concentration of 50 mg/ml [17] – and it is also the most critical component in terms of the physico-chemical properties of the mucus gel [18, 20].

1.1.2. Mucin

As mentioned above, the viscoelastic properties of the mucus are determined by the mucin molecules. Mucin consists of high molecular weight (ranging from 0.5 to 20 M g mol^{-1}) O-linked glycoproteins. Even though some differences can be found from one mucous barrier to another, the chemical composition and the physico-chemical properties described below can be considered as representative for all types of mucin.

1.1.2.1. Chemical composition of the mucin

The chemical composition of the mucin depends on the origin of the sample as well as the physiological conditions of the host from which the sample is taken. Therefore, it can be difficult to determine the exact chemical composition of the mucin. Studies on mucin can be performed after purification of a mucus extract with the purification process involving several steps during which mucin degradation can occur.

Polypeptide backbone

Mucin monomers comprise glycosylated and non-glycosylated peptide blocks linked by intra-molecular disulphide bridges. The polypeptide backbone of mucin (Table 1.2) contributes to 10-30% of the total weight of the mucin molecule. The polypeptide chain consists of a large number of repeated units rich in serine, threonine and proline. The presence of the serine and threonine amino acids is fundamental in forming the link between the protein backbone and the carbohydrate side chains via their hydroxyl group. The high level of proline is important in determining the conformation of the mucin molecule.
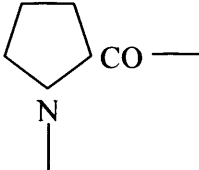
$\begin{array}{c} -CO-CH-NH- \\ \mid \\ R \end{array}$	-R	% in small intestine mucin	% in stomach mucin
Thr	$\begin{array}{c} -CH-OH \\ \mid \\ CH_3 \end{array}$	16.8%	25.3%
Ser	$-CH_2-OH$	10.5%	14.2%
Pro	(pyrrolidine ring) $CO\!-\!\!-$ with N	9.8%	17.8%
Glu	$-CH_2-CH_2-COOH$	8.7%	4.7%
Asp	$-CH_2-COOH$	8.1%	2.4%
Ala	$-CH_3$	6.5%	10.8%
Gly	$-H$	7.4%	6.7%
Arg	$\begin{array}{c} NH \\ \parallel \\ -(CH_2)_3-NH-C-NH_2 \end{array}$	3.1%	2.1%
Lys	$-(CH_2)_4-NH_2$	3.3%	4.8%
Cys	$-CH_2-SH$	1.5%	-

Table 1.2 *Amino acids composition of the gastrointestinal mucin.*

Oligosaccharide side chains

The oligosaccharide side chains are mainly composed of five different monosaccharides: galactose, fucose, N-acetylglucosamine, N-acetylgalactosamine and sialic acid (Figure 1.1). The carboxyl group on the sialic acid molecules (pKa ~ 2.6), together with the sulphated sugars (pKa ~ 1), is responsible of the negative charge on the mucin glycoprotein contributing to the low isoelectric point (IEP) of mucin estimated to be between 2 and 3 [21-23]. Typically a mucin side chain consists of 2-20 monomers, even though these chains are branched and can exhibit heterogeneity in terms of length and complexity [24]. They represent more

than 50% of the molecular weight of the mucin molecule [17, 25]. A schematic representation of the mucin molecule is illustrated in Figure 1.2. Furthermore, the high degree of mucin glycosylation provides resistance to proteolysis by rendering the peptide core less accessible to enzymatic hydrolysis and therefore affording a protective role for the mucus layer in mammalian organs [3, 26].
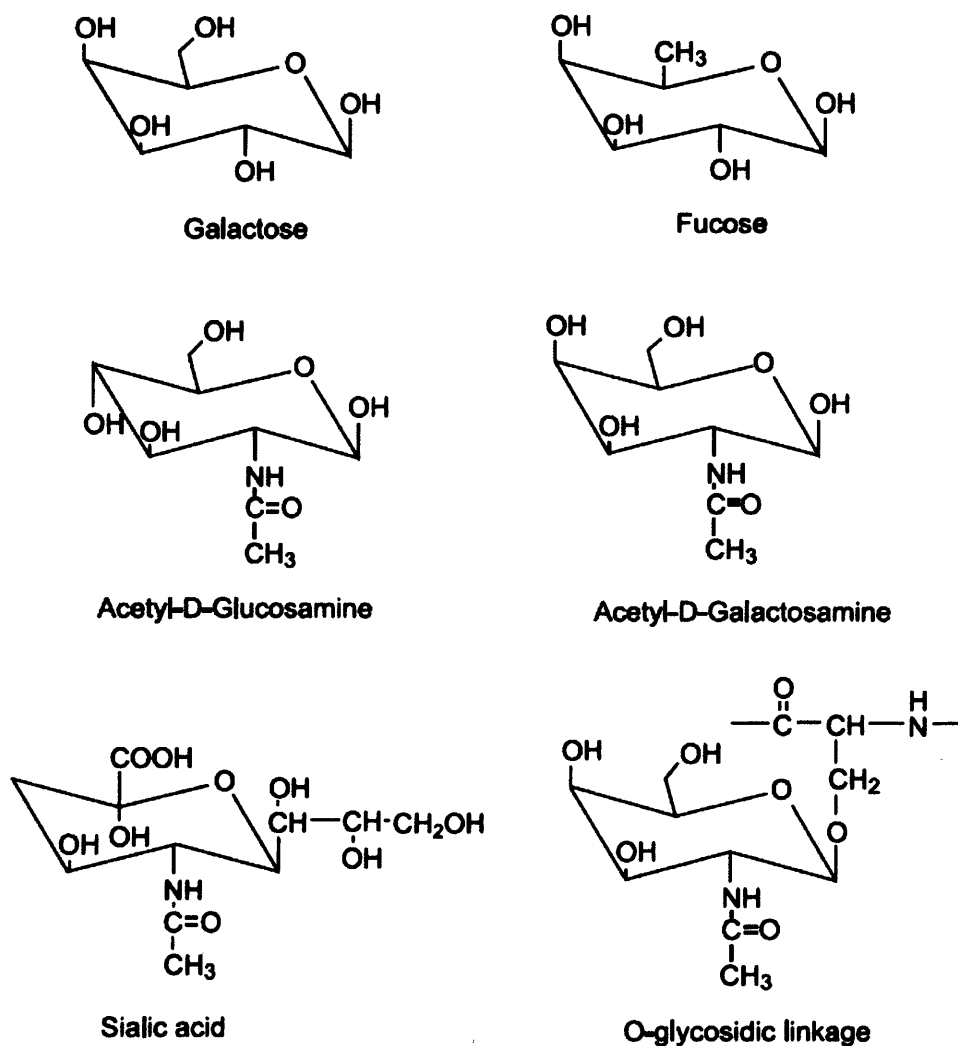
Figure 1.1 Chemical structures of the sugar units generally found in mucin.

6

■■■■ **Polypeptide backbone**   ⅄ **N- and C- terminal end**

⌇⌇⌇⌇ **Polysaccharide**   ∿∿ **Cysteine rich-domains**
side chain   **(hydrophobic patches)**
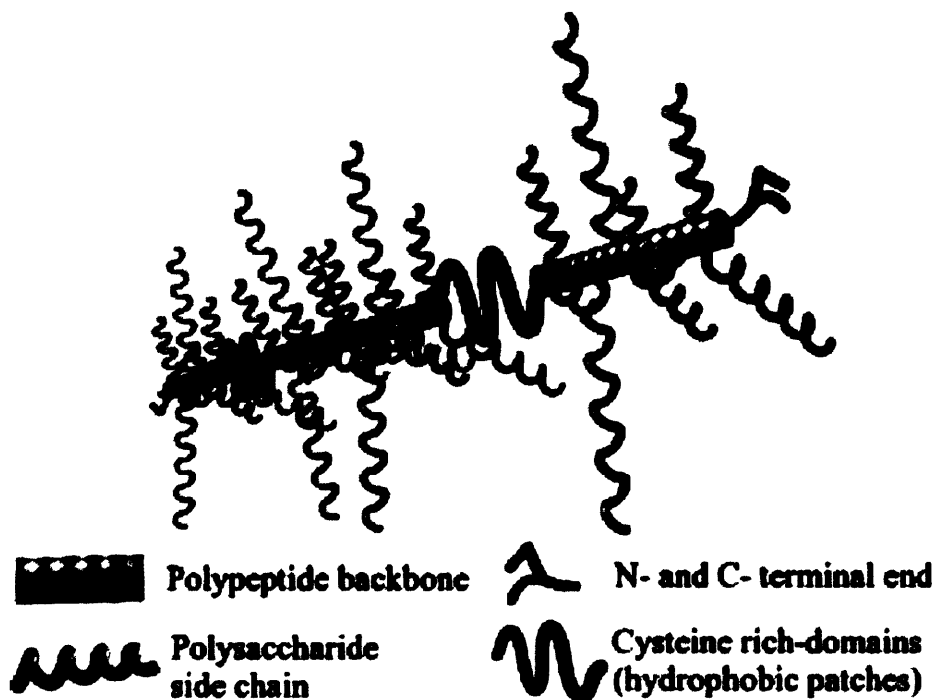
Figure 1.2 Schematic representation of the mucin molecule. Taken from Lafitte G. [27].

<u>Cysteine-rich domains</u>

Apart from the glycosylated domains, the mucin contains non-glycosylated regions called 'naked domains'. They are typically found in the N-terminal and C-terminal part of the polypeptide backbone and are enriched in cysteine residues. These domains have been shown to be involved in the dimerization and eventual mucin polymerization to form large mucin supramolecular complexes connected via disulfide bond formation [28].

1.1.2.2. Mucin conformation in solution

Since the mucin is a large and complex molecule, it is hard to determine its exact conformation. However, despite it being a glycoprotein no evidence of folded structures, such as α-helix and/or β-sheet, is observed [24]. The glycosylated domains of the mucin tend to interact well with water, resulting in an extended random coil conformation for the mucin molecule

7

[24, 29] with a length ranging from a few hundred nanometres up to several microns [30, 31].

1.1.2.3. Mucin association in solution

A general characteristic of polymer solutions is their aggregation which depends on the molecular weight of the polymer as well as the concentration of the polymer in solution.

For a polymer solution, three regimes can be distinguished: dilute, semi-dilute and concentrated [32]. The concentration at which the polymer coils start to overlap is known as the overlap concentration C^*. For concentrations at less than the overlap concentration – *i.e.*, $c<C^*$ – each polymer molecule can be considered as a single non-interacting chain and any interaction between polymer molecules can be neglected. In the semi-dilute regime, the chain of one polymer is likely to come in contact with chains of other polymers, forming a non-connected network. In the concentrated regime $c>>C^*$, all polymer chains become highly entangled and the properties of the system come close to those of a polymer melt. A summary of the three regimes described is described in Figure 1.3.

$c<C^*$ $\qquad$ $c>C^*$ $\qquad$ $c>>C^*$
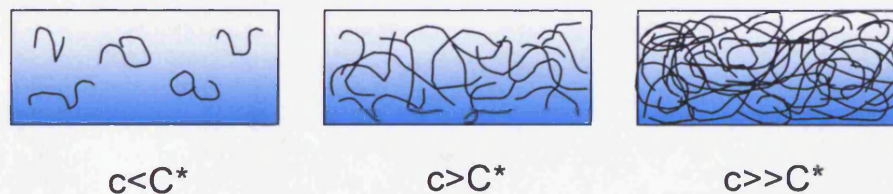
Figure 1.3 Dilute, semi-dilute and concentrated regimes in a polymer solution.

Since mucin is a high molecular weight molecule, the overlap concentration is low (2-4 mg/ml) [33], and at physiological concentration in the mucus gel (~ 50 mg/ml) mucin molecules are expected to be highly entangled. This type of interaction is also the main type of interaction responsible of the viscoelastic properties of concentrated mucin solutions. Bhaskar *et al.* [34] reported viscometry, analytical ultracentrifugation and

dynamic light scattering (DLS) studies that showed a noticeable increase in the viscosity and aggregation of mucin *in vitro* when the pH was lowered from pH 7 to pH 2. Similarly, Hong *et al.* [35] used atomic force microscopy (AFM) to show that mucin aggregates at low pH forming clusters of 10 or fewer molecules at pH 2, and suggesting that oligosaccharide side chains are not directly involved in the aggregation process. DLS, turbidity and rheo-small angle light scattering (rheo-SALS) methods have also shown that mucin solutions tend to aggregate at pH 2 [36].

The aggregation/gelation behaviour of mucin is essential, for example, in the protection of the stomach from auto-digestion, at the physiological gastric pH of 2. Cao *et al.* [37-39] studied the pH-dependent conformational change of gastric mucin by DLS and showed that mucin undergoes a reversible conformational change from a random coil at pH> 4 to an extended conformation at pH< 4, interpreted as a sol-gel transition. At low pH, the extended conformation exposes the hydrophobic regions of the mucin polymer, leading to a more accessible protein-protein interaction, which increases the viscosity. Pig gastric mucin (PGM) gelatination involves interactions between aspartic acid and glutamic acid residues (pKa ~ 4) from the non-glycosylated side chains of the molecule. At pH>4, salt bridges between negatively charged carboxylate side chains and positively charged amine groups in the non-glycosylated regions induce a random coil that results in the hydrophobic domains becoming folded and hidden. At pH<4, the carboxylate groups of the salt bridges become protonated and mucin unfolds, exposing the hydrophobic and promoting a more extended conformation [20]. A model showing the conformational change of the mucin with the pH is illustrated in Figure 1.4.
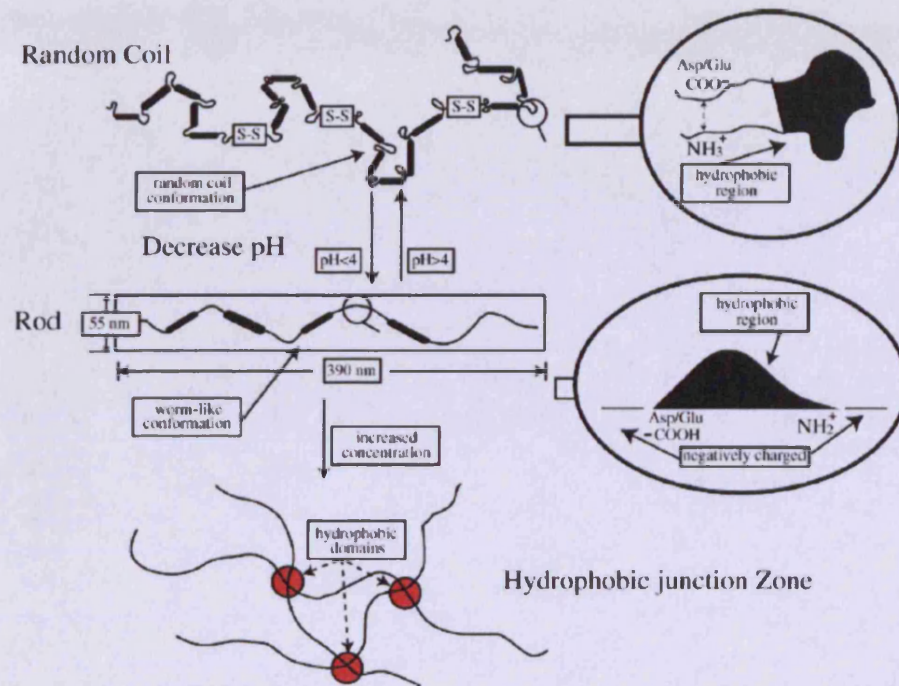
Figure 1.4 *A model showing how the electrostatic interactions at pH < 4 can produce a conformational change from a random coil to a rod, leading to gelation. Taken from Bansil R.* [20].

1.1.2.4. *Physico-chemical properties of the mucin*

As mentioned earlier, the presence of sialic acid molecules in the carbohydrate side chains makes the mucin a highly negatively charged polymer. However, the glutamic acid and aspartic acid in the protein core as well as the sulphate groups on the side chains contribute also to the negative charge of the mucin molecule. Considering an isoeletric point (IEP) between 2 and 3, the mucin molecule can be assumed to be fully charged at a pH above 2.6, which is the pKa of sialic acid. Thus, the mucin is fully charged at pH 7 and the degree of negative charge decreases with decreasing pH. From a physiological point of view, this means that the charge of mucin changes from being fully charged at physiological pH (~ pH 7.4) to weakly positively charged at the low pH (pH 1-2) in the gastric tract.

Another important aspect from a physico-chemical point of view is the presence of hydrophobic patches in the mucin molecule. Even though most hydrophobic groups belong to the polypeptide backbone and in particular to the cysteine-rich domains, some functional groups in the oligosaccharide side chains – for example, the fucose – can have similar properties: in fact, the methyl group at the equatorial position in the fucose molecule (Figure 1.1) confers some hydrophobicity to that specific region of the molecule [40].

The rheological properties of mucin are mainly determined by the intermolecular disulfide bridges between the polypeptide backbones in mucin molecules, responsible of the mucin gel-network formation. This makes the mucin a viscoelastic gel. However, mucin molecules are differently able to form intermolecular disulfide bridges, probably due to a different chemical composition and arrangement of the amino acids on the peptide backbone. Therefore, some molecules are able to form viscoelastic gels while others can only form loose gels [17].

Summarizing the physico-chemical properties of mucin as hydrophobic patches, negative charges and disulfide bridges, it is easy to understand why mucin molecules have been compared to hydrophobically modified polyelectrolytes [24]. Similarly to polyelectrolytes, mucin molecules are subjected to structural changes when changing the external conditions and they are also able to form a loose, highly solvated, and greatly expanded structure.

1.1.3. Advantages and limitations of using commercial mucin compared to 'real' mucus

Mucin can be easily purchased from Sigma Aldrich in the form of dried porcine gastric mucin (PGM), from which mucin solutions can be readily made up. Commercial porcine gastric mucin is widely used in several mucin-related studies [41-43] since: (i) it is quite well representative of the mucin present in 'real' mucus; (ii) it does not require all the extraction and purification processes of the mucin extracted from fresh mucus samples.

Indeed, the purification of pig gastric mucin from fresh mucus involves several steps: (i) collection of the mucus after gently scraping the surface of the stomachs of freshly slaughtered pigs; (ii) purification of mucin samples through exhaustive dialysis, high-speed centrifugation and isopycnic density-gradient centrifugation.

Although all the advantages in using commercial pig gastric mucin (*i.e.*: avoiding long and tedious purification processes), it has been found that the gel properties of the commercial mucin cannot reproduce those observed *in-vivo*, as demonstrated by rheological studies performed by Kocevar-Nared *et al.* [44]. The rheological investigation of rehydrated dried Sigma porcine gastric mucin and natural pig gastric mucus demonstrated that after rehydration of Sigma mucin, a model mucus system with rheological properties equivalent to fresh isolated natural mucus cannot be obtained. Obviously, the isolation procedure of commercial mucin changes the physico-chemical properties of the PGM. The commercial mucin is highly degraded: in fact, the extraction and purification processes damage the disulfide bridges in the cysteine-rich domain, leading to a lack of gel formation and, therefore, to a much weaker sol-gel transition around pH 4. Nevertheless, the protein backbone and the carbohydrate side-chains appear to be unchanged during the purification process.

Therefore, commercial PGM can then be regarded as an interesting material to study the mobility through, and interactions with, mucin solutions of other molecules, while investigation of the mucin gel properties should be carried out on mucin purified from fresh natural mucus.

1.2. Polymer architecture and drug delivery

1.2.1. Use of water-soluble polymers to promote targeting and delivery of therapeutic agents

A successful drug delivery system should be able to traverse several physicochemical and biological barriers en-route to the site of action and provide for a sufficient uptake of the active therapeutic. The interface of polymer chemistry and biomedical science has given birth to nano-sized (5-100 nm) polymer-based pharmaceuticals, which have been termed 'polymer therapeutics' [45]. The term 'polymer therapeutics' is used to describe polymeric drugs [46], polymer-drug conjugates [47] and polymer-protein conjugates [48, 49], drug entrapment in polymer micelles [50] and polymeric multicomponents polyplexes used as non-viral vectors [51]. A schematic diagram of polymer therapeutics is illustrated in Figure 1.5.

In polymer-drug systems, the polymer is seen as a physical carrier for low-molecular-weight drugs to improve their tissue targeting specificity. Polymer and drug can be, for example, coupled via biodegradable linkers that release the drug at the target site upon exposure to a given biological stimuli. In polymer-protein conjugates – *e.g.*, PEGylation – the polymer may also increase protein solubility and stability, reduce protein immunogenicity and prolong plasma half-life.

The polymer, as a delivery vehicle, must be [52]:

> ➤ Biocompatible, non-toxic, non-immunogenic and non-pathogenic
> ➤ Able to carry and protect the payload from degradation
> ➤ Stable
> ➤ Able to:
>   - target the appropriate cell type
>   - avoid the accumulation in the liver
>   - release the therapeutic agent at the target site
> ➤ Easy to administer
> ➤ Inexpensive to synthesize and purify

Advances in polymer chemistry have allowed the synthesis of polymers with specific chemical structure. These structures can go from simple linear polymers to highly branched dendrimers [53] and they can be designed to have well defined physical and chemical properties, as well as three-dimensional structure in the case of dendrimers.
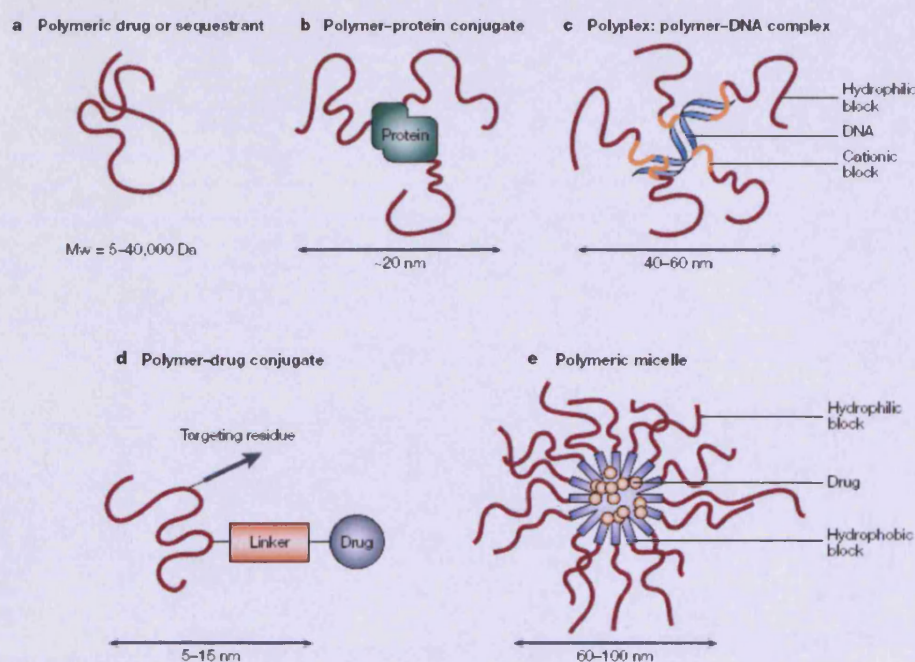
Figure 1.5 Schematic representation of polymer therapeutics. Taken from Duncan R. [45].

1.2.2. Polymer architecture

For a controlled release formulation and a drug-targeting system, polymeric materials, including natural, semi-natural and synthetic polymers, provide several opportunities to modulate the properties of drug delivery systems. Any polymer selected for drug delivery formulations is usually classified according to (i) chemical nature (such as polyester, polyanhydride), (ii) backbone stability (biodegradable, non-biodegradable), (iii) and water solubility (hydrophobic, hydrophilic) [54].

14

Polymer architectures relevant to drug delivery application are presented in Figure 1.6 . Linear polymers considered are water-soluble polymers to create polymer-drug conjugates. Branched polymers are characterized by the presence of branch points. Some studies have revealed that branched polymers have significantly different physical properties from linear polymers and polymer networks, such as melt rheology, mechanical behaviour, and solution properties [55]. Although undesirable branching can occur in several polymerization reactions, branches in branched polymers should be preferably prepared via controlled polymerization techniques. Most of the cross-linked polymers, including the interpenetrating polymer networks (IPN), involve chemical cross-linking techniques to form drug delivery systems which go beyond nanoscale in size. Therefore, they will not be considered in the following descriptions.

a. Linear Polymers

homopolymer

AB-type diblock copolymer

b. Branched Polymers
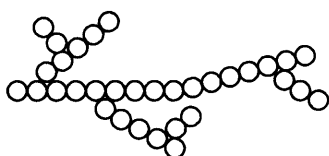
hyper-branched polymer
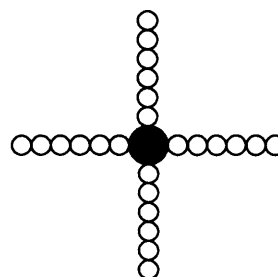
star-shaped polymer
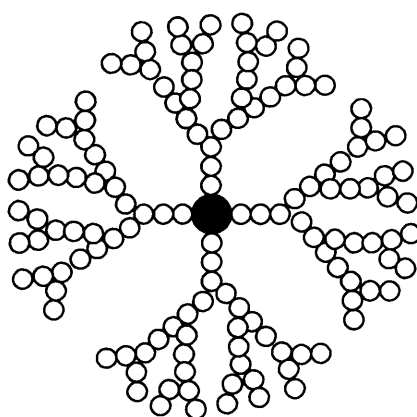
dendrimer

c. Cross-linked Polymers
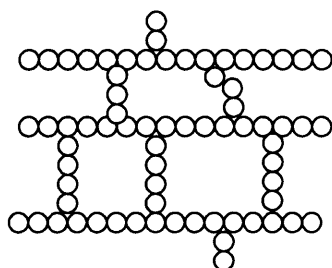
polymer network
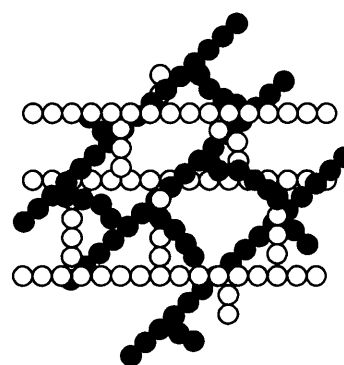
interpenetrating polymer network (IPN)

Figure 1.6 Polymer architecture: (a) linear polymers, (b) branched polymers, and (c) cross-linked polymers. Adapted from Qui L. Y. [53].

<u>Linear water-soluble polymers</u>

Linear polymers present the simplest architecture form. Two are the main advantages that have been specially noted: (i) the formation of random coil structures of 5-15 nm in size in good solvents depending on molecular weight and polymer-solvent interactions; (ii) a tailored multivalency achieved by introducing functional groups along the polymer backbone, typically used as centres for polymer-drug conjugations.

Polymers frequently used for drug carriers include vinyl polymers, polysaccharides, poly(amino acids), proteins and poly(ethylene glycol) (PEG) [54, 56]. Poly(N-vinylpyrrolidone) (PVP) with an active group on one chain end introduced during polymerization can conjugate with certain drugs (*e.g.*, *para*-nitroaniline) to increase drug solubility and stability [57-59]. The functional side groups of poly(amino acids), such as poly(L-lysine), poly(L-glutamic acid), and poly[(N-hydroxyalkyl) glutamine], can be also coupled with drug molecules [60]. These polymers have the disadvantage to have complicated chemical compositions, which make it difficult to characterize the product. Polysaccharides, such as dextran, alginate, chitosan, have been well used because of their good compatibility as natural polymers and their possibility of drug conjugation through their functional side groups [61-63]. PEG has been widely used to modify several therapeutic proteins (PEGylation of a protein) by enhancing their stability, plasma half-life, and reducing their immunogenicity *in vivo* [64-66]. PEGylation has been able to improve the low solubility of small drugs.

<u>Branched polymers</u>

A general problem encountered with linear polymers is the low loading of these polymers: a PEG chain, for instance, possess only one or two hydroxyl terminal groups that can be activated. To overcome this limitation, branched and dendritic polymer structures have been considered.

A typical example of branched polymer used in drug delivery is polyethylenimmine (PEI). This hyper-branched polymer possesses primary, secondary and tertiary charged amino groups. Therefore, it can work as a cationic polyelectrolyte which can strongly attract anionically charged organic and inorganic materials, colloids and surfaces: in fact, PEI is widely involved in the applications for anionic DNA delivery.

Star polymers have a three-dimensional hyper-branched structure where linear arms radiate from a central core. The most significant advantage for star polymer-shape unimolecular micelles is the higher stability when compared with micelles formed from amphiphilic molecules because these unimolecular micelles have covalently fixed branching points.

Another class of polymers possessing a three-dimensional structure are represented by the dendrimers, where a series of layered branches regularly extend from a central core [67, 68]. A typical dendrimer comprises three main structural components: a multifunctional central core, branched units and surface groups. The repeated layers are called "generations". Compared to linear polymers, dendrimer polymers architecture can be favourably used for drug delivery applications. The internal cavity of the dendrimer provides a location for non-covalent encapsulation of hydrophobic drugs and possibly controls the release afterwards. Furthermore, the controlled multivalency of dendrimers can be used to attach combination of drug molecules and targeting groups in a well-defined way. Dendrimers are usually low polydiperse which should provide a more reproducible pharmacokinetic behaviour. Like the star polymers, dendrimers are more stable when compared to polymeric micelles at any concentration because they are unimolecular covalently bound micelles and they do not dissociate. It has been studied [69, 70] that the generation of dendrimers also affects the drug release. For polyamidoamines (PAMAM) dendrimers, an increase in generation means a transform from a flexible (G0-3) to semi-rigid container-type structure (G4-6). Obviously, dendrimers with larger generation show longer

retention in drug release because with increased generation the structure becomes more compact.

1.3. Diffusion and permeability of macromolecules through mucus

The mucus is a thick and viscous gel. Its physicochemical properties, afford bio-adhesion which has been extensively used to promote localised delivery. Mucoadhesive drug delivery systems require an interaction between the mucus and the drug delivery device [71-73] which results then in: (i) a prolonged residence time of the delivery system, (ii) a localization of the delivery device at a specific target site, and (iii) an increase in the drug concentration gradient [8, 74, 75]. Despite the value of bio-adhesion in promoting localised delivery, the focus of this thesis is on quantifying the mobility and permeability of macromolecules (polymers, nano-sized drug delivery constructs) through the mucosal layer and to develop an understanding how molecular interactions affect the pharmacokinetics.

Many studies have considered the ability of macromolecules to diffuse within the mucosal network using a range of different techniques, including multiple-particle tracking (MPT), diffusion chamber system and fluorescence recovery after photobleaching (FRAP). An overview of these techniques will be given together with their findings on the mobility of nano-sized drug delivery constructs in bio-gels.

1.3.1. Multiple particle tracking (MPT)

Multiple-particle tracking (MPT) is a well established technology which can be used to study the diffusion of particles through biological environments. In this method, the microscopic motion of hundreds of particles is recorded by video microscopy. The kind of information that can be extracted from the analysis of time-resolved particle trajectories are both quantitative (diffusion coefficients related to the mobility of the particle) and qualitative (direction and transport mode). Data thus obtained can provide direct and indirect information about particle-environment

interactions and it can be easily applied to study the effect of intracellular (*e.g.*, cell cytoplasm) [76] and extra-cellular media (*e.g.*, mucus) [77].

MPT has been applied to study the diffusion of uniform polystyrene (PS) particles of various diameters (100, 200 and 500 nm) in cystic fibrosis mucus. Smaller particles showed a greater transport rate compared with larger particles, revealing their more facile mobility within pores formed in the cystic fibrosis mucus network [13, 76]. Similarly, Lai *et al.* [78] found that larger polystyrene nanoparticles (500 and 200 nm in diameter), when coated with poly(ethylene glycol), diffuse faster through cervico-vaginal mucus compared to smaller 100 nm coated particles. These same workers showed that PEGylation not only reduced obstruction for larger PEG-PS (200 and 500 nm) but also increased the homogeneity of transport compared with similar sized PS particles.

Furthermore, Dawson *et al.* [79] investigated the transport rates in mucus of cationic nanoparticles made from poly(D,L-lactic-co-glycolic) acid (PLGA) and the cationic surfactant dimethyldioctadecylammonium bromide (DDAB) coated with DNA (PLGA-DDAB/DNA) as potential nanoparticle gene carriers. Their results showed that transport rates of PLGA-DDAB/DNA nanoparticles in mucus were higher than that of the slightly smaller PS nanoparticles because the DNA coating makes the PLGA-DDAB/DNA nanoparticles moderately hydrophilic when compared to PS nanoparticles, allowing a greater mobility within the relatively hydrophobic mucus media.

1.3.2. Diffusion chamber system

The diffusion chamber is somewhat dated but is still used to study diffusion of particles through bio-gels. It involves the vertical mounting of two chambers, one donor and one receiver, either side of a mucus or gel solution as shown in Figure 1.6. The donor compartment is filled with the drug delivery system (DDS) under investigation, while the receiver is filled with the buffer solution of the same composition but without the DDS. Diffusion rates of the drug or DDS through the mucus are calculated

by measuring the change in drug concentration in serial samples removed from donor, receiver or both compartments as a function of time. The advantages of this method are its simplicity and the fact that the mucus composition can be changed or altered, simulating several disease states or physiological situations. Disadvantages include the need for lengthy experiments (usually several hours) and that during this period, native mucus with its endogenous proteolytic enzymes can degrade the mucus glycoproteins [1, 18].
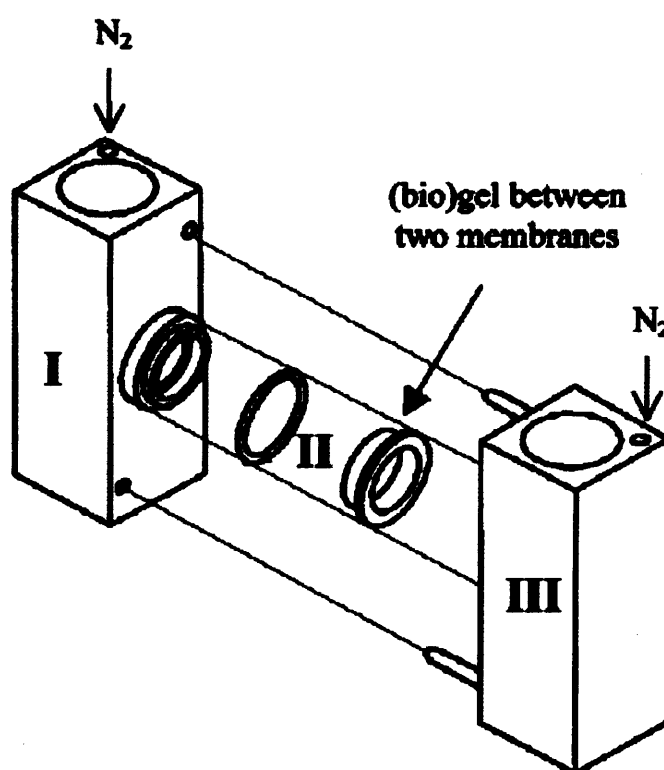
Figure 1.6 Schematic representation of a model diffusion chamber system. Donor compartment (I) is filled with drug and the acceptor compartment (III) with buffer. A thin layer of a bio-gel (II) is placed between the two compartments and hold between two membranes. Taken from Sanders N.N. [1].

Sanders *et al.* [12, 80] studied the transport of fluorescently labelled polystyrene particles (with size comparable to that of some transfection systems for cystic fibrosis gene therapy) through a 220 μm thick cystic

fibrosis mucus layer with a vertical diffusion chamber system. It was found that the largest PS nanospheres (560 nm) were sterically obstructed by the mucus network, while the smaller nanospheres (124 nm) were retarded only by a factor of 1.3 when compared with buffer.

The diffusion of a selection of drugs, such as isoniazid, pentamidine, rifampicin, *p*-aminosalicylic acid and pyrazinamide (which can be all potentially delivered as pulmonary aerosols) through mucin has been carried out by Bhat *et al.* [81, 82]. They showed that the mucus layer presented an additional diffusional barrier to the drugs of 50-57% of the total observed resistance, the latter due to a combination of factors including protein binding, viscosity and physical obstruction. When the mucus was replaced with different cystic fibrosis mucus solutions, there was a 28-75% decrease in drug permeability [83], indicating that significant decreases in drug transport rate occur when crossing cystic fibrosis mucus and that these could play an important role in reduced pulmonary bioavailability.

Similarly, Desai *et al.* [84, 85] investigated the diffusion through mucus gel of a range of solutes with various molecular weights ($126 < M_w < 14{,}400$ g mol^{-1}) and physical properties, including phloroglucinol, 5-hydroxy-L-tryptophan, β-nicotinamide adenine dinucleotide (NAD) and ribonucleic acid (RNA). This study showed, for all solutes studied, a retardation of solute flux in mucus by a factor of at least two when compared to the diffusion of the same solute in aqueous solutions. The limitations of the diffusion chamber methodology centre on the risk of artefacts arising from practical difficulties, principally the inability to control the layer of bio-gel and its propensity to obstruct the filters, reducing the apparent diffusion coefficient.

1.3.3. Fluorescence recovery after photobleaching (FRAP)

Many studies have used fluorescence recovery after photobleaching (FRAP) to investigate the mobility of a range of solutes in sub-cellular compartments. Besides this application, FRAP has also been used to study

the mobility of molecules in extracellular matrices such as mucus and related bio-gels. In a FRAP experiment, one component in a multi-component system is selectively fluorescently labelled. The sample is placed on a microscope and a high intensity laser beam is rastered across the sample, bleaching the fluorescence of the labelled molecules, causing a drop in the fluorescence intensity. Diffusion of the non-bleached molecules into the area previously bleached results in recovery of the fluorescence intensity, Figure 1.7. The diffusion coefficient is then obtained by fitting the curve of the recovery profile [86].
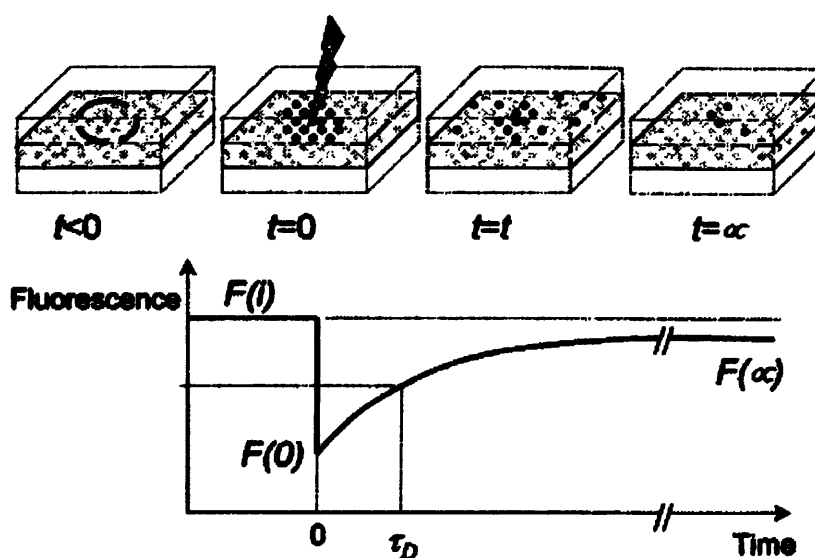
Figure 1.7 Schematic representation of a FRAP experiment. Before bleaching, the initial fluorescence is recorded as F(i). At t = 0, a high intensity light beam bleaches the molecules causing a drop in fluorescence to F(0). Due to the random motion/diffusion, the bleached molecules will exchange their position in the bleached area with non bleached fluorescent molecules from the surrounding. This results in a recovery of the observed fluorescence. The characteristic diffusion time (τ_D) is indicated as the time at which half of the fluorescence has recovered. Taken from Meyvis T. K. L. [86].

The diffusion of polystyrene microspheres (59-1000 nm) viruses, and artificial virus-like particles derived from the capsid layers of human

papilloma virus HPV (55 nm, ~ 20,000 g mol^{-1}) and Norwalk virus (38 nm, ~ 10,000 g mol^{-1}) in fresh human cervical mucus were quantified using FRAP [87]. When compared to virus-like particles of similar size, the PS microspheres were bound more tightly to the mucin fibres. Even the smallest microspheres (59nm) showed no detectable diffusion by FRAP.

FRAP was also used by Afdhal et al. to examine the influence of mucin in the aggregation of cholesterol enriched vesicles [88]. An increase in the vesicle size (calculated from the diffusion coefficients measured by FRAP) was explained by binding of the vesicles to the mucin, suggesting that both glycosylated and non-glycosylated domains of the mucin are involved in the interaction even though the effect is reversible in the absence of non-glycosylated domains.

1.4. Aims and overview of the studies in this thesis

The overall aim of this thesis was to exploit the technologies of small-angle neutron scattering (SANS) and pulsed-gradient spin-echo nuclear magnetic resonance (PGSE-NMR) to reveal physicochemical interaction of mucin with polymer-based DDS.

Using SANS, conformation of the mucin molecule in solution was determined. The behaviour of mucin in solution was studied as function of the concentration, pH, ionic strength and in the presence of N-Acetyl-L-cysteine (NAC) as mucolytic agent (Chapter 4). The conformation of mucin in solution was described by mathematical scattering models.

The mobility through, and interactions with, mucin solutions of model polymer DDS were then studied. SANS was able to detect the influence/perturbation of the polymeric DDS on the scattering from mucin. PGSE-NMR was used to investigate the diffusion through mucin solution of the polymeric DDS. Theories relative to these techniques are explained in Chapter 3.

Non-ionic/cationic/anionic polymeric DDS with different structures (linear, branched, dendritic) were then considered and the influence of

their electrical charge and structure upon mobility through, and interactions with, mucin solutions studied by SANS and PGSE-NMR (Chapter 5).

The effect of covalently linking polyethylene glycol (PEG) chains to polymers exhibit binding towards mucin molecules was then explored. PEG is widely used for the modification (PEGylation) of interactive molecules. The synthesis of these conjugates with different degrees of PEGylation (from 10% to 100%) was performed. The effect of these PEG-modified polymers on mucin solutions were explored by PGSE-NMR and SANS (Chapter 6).

Finally, a more complex mucus model was studied comprising phospholipids and serum albumin. SANS was used to investigate the conformation of this more complex model (Chapter 7).

References

1. Sanders, N. N.; De Smedt, S. C.; Demeester, J., The physical properties of biogels and their permeability for macromolecular drugs and colloidal drug carriers. *Journal of Pharmaceutical Sciences* **2000,** 89, 835-849.

2. Norris, D. A.; Puri, N.; Sinko, P. J., The effect of physical barriers and properties on the oral absorption of particulates. *Advanced Drug Delivery Reviews* **1998,** 34, 135-154.

3. Linden, S. K.; Sutton, P.; Karlsson, N. G.; Korolik, V.; McGuckin, M. A., Mucins in the mucosal barrier to infection. *Mucosal Immunology* **2008,** 1, 183-197.

4. Bhat, P. G.; Flanagan, D. R.; Donovan, P. D., Drug binding to gastric mucus glycoproteins. *International Journal of Pharmaceutics* **1996,** 134, 15-25.

5. Rahmoune, H.; Shephard, K. L., State of airways surface liquid on guinea-pig trachea. *Journal of Applied Physiology* **1995,** 178, 2020-2024.

6. Sims, D. E.; Horne, M. M., Heterogeneity of the composition and thickness of tracheal mucus in rats. *American Journal of Physiology - Lung Cellular and Molecular Physiology* **1997,** 273, L1036-L1041.

7. Neutra, M. R.; Forstner, J. F., Gastrointestinal mucus: synthesis, secretion, and function. In *Physiology of the Gastrointestinal Tract*, 2nd ed. ed.; Johnson, L. R., Ed. New York, 1986; pp 975-1009.

8. Ponchel, G.; Irache, J. M., Specific and non-specific bioadhesive particulate systems for oral delivery to the gastrointestinal tract. *Advanced Drug Delivery Reviews* **1998,** 34, 191-219.

9. Kerss, S.; Allen, A.; Garner, A., A simple method for measuring thickness of the mucus gel layer adherent to rat, frog and human gastric mucosa: influence of feeding, prostaglandin, N-acetylcysteine and other agents. *Clinical Science* **1982,** 63, 187-195.

10. Sakata, T.; Engelhardt, W. V., Luminal mucin in the large intestine of mice, rats and guinea pigs. *Cell and Tissue Research* **1981,** 219, 629-635.

11. Sellers, L. A.; Allen, A.; Morris, E. R.; Ross-Murphy, S. B., Mechanical characterization and properties of gastrointestinal mucus gel. *Biorheology* **1987,** 24, 615-623.

12. Sanders, N. N.; De Smedt, S. C.; Van Rompaey, E.; Simoens, P.; De Baets, F.; Demeester, J., Cystic fibrosis sputum: a barrier to the transport of nanospheres. *American Journal of Respiratory and Critical Care Medicine* **2000,** 162, 1905-1911.

13. Dawson, M.; Wirtz, D.; Hanes, J., Enhanced viscoelasticity of human cystic fibrotic sputum correlates with increasing microheterogeneity in particle transport. *The Journal of Biological Chemistry* **2003,** 278, 50393-50401.

14. Gulbins, E., Lipids control mucus production in cystic fibrosis. *Nature Medicine* **2010,** 16, 267-268.

15. Pullan, R. D., Colonic mucus, smoking and ulcerative colitis. *Annals of The Royal College of Surgeons of England* **1996,** 78, 85-91.

16. Matthes, I.; Nimmerfall, F.; Sucker, H., Mucus models for investigation of intestinal absorption mechanisms. 2. Mechanisms of drug interactions with intestinal mucus. *Die Pharmazie* **1992,** 47, 609-613.

17. Strous, G. J.; Dekker, J., Mucin-type glycoproteins. *Critical Reviews in Biochemistry and Molecular Biology* **1992,** 27, 57-92.

18. Khanvilkar, K.; Donovan, M. D.; Flanagan, D. R., Drug transfer through mucus. *Advanced Drug Delivery Reviews* **2001,** 48, 173-193.

19. Larhed, A. W.; Artursson, P.; Bjork, E., The influence of intestinal mucus components on the diffusion of drugs. *Pharmaceutical Research* **1998,** 15, 66-71.

20. Bansil, R.; Turner, B. S., Mucin structure, aggregation, physiological functions and biomedical applications. *Current Opinion in Colloid and Interface Science* **2006,** 11, 164-170.

21. Perez, E.; Proust, J. E., Forces between mica surfaces covered with adsorbed mucin across aqueous solution *Journal of Colloid and Interface Science* **1987,** 18, 182-191.

22. Durrer, C.; Irache, J. M.; Duchene, D.; Ponchel, G., Mucin interactions with functionalized polystyrene latexes. *Journal of Colloid and Interface Science* **1995**, 170, 555-561.

23. Lee, S.; Muller, M.; Rezwan, K.; Spencer, N. D., Porcine gastric mucin (PGM) at the water/poly(dimethylsiloxane) (PDMS) interface: influence of pH and ionic strength on its conformation, adsorption, and aqueous lubrication properties. *Langmuir* **2005**, 21, 8344-8353.

24. Harding, S. E., The macrostructure of mucus glycoproteins in solution. *Advances in Carbohydrate Chemistry and Biochemistry* **1989**, 47, 345-381.

25. Dekker, J.; Rossen, J. W. A.; Buller, H. A.; Einerhand, A. W. C., The MUC family: an obituary. *Trends in Biochemical Sciences* **2002**, 27, 126-131.

26. Jentoft, N., Why are proteins O-glycosylated? *Trends in Biochemical Sciences* **1990**, 15, 291-294.

27. Lafitte, G.; Soderman, O.; Thuresson, K.; Davies, J., PFG-NMR diffusometry: a tool for investigating the structure and dynamics of non commercial purified gastric mucin in a wide range of concentrations. *Biopolymers* **2007**, 86, 165-175.

28. Carlstedt, I.; Lindgren, H.; Sheehan, J. K., The macromolecular structure of human cervical-mucus glycoproteins. Studies on fragments obtained after reduction of disulphide bridges and after subsequent trypsin digestion. *Biochemical Journal* **1983**, 213, 427-435.

29. Schimmel, P. R.; Flory, P. J., Conformational energies and configurational statistics of copolypeptides containing L-proline. *Journal of Molecular Biology* **1968**, 34, 105-120.

30. McMaster, T. J.; Berry, M.; Corfield, A. P.; Miles, M. J., Atomic force microscopy of the submolecular architecture of hydrated ocular mucins. *Biophysical Journal* **1999**, 77, 533-541.

31. Oates, M. D. G.; Rosbottom, A. C.; Schrager, J., Further investigations into the structure of human gastric mucin: the

structural configuration of the oligosaccharide chains. *Carbohydrate Research* **1974**, 34, 115-137.

32. Gedde, U. W., *Polymer physics*. Kluwer Academic Publishers: Dordrecht, 1999.

33. Bansil, R.; Stanley, E.; LaMont, T. J., Mucin biophysics. *Annual Review of Physiology* **1995**, 57, 635-657.

34. Bhaskar, K. R.; Gong, D.; Bansil, R.; Pajevic, S.; Hamilton, J. A.; Turner, B. S.; LaMont, J. T., Profound increase in viscosity and aggregation of pig gastric mucin at low pH. *American Journal of Physiology* **1991**, 261, 827-832.

35. Hong, Z.; Chasan, B.; Bansil, R.; Turner, B. S.; Bhaskar, K. R.; Afdhal, N. H., Atomic force microscopy reveals aggregation of gastric mucin at low pH. *Biomacromolecules* **2005**, 6, 3458-3466.

36. Maleki, A.; Lafitte, G.; Kjoniksen, A.-L.; Thuresson, K.; Nystrom, B., Effect of pH on the association behaviour in aqueous solutions of pig gastric mucin. *Carbohydrate Research* **2008**, 343, 328-340.

37. Bansil, R.; Cao, X.; Afdhak, N. H.; Niu, N.; Bhaskar, K. R.; LaMonte, J. T., Mucin: aggregation and colloidal interactions of relevance to some biomedical problems. *Il Nuovo Cimento D* **1994**, 16, (9), 1411-1418.

38. Cao, X.; Bansil, R.; Bhaskar, R.; Turner, B. S.; LaMont, J. T., pH-dependent conformational change of gastric mucin leads to sol-gel transition *Biophysical Journal* **1999**, 76, 1250-1258.

39. Bansil, R.; Cao, X.; Bhaskar, K.; Ramakrishnan, K.; LaMont, J. T., Gelation and aggregation of mucin in relation to the stomach's protective barrier. *Macromolecular Symposia* **1996**, 109, 105-113.

40. Jimenez-Castellanos, M. R.; Zia, H.; Rhodes, C. T., Mucoadhesive drug delivery systems. *Drug Development and Industrial Pharmacy* **1993**, 19, 143-194.

41. Tian, P.; Brandl, M.; Mandrell, R., Porcine gastric mucin binds to recombinant norovirus particles and competitively inhibits their binding to histo-blood group antigens and Caco-2 cells. *Letters in Applied Microbiology* **2005**, 41, 315-320.

42. Chen, E. Y. T.; Wang, Y.-C.; Chen, C.-S.; Chin, W.-C., Functionalized positive nanoparticles reduce mucin swelling and dispersion. *PLoS ONE* **2010**, 5, e15434.

43. Waigh, T. A.; Papagiannopoulos, A.; Voice, A.; Bansil, R.; Unwin, A. P.; Dewhurst, C. D.; Turner, B.; Afdhal, N., Entanglement coupling in porcine stomach mucin. *Langmuir* **2002**, 18, 7188-7195.

44. Kocevar-Nared, J.; Kristl, J.; Smid-Korbar, J., Comparative rheological investigation of crude gastric mucin and natural mucus. *Biomaterials* **1997**, 18, 677-681.

45. Duncan, R., The dawning era of polymer therapeutics. *Nature Reviews Drug Discovery* **2003**, 2, 347-360.

46. Donaruma, L. G., Synthetic biologically active polymers. *Progress in Polymer Science* **1974**, 4, 1-25.

47. Duncan, R., Polymer-drug conjugates. In *Handbook of Anticancer Drug Development*, Budman, D.; Calvert, H.; Rowinsky, E., Eds. Lippincott Williams & Wilkins: Baltimore, 2003; pp 239-260.

48. Harris, J. M.; Chess, R. B., Effect of PEGylation on pharmaceuticals. *Nature Reviews Drug Discovery* **2003**, 2, 214-221.

49. Veronese, F. M.; Harris, J. M., Peptide and protein PEGylation. *Advanced Drug Delivery Reviews* **2002**, 54, 453-609.

50. Masayuki, Y.; Mizue, M.; Noriko, Y.; Teruo, O.; Yasuhisa, S.; Kazunori, K.; Shohei, I., Polymeric micelles as novel drug carrier: Adriamycin-conjugated poly(ethylene glycol)-poly(aspartic acid) block copolymers. *Journal of Controlled Release* **1990**, 11, 269-278.

51. Kabanov, A. V.; Felgner, P. L.; Seymour, L. W., *Self-assembling complexes for gene delivery: From Laboratory to Clinical Trial.* John Wiley & Sons: Chichester, 1998.

52. Twaites, B.; de las Heras Alarcon, C.; Alexander, C., Synthetic polymers as drugs and therapeutics. *Journal of Materials Chemistry* **2005**, 15, 441-445.

53. Qiu, L. Y.; Bae, Y. H., Polymer architecture and drug delivery. *Pharmaceutical Research* **2006**, 23, 1-30.

54. Hoste, K.; De Winne, K.; Schacht, E., Polymeric prodrugs. *International Journal of Pharmaceutics* **2004**, 277, 119-131.

55. McKee, M. G.; Unal, S.; Wilkes, G. L.; Long, T. E., Branched polyesters: recent advances in synthesis and performance. *Progress in Polymer Science* **2005**, 30, 507-539.

56. Okana, T.; Yui, N.; Yokoyama, M.; Yoshida, R., *Advances in polymeric systems for drug delivery*. Gordon and Breach Science Publisher: Tokyo, 1994.

57. Tsunoda, S.; Kamada, H.; Yamamoto, Y.; Ishikawa, T.; Matsui, J.; Koizumi, K.; Kaneda, Y.; Tsutsumi, Y.; Ohsugi, Y.; Hirano, T.; Mayumi, T., Molecular design of polyvinylpyrrolidone-conjugated interleukin-6 for enhancement of in vivo thrombopoietic activity in mice. *Journal of Controlled Release* **2000**, 68, 335-341.

58. D'Souza, A. J. M.; Schowen, R. L.; Topp, E. M., Polyvinylpyrrolidone-drug conjugate: synthesis and release mechanism. *Journal of Controlled Release* **2004**, 94, 91-100.

59. Kaneda, Y.; Tsutsumi, Y.; Yoshioka, Y.; Kamada, H.; Yamamoto, Y.; Kodaira, H.; Tsunoda, S.; Okamoto, T.; Mukai, Y.; Shibata, H.; Nakagawa, S.; Mayumi, T., The use of PVP as a polymeric carrier to improve the plasma half-life of drugs. *Biomaterials* **2004**, 25, 3259-3266.

60. Franssen, E. J. F.; Moolenaar, F.; De Zeeuw, D.; Meijer, D. K. F., Drug targeting to the kidney with low-molecular weight proteins. *Advanced Drug Delivery Reviews* **1994**, 14, 67-88.

61. Matsumoto, S.; Yamamoto, A.; Takakura, Y.; Hashida, M.; Sezaki, H., Cellular interaction and in vivo antitumour activity of mitomycin C-dextran conjugate. *Cancer Research* **1986**, 46, 4463-4468.

62. Al-Shamkhani, A.; Duncan, R., Synthesis, controlled release properties and antitumour activity of alginate-cis-aconityl-daunomycin conjugates. *International Journal of Pharmaceutics* **1995**, 122, 107-119.

63. Son, Y. J.; Jang, J. S.; Cho, Y. W.; Chung, H.; Park, R. W.; Kwon, I. C.; Kim, I. S.; Park, C. R.; Jeong, S. Y., Biodistribution and anti-

tumor efficacy of daxorubicin loaded glycol-chitosan nanoaggregates by EPR effect. *Journal of Controlled Release* **2003**, 91, 135-145.

64. Ho, D. H. W.; Wang, C.; Lin, J.; Brown, N.; Newman, R. A.; Krakoff, I. H., Polyethylene glycol-L-asparaginase and L-asparaginase studies in rabbits. *Drug Metabolism and Disposition* **1988**, 16, 27-29.

65. Tanaka, H.; Satake-Ishakawa, R.; Ishakawa, M.; Matsuki, S.; Asano, K., Pharmacokinetics of recombined human granulocyte colony-stimulating factor conjugated to poly(ethylene glycol) in rats. *Cancer Research* **1991**, 51, 3710-3714.

66. Veronese, F. M.; Pasut, G., PEGylation, successful approach to drug delivery. *Drug Discovery Today* **2005**, 10, 1451-1458.

67. Aulenta, F.; Hayes, W.; Rannard, S., Dendrimers: a new class of nanoscopic containers and delivery devices. *European Polymer Journal* **2003**, 39, 1741-1771.

68. Gillies, E. R.; Frechet, J. M. J., Dendrimers and dendritic polymers in drug delivery. *Drug Discovery and Therapeutics* **2005**, 10, 35-43.

69. Ooya, T.; Lee, J.; Park., K., Effects of ethylene glycol-based graft, star-shaped, and dendritic polymers on solubilization and controlled release of paclitaxel. *Journal of Controlled Release* **2003**, 93, 121-127.

70. Jansen, J. F. G. A.; De Brabander-van den berg, E. M. M.; Meijer, E. W., Encapsulation of guest molecules into a dendritic box. *Science* **1994**, 266, 1226-1229.

71. Fiebrig, I.; Varum, K. M.; Harding, S. E.; Davis, S. S.; Stokke, B. T., Colloidal gold and colloidal gold labelled wheat germ agglutinin as molecular probes for identification in mucin/chitosan complexes. *Carbohydrate Polymers* **1997**, 33, 91-99.

72. Genta, I.; Costantini, M.; Asti, A.; Conti, B.; Montanari, L., Influence of glutaraldehyde on drug release and mucoadhesive properties of chitosan microsphere. *Carbohydrate Polymers* **1998**, 36, 81-88.

73. Bernkop-Schnurch, A.; Schwarz, V.; Steininger, S., Polymers with thiol groups: a new generation of mucoadhesive polymers? *Pharmaceutical Research* **1999**, 16, 876-881.

74. Peppas, N. A.; Huang, Y., Nanoscale technology of muchoadhesive interactions. *Advanced Drug Delivery Reviews* **2004**, 56, 1657-1687.

75. Peppas, N. A.; Sahlin, J. J., Hydrogels as mucoadhesive and bioadhesive materials: a review. *Biomaterials* **1996**, 17, 1553-1561.

76. Suh, J.; Dawson, M.; Hanes, J., Real-time mulptiple-particle tracking: applications to drug and gene delivery. *Advanced Drug Delivery Reviews* **2004**, 57, 63-78.

77. Dawson, M.; Wirtz, D.; Hanes, J., Real-time tracking of nanoparticle gene carriers in gastrointestinal mucus. *Biophysical Journal* **2004**, 86, 598A.

78. Lai, S. K.; O'Hanlon, D. E.; Harrold, S.; Man, S. T.; Wang, Y.-Y.; Cone, R.; Hanes, J., Rapid transport of large polymeric nanoparticles in fresh undiluted human mucus. *Proceedings of the National Academy of Sciences of the United States of America* **2007**, 104, 1482-1487.

79. Dawson, M.; Krauland, E.; Wirtz, D.; Hanes, J., Transport of polymeric nanoparticle gene carriers in gastric mucus. *Biotechnology Progress* **2004**, 20, 851-857.

80. Sanders, N. N.; De Smedt, S.; Demeester, J., Mobility and stability of gene complexes in biogels. *Journal of Controlled Release* **2003**, 87, 117-129.

81. Bhat, P. G.; Flanagan, D. R.; Donovan, M. D., The limiting role of mucus in drug adsorption: drug permeation through mucus solution. *International Journal of Pharmaceutics* **1995**, 126, 179-187.

82. Bhat, P. G.; Flanagan, D. R.; Donovan, M. D., Drug-permeation studies through cystic fibrotic mucus solution. *Pharmaceutical Research* **1995**, 12, S244.

83. Bhat, P. G.; Flanagan, D. R.; Donovan, M. D., Drug diffusion through cystic fibrotic mucus: steady-state permeation, rheologic

properties, and glycoprotein morphology. *Journal of Pharmaceutical Sciences* **1996**, 85, 624-630.

84. Desai, M. A.; Vadgama, P., Estimation of effective diffusion coefficients of model solutes through gastric mucus: assessment of a diffusion chamber technique based on spectrophotometric analysis. *Analyst* **1991**, 116, 1113-1116.

85. Desai, M. A.; Mutlu, M.; Vadgama, P., A study of macromolecular diffusion through native porcine mucus. *Experientia* **1992**, 15, 22-26.

86. Meyvis, T. K. L.; De Smedt, S. C.; Van Oostveldt, P.; Demeester, J., Fluorescence recovery after photobleaching: a versatile tool for mobility and interaction measurements in pharmaceutical research. *Pharmaceutical Research* **1999**, 16, 1153-1162.

87. Olmsted, S. S.; Padgett, J. L.; Yudin, A. I.; Whaley, K. J.; Moench, T. R.; Cone, R. A., Diffusion of macromolecules and virus-like particles in human cervical mucus. *Byophysical Journal* **2001**, 81, 1930-1937.

88. Afdhal, N. H.; Cao, X.; Bansil, R.; Hong, Z.; Thompson, C.; Brown, B.; Wolf, D., Interaction of mucin with cholesterol enriched vesicles: role of mucin structural domains. *Biomacromolecules* **2004**, 5, 269-275.

Chapter 2. Theory and techniques

This chapter presents some of the theoretical aspects of the major techniques used for the studies presented in this thesis: pulsed-gradient spin-echo nuclear magnetic resonance (PGSE-NMR), small-angle neutron scattering (SANS) and viscosimetry. In particular, it focuses on those aspects relevant to the data analysis showed in the subsequent chapters. More detailed theoretical aspects can be found in the Appendix.

2.1. Pulsed-Gradient Spin-Echo NMR (PGSE-NMR)

2.1.1. Introduction

Like all nuclear magnetic resonance (NMR) techniques, the pulsed-gradient spin-echo NMR (PGSE-NMR) offers a numbers of advantages when applied to multi-component or heterogeneous systems: it is non-invasive, non-destructive but most importantly the chemical specificity of NMR enables the behaviour of each component within the mixture to be identified and analysed in a single experiment. This powerful technique provides information on the self-diffusion coefficient of the species under investigation which is determined by the structure of the condensed matter [1].

2.1.2. Self-diffusion and self-diffusion coefficient

Diffusion, as a translational mass transfer process, is manifest as physical (permeation of fluids through porous adsorbents such as oil reservoir rocks), chemical (properties of ordered fluids such as liquid crystals) or biological (circulation of body fluids), and spans a very wide range of timescales [2].

When external forces are applied such as electric fields or other gradients (e.g.: concentration, temperature, pressure), the diffusion process is said to be directed. In the absence of these external forces, the displacements of the particles result from their internal thermal agitation.

The process is known as self-diffusion and is defined as the random translational motion ('random walk') of the particles driven by their internal kinetic energy. Figure 2.1 illustrates the random walk of a particle between time $\tau = 0$ and $\tau = t$ due to its self-diffusion.

Position at time
$\tau = t$

Initial position at
$\tau = 0$

X
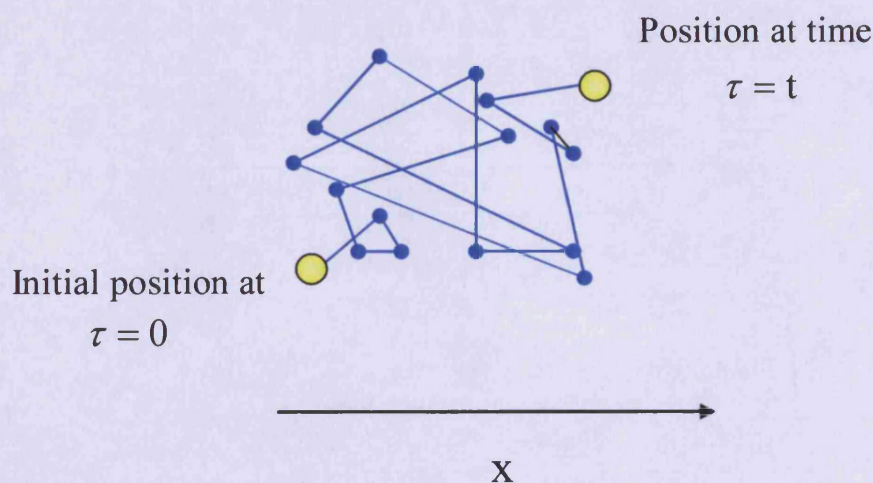
Figure 2.1 Illustration of the random walk of a particle resulting from its thermal motion – i.e., self-diffusion.

The trajectory of a particle experiencing a Brownian walk in a three dimensional space is parameterized by its self-diffusion coefficient, D_s, given by the Einstein-Smoluchowsky equation (Eq. 2.1):

$$D_s = \frac{\langle |\Delta x|^2 \rangle}{6\Delta\tau}$$

Eq. 2.1

where $\langle |\Delta x|^2 \rangle$ is the mean square displacement of the particle over a diffusion time $\Delta\tau$, the angular brackets signifying an average [3].

For solutions with low viscosity, the displacement of a particle due to the diffusion corresponds to a self-diffusion coefficient D_s of the order of 10^{-9}-10^{-12} m^2 s^{-1}. For highly viscous liquids, the mobility of the particle can be significantly retarded by several order of magnitudes [4]. The self-diffusion coefficient provides also information about the size and shape of

the species of interest. The diffusion of a molecule is closely related to its molecular size, as shown by the Stokes-Einstein equation (Eq. 2.2) [1]:

$$D_s = \frac{k_B T}{f}$$ **Eq. 2.2**

where k_B is the Boltzmann's constant, T represents the absolute temperature and f is the frictional factor. For a spherical particle with hydrodynamic radius R_h and viscosity η, the frictional factor is given by the Eq. 2.3:

$$f = 6\pi\eta R_h$$ **Eq. 2.3**

By combining the equations Eq. 2.2 and Eq. 2.3, the self-diffusion coefficient is expressed by the familiar Stokes-Einstein relation (Eq. 2.4) [3]:

$$D_s = \frac{k_B T}{6\pi\eta R_h}$$ **Eq. 2.4**

However, the Stokes-Einstein equation is valid only under ideal conditions in which diffusing species sees the solvent as a continuum and that the diffusing species are essentially at infinitive dilution (*i.e.*, interactions between diffusing species can be ignored). Despite its limitations, the Stoke-Einstein equation provides a useful and intuitive framework for the interpretation of the diffusion data [5].

In the case of a polymer in a dilute solution, the polymer molecules can be considered greatly separated, so that they do not interact with each other, but only with the solvent. In some cases, the solvent will expand the polymer chain in the solution: such solvent is referred as 'good' solvent. In other cases the solvent and polymer will not strongly interact, and the polymer chain will fold back on itself in order to minimize its contacts with the solvent, giving rise to a small globular conformation: such solvent is called 'poor' solvent.

Between these two extreme situations, the polymer and the solvent can interact just enough so that the polymer chain is randomly distributed. This limit of a 'random coil' of a polymer is conventionally chosen as the 'ideal' polymer solution, and a solvent showing these characteristics is called *'theta'* (θ) solvent. Under these conditions, the diffusion of the polymer can be calculated as a correction of the Stoke-Einstein equation:

$$D_s = \frac{k_B T}{6\pi\eta R_e} \qquad\qquad \textbf{Eq. 2.5}$$

where R_e is the equivalent radius of the polymer. This radius is calculated to be

$$R_e = 0.676 \langle R^2 \rangle^{1/2} \qquad\qquad \textbf{Eq. 2.6}$$

in which $\langle R^2 \rangle^{1/2}$ is the root-mean-square radius of gyration, the common measure of the size of the polymer molecule in solution.

In 'good' solvents and 'poor' solvents, the diffusion coefficient still is estimated from the Stoke-Einstein equation, but the relation between the equivalent radius R_e and the root-mean-square radius $\langle R \rangle$ seems less well known [6].

The self-diffusion process can be quantified by PGSE-NMR to provide the measurement of the self-diffusion coefficient of the species investigated. Before analyzing in more details the theory behind the PGSE-NMR technique, a summary of the basis of NMR is given.

2.1.3. Measuring diffusion with magnetic field gradients

The basis of all diffusion NMR measurements is spatially resolved NMR achieved by superimposing pulsed magnetic field gradients on the static magnetic field. Therefore, the central feature of a diffusion NMR experiment is a spatially varying magnetic field produced by the application of a magnetic field gradient *G(r)* that encodes into the NMR

signal (via the frequency, ω) the position of the molecule, r, as shown by Eq. 2.7:

$$B(r) = B_0 + \gamma G(r) \qquad \textbf{Eq. 2.7}$$

where $B(r)$ is the effective field at the position r, B_0 the static field strength and γ the gyromagnetic ratio, constant for a particular nucleus.

Therefore, the addition of magnetic field gradients in the z-axis to the external magnetic field B_0 affects the frequency of a nucleus such as

$$\omega_{eff} = \omega_0 + \gamma G(r) \qquad \textbf{Eq. 2.8}$$

The Larmor frequency of the nucleus becomes a spatial label with respect to the direction of the gradient because any nucleus changing its location will have a Larmor frequency varied. This frequency change is observed in a spin-echo (SE) experiment [4]. More detailed aspects on the basics of NMR and the pulse programmes can be found in the Appendix A.

2.1.4. Calculating the self-diffusion coefficient

The spin-echo recorded in the PGSE experiment can be Fourier transformed to get the spectrum. The spectrum obtained presents all the peaks belonging to the different components in the system: the peak intensities decay differently. Therefore, the self-diffusion coefficients of several species present in a multi-component system can be measured simultaneously from their attenuation functions, as illustrated in Figure 2.2.
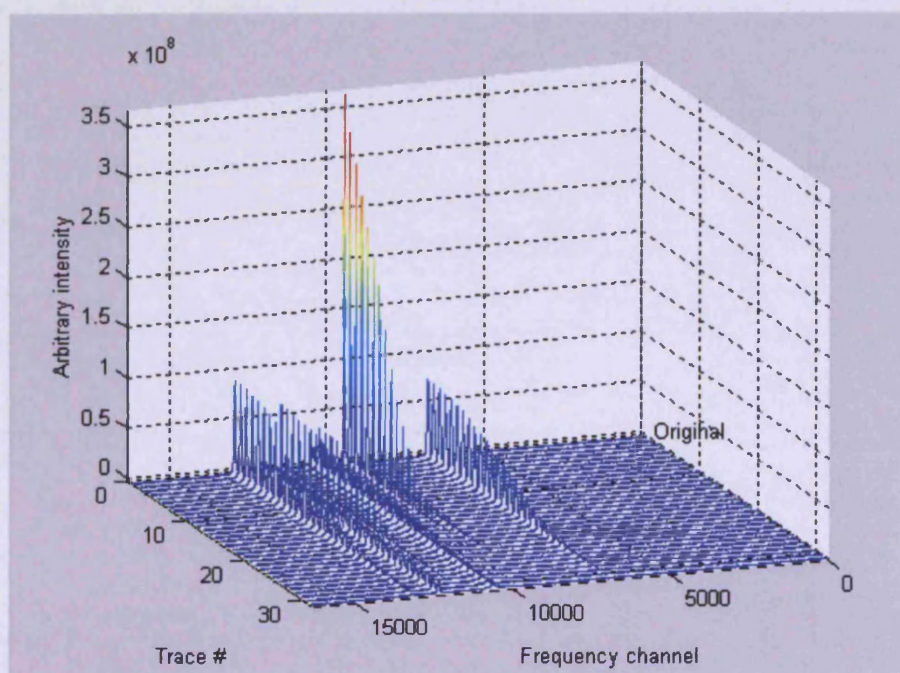
Figure 2.2 *Attenuation decays of peaks belonging to various species in a multi-component system.*

The well-established procedure for extracting the self-diffusion coefficient, D_s, quantifying the Brownian motion of a specie in a complex NMR dataset is to isolate a peak assignable in an unambiguous manner to one of the components, extract the peak height or integral and fit the signal decay to Equation 2.9:

$$A(\delta, g, \Delta) = A_0 \left[\exp - (kD_s)^{\beta} \right] \qquad \textbf{Eq. 2.9}$$

where A is the peak amplitude in the absence (A_o) or presence of the field gradient pulses of duration δ, ramp time σ, intensity G and diffusion time Δ; β characterize the polydispersity of that component: it may assume values between 0 and 1, the latter of which is related to the monodipserse case.

Being γ the gyromagnetic ratio of the nucleus probed, k is given by Eq. 2.10:

$$k = -\gamma^2 G^2 \left(\frac{30\Delta(\delta+\sigma)^2 - (10\delta^3 + 30\sigma\delta^2 + 35\sigma^2\delta + 14\delta^3)}{30} \right)$$ **Eq. 2.10**

The self-diffusion coefficients are obtained from Eq. 2.9. By plotting the attenuation functions versus k, it is possible to determine the self-diffusion coefficient, D_s.

In the case of a biexponential decay (*i.e.*, when there are two different species diffusing in the same sample), the Eq. 2.11 becomes:

$$A(\delta, g, \Delta) = A_0 \left[\exp-(kD_{s1})^{\beta_1} + \exp(-kD_{s2})^{\beta_2} \right]$$ **Eq. 2.11**

where D_{s1} and D_{s2} are the self-diffusion coefficients of the two molecules in the sample, with one usually diffusing faster than the other; β_1 and β_2 characterize the polydispersity of the two components.

Attenuation functions of polymers in solution displaying a monodisperse, biexponential and polydisperse behaviour are illustrated in Figure 2.3.

(a) (b) (c)
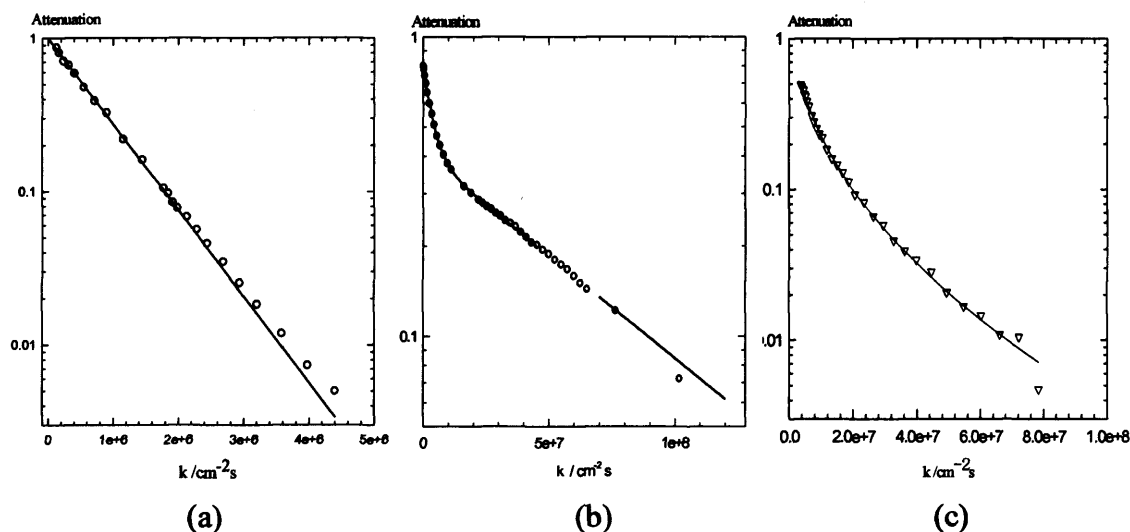
Figure 2.3 Attenuation functions arising from the integral of a simple polymer in solution and in a polymer blend showing (a) monodisperse, (b) bi-exponential and (c) polydisperse behaviour.

41

2.1.5. Protocols for quantifying self-diffusion coefficients

The method to calculate the self-diffusion coefficient just discussed involves measuring the integral of a characteristic peak arising from the molecule of interest and fitting the exponential attenuation of this signal. However, there are various analysis protocols for quantifying the self-diffusion coefficient. More elaborate protocols also exist where *a priori* information is used to further refine the analysis by constraining input parameters to known spectra or to the known number of diffusion coefficients.

A protocol commonly employed is the DOSY (Diffusion Ordered SpectroscopY) NMR approach. This method is normally based on routines developed by Provencher *et al.* [7] (*i.e.*, CONTIN). After some interpolation and smoothing, the combined results are displayed in a two-dimensional (2D) representation of the diffusion coefficients versus spectral characteristics [8].

This is a particularly powerful approach if one is interested in editing or resolving spectra based on diffusion rates since discriminates between chemical compounds both on the basis of their chemical shifts and diffusion coefficients. However, one of the limits of this method is the smoothing feature broadens all of the peaks and even the monodisperse components show significant linewidths.

Another approach, which is found of particular use in studies on complex systems, is called CORE-NMR (Component Resolved NMR spectroscopy). Complex systems in these aspects are systems in which, for example, the signal from different compounds are overlapping and/or the echo decays are multiexponential (*i.e.*, studies on aggregation and/or binding in polymer solutions).

In CORE-NMR applications, usually the number of components in the sample are known beforehand and also if one or more component are likely to show polydispersity behaviour. CORE permits the selection of significant frequency channels and to mask out unwanted regions. CORE

evaluates the experimental data in two dimensions by a global least-squares fit, yielding estimations of the diffusion coefficients for each species in the sample. The output data include the fitted parameters of the optimized model, the global fit and the global difference map.

CORE processing is well applied in data evaluation of PGSE-NMR data sets for very complex systems. It is used to solve or improve estimation problems originating from poor signal/noise or overlapping bandshapes [9].

2.2. Small-angle neutron scattering (SANS)

2.2.1. Introduction

When investigating relationships between physical properties and molecular structure, the determination of molecular organization within colloidal systems is fundamental. Small-angle neutron scattering is a powerful technique providing useful information on molecular size, shape and structure of colloidal systems. SANS belongs to a wider range of small-angle scattering techniques, which also includes small-angle light scattering (SALS), small-angle X-ray scattering (SAXS), etc. All these techniques are based on the interaction occurring between the incident radiations (neutrons, light, X-rays) and the particles present in the system under investigation.

One of the differences in the three small-angle scattering methods is the nature of the radiation, which has a fundamental impact on the actual length scale that can be probed as well as the kind of system that can be analysed. Typical colloidal systems (*i.e.*, micelles, microemulsions, microgels) lay in a size range of 10-10,000 Å; comparable wavelengths, λ, are needed to probe these systems and obtain information about the size, the shape and interactions between the different components present [10].

Light and X-rays are both electromagnetic radiation and interact with the electron cloud surrounding the atomic nuclei. SALS, with a wavelength range of 4000-8000 Å, is mostly used for the characterization of larger colloidal particles even though it cannot be used for optically opaque samples. Smaller systems with a size order of 100 Å can be probed by SAXS (λ = 0.5-2.3 Å) although the high energy of the X-ray photons can damage more sensitive and delicate samples such as biological ones.

Neutron radiation wavelengths, typically comprising between 0.1-30 Å, can be used to investigate sizes in the range of 10-1000 Å. As the energy of a neutron is lower than that of the X-ray photon for a comparable wavelength, neutrons provide a non-invasive and non-destructive method

to study colloidal systems. Moreover, neutrons are scattered by the nuclei of the atoms and not by the electron cloud, which has important implications on the way neutrons/X-rays interact with the nuclei of various atoms (Figure 2.4). Therefore, SANS can discriminate different isotopes of a given element, the most used example being the Hydrogen – Deuterium contrast, allowing an experimental approach called 'contrast variation' (for further details see the Appendix B).
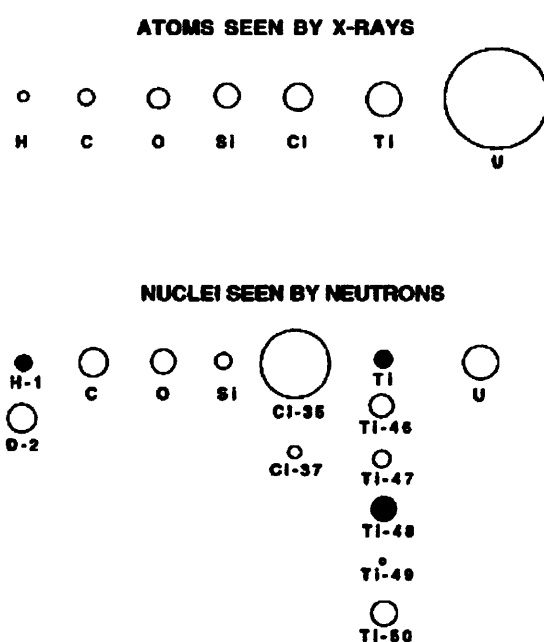
Figure 2.4 Schematic diagram of the neutron interaction with atoms of various elements (nuclei dependant) compared to the X-rays interaction (electron cloud dependant). Negative neutron scattering length are represented in dark. Taken from Hammouda B. [11].

2.2.2. SANS instrument

In a SANS experiment, the neutron beam is scattered by the sample and the intensity, I(Q), of the scattered beam at the angle θ is measured. Figure 2.5 shows a schematic view of the scattering geometry, where the detector is placed at a distance L from the sample and the scattered beam is

measured at a radial distance R_d. A more extended explanation on neutron production and scattering theory can be found in the Appendix B.
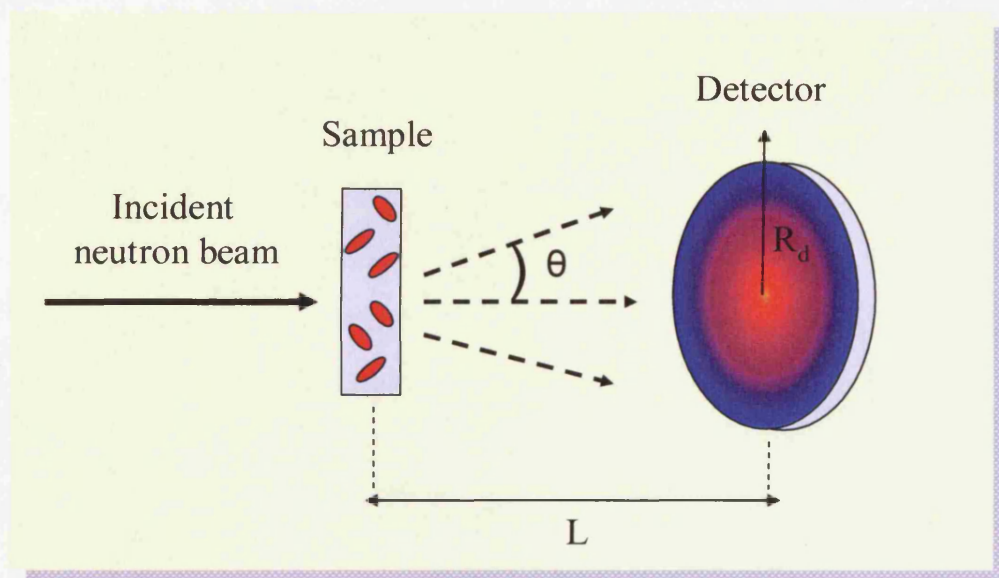
Figure 2.5 *Schematic representation of the SANS experiment. Usually, 1m<L<20m and θ<10°.*

2.2.2.1. The scattering intensity

Scattering data are usually presented as plots of the intensity of the scattered neutron beam, I(Q), versus the scattering vector, Q. The scattering vector Q is proportional to the scattering angle, θ, and is the modulus of the resultant between the incident and the scattered wavevectors. The geometrical relationship for the determination of the scattering vector Q is given in details in the Appendix B.

In a SANS experiment, the collimated neutron beam illuminates a small volume of the sample, typically < 0.5 cm^3. Some of the incident radiation can be scattered, some can be transmitted and some can be adsorbed. The

detector then records the flux of radiation scattered into a solid angle element, which can be expressed as the following:

$$I(\lambda,\theta) = I_0(\lambda)\Delta\Omega\eta(\lambda)T(\lambda)V_s \frac{d\Sigma}{d\Omega}(Q) \qquad \textbf{Eq. 2.12}$$

being $I_0(\lambda)$ the incident flux, $\Delta\Omega$ the solid angle element, η the detector efficiency, $T(\lambda)$ the sample transmission, V_s the illuminated sample volume and $\frac{d\Sigma}{d\Omega}(Q)$ the differential scattering cross-section which contains information on the size, shape and interactions of the scatter bodies [12].

The differential scattering cross-section $\frac{d\Sigma}{d\Omega}(Q)$, also indicated as $I(Q)$ (scattering intensity), provides structural information of the sample, is measured and can be expressed as follows:

$$\frac{d\Sigma}{d\Omega}(Q) = I(Q) = N_p V_p^2 (\Delta\rho)^2 P(Q)S(Q) + B_{inc} \qquad \textbf{Eq. 2.13}$$

where N_p is the number of scattering bodies, V_p the volume of the scattering body, $(\Delta\rho)^2$ the contrast term, $P(Q)$ the form factor, $S(Q)$ the structure factor and B_{inc} the incoherent background.

Eq. 2.14 shows that the contrast term can be described as the squared difference in scattering length densities between the particle, ρ_p, and the solvent, ρ_s:

$$(\Delta\rho)^2 = (\rho_p - \rho_s)^2 \qquad \textbf{Eq. 2.14}$$

The scattering length density ρ of a molecule of i atoms can be calculated as follows:

$$\rho = \sum_i b_i \frac{\rho_{bulk} N_A}{M_w} \qquad \textbf{Eq. 2.15}$$

where b_i is the coherent neutron scattering length of the nucleus, ρ_{bulk} the bulk density of the scattering body, N_A Avogadro's number and M_w the molecular weight.

The scattering length of an atom can be described as the strength of the interaction of free neutrons with the nucleus; its value can vary randomly through the periodic table and it is isotope dependent. This is used to differentiate the scattering of the hydrogen (b_H) from the scattering of the deuterium (b_D) since their scattering lengths are widely different ($b_H = -3.739 \times 10^{-15}$ m and $b_D = 6.671 \times 10^{-15}$ m; the negative sign in front of b_H means that the scattered neutrons wavefunction is out of phase with respect to the incident neutrons wavefunction).

2.2.3. Form and structure factor

The Eq. 2.22 describing the scattering intensity I(Q) contains two important factors: (i) the form factor, P(Q), and (ii) the structure factor, S(Q). Both of them are mathematical functions giving information to a intra- and inter-molecular level respectively.

The form factor is a function that describes how the angular dependence of the scattering, $\dfrac{d\Sigma}{d\Omega}(Q)$, is modulated by interference effects between radiation scattered by different parts of the same scattering body. Therefore, P(Q) is very dependent on the shape of the scattering body.

The structure factor is a function that explains how the angular dependence of the scattering, $\dfrac{d\Sigma}{d\Omega}(Q)$, is modulated by interference effects between radiation scattered by different scattering bodies. Therefore, S(Q) is dependent on the degree of local order in the sample.

2.2.3.1. Form factor

The form factor P(Q) provides information on the size and shape of the scattered bodies on an intra-molecular level. P(Q) functions are known for the most common molecular shapes such as sphere, disc, rod. Table 2.1 includes some of the P(Q) analytical expressions for a solid spherical particle of radius R [13], a disc shape particle of radius R and small thickness, and a rod shape particle of length L and small cross-section [12].

Shape	Form factor P(Q)
Sphere, radius R	$P(Q) = \left[\dfrac{3(\sin(QR) - QR\cos(QR))}{(QR)^3}\right]^2$
Disc, radius R, small thickness (J_1: a first order Bessel function)	$P(Q) = \dfrac{2}{(QR)^2}\left[1 - \dfrac{J_1(2QR)}{QR}\right]$
Rod, length L, small cross-section S_i: the Sine integral function)	$P(Q) = \dfrac{2S_i(QL)}{QL} - \dfrac{\sin^2(QL/2)}{QL/2}$

Table 2.1 *P(Q) mathematical functions for sphere, disc and rod shapes.*

2.2.3.2. Structure factor

The structure factor S(Q) depends on the inter-particle interactions in the system, which can be of attractive, repulsive or excluded volume. The inter-particle structure factor is expressed as:

$$S(Q) = 1 + \frac{4\pi N_p}{QV}\int_0^\infty [g(r) - 1]r\,\sin(Qr)dr \qquad \textbf{Eq. 2.16}$$

where r is the radial distance from the centre of any scattering body in the sample. Therefore, scattering can be used to achieve information about the location of the scattering centres, usually through the 'radial distribution function' (r.d.f.):

$$r.d.f. = \frac{4\pi N_p r^2}{V}g(r) \qquad \textbf{Eq. 2.17}$$

where the density distribution $g(r)$ is obtained from Eq. 2.25 by Fourier inversion.

An effective way of reducing S(Q) for interacting systems is by diluting the sample (in the case of concentrated dispersions) or by adding salt (in the case of charged particles). However, for diluted non-interacting systems $N_p \rightarrow 0$, so, from Eq. 2.25, $S(Q) \rightarrow 1$ [12].

2.2.4. SANS approximations

After having recorded the scattering pattern I(Q) versus Q for a given sample, a first information of the size and shape of the scattering particles can be estimated from linear plots of the functions of the scattered intensity, I(Q), plotted against functions of the scattering variable, Q. This can also serve as a starting point for the data fitting using more refined and complex models.

These approximations are known as the Guiner, Porod and Zimm approximations. A description of the Zimm approximation is given since this is the SANS approximation used in the scattering data analysis discussed in Chapter 4. The Guiner and Porod approximations are described in details in the Appendix B.

Zimm approximation

The Zimm approximation applies to low Q range values and finds wide use in polymer solutions. The Zimm approximation relates the scattering intensity I(Q) to the correlation length ξ.

Assume a Lorentzian form for the Q-dependance of the scattering intensity:

$$I(Q) = \frac{I_0}{1 + Q^2 \xi^2}$$

Eq. 2.18

A plot of $1/I(Q)$ versus Q^2 yields $1/I_0$ as intercept and ξ^2/I_0 as slope. The correlation length is obtained as $\xi = \sqrt{\dfrac{slope}{intercept}}$.

In the low-Q region, Eq. 2.18 can also be expressed as follow:

$$I(Q) = \frac{I_0}{1 + \dfrac{Q^2 R_g^2}{3}}$$

Eq. 2.19

Therefore, $R_g = \xi \sqrt{3}$ for the low-Q region.

The Zimm plot can be applied also beyond the low-Q region. In the high Q regime where $Q^2\xi^2$ is smaller than 1, Eq. 2.18 can be written as follows:

$$I(Q) = \frac{I_0}{Q^2\xi^2} \qquad\qquad \textbf{Eq. 2.20}$$

In this region, the form factor for a single polymer chain behaves as $2/Q^2R_g^2$, so that $\xi = R_g / \sqrt{2}$. Therefore, $R_g = \xi\sqrt{2}$ for high-Q.

In the case of polymer solutions with excluded volume interactions, Eq. 2.20 becomes:

$$I(Q) = I_0 \frac{2}{\left(QR_g\right)^{1/\upsilon}} \qquad\qquad \textbf{Eq. 2.21}$$

where υ is the excluded volume exponent ($\upsilon = 3/5$ for fully swollen chains, $\upsilon = 1/2$ for theta chains and $\upsilon = 1/3$ for collapsed chains) [14].

2.2.5. SANS data analysis

Once the scattering profile is obtained as a plot of the intensity of the scattered neutron beam, I(Q), versus the scattering vector, Q, a model-fitting approach using programs like *Fish* is commonly used to analyse the scattering data. *Fish* is a powerful program developed by Richard Heenan [15] and it is able to fit the scattering data to a specific model: an iterative least-squared algorithm determines the best structural parameters and residuals for the specific scattering data set chosen within the specific model used. Obviously, depending on the specific conformation of the scattering bodies, different fitting models can be applied to each data set.

When fitting a scattering data set to a specific model with *Fish*, the following steps need to be followed: (i) *Fish* will first read in the data set to be fitted; (ii) then, *Fish* will load all the model files among which the specific model of interest can be selected; (iii) each fitting model will have specific parameters which will fit specific sizes in the model (*e.g.*: the sphere radius, the length of the rod, the thickness of the shell); (iv) by

setting appropriately the values of the parameters, by constrain some of the values and by allowing a continue cycle through the fitting routine, a good fit to the data can be obtained.

The model used to fit the scattering data from mucin solutions (as it will be extensively discussed in Chapter 4) is a quite complex model which includes several parameters taking into account contributions for: (i) radius (R) of polydisperse solid spherical particles; (i) volume fraction (ϕ) of the dispersed spheres; (iii) radius of gyration (R_g) for Gaussian coil; (iv) correlation length (ξ) as gel-network term. The radius of gyration, R_g, and the correlation length, ξ, were obtained from the Zimm plots for each data set as explained in the section above. The values of these parameters were inputted in the fitting model and constrained. The radius of polydisperse solid spherical particles, R, the volume fraction of the dispersed spheres, ϕ, were obtained as fitted parameters of the model using Fish program. Fitted parameters showed no change in the fit up to a $\pm$ 5% change in the value of the parameters. Therefore, 5% was considered the sensitivity of the parameters to the overall fit.

2.3. Viscosimetry

Viscosity is an internal property of a fluid and is described as a fluid's resistance to flow. Therefore, viscosity measurements consider the resistance of a fluid deformed by shear stress. All real fluids show some resistance to stress; a fluid which does not exhibit resistance to shear stress is known as an ideal fluid.

Generally, when a shear stress is applied to a fluid, layers will flow at different velocities and the viscosity will be determined by the shear stress between the layers that opposes any applied force. Thus, for a parallel and uniform flow, the shear stress, τ, between layers is proportional to the velocity gradient, $\dfrac{\partial u}{\partial y}$, in the direction perpendicular to the layers, as shown in the following equation :

$$\tau = \eta \frac{\partial u}{\partial y} \qquad\qquad \textbf{Eq. 2.22}$$

where η is a constant known as the coefficient of viscosity or viscosity.

There are several ways for characterizing the solution viscosity. Considering η_o the viscosity of the pure solvent, η the viscosity of a solution using that solvent and c the solution concentration, the solution viscosity can be expressed as the following:

(i) Relative viscosity $\eta_r = \dfrac{\eta}{\eta_0}$

(ii) Specific viscosity $\eta_{sp} = \dfrac{\eta - \eta_0}{\eta_0} = \eta_r - 1$

(iii) Inherent viscosity $\eta_i = \dfrac{\ln \eta_r}{c}$

(iv) Intrinsic viscosity $[\eta] = \lim\limits_{c \to 0} \dfrac{\eta_{sp}}{c}$

Relative viscosity is self-explanatory. Specific viscosity expresses the incremental viscosity due to the presence of a solute (*i.e.*, polymer) in

solution. Normalizing η_{sp} to concentration gives $\dfrac{\eta_{sp}}{c}$ which expresses the

capacity of a solute to cause the solution viscosity to increase. Since $\dfrac{\eta_{sp}}{c}$

will be concentration dependent, it is useful to extrapolate it to zero

concentration. The extrapolated value of $\dfrac{\eta_{sp}}{c}$ at zero concentration is

known as the intrinsic viscosity, $[\eta]$.

Like η_{sp}, $\ln\eta_r$ is zero for pure solvent and increases with increasing

concentration. Thus, $\ln\eta_r$ also expresses the incremental viscosity due to

the presence of the solute in solution. Normalizing $\ln\eta_r$ to the

concentration, $\dfrac{\ln\eta_r}{c}$ gives the inherent viscosity, η_i. In the limit of zero

concentration, η_i extrapolates the same as $\dfrac{\eta_{sp}}{c}$ and becomes equal to the

intrinsic viscosity. This can be demonstrated by:

$$\lim_{c\to0}\frac{\ln\eta_r}{c} = \lim_{c\to0}\frac{\ln(1+\eta_{sp})}{c} = \lim_{c\to0}\frac{\eta_{sp}}{c} = [\eta] \quad \textbf{Eq. 2.23}$$

Therefore, $[\eta]$ can be found by extrapolating $\dfrac{\eta_{sp}}{c}$ or η_i to zero

concentration. When c is not equal to zero the specific viscosity and

inherent viscosity will be different, even for an ideal solution. In ideal

solutions $\dfrac{\eta_{sp}}{c}$ will be independent of concentration, but η_i will depend on

concentration [16].

2.3.1. Viscosity measurement of a fluid

To measure the viscosity of a fluid, a viscometer is usually required.
A standard laboratory viscometer for liquids is a U-tube viscometer. This
device shown in Figure 2.18 is also known as glass capillary viscometer or
Ostwald viscometer. It consists of a U-shaped glass tube placed in a

controlled temperature bath. The glass capillary is located in one arm of the U-tube. On top of the capillary there is a bulb and another bulb can be found lower down on the other arm. The lower bulb in the viscometer is filled in with the test solution up to the mark level (mark C in Figure 2.18). The solution is then transferred to the upper bulb by suction and allow to flow down through the capillary into the lower bulb. The time required by the solution to move between the two marks in the upper bulb (marks A and B in Figure 2.18) is then recorded. It is best to chose a viscometer such that the flow time is greater than 100 seconds so to ignore any kinetic energy term.

Viscometers are usually supplied with a conversion factor or they can be calibrated by a fluid of known properties. The relative and specific viscosity of the solution is then calculated by comparing the flow time of the solution, t, to the flow time of the pure solvent, t_0:

$$\eta_r = \frac{t}{t_0} \quad \text{and} \quad \eta_{sp} = \frac{t - t_0}{t_0} \qquad \textbf{Eq. 2.24}$$
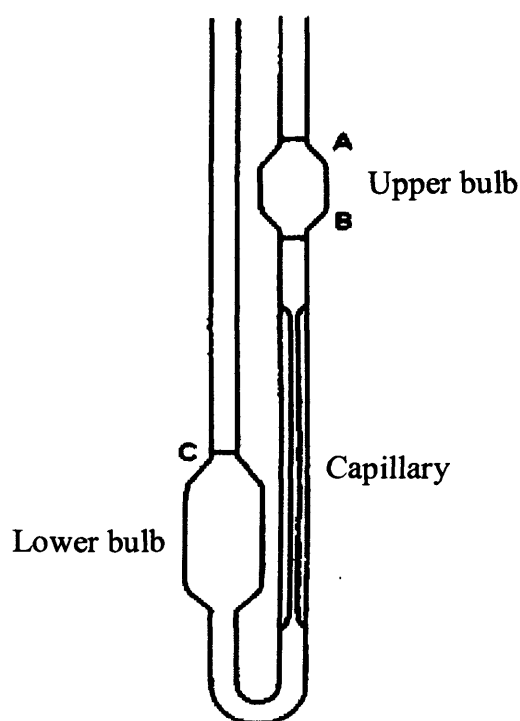

Figure 2.18 Illustration of a standard laboratory U-tube viscometer.

References

1. Price, W. S., Pulsed-field gradient nuclear magnetic resonance as a tool for studying translational diffusion: Part 1. Basic theory. *Concepts in Magnetic Resonance* **1997**, 9, 299-336.

2. Parker, K. J., Diffusion and flow in fluids. In *Encyclopedia of Nuclear Magnetic Resonance*, Grant, D. M.; Harris, R. K., Eds. Wiley: Chichester, 1996.

3. Stilbs, P., Fourier transform pulsed-gradient spin echo studies of molecular diffusion. *Progress in Nuclear Magnetic Resonance Spectroscopy* **1987**, 19, 1-45.

4. Weingartner, H.; Holz, M., NMR studies of self-diffusion in liquids. *Annual Reports on the Progress of Chemistry Section C* **2002**, 98, 121-155.

5. Price, W. S., Applications of pulsed gradient spin-echo NMR diffusion measurements to solution dynamics and organization. *Diffusion Fundamentals* **2005**, 2, 112.1-112.19.

6. Cussler, E. L., *Diffusion: mass transfer in fluid system*. Cambridge University Press: 1997.

7. Provencher, S. W., CONTIN: a general purpose constrained regularization program for inverting noisy linear algebrical and integral equations. *Computer Physics Communications* **1982**, 27, 229-242.

8. Johnson, C. S., Diffusion ordered nuclear magnetic resonance spectroscopy: principles and applications. *Progress in Nuclear Magnetic Resonance Spectroscopy* **1999**, 34, 203-256.

9. Stilbs, P.; Paulsen, K.; Griffiths, P. C., Global least-squares analysis of large, correlated spectral data sets: application to component-resolved FT-PGSE NMR spectroscopy. *Journal of Physical Chemistry* **1996**, 100, 8180-8189.

10. Eastoe, J., *Surfactant Chemistry*. (Book arising from a series of advanced lectures given in October 2002 at the China Research Institute for Daily Chemical Industry (RIDCI) TaiYuan), 2003.

11. Hammouda, B., A tutorial on small-angle neutron scattering from polymers. In 1995.

12. King, S. M., Small angle neutron scattering. In *Techniques for Polymer Characterisation*, Pethrick; Dawkins, Eds. Wiley: 1999.

13. Castelletto, V.; Hamley, I. M., Modelling small-angle scattering data from micelles. *Current Opinion in Colloid & Interface Science* **2002,** 7, 167-172.

14. Hammouda, B., *Probing nanoscales structures - The SANS toolbox.* 2008.

15. Hennan, R. K. *FISH Data analysis program*; Rutherford Appleton Laboratory Report RAL-89-129: 1989.

16. Atkins, P. W., *Physical Chemistry*. Oxford University Press: 1994.

Chapter 3.   Materials and methods

All materials used and experimental approaches applied in the studies presented in this thesis have been collected in Chapter 3 herein. Some materials are common to all the studies; some others have been used only in specific studies and the related chapters are specified.

3.1.   Materials

3.1.1.   Mucin

Dried porcine gastric mucin (PGM) type III used in all experiments was purchased from Sigma Aldrich (UK) and used without any further treatment.

3.1.2.   Chemicals

<u>Solvents</u>

Samples for viscosity measurements have been prepared in Millipore water.

Samples for SANS and PGSE-NMR experiments have been made up in deuterium oxide (D_2O) purchased from Fluochem Ltd., UK.

Dimethyl sulfoxide (DMSO) anhydrous, $\geq$ 99.9%, was purchased from Sigma Aldrich (UK) and used for the synthesis of the PEG-PAMAM dendrimer conjugates.

<u>Bases and acids</u>

Sodium deuteroxide (NaOD) solution 40 wt% in D_2O, 99 atom % D (Sigma Aldrich, UK) and deuterium chloride solution (DCl) 35 wt% in D_2O, 99 atom % D (Sigma Aldrich, UK) were used for changing the pH in mucin samples in SANS and PGSE-NMR experiments.

Sodium hydroxide (NaOH) beads (Sigma Aldrich,UK) and hydrochloric acid (HCl) 37% (Sigma Aldrich ,UK) were used for changing the pH in mucin samples in viscosity measurements.

<u>Mucolytic agent</u> (Chapter 4)

N-Acetyl-L-Cysteine (NAC), $\geq$ 99% was purchased from Sigma Aldrich (UK) and used without any further treatment.

<u>Polymers</u> (Chapter 5 and 6)

A series of water-soluble polymers – termed 'probe' polymer – were examined and their characteristics are presented in Table 3.1. Polymers were used as received.

Linear poly(ethylene glycol) (PEG) and branched polyethylenimine (PEI) with different molecular weights were studied in this work.

Polyamidoamine (PAMAM) dendrimers with a tetra-functional ethylenediamine core have been investigated. PAMAM dendrimers generation 2.0 and 4.0 contain 16 and 64 surface amino groups, respectively. PAMAM dendrimers generation 3.5 and 5.5 contain 64 and 256 surface carboxylate groups, respectively.

Polymer	Molecular weight / g mol^{-1}	Source
[Linear] Poly(ethylene glycol) (*l*-PEG10K)	10,000	Sigma-Aldrich (UK)
[Linear] Poly(ethylene glycol) – deuterated (*l-(d)*PEG10K)	10,000	Polymer Laboratories (UK)
4-arms-Poly(ethylene glycol) (*b*-PEG20K)	20,000	Nektar (US)
[Linear] Poly(ethylene glycol) (*l*-PEG50K)	50,000	Polymer Laboratories (UK)
Dextrin (Dextrin50K)	50,000	ML laboratories (UK)
[Linear] Poly(ethylene oxide) (*l*-PEG100K)	100,000	Sigma-Aldrich (UK)
[Branched] Polyethylenimine (*b*-PEI2K)	2,000	Sigma-Aldrich (UK)
[Branched] Polyethylenimine (*b*-PEI25K)	25,000	Sigma Aldrich (UK)
Polyamidoamine dendrimer G2.0 (PAMAM G2.0)	3,260	Dendritech Inc. (US)
Polyamidoamine dendrimer G4.0 (PAMAM G4.0)	14,210	Dendritech Inc. (US)
Polyamidoamine dendrimer G3.5 (PAMAM G3.5)	12,930	Dendritech Inc. (US)
Polyamidoamine dendrimer G5.5 (PAMAM G5.5)	52,900	Dendritech Inc. (US)

Table 3.1 Molecular characteristics of the polymers used in this thesis.

PEGylation reagent (Chapter 6)

Methyl-PEG$_{12}$-*N*-Hydroxysuccinimide (NHS) Ester was purchased from Thermo Scientific (USA) and used for the synthesis of the PEG-PAMAM dendrimer conjugates.

Lipids and albumine (Chapter 7)

The lipids 1,2-dihexanoyl-*sn*-glycero-3-phosphocoline (DHPC) and 1,2-dipalmitoyl-*sn*-glycero-3-phosphocholine (DPPC) were obtained from Avanti Polar Lipids (US). Both phosphocholines were purchased in the hydrogenated (h) and deuterated (d) form. Their chemical structures are illustrated in Figure 3.1. The critical micelle concentrations (c. m. c.) of the two phospholipids are 0.46 nM for the DPPC and 1.4 mM for the DHPC, respectively.

Bovine serum albumine (BSA) was obtained from Sigma Aldrich (UK).
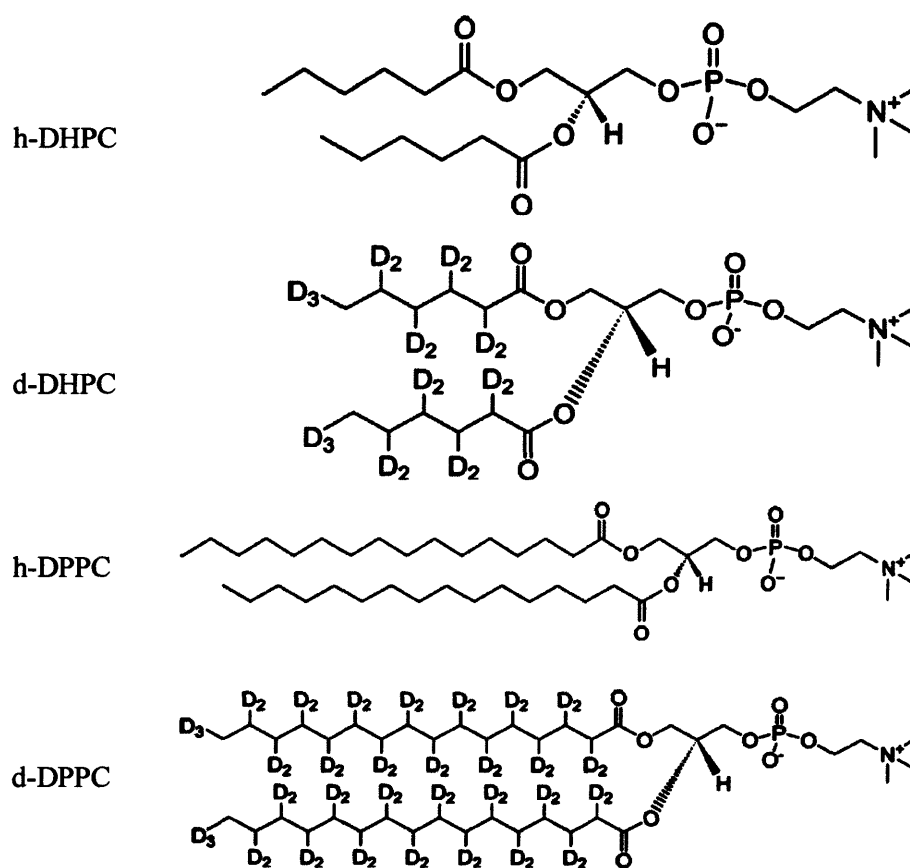
Figure 3.1 *Chemical structures of the hydrogenated (h), and deuterated (d) DHPC and DPPC.*

3.2. Methods

3.2.1. Samples preparation

Preparation of mucin solutions

Solutions with different mucin concentrations (1 wt% ≤ [mucin] ≤ 5 wt%) were prepared by simply dissolving the required mass of mucin in D_2O (99.5 atom % D) or H_2O. Samples were left for at least 2h but typically overnight at room temperature to allow full dissolution and equilibration. The solutions were not filtered.

Preparation of the mucin samples with the mucolytic agent (Chapter 4)

Mucin solution 5 wt% in the presence of 0.5% NAC were prepared in the following way. A stock solution of 5% NAC was made up in distilled water. 250 mg of mucin were dissolved in 4.5 ml of distilled water. Once mucin was dissolved in water, 0.5 ml of the NAC 5% stock solution were added. In this way a 5 ml mucin solution 5 wt% in the presence of NAC 0.5% was obtained. Since the mucolytic agent performs better at pH 7.0-9.0, the pH of the sample was then adjusted within a pH range of 7.0-9.0 adding sodium hydroxide. The mucin sample in the presence of NAC at pH 7.0-9.0 exhibited a light purple color. This is due to the fact that the commercial NAC contains a chelating agent, ethylendiaminetetra-acetic acid (EDTA). The light purple color indicates metal ion removal [1].

Preparation of mucin- polymer solutions (Chapter 5 and 6)

Solutions with different mucin concentrations (1 wt% ≤ [mucin] ≤ 5 wt%) and a constant 'probe' polymer concentration (0.5 wt%) were prepared by simply dissolving the required masses of polymer in D_2O (99.5 atom % D) or H_2O. Samples were left for at least 2h but typically overnight at room temperature to allow full dissolution and equilibration. The solutions were not filtered.

<u>Preparation of mucin-lipid/protein solutions</u> (Chapter 7)

Solutions containing a constant concentration of DHPC (5 mM), and/or BSA (500 ppm and 5000 ppm) in mucin (1 wt% ≤ [mucin] ≤ 5 wt%) were prepared by simply dissolving the required masses of polymer in D_2O (99.5 atom % D). Solutions containing a constant concentration of DPPC (5 mM) in mucin (1 wt% ≤ [mucin] ≤ 5 wt%) were made up by adding the dried amount of mucin in the DPPC vesicles solution already done. Samples were left for at least 2h but typically overnight at room temperature to allow full dissolution and equilibration. The solutions were not filtered.

3.2.2. Synthesis of the PEG-PAMAM dendrimers (Chapter 6)

PEG-PAMAM dendrimers G2.0 and G4.0 conjugates with different degrees of PEGylation – 10%, 50% and 100% PEGylated – were synthesized *via* the procedure shown in Scheme 3.1. Methyl-PEG$_{12}$-*N*-Hydroxysuccinimide (NHS) Ester was used as activated PEG for the modification of the PAMAM dendrimer surfaces.

N-Hydroxysuccinimide (NHS) Ester is one of the most popular type of reactive groups used for protein modification or any macromolecule bearing primary amino groups (–NH$_2$). NHS-ester reagents react efficiently at pH 7-9 with primary amino groups by nucleofilic attack, forming stable amide bonds and releasing the NHS, as shown in Scheme 3.1.

To a solution of a second (G2.0, Mw = 3,260 g mol^{-1}) or fourth (G4.0, Mw = 14,210 g mol^{-1}) generation PAMAM dendrimer (2 mg ml^{-1}) in dimethyl sulfoxide anhydrous (DMSO), methyl-PEG$_{12}$-*N*-Hydroxysuccinimide (NHS) Ester (Mw = 685.71 g mol^{-1}) was added and the solution stirred for two hours at room temperature under nitrogen. Obviously, the amount of NHS-PEGylation reagent added depended on the degree of PEGylation and the generation of the PAMAM dendrimer. For the 100% PEGylated PAMAM dendrimers G2.0 and G4.0, 6.6 mg

(9.6 μmol) and 4.4 mg (6.4 μmol) of NHS-PEGylating reagent were respectively added to a solution of 2 mg ml^{-1} (0.6 μmol ml^{-1}) PAMAM dendrimer G2.0 and 2 mg ml^{-1} (0.1 μmol ml^{-1}) PAMAM dendrimer G4.0. The following amount of methyl-PEG$_{12}$-NHS ester were used for a 10% PEGylation of PAMAM dendrimer G2.0 and G4.0: 0.62 mg (0.9 μmol) for a 2 mg ml^{-1} PAMAM dendrimer G2.0; 0.41 mg (0.5 μmol)for a 2 mg ml^{-1} PAMAM dendrimer G4.0. For a 50% PEGylation of PAMAM dendrimer G2.0 and G4.0, the quantity of methyl-PEG$_{12}$-NHS ester used was: 3.3 mg (4.8 μmol) for a 2 mg ml^{-1} PAMAM dendrimer G2.0; 2.2 (3.1 μmol) mg for a 2 mg ml^{-1} PAMAM dendrimer G4.0.

The products from the syntheses were purified by dialysis against water for 48 hours using a membrane with a different molecular weight cut-off (MWCO), depending on the molecular weights of the synthesized conjugates. Given that the molecular weights of the 100% PEG-PAMAM G2.0 and G4.0 conjugates 12,650 g mol^{-1} and 51,760 g mol^{-1} respectively, dialysis tubes with a MWCO of 12-14000 Daltons (Medicell International Ltd, UK) were used. The same dialysis tubes were used for the 10% and 50% PEG-PAMAM dendrimer G4.0 conjugates, given their molecular weights 17,953 g mol^{-1} and 32,953 g mol^{-1}, respectively. Whereas, for the 10% and 50% PEG-PAMAM dendrimer G2.0 conjugates – bearing molecular weights 4,492 g mol^{-1} and 7,946 g mol^{-1}, respectively – dialysis tubes with a MWCO of 2000 Daltons (Sigma Aldrich, UK) were employed. The dialyzed products were then lyophilized and used for further characterization. Finally, with the aid of a freeze-drier, the water was removed from the products. Yields were ~ 75% for all conjugates synthesized.

The synthesized PEG-PAMAM conjugates were characterized by ^{1}H-NMR spectroscopy using D$_2$O as solvent (the chemical shift of HDO is 4.8 ppm). ^{1}H-NMR spectra were recorded on a Bruker Avance 500 MHz spectrometer. PEGylation was confirmed by the appearance of signals at 3.52-3.67 ppm and 3.28 ppm in ^{1}H NMR spectra of the conjugates, which correspond to the protons of CH$_2$CH$_2$O repeat unit and terminal OCH$_3$

groups of PEG, respectively. The degree of PEGylation (the actual average number of PEG arms per dendrimer) was estimated using the proton integration method, by taking the characteristic peaks of PEG and PAMAM into account [4].

Scheme 3.1 *Schematic mechanism of PEGylation of PAMAM dendrimer. Adapted from Kojima C.* [5].

67

3.2.3. Preparation of the DPPC vesicles (Chapter 7)

h-DPPC and d-DPPC vesicles were prepared in D_2O following exactly the same procedure.

A 5 mM DPPC solution was prepared by dissolving 11 mg of phospholipid in 3 ml of chloroform. The solvent was then completely removed by the rotavap until a film was formed. At this stage, 3 ml of D_2O were added to the film for hydration to deliver a final concentration of 5 mM. The solution was left in a water bath set at 52 °C (~ 10 °C higher than the phospholipid transition temperature) for half an hour, mixing occasionally. After, the solution was first dipped into liquid nitrogen for five minutes, then defrosted in warm water for five minutes and finally vortex for five minutes. This cycle (water bath/liquid nitrogen/vortex) was repeated three times to break multilamellar vesicles (MLV) into unilamellar vesicles (ULV) [2, 3]. At this point the DPPC vesicles are ready to be extruded. The extrusion process was performed above the lipid transition temperature using an extrusion unit (Lipex Biomembranes Inc., Canada) illustrated in Figure 3.2. The DPPC vesicles were produced by extrusion through polycarbonate nucleopore membrane filters (Whatman International Ltd., UK), starting with membranes having a pore size of 400 nm to finish with membranes with a pore size of 100 nm. The opalescent blue-ish solution obtained was kept at + 4 °C.

Nitrogen pipe

Clip-on cap

Lid

Central chamber

Nucleopore membrane filters are placed inside here

Tubes connected to the water bath

Tube for vesicles solution collection

Figure 3.2 *Extruder unit used for extrusion of the DPPC vesicles.*

3.2.4. Samples for SANS

SANS measurements were used to study the conformation of mucin in solution and to detect any change in the mucin conformation due to possible mucin-'probe' polymer interaction.

SANS measurements were performed on the fixed-geometry, time-of-flight LOQ diffractometer at the ISIS spallation neutron source, Rutherford Appleton Laboratories (Didcot, UK). A $Q = (4\pi / \lambda)\sin(\theta / 2)$ range between 0.008 and 0.25 Å^{-1} was obtained by using neutron wavelengths (λ) spanning 2.2 to 10 Å with a fixed sample-detector of 4.1 m. The samples were contained in 2 mm path length, UV-spectrophotometer grade, quartz cuvettes (Hellma Ltd, UK) and mounted in aluminium holders on top of an enclosed, computer-controlled, sample chamber. Sample volumes were around 0.4 cm^3. All experiments were conducted at 37 °C (unless otherwise stated). Temperature control was achieved by using a thermostatic circulating bath pumping fluid through the base of the sample chamber, achieving a temperature stability of ± 0.2 °C. Experimental measuring times were approximately 40 minutes.

All scattering data were (a) normalized for the sample transmission, (b) background corrected using a quartz cell filled with D_2O, and (c) corrected for the linearity and efficiency of the detector response using the instrument specific software package.

3.2.5. Samples for PGSE-NMR

PGSE-NMR was used to investigate the mobility of the 'probe' polymers in mucin solutions by measuring their diffusion coefficients as function of the mucin concentration. For each polymer probed in the mucin media, six samples were prepared in D_2O spanning a mucin concentration 0 wt% $\leq$ [mucin] $\leq$ 5 wt%. The diffusion coefficients of the probe polymers were measured for each solution at 310.3 K.

PGSE-NMR experiments were performed on a Bruker AMX360 spectrometer, operating at 360 MHz (^{1}H) and using a stimulated echo sequence together with current-regulated field gradient drivers and ramped gradient pulses [6]. Three field gradient pre-pulses were applied before every scan. Experiments were performed in a 5 mm diffusion probe at the set temperature of 310.3 K. Temperature stability was maintained by the standard air heating/cooling system of the spectrometer, to an accuracy of $\pm$ 0.3 °C.

^{1}H-NMR signals from mucin result in broad peaks at 3.65 ppm. This caused often an overlap between the wide peaks from mucin and the peaks from the polymer under investigation: therefore, the self-diffusion of the polymer might be affected by the diffusion of the mucin.

For instance, the ^{1}H-NMR spectrum of *l*-PEG in D_2O consists of a singlet at 3.50 ppm. When in mucin solutions, the peak from the PEG results in a broad peak which include buried signals belonging to the mucin.

For this reason two approaches to analyzing the data were employed: where there was a little spectral overlap of the signals from mucin with the peak of interest of the polymer (*e.g.*, PAMAMs in mucin), the diffusion coefficients have been extracted by an analysis of the peak integrals (Figure 3.3); however, where spectral overlap was pronounced (*e.g.*, PEGs

in mucin), a more involved component-resolved (CORE) approach was adopted (Figure 3.4) [7]. Both methods have been already discussed in sections 2.1.6 and 2.1.7 in Chapter 2.

In both approaches, a double exponential fitting was applied for the diffusion of the species in mucin solutions, considering the 'probe' polymer always the specie diffusing faster than mucin (the diffusion of mucin as a thick gel was slow compared to the diffusion time of the other species considered).

In both cases, the self-diffusion coefficient D_s was extracted from an analysis of the peak amplitude according to the Eq. 4.1:

$$A(\delta, g, \Delta) = A_0 \left| \exp{-(kD_s)^\beta} \right| \qquad \textbf{Eq. 4.1}$$

where A is the peak amplitude in the absence (A_o) or presence of the field gradient pulses of duration δ (400 μs $< \delta <$ 2.8 ms), ramp time σ (250 μs), strength G (0.86 T m^{-1}) and diffusion time Δ (140 ms); β is an empirical parameter relating to the polydispersity which was kept to 1; k is given by Eq. 4.2:

$$k = -\gamma^2 G^2 \left(\frac{30\Delta(\delta + \sigma)^2 - \left(10\delta^3 + 30\sigma\delta^2 + 35\sigma^2\delta + 14\delta^3\right)}{30} \right) \qquad \textbf{Eq. 4.2}$$

being γ the gyromagnetic ratio (for protons, γ = 26.7520 e^{-7} T^{-1}s^{-1}).

Samples were prepared in vials and then pipetted to the NMR tubes when liquid. Since the experiments were conducted at the temperature of 310.3 K, a 30 minutes equilibration time was allowed to the sample in the NMR spectrometer before starting the experiment. An experimental error of ± 5% is considered for all data, representing the sample to sample reproducibility achieved.
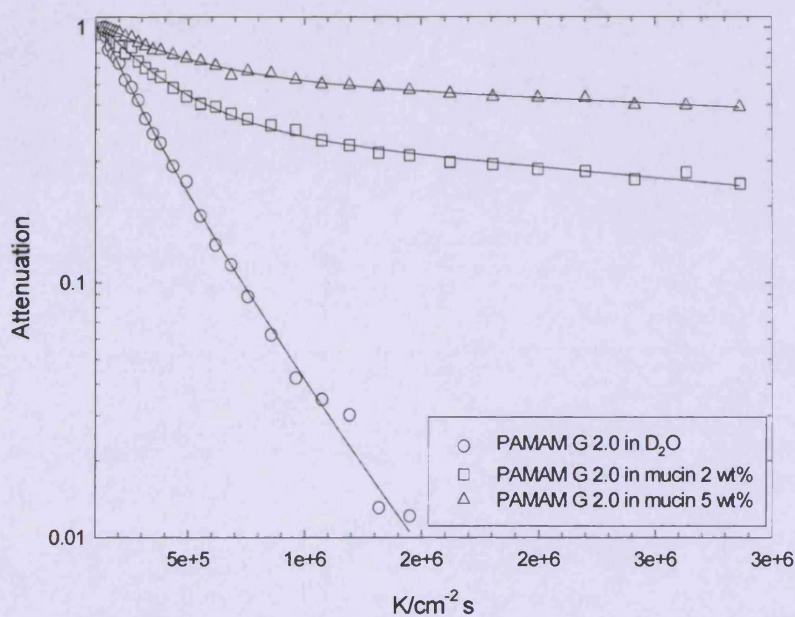
Figure 3.3 *Attenuation functions from the integral of the peak at 2.57 ppm of the PAMAM dendrimer G2.0 in D_2O (open circles), in mucin 2 wt% (open squares) and in mucin 5 wt% (open triangles).*
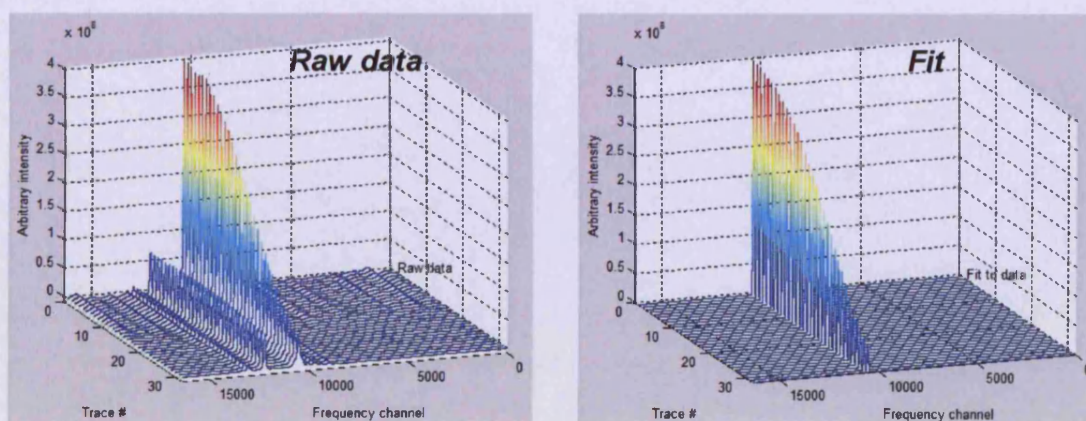

Figure 3.4 *Sequence of FT-PGSE spectra (left panel) and CORE fit to the data set (right panel) for the system of l-PEG 10K g mol^{-1} in mucin 3 wt%.*

3.2.6. Samples for viscosity measurements

Viscosity measurements were performed using U-tube viscometers (also known as glass capillary viscometers or Ostwald viscometers) purchased from Poulten Selfe & Lee Ltd. (England, UK). Different viscometers sizes (B, C, D) were used depending on the viscosity of the solution measured. The sample volume required for each measurement may vary from 15 up to 30 ml, depending on the size of the viscometer. Experiments were performed at 37 °C. Temperature was controlled by using a thermostatic water bath. An experimental error of ± 0.4% was considered for all data according to the viscometers manufacture. Viscosity values were calculated considering viscosity of water at 37 °C equal to 0.696 mPa s.

References

1. Henke, M. O.; Ratjen, F., Mucolytics in cystic fibrosis. *Paediatric Respiratory Reviews* **2007**, 8, 24-29.

2. Hunter, D. G.; Frisken, B. J., Effect of extrusion pressure and lipid properties on the size and polydispersity of lipid vesicles. *Biophisical Journal* **1998,** 74, 2996-3002.

3. MacDonald, R. C.; MacDonald, R. I.; Menco, B. P.; Takeshita, K.; Subbarao, N. K.; Hu, L. R., Small-volume extrusion apparatus for preparation of large, unilamellar vesicles. *Biochimica et Biophysica Acta* **1991,** 1061, (297-303).

4. Luo, D.; Haverstick, K.; Belcheva, N.; Han, E.; Saltzman, W. M., Poly(ethylene glycol)-conjugated PAMAM dendrimer for biocompatible, high-efficiency DNA delivery. *Macromolecules* **2002,** 35, 3456-3462.

5. Kojima, C.; Kono, K.; Maruyama, K.; Takagishi, T., Synthesis od polyamidoamine dendrimers having poly(ethylene glycol) grafts and their ability to encapsulate anticancer drugs. *Bioconjugate Chemistry* **2000,** 11, 910-917.

6. Griffiths, P. C.; Cheung, A. Y. F.; Davies, J. A.; Paul, A.; Tipples, C. N.; Winnington, A. L., Probing interactions within complex colloidal systems using PGSE-NMR. *Magnetic Resonance in Chemistry* **2002,** 40, S40-S50.

7. Stilbs, P.; Paulsen, K.; Griffiths, P. C., Global least-squares analysis of large, correlated spectral data sets: application to component-resolved FT-PGSE NMR spectroscopy. *Journal of Physical Chemistry* **1996,** 100, 8180-8189.

Chapter 4. Study of the conformation of mucin in solution by SANS

This chapter focuses on the behaviour of mucin glycoprotein in solution. An introduction on previous studies performed on the conformation of mucin in solution is provided. In the present study, the conformation of the mucin was investigated by small-angle neutron scattering (SANS). Characterization of the behaviour of mucin in solution upon changing concentration, pH, ionic strength, temperature and in the presence of a mucolytic agent was explored and discussed.

4.1. Introduction

Understanding the molecular structure of mucin is still a challenging question. The conformation of mucin in solution has been difficult to characterize due to the large molecular weight, polydispersity and high degree of glycosylation of the mucin molecule. Furthermore, the chemical heterogeneity, the long-range charge effects and the tendency of the mucin molecules to associate make the overall study more complex.

However, several models have been proposed to describe the solution structure of mucin: (i) aggregates of rod-shaped molecules comprising a central linear polypeptide core of $100,000 < M_w < 250,000$ g mol^{-1} with radial oligosaccharide side chains of 2 to 12 monosaccharide residues, attached to serine and threonine residues by O-glycosidic linkages [1,2]; (ii) a solvated random coil of flexible linear glycoprotein[3,4], that is either stiffened by the glycosylated fragments [5] or their interaction – the so-called "zipper" or bottle-brush model [6,7]; (iii) liquid crystalline structures [3]; and (iv) a double globule comb structure[8]. This complexity is amplified by the tendency of mucin to aggregate at low concentration and low pH [1,9,10].

Despite these models, only a few studies have considered a either neutron or X-ray scattering approach to describe the conformation of mucin in solution [8, 11]. Therefore, the aim of this current work is to quantify the conformation of non-purified porcine gastric mucin (PGM) in solution by small-angle neutron scattering (SANS). As a non-destructive technique, SANS can be easily applied for the study of delicate biological materials such as mucin. Mucin molecules in solution were studied by SANS as function of concentration, pH, ionic strength and temperature. Moreover, studies on mucin conformation in the presence of *N*-Acetyl-L-cysteine as mucolytic agent were performed by SANS to better understand changes in the mucin structure caused by the mucolytic agent.

4.2. Studies of the conformation of mucin in solution

4.2.1. SANS from PGM solutions

The typical scattering from 5 wt% non-purified porcine gastric mucin (PGM) solutions at 37 °C is presented in Figure 4.1. As may be seen, there are a number of features in the data, including pronounced maxima against a slowly decaying background signal. The two main maxima are at Q values (Q_{max}) of 0.031 Å^{-1} and 0.063 Å^{-1}. Considering the relationship between the wavevector Q and a distance/size R (Eq. 4.1):

$$Q = \frac{2\pi}{R}$$

Eq. 4.1

the Q_{max} values correspond to distances/sizes of 20.3 nm and 10.0 nm, respectively. Interestingly, the location (Q value) of the second maxima occurs at twice Q of the first, *i.e.*, $Q_{max}(peak2) = 2Q_{max}(peak1)$, indicating a regular distribution of scatterers. Therefore, these maxima arise due to interference from scattering centres within the solution, implying some level of order.
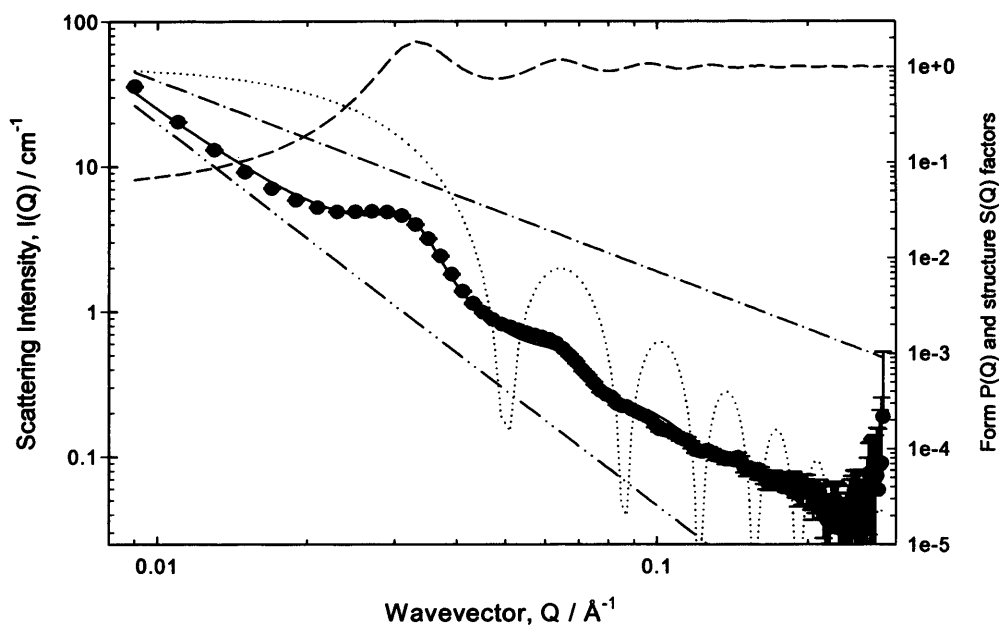
Figure 4.1 *Scattering from mucin 5 wt% (closed circles) at 37 °C, pH 7; fitting to the scattering data (solid line); globule form factor P(Q) (dotted line); globule structure factor S(Q) (dashed line); Q^{-2} (dashed-dotted line); and Q^{-4} (dashed-dotted-dotted line) terms.*

Early SANS studies on mucin were performed by Waigh *et al.* [11]. Although the same type of mucin was used (porcine gastric mucin purchased from Sigma Aldrich), the first important difference observed between the scattering data from mucin solutions presented by Waigh's group and the scattering data here presented is the absence of the two main maxima in the scattering profile from mucin solutions obtained by Waigh. Therefore, Waigh could approximate the scattering from mucin to a homogeneous cylinder and fit the scattering data to a Guiner expression, from which the cross section and the radius of gyration of the cylindrical molecule was obtained. Unfortunately, this model was not able to fit the scattering data from mucin solution presented in Figure 4.1. Subsequently, the same group re-analyzed their SANS data in light of the SAXS study [8] and invoked a dumbbell model in which two globular structures are

connected by a glycosylated spacer with a thickness of a few nanometers: a double Guiner fit was developed for the analysis of the dumbbell structure which suggested two globular structure with dimension of 10-20 nm linked by a glycosylated spacer of 40-50 nm.

The dumbbell model described by Waigh's group on the basis of their SAXS results on mucin contained the essential features which represented a starting point to build up a model able to fit the complex SANS data from mucin here presented (Figure 4.1). Therefore, a more complex form factor approach has been adopted here that embodies the essence of the dumbbell model, in which the scattering from mucin solutions has been analyzed using a model that comprises two main scattering terms:

$$I(Q) = I(Q)_{peptide\ backbone} + I(Q)_{globule} \qquad \textbf{Eq. 4.2}$$

The first term of the Eq. 4.2 is the contribution from the glycosylated peptide backbone whilst the second term accounts for the dispersion of hydrophobic globules connected by the glycosylated peptide backbone. A graphic representation of this model from a polymeric mucin molecule is idealized in Scheme 4.1.
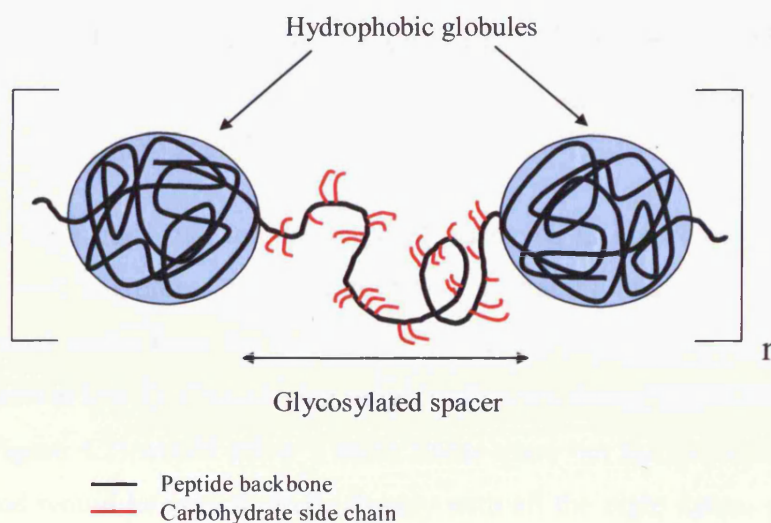
Scheme 4.1 *Solution conformation of a polymeric mucin molecule comprising hydrophobic globules connected by a glycosylated spacer. Adapted from Yakubov G. E. [12].*

The peptide backbone is modeled as

$$I(Q)_{\text{peptide backbone}} = \frac{I_1}{\xi^2 Q^2} + \frac{I_2}{\zeta^4 Q^4}$$
Eq. 4.3

where I_1 and I_2 characterize the contribution to the scattering arising from the peptide backbone with characteristic length scale ξ (where $\xi^2 Q^2 > 1$) and from some larger, ill-defined structure, ζ. Figure 4.1 illustrates the contributions of Q^{-2} (dashed-dotted line) and Q^{-4} (dashed-dotted-dotted line) terms to the fit of the scattering data. As may be seen from Figure 4.1, the Q^{-4} term contributes rather weakly to the overall fit; indeed, the fit is dominated by the Q^{-2} and globule terms.

Considering the Lorentzian form for the Q-dependence of the scattering intensity as expressed in Eq. 2.18 in Chapter 2, an analysis of the low-Q region of the scattering data in a Zimm plot (1/I(Q) versus Q^2) would provide information on the correlation length ξ, which gives a good estimation of the average entanglement length for mucin solutions, and the radius of gyration R_g. Figure 4.2 shows the Zimm plot for mucin 5 wt% at low-Q region. From the analysis of the Zimm plot, the correlation length ξ

is obtained as $\xi = \sqrt{\dfrac{slope}{intercept}}$ while the radius of gyration $R_g = \xi\sqrt{3}$.

The fit resulted in a correlation length ξ of 23.5 nm and a radius of gyration R_g of 41.0 nm. These data are in good agreement with those obtained by Yakubov *et al.* [12].

It could be argued that the datum point displayed in Figure 4.2 are not lined up and, therefore, not easy to fit to a straight line. The slightly curved trend arises from the presence of the main peak in the scattering from mucin at low Q. Considering only the first six datum points (dashed line in Figure 4.2) would allow a more linear trend but the low-Q region considered would be very limited (already with all the eight datum points is limited and that it is due to the main peak in the low-Q region). The correlation lengths (ξ) and radius of gyration values (R_g) − given by

$$\xi = \sqrt{\frac{slope}{intercept}} \text{ and } R_g = \xi\sqrt{3}$$ – considering a six or eight datum points

fit were calculated: the correlation length resulted 21.0 nm and 23.5 nm

for a six and eight datum points fit, respectively; the radius of gyration

was 36.4 nm and 41.0 nm for a six and eight datum points fit, respectively.

The difference in the correlation length and radius of gyration values when

considering a six or eight datum points fit was about 10%. Therefore, 10%

can be considered the sensitivity of these parameters (correlation length
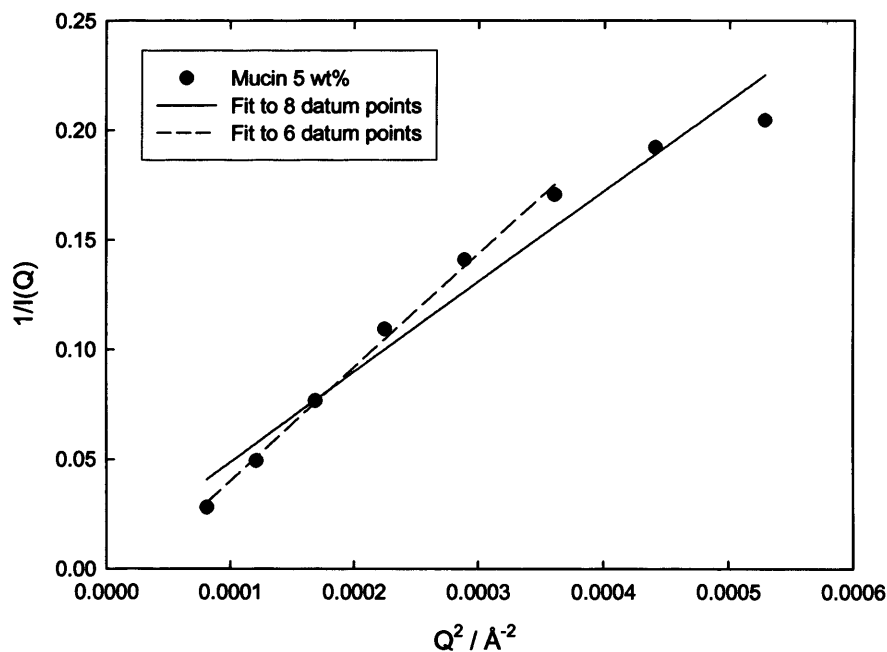
and radius of gyration) to the fit.

Figure 4.2 Zimm plot for mucin 5 wt% (37 °C, pH 7) at low-Q region
(0.009 $Å^{-1}$ < Q < 0.023 $Å^{-1}$), with linear fit to eigth datum points (solid
line) and six datum points (dashed line).

The second term in Eq. 4.2, $I(Q)_{globule}$, is responsible for the scattering

from the locally ordered hydrophobic globules, and it was thought most

appropriate to model this structure as a concentrated dispersion of

uncharged (polydisperse) spheres, given (i) the liquid ordering scaling of

the peak positions with concentration (see Figure 4.3) and (ii) the fact that no change in their scattering profile is observed as result of the increase in the ionic strength (see Figure 4.8), as it will be discussed afterwards. Therefore,

$$I(Q)_{globule} = NV^2 (\rho_m - \rho_s)^2 P(Q)S(Q) \qquad \textbf{Eq. 4.4}$$

where N is the number of scatterers of volume V per unit volume and $(\rho_m - \rho_s)^2$ is their contrast against the solvent (D$_2$O). The form factor *P(Q)* is calculated using a distribution of polydisperse spherical scatterers with

$$P(Q) = \left[\frac{3(\sin(QR) - QR\cos(QR))}{(QR)^3} \right]^2 \qquad \textbf{Eq. 4.5}$$

integrated over a modified Schulz distribution [13]:

$$f(R) = \left[\frac{(z+1)}{\overline{R}} \right]^{z+1} R^z \exp\left[-\left(\frac{z+1}{\overline{R}} R \right) \right] \frac{1}{\Gamma(z+1)} \qquad \textbf{Eq. 4.6}$$

where $\overline{R}$ is the mean sphere radius, z is a parameter related to the width of the distribution.

In particular, one has a polydispersity index ρ

$$\rho = \frac{\sigma_R}{\overline{R}} \qquad \textbf{Eq. 4.7}$$

where σ_R is the root-mean-square deviation from the mean size,

$$\sigma_R = \frac{\overline{R}}{\sqrt{(z+1)}} \qquad \textbf{Eq. 4.8}$$

Therefore, combining Eq. 4.7 and Eq. 4.8, ρ is given by

$$\rho = \frac{1}{\sqrt{(z+1)}} \qquad \textbf{Eq. 4.9}$$

This model, idealized in Scheme 4.1 with the various contributions to the overall fit illustrated in Figure 4.1, is most sensitive to the position of the peaks, allowing the size, R, and volume fraction, ϕ (= NV), of the globules to be readily parameterized (R = 9.0 nm, ϕ = 0.37). The values obtained are in very good agreement with those obtained by Waigh *et al.* [8].

For a two globule chain structure, it has been shown that the radius of gyration R_g is related to the radius of the globule R (assumed equal for both globules) and the distance between the globules centres L [14]. The relationship is expressed by the following equation:

$$R_g{}^2 = R^2 + \frac{L^2}{4}$$

Eq. 4.10

Therefore, considering a R_g value of 41.0 nm and a radius of the globule R equal to 9.0 nm, L results equal to 80.0 nm.

All the parameters obtained from this model describing the mucin molecule and the Zimm plot are summarized in Table 4.1.

Radius of gyration, R_g (nm)	Correlation length, ξ (nm)	Radius of the globule, R (nm)	Volume fraction, ϕ	Distance between the globule centres, L (nm)
41.0 ± 4.1	23.5 ± 2.4	9.0 ± 0.5	0.37 ± 0.02	80.0 ± 18.3

Table 4.1 *Parameters obtained from the model which describes the mucin molecule.*

4.2.2. SANS from PGM solutions as function of concentration, pH, ionic strength and temperature

Mucin solutions have been analyzed by SANS over a range of concentrations (1 wt% ≤ [mucin] ≤ 5 wt%), pH (2 ≤ pH ≤ 9), ionic strength (0 ≤ [salt] ≤ 0.1 M NaCl) and temperature (25 °C and 37 °C) to

better understand the effect of these parameters on the conformation of mucin in solution.

Concentration

Scattering from mucin solutions over the entire concentration range studied, 1 wt% ≤ [mucin] ≤ 5 wt%, at 37 °C are showed in Figure 4.3. The scattering profiles revealed a decrease in intensities of the main peaks while decreasing the mucin concentration. However, these maxima are still present in the scattering even at concentration as low as 1 wt%. Again, the location of the second maxima for each concentration moves regularly at twice Q of the first, *i.e.*, $Q_{max}(peak2) = 2Q_{max}(peak1)$, indicating still a regular distribution of scatterers. The position of the main peak corresponds to a distance of 20 nm at 5 wt% mucin increasing to 42 nm at 1 wt% mucin, implying larger separation in the mucin network.

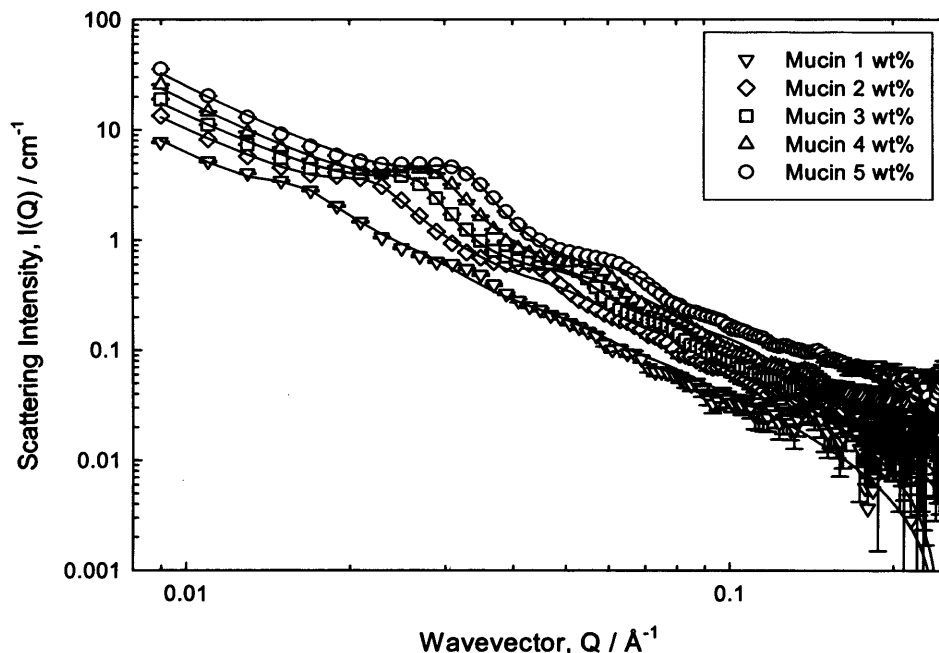*Figure 4.3 Scattering (symbols) and fit(solid lines) to the scattering model from mucin solutions over a concentration range (1 wt% ≤ [mucin] ≤ 5 wt%) at 37 °C.*

Upon dilution from [mucin] = 5 wt% to 1 wt%, the peaks in the data move to lower Q. Figure 4.4 shows the Q values of the main peak in the scattering from mucin plotted against mucin concentration. There is a power dependence found for Q on concentration c as expressed by the Eq. 4.11:

$$Q = \alpha c^{\beta}$$
Eq. 4.11

From the fitting of the data, α is 0.016, while β is 0.41.

The position of the peak is known to follow a $c^{1/2}$ dependence in semi-diluted hydrophobic polyelectrolytes solutions [15, 16]; the $c^{1/3}$ dependence is characteristic of liquid-like ordering. The $c^{(0.41\pm0.05)}$ scaling of the peak position observed is, therefore, denoting an intermediate behaviour of the mucin solutions.
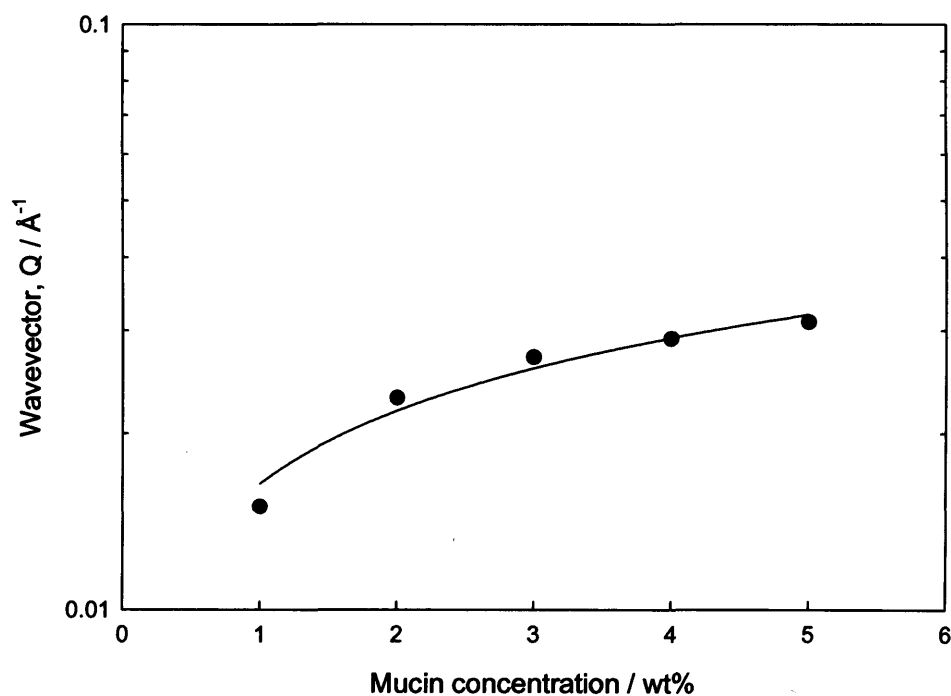

Figure 4.4 *Plot of the Q values for the main peak in the scattering from mucin against mucin concentration.*

Zimm plots in the low-Q region for the scattering from mucin at different concentrations are presented in Figure 4.5. Zimm plots were analyzed to obtain the correlation length ξ and radius of gyration R_g for each sample.

Since the main peak in the scattering from mucin solutions shifts to lower Q while decreasing the mucin concentration, the low-Q region considered for the Zimm plots was reduced to very low-Q values when decreasing the mucin concentration: avoiding the low-Q region comprising the main peak in the scattering allowed to have a linear decay in the Zimm plots. However, for the scattering from 1 wt% mucin solution this was not applicable because the main peak in the scattering profile is situated at very low-Q values: therefore, no Zimm plot was considered for this specific mucin concentration.

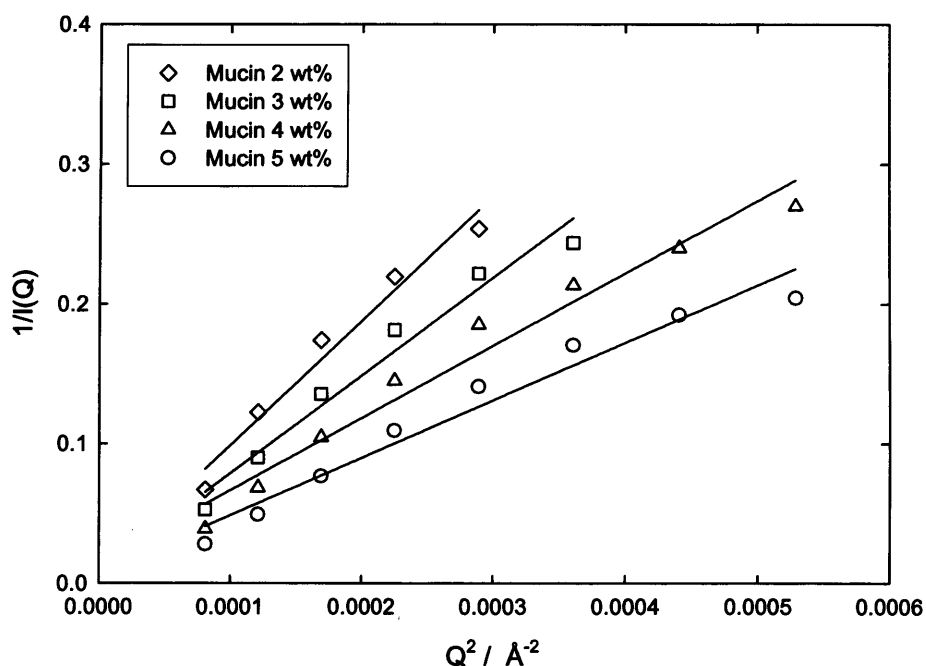

Figure 4.5 *Zimm plots at low-Q region (0.009 $\mathring{A}^{-1}$ $\leq$ Q $\leq$ 0.023 $\mathring{A}^{-1}$) for mucin solutions over a concentration range (2 wt% $\leq$ [mucin] $\leq$ 5 wt%), with linear fit to the data (solid line).*

The correlation length, the radius of gyration, the distance L together with the radius of the globule and the volume fracture obtained for each sample are summarized in Table 4.2. The distance L between the globule centres was calculated using Eq. 4.10.

Clearly, the radius of gyration, the correlation length and the distance between the globule centres increase while mucin concentration decreases. The volume fraction seems not to be particularly affected by the dilution while the radius of the globule decreases slightly when the mucin reaches concentrations of 4-5 wt%.

Mucin concentration (wt%)	Radius of gyration, R_g (nm)	Correlation length, ζ (nm)	Radius of the globule, R (nm)	Volume fraction, ϕ	Distance between the globule centres, L (nm)
5	41.0 ± 4.1	23.5 ± 2.4	9.0 ± 0.5	0.37 ± 0.02	80.0 ± 18.3
4	45.0 ± 4.5	26.0 ± 2.6	9.0 ± 0.5	0.38 ± 0.02	89.0 ± 20.5
3	49.0 ± 4.9	28.0 ± 2.8	11.5 ± 0.6	0.38 ± 0.02	95.0 ± 21.8
2	52.5 ± 5.2	30.0 ± 3.0	11.5 ± 0.6	0.36 ± 0.02	102.5 ± 23.6
1	-	-	11.5 ± 0.6	0.36 ± 0.02	-

Table 4.2 Parameters obtained from the model for the scattering from mucin solutions over a concentration range (1 wt% ≤ [mucin] ≤ 5 wt%).

Effects of the concentration on mucin solutions have been explored also by viscosity measurements. Viscosity experiments were performed on mucin solutions over a concentration range $0.1 \le$ [mucin] ≤ 5 wt% - at pH 7 and 37 °C - in an Ostwald viscometer. Over the concentration range 0.1 $\le$ [mucin] ≤ 5 wt%, solutions of PGM are viscous, as viscosity measurements show in Figure 4.6, and follow a trend such as $\eta \propto [mucin]^2$. Results obtained were consistent with results found by Naresh *et al.* [17].
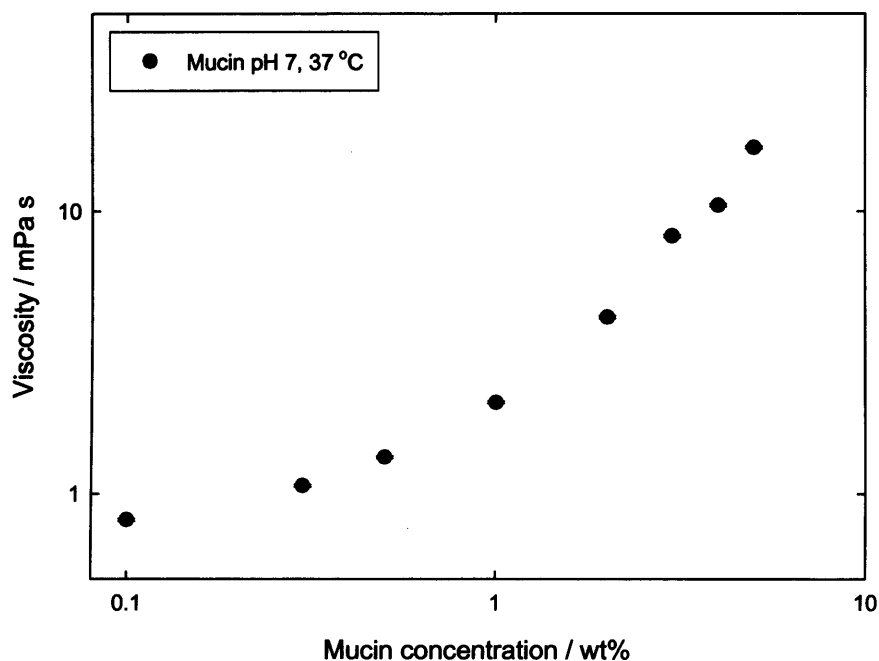
Figure 4.6 *Viscosity of PGM solutions as function of mucin concentration measured at pH 7 and 37 °C.*

pH

Scattering profiles from mucin solutions 5 wt% over the pH range studied, $2 \leq$ pH ≤ 9, at 37 °C are illustrated in Figure 4.7. Upon alteration of the pH, the scattering from 5 wt% mucin solutions showed identical maxima, like if the conformation of the mucin does not change over this pH range. However, the sample at pH 2 did exhibit a little difference in the scattering: the intensity of the maxima is slightly reduced but there is no change in the peak position.

Also the viscosity data of mucin 5 wt% over a pH range of $2 \leq$ pH ≤ 9 showed that mucin solutions did not exhibit relevant change in the viscosity upon alteration of the pH (Figure 4.8). Therefore, no pH-dependent sol-gel transition was observed in these mucin sample. The problem is that the gel properties of the commercial mucin cannot reproduce those observed *in-vivo*, as demonstrated by rheological studies performed by Kocevar-Nared *et al.* [18]. The commercial mucin is highly

degraded: in fact, the extraction and purification processes damage the disulfide bridges in the cysteine-rich domain, leading to a much weaker sol-gel transition around pH 4 and the lack of gel formation. Nevertheless, the protein backbone and the carbohydrate side-chains appear to be unchanged during the purification process.

Therefore, commercial mucin can then be regarded as an interesting material to study the interaction between the glycoprotein and other molecules, while investigation of the mucin gel properties should be carried out on mucin purified from fresh natural mucus.
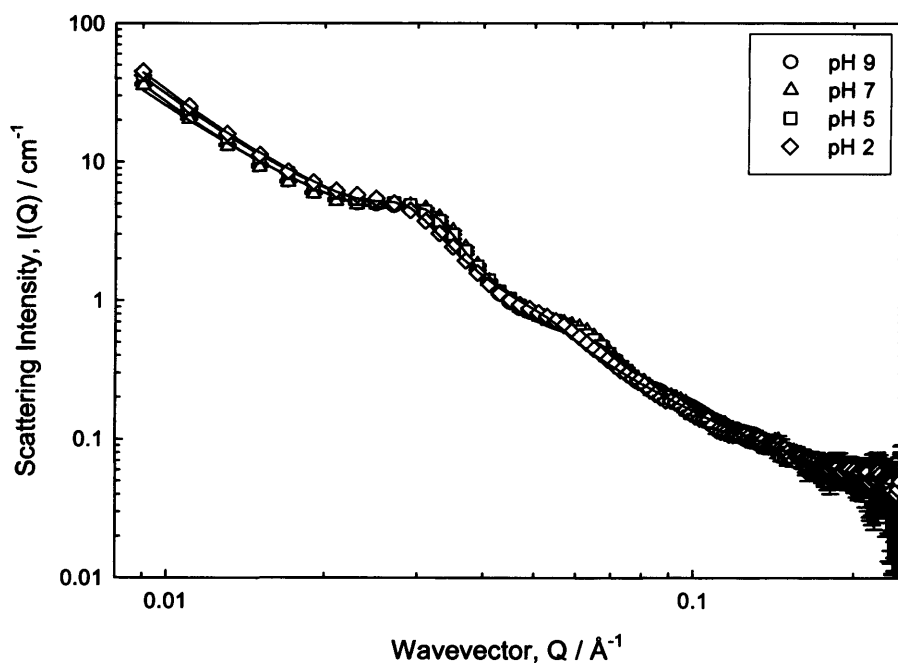

Figure 4.7 Scattering (symbols) and fit (solid lines) to the scattering model from mucin solutions 5 wt% over a range of pHs ($2 \leq pH \leq 9$) at 37 ^oC.
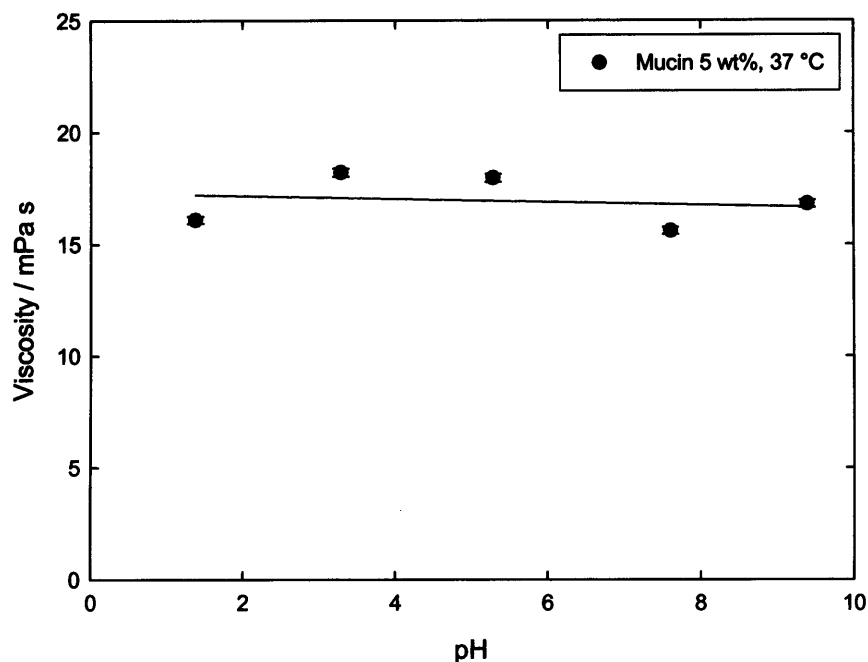
Figure 4.8 *Viscosity of mucin 5 wt% as function of pH at 37 °C.*

Zimm plots in the low-Q region for the scattering from mucin 5 wt% over a pH range are shown in Figure 4.9. Zimm plots were analyzed to get the correlation length ζ and radius of gyration R_g for each sample.

Table 3.3 summarizes all the parameters obtained from the model and the Zimm plots for each mucin 5 wt% sample over the pH range considered. The data obtained resulted of particular interest: in fact, when decreasing the pH, the correlation length together with the radius of gyration and the distance between the globules exhibited an increase. This variation is consistent with the more extended conformation that mucin reveals at pH lower than 4. Also the hydrophobic globule shows a reduction in size, probably as a consequence of a stronger hydrophobic interaction when lowering the pH.

Therefore, although from a rheological point of view it is not possible to observe a pH-dependent sol-gel transition, the scattering on mucin sample at pH lower than 4 can give some information revealing that commercial mucin can still exhibit a more extended, unfolded conformation when the pH is lower than 4.

Figure 4.9 *Zimm plots at low-Q region (0.009 $\mathring{A}^{-1} \leq Q \leq 0.023 \mathring{A}^{-1}$) for mucin solution 5 wt% over a pH range (2 ≤ pH ≤ 9), with linear fit to the data (solid line).*

Mucin 5 wt% pH	Radius of gyration, R_g (nm)	Correlation length, ζ (nm)	Radius of the globule, R (nm)	Volume fraction, ϕ	Distance between the globule centres, L (nm)
2	71.0 ± 7.1	41.0 ± 4.1	7.0 ± 0.3	0.34 ± 0.02	141.0 ± 32.4
5	61.5 ± 6.2	35.5 ± 3.6	9.0 ± 0.5	0.33 ± 0.02	122.0 ± 28.1
7	41.0 ± 4.1	23.5 ± 2.4	9.0 ± 0.5	0.37 ± 0.02	80.0 ± 18.3
9	43.0 ± 4.3	25.0 ± 2.5	9.0 ± 0.5	0.34 ± 0.02	83.5 ± 19.2

Table 4.3 *Parameters obtained from the model for the scattering from mucin solution 5 wt% over a pH range (2 ≤ pH ≤ 9).*

<u>Ionic strength</u>

Scattering from mucin solutions 5 wt% in a sodium chloride ambient over a range of $0 \leq$ [salt] ≤ 0.1 M NaCl are displayed in Figure 4.10. Interestingly, the main peaks do not move with increasing ionic strength implying that they do not arise due to an electrostatic structure factor.

The Zimm plots in the low-Q region for the scattering from mucin 5 wt% over a range of NaCl concentration are presented in Figure 4.11. The results from the analysis from the Zimm plots together with the other parameters obtained from the fit of the SANS datasets are reported in Table 4.4. A significant difference in the radius of gyration, correlation length and distance between the globules is observed only when a concentration of 100 mM is added to the 5 wt% mucin solution, while the size of the globules is not affected by the presence of the salt.

These results are in agreement with those found by Waigh *et al.* [8], who performed SAXS studies on mucin in the presence of salt. They showed that the addition of salt ($0 \leq$ [NaCl] ≤ 0.1 M) caused a decrease in the radius of gyration of the mucin molecule due to a contraction of the distance between the globules attributed to an increased screening of the electrostatic interactions of the peptide backbone.

Figure 4.10 *Scattering (symbols) and fit(solid lines) to the scattering model from mucin 5 wt% solutions in a NaCl ambient over a range of $0 \leq [NaCl] \leq 100$ mM at 37 °C.*
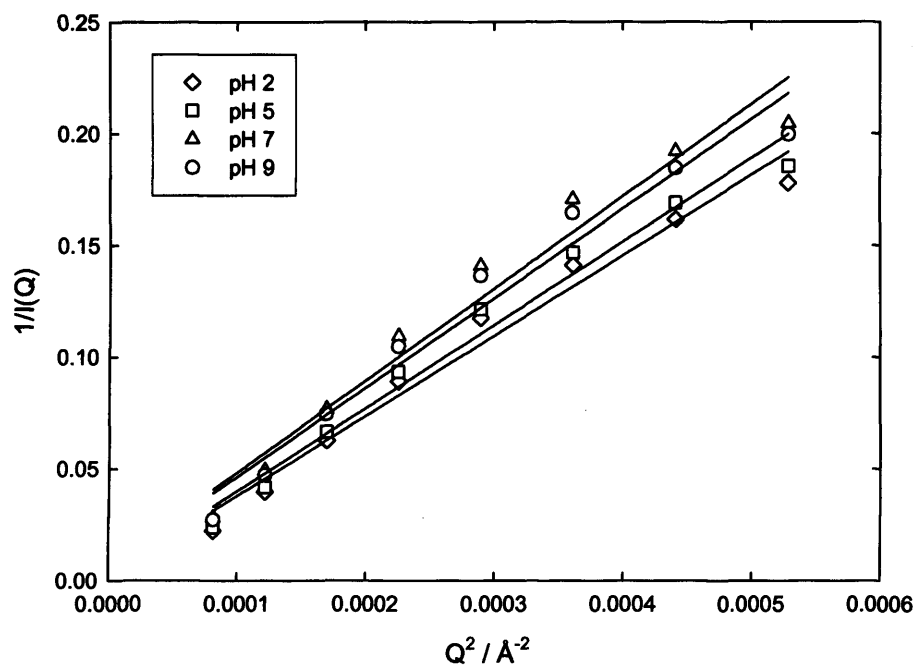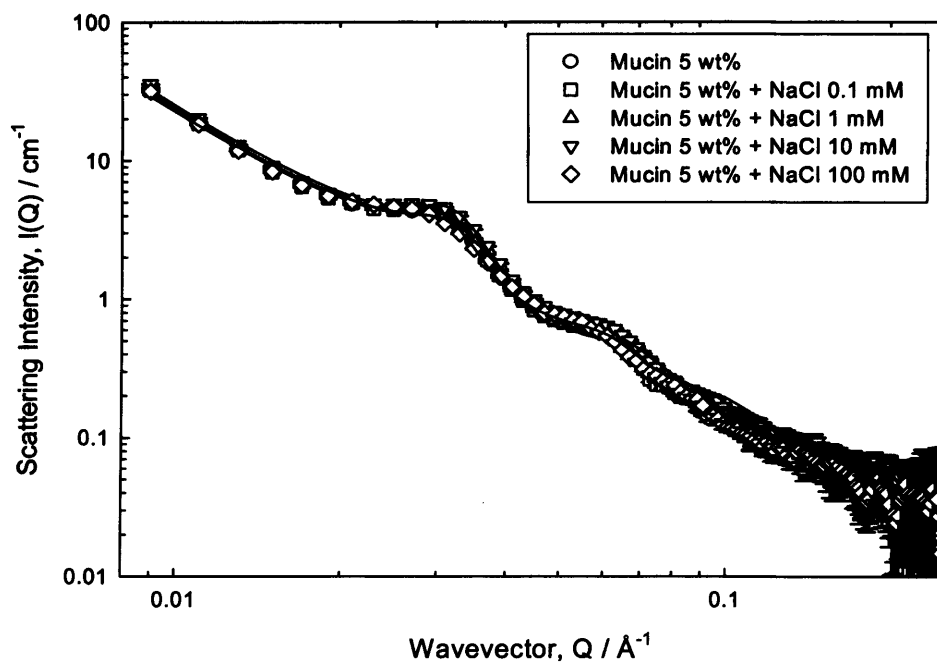

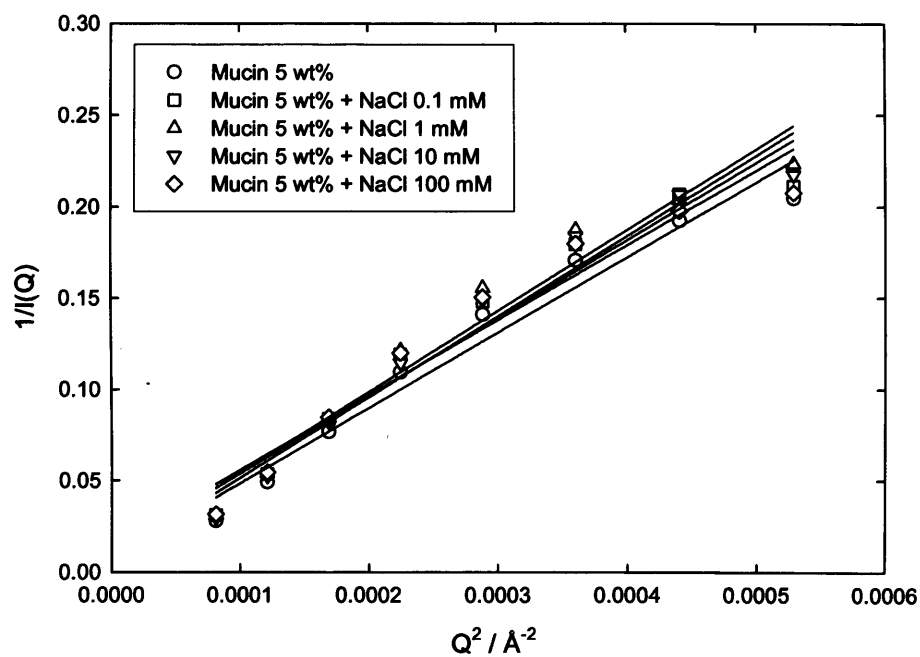***Figure 4.11*** *Zimm plots at low-Q region $(0.009 \text{ Å}^{-1} \leq Q \leq 0.023 \text{ Å}^{-1})$ for mucin solution 5 wt% over a range of $0 \leq [salt] \leq 0.1$ M NaCl, with linear fit to the data (solid line).*

[NaCl] added to mucin 5 wt% (mM)	Radius of gyration, R_g (nm)	Correlation length, ξ (nm)	Radius of the globule, R (nm)	Volume fraction, ϕ	Distance between the globule centres, L (nm)
0	41.0 ± 4.1	23.5 ± 2.4	9.0 ± 0.5	0.37 ± 0.02	80.0 ± 18.3
0.1	33.0 ± 3.3	19.0 ± 1.9	9.5 ± 0.5	0.37 ± 0.02	64.0 ± 14.7
1	36.5 ± 3.6	21.5 ± 2.2	9.5 ± 0.5	0.37 ± 0.02	70.5 ± 16.2
10	42.0 ± 4.2	24.0 ± 2.4	9.0 ± 0.5	0.36 ± 0.02	82.0 ± 18.9
100	29.0 ± 2.9	17.0 ± 1.7	9.0 ± 0.5	0.37 ± 0.02	54.5 ± 12.4

Table 4.4 *Parameters obtained from the model for the scattering from mucin solution 5 wt% over a range of $0 \leq [salt] \leq 0.1$ M NaCl.*

Temperature

The effect of the temperature on the mucin conformation was also studied. Scattering from mucin 4 wt% at 25 °C and 37 °C are presented in Figure 4.12. The scattering from mucin does not appear to be affected by a temperature variation, implying that no change in the mucin conformation is observed upon the temperature interval investigated. These results are in agreement with what found by Nystrom *et al.* [19], who reported that no change in the mucin structure could be observed in this temperature interval.
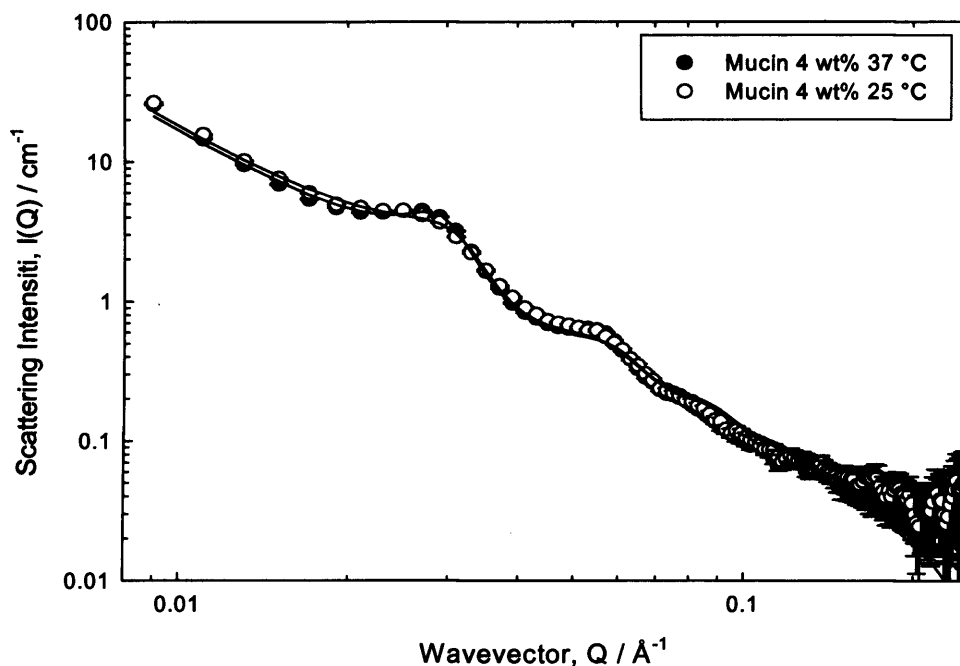
Figure 4.12 Scattering (symbols) and fit (solid lines) to the scattering model from mucin 4 wt% solutions at 37 °C and 25 °C.

4.2.3. The effect of mucolytic agents on the mucin structure

After having defined a model able to explain and to fit the scattering from PGM solutions, we wanted to explore the scattering from mucin solution in the presence of *N*-Acetyl-L-Cysteine (NAC), a mucolytic agent. The interest focused on studying the effect of the mucolytic agent on the mucin structure as function of the incubation time of the mucin with the mucolytic agent.

4.2.3.1. The mucolytic agents

Mucolytic agents are able to dissolve thick mucus and they are usually used for treatment in respiratory difficulties. A mucolytic agent tends to break down the gel structure of mucus and therefore decreases its elasticity and viscosity, helping to clear the mucus from the airways which makes it difficult to breath.

The most common mucolytic agents are *N*-Acetyl-L-Cysteine (NAC) and dornase alfa. The NAC disrupts disulfide bonds in mucus as mode of

action, while the dornase alfa acts enzymatically breaking down DNA in airways secretions. Since the interest is on mucus structure and how this can be altered by mucolityc agents, we will focus on N-Acetyl-L-Cysteine. The mechanism of action of NAC on mucin molecules consists of reducing the disulfide bridges in mucin to free thiol (sulfhydryl) groups, breaking the mucin polymer into smaller, less viscous units [20], as shown in Figure 4.13. As a result both the viscosity and the elasticity of the mucus are lowered. NAC begins to reduce viscosity immediately. Its mucolytic activity increases with higher pH and is optimal with a pH of 7.0-9.0 [21].
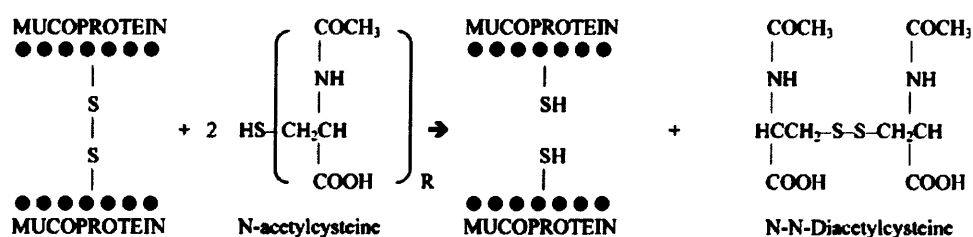
Figure 4.13 Mechanism of action of N-Acetyl-L-Cysteine on mucin molecules. Taken from Schrier B. [20].

4.2.3.2. Viscosity study

A viscosity study was carried out on mucin solution 5 wt% in the presence of NAC 0.5% at pH 7 and 37 °C as function of incubation time of the mucin with the NAC. Viscosity data in Figure 4.14 illustrates how the viscosity of mucin was affected greatly by the presence of NAC. After only an incubation time of 10 minutes, the viscosity of the mucin reduced by 33%. After 10 minutes, the viscosity of mucin shows a continuous decrease reaching a 50% viscosity reduction after 135 minutes.
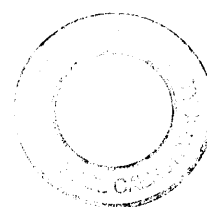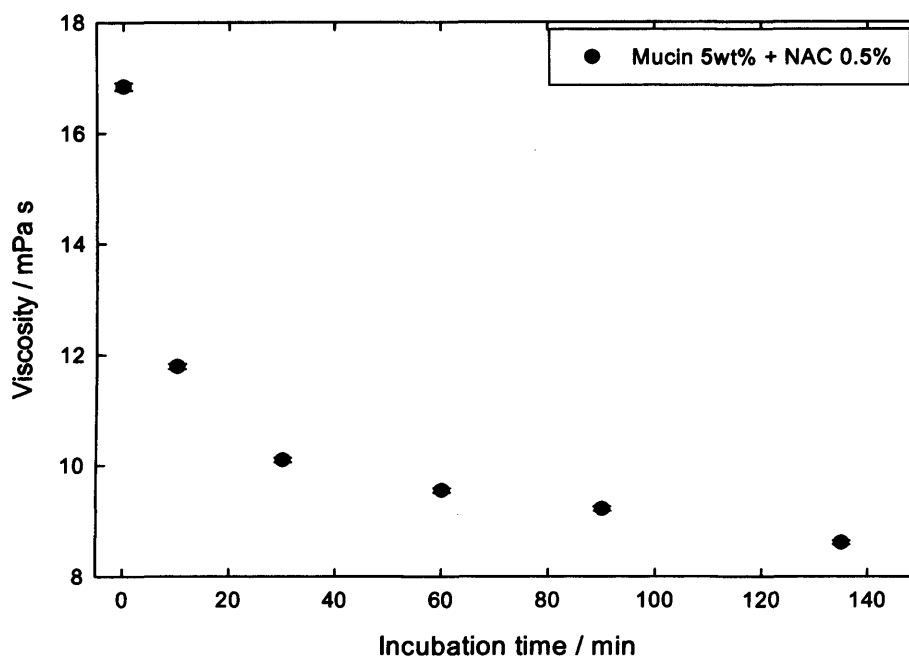
Figure 4.14 Viscosity of mucin solution 5 wt% in the presence of NAC 0.5% at pH 7 and 37 °C as function of the incubation time.

4.2.3.3. Kinetic study by SANS

The effect of NAC consists of breaking down the disulfide bridges in mucin which are relevant in determining the mucin structure [20]. Furthermore, the presence of NAC in mucin solutions affected significantly the viscosity of the mucin. Therefore, a SANS study looking at the changes of mucin structure as function of the incubation time with the mucolytic agent would be of interest.

Scattering from mucin 5 wt% in the presence of NAC 0.5 % at pH 7 was recorded as function of time, considering an incubation time range of mucin solution up to 25 minutes at 37 °C (Figure 4.15). Despite the great changes observed in the viscosity of mucin solutions immediately after the NAC was added, changes in scattering from mucin 5 wt% in the presence of NAC were less pronounced.

The position of the main peaks in the scattering from mucin did not result affected by the incubation of the mucin with NAC. The major changes

were related to the two main maxima at Q values (Q_{max}) of 0.031 Å^{-1} and 0.063 Å^{-1} which appeared to be weaker in intensity when increasing the incubation time of mucin with NAC. Figure 4.16 shows the scattering intensity of the main peak from the scattering from mucin (0.031 Å^{-1}) plotted against the incubation time of the mucin with NAC: the scattering intensity decreases of 1 cm^{-1} from the incubation time t = 0 to the time t = 5 minutes; after this time, any prolonged incubation time did not affect the scattering intensity of the peak any further.
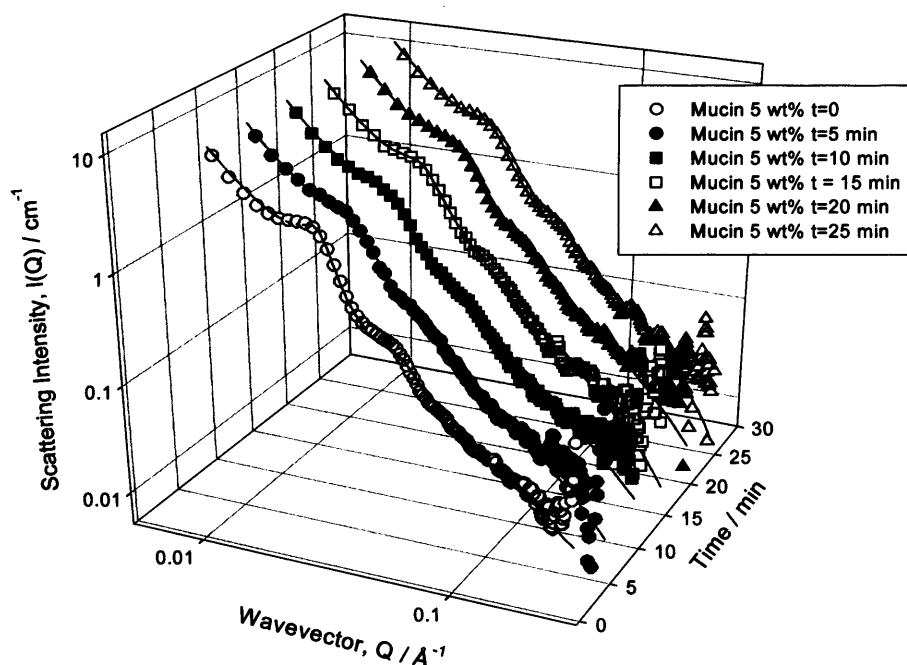
Figure 4.15 Ternary plot displaying scattering (symbols) and fit (solid lines) to the scattering model from mucin 5 wt% solutions in the presence of NAC 0.5% at pH 7 as function of the incubation time at 37 °C.
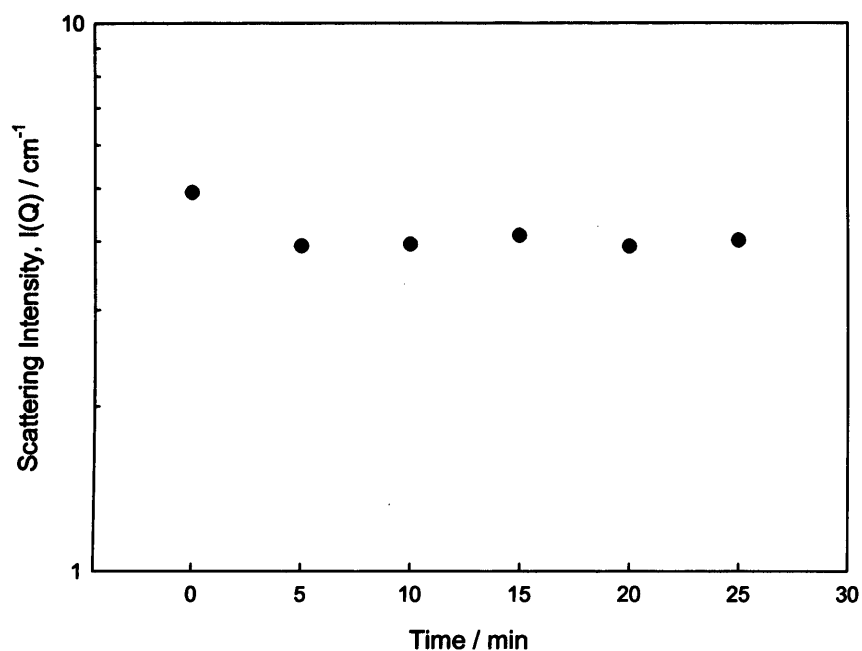
Figure 4.16 *Plot of the scattering intensities of the main peak in the scattering from mucin against incubation time of mucin with NAC.*

The Zimm plots in the low-Q region for the scattering from mucin 5 wt% over an incubation time with NAC are presented in Figure 4.17. The results from the analysis from the Zimm plots together with the other parameters obtained from the fit of the SANS datasets are reported in Table 4.5. A decrease in the radius of gyration, correlation length, distance between the globule and also the radius of the globules is observed 5 minutes after the incubation of mucin with NAC. These alterations could imply a break-down in the mucin structure as effect of the mechanism of action of the mucolytic agent. However, after this time, no significant changes are recorded.

The fact that changes in mucin structure are not particularly pronounced could be due to a degradation that commercial pig gastric mucin experiences during the purification process. The degradation occurs mainly in the cysteine-rich domain and consequently the disulfide bridges are damaged [18].
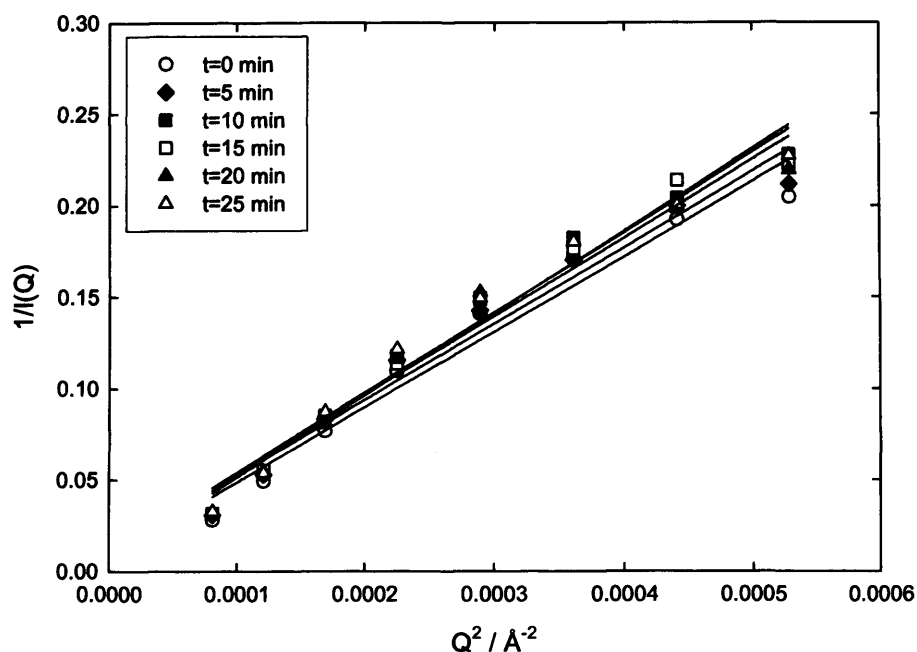
Figure 4.17 *Zimm plots at low-Q region (0.009 $Å^{-1}$ < Q < 0.023 $Å^{-1}$) for mucin solution 5 wt% over an incubation time (0 min ≤ time ≤ 25 min) with NAC, with linear fit to the data (solid line).*

Incubation time of mucin 5 wt% with NAC (min)	Radius of gyration, R_g (nm)	Correlation length, ξ (nm)	Radius of the globule, R (nm)	Volume fraction, ϕ	Distance between the globule centres, L (nm)
0	41.0 ± 4.1	23.5 ± 2.4	9.0 ± 0.5	0.37 ± 0.02	80.0 ± 18.3
5	35.0 ± 3.5	20.0 ± 2.0	7.5 ± 0.4	0.29 ± 0.01	68.0 ± 15.6
10	36.0 ± 3.6	21.0 ± 2.0	7.7 ± 0.4	0.27 ± 0.01	71.0 ± 16.3
15	35.5 ± 3.6	20.5 ± 2.0	7.8 ± 0.4	0.31 ± 0.02	69.0 ± 15.9
20	35.0 ± 3.5	20.0 ± 2.0	7.7 ± 0.4	0.29 ± 0.01	67.5 ± 15.5
25	36.0 ± 3.6	21.0 ± 2.1	7.7 ± 0.4	0.31 ± 0.02	71.0 ± 16.3

Table 4.5 *Parameters obtained from the model for the scattering from mucin solution 5 wt% over an incubation time (0 min ≤ time ≤ 25 min) with NAC.*

4.3. *Conclusions*

The conformation of mucin in solution has been explored by SANS and a more comprehensive approach was applied to analyze the scattering from mucin in solution. The analysis of the complex scattering profile from mucin solution was believed to most appropriate model a dispersion of hydrophobic globules – described as a dispersion of uncharged polydisperse spheres – connected by the glycosylated peptide backbone. According to this model, the radius of the globule, R, and the volume fraction, ϕ, resulted to be 9.0 nm and 0.37, respectively. Furthermore, a Zimm plot analysis of the low-Q region revealed a radius of gyration, R_g, of the mucin equals to 41.0 nm, a correlation length, ξ, of 23.5 nm and distance between the two globules of 80.0 nm. Despite the scattering profile from mucin did not change upon alteration of the ionic strength of the mucin solutions, a Zimm plot analysis showed a decrease in the R_g of the mucin molecule due to the addition of NaCl, attributed to a contraction of the glycosylated peptide spacer. These results are in agreement with SAXS studies on mucin solutions performed by Waigh *et al* [8].

Upon dilution, the scattering from mucin exhibited the characteristic peaks even at concentration as low as 1 wt%. However, these peaks resulted shifted at lower Q, interpreted as a larger separation in the mucin network when diluted. Indeed, the correlation length, the radius of gyration and the distance between the globules exhibited an increase while decreasing the mucin concentration, while no change in the radius of the globules was observed.

Changes on the temperature did not affect the scattering from mucin at all.

Notwithstanding the sol-gel transition observed by Cao *et al.* [22] on mucin solutions at pH lower than 4, interestingly the commercial PGM mucin here employed did not exhibit any relevant sol-gel transition over a broad pH range. The main reason seemed to be the fact that commercial mucins undergo to extraction and purification processes which damage the disulfide bridges in the cysteine-rich domain, main responsible of the sol-

100

gel transition. However, scattering from mucin upon alteration of the pH showed that a pH < 4 the mucin conformation exhibited an increase in the correlation length, in the distance between the two globules and in the radius of gyration: this could be related to a more extended conformation, typical of the mucin molecule at pH lower than 4.

The rapid decrease of the viscosity of mucin solutions caused by the mucolytic agent NAC was in agreement with what found by Schrier *et al.* [20]. However, the relevant effect of the NAC on the viscosity of mucin was not equally supported by the effect of the mucolytic agent on the conformation of mucin: a decrease of the correlation length and radius of gyration of the mucin was observed over the incubation time with the NAC; however, these changes were not as pronounced as the variation in viscosity due to the mechanism of action of NAC on mucin. The reason why changes in mucin structure were not particularly evident could be related, once more, to the degradation of the commercial mucin.

Understanding the conformation of mucin in solution upon the alteration of some external conditions (concentration, pH, ionic strength, temperature, the presence of a mucolytic agent) was of fundamental importance from a physiochemical point of view because it provided a complete picture of the behaviour of mucin in solution when changing the external environment. Moreover, SANS studies on the conformation of mucin here presented put the bases for undertaking any further and deeper SANS studies on mucin in solution: in fact, when considering delivering particles (*i.e.*: therapeutic molecules) through the mucosal barrier it fundamental to understand first the conformation of the mucin in solution to better evaluate the impact that the mucin gel-network might have on the transport of the particles.

References

1. Bansil, R.; Stanley, E.; LaMont, T. J., Mucin Biophysics. *Annual Review Physiology* **1995**, 57, 635-57.

2. Sheehan, J. K.; Oates, K.; Carlstedt, I., Electron microscopy of cervical, gastric and bronchial mucus glycoproteins. *The Biochemical Journal* **1986**, 239, 147-53.

3. Shogren, R. L.; Jamieson, A. M.; Blackwell, J.; Jentoft, N., Conformation of mucous glycoproteins in aqueous solvents. *Biopolymers* **1986**, 25, 1505-1517.

4. Gupta, R.; Jentoft, N.; Jamieson, A. M.; Blackwell, J., Structural analysis of purified human trancheobronchial mucins. *Biopolymers* **1990**, 29, 347-355.

5. Shogren, R. L.; Gerken, T. A.; Jentoft, N., Role of glycosylation on the conformation and chain dimensions of O-linked glycoproteins: light-scattering studies of ovine submaxillary mucin. *Biochemistry* **1989**, 28, 5525-5536.

6. Meyer, F. A.; Silberberg, A., Structure and function of mucus. In *Respiratory Tract Mucus*, Elsevier: Amsterdam, 1978; Vol. 54, pp 203-218.

7. Allen, A., Structure and function of gastrointestinal mucus. In *Physiology of Gastrointestinal Tract* Johnson, L. R., Ed. Raven Press: New York, 1981; pp 617-639.

8. Di Cola, E.; Yakubov, G. E.; Waigh, T. A., Double-globular structure of porcine gastric mucin: a small-angle X-ray scattering study. *Biomacromolecules* **2008**, 9, 3216-3222.

9. Bhaskar, K. R.; Gong, D.; Bansil, R.; Pajevic, S.; Hamilton, J. A.; Turner, B. S.; LaMont, J. T., Profound increase in viscosity and aggregation of pig gastric mucin at low pH. *American Journal of Physiology* **1991**, 261, 827-832.

10. Hong, Z.; Chasan, B.; Bansil, R.; Turner, B. S.; Bhaskar, K. R.; Afdhal, N. H., Atomic force microscopy reveals aggregation of gastric mucin at low pH. *Biomacromolecules* **2005**, 6, 3458-3466.

11. Waigh, T. A.; Papagiannopoulos, A.; Voice, A.; Bansil, R.; Unwin, A. P.; Dewhurst, C. D.; Turner, B.; Afdhal, N., Entanglement coupling in porcine stomach mucin. *Langmuir* **2002**, 18, 7188-7195.

12. Yakubov, G. E.; Papagiannopoulos, A.; Rat, E.; Easton, R., L.; Waigh, T. A., Molecular structure and rheological properties of short-side-chain heavily glycosylated porcine stomach mucin. *Biomacromolecules* **2007**, 8, 3467-3477.

13. Kotlarchyk, M.; Stephens, R. B.; Huang, J. S., Study of Schultz distribution to model polydispersity of microemulsion droplets. *The Journal of Physical Chemistry* **1988**, 92, 1533-1538.

14. Fujisawa, T.; Ueki, T.; Inoko, Y.; Kataoka, M., X-ray scattering from a Troponin C solution and its interpretation with a dumbell-shaped-molecule model. *Journal of Applied Crystallography* **1987**, 20, 349-355.

15. Dobrynin, A. V.; Colby, R. H.; Rubinstein, M., Scaling theory of polyelectrolyte solutions. *Macromolecules* **1995**, 28, 1859-1871.

16. Dobrynin, A. V.; Rubinstein, M., Counterion condensation and phase separation in solutions of hydrophobic polyelectrlytes. *Macromolecules* **2001**, 34, 1964-1972.

17. Naresh, R.; Hampson, D. J., Attraction of Brachyspira pilosicoli to mucin. *Microbiology* **2010**, 156, 191-197.

18. Kocevar-Nared, J.; Kristl, J.; Smid-Korbar, J., Comparative rheological investigation of crude gastric mucin and natural mucus. *Biomaterials* **1997**, 18, 677-681.

19. Nystrom, B.; Kjoniksen, A.-L.; Beheshti, N.; Maleki, A.; Zhu, K.; Knudsen, K. D.; Pamies, R.; Hernandez Cifre, J. G.; Garcia de la Torre, J., Characterization of polyelectrolyte features in polysaccharide systems and mucin. *Advances in Colloid and Interface Science* **2009**.

20. Schrier, B. P.; Lichtendonk, W. J.; Witjes, J. A., The effect of N-acetyl-L-cysteine on the viscosity of ileal neobladder mucus. *World Journal of Urology* **2002**, 20, 64-67.

21. Henke, M. O.; Ratjen, F., Mucolytics in cystic fibrosis. *Paediatric Respiratory Reviews* **2007**, 8, 24-29.

22. Cao, X.; Bansil, R.; Bhaskar, R.; Turner, B. S.; LaMont, J. T., pH-dependent conformational change of gastric mucin leads to sol-gel transition *Biophysical Journal* **1999**, 76, 1250-1258.

Chapter 5. SANS and PGSE-NMR studies on the interaction between polymers and mucin solutions

This chapter presents a comprehensive study on the diffusion and interaction of a series of water-soluble polymers with mucin solutions. The polymers considered are of interest in the field of polymer-drug delivery systems because they can be conjugated to liposomal carriers, nanoparticles and proteins to increase their solubility and stability or they can be involved in applications for gene delivery. Therefore, an understanding of the dynamics of the mobility through and/or binding of these polymers to the mucosal barrier is of fundamental interest for the design and development of polymer-drug delivery constructs. An introduction to the applications of pulsed-gradient spin-echo NMR (PGSE-NMR) and small-angle neutron scattering (SANS) on bio-gel system is first given.

5.1. Introduction

5.1.1. Application of PGSE-NMR to bio-gel systems

As a non-invasive technique, PGSE-NMR can be used to quantify the diffusion of micro- and nano-sized drug delivery constructs (liposomes, surfactant micelles, micro-emulsions, polymers) [1,2] in colloidal systems [3-7] and bio-gels such as mucin glycoprotein solutions [8-10], cartilage [11], curdlan gels [12], whey and casein protein gels [13-16].

As explained in Chapter 2, a PGSE-NMR experiment quantifies the measurement of the self-diffusion coefficient of the species investigated within the solution. The diffusion coefficient thus determined contains dynamical and structural information defined by the size and shape of the diffusing species and the solution within which it is dispersed. Diffusion coefficients decrease with increasing molecular size and as a reflection of

any binding or obstruction the diffusing species experience within the solution [17]. In dilute solutions, hydrodynamic radii are most frequently calculated from self-diffusion coefficients via the Stokes-Einstein relationship (Eq. 2.4), notwithstanding its limitations (since it applies best for large, spherical molecules).

Associations and other interactions (such as binding) between diffusing species leads to a reduction in diffusion rate, commensurate with the increased size of the aggregate, modulated by the lifetime and concentration of the aggregate. For the situation where the aggregate is long-lived compared to the NMR timescale, two discrete NMR populations are manifest, sometimes giving rise to two discrete NMR signals [10]. More commonly, fast exchange occurs and the effective diffusion coefficient is a population weighted average of the two discrete environments, the faster rate associated with the non-aggregated species and the slower rate associated with aggregates, as shown in Eq. 5.1:

$$D_s{}^{average} = \frac{C_{non-aggregated}D_s{}^{fast} + C_{aggregated}D_s{}^{slow}}{C_{total}} \qquad \textbf{Eq. 5.1}$$

In the case of small, rapidly diffusing molecules interacting with large, slowly diffusing structures, there is a significant sensitivity to the concentration of the non-aggregated fraction of the small molecule, and thus NMR diffusion measurements are highly useful for the study of weak interactions.

In this context, diffusion NMR is used here to probe either the diffusion, binding, interaction of polymers with mucin solutions. The polymers considered in this study – such as poly(ethylene glycol), polyamidoamine dendrimers, polyethylenimines – are usually employed in the construction of drug delivery systems, in particular they are polymeric carriers which can be conjugated via covalent (often cleavable) bond to the therapeutic moiety [18]. The polymeric carrier confers aqueous solubility, biocompatibility to and improves the pharmacokinetics of the therapeutic agent. The bioavailability of the therapeutic agent is closely coupled to its

ability to be transported to the site of action. Therefore, a key aspect in defining structure-activity relationships for drug delivery systems derived from polymer diffusion data is the requirement to separate the effects of obstruction – the reduction in polymer mobility due to the increased diffusion path-length associated with the polymer having to diffuse around and through the mucin network – from the effects of binding – the reduction in polymer mobility due to a specific interaction between the polymer and the mucin molecules.

5.1.2. Application of SANS to bio-gel systems

Small-angle neutron scattering (SANS) has been proved to be a unique and powerful tool to probe not only structures of macromolecules in solutions, but also interactions of different components in the system under investigation, and phase transitions of soft-matter systems [19]. The understanding of inter-particle interactions, aggregation and cluster formation is still an important aspect in a number of areas, ranging from cluster formation in various diseases process (*i.e.*, Alzheimer's disease) [20] to the design of drug-delivery systems [21]. Several studies have used SANS to investigate protein-protein [22] or protein-surfactant interaction [23], to follow the cluster formation in protein solutions and colloids [24], to study the aggregation of amphiphilic molecules into micelles and microemulsions [19].

In the present study, the use of SANS has been applied to quantify changes induced in the structure of mucin by the addition of a second polymer. The polymers tested are considered of particular interest in the construction of polymer-drug delivery systems: (i) poly(ethylene glycol) (PEG) has been widely used in the PEG coating (PEGylation) of nanoparticle [25], liposomal carriers [26] and proteins [27] to enhance their stability and solubility; (ii) polyamidoamine (PAMAM) dendrimers and polyethyleneimine (PEI) find large applications in drug encapsulation[28] and in polyelectrolyte complexes (polyplexes) for gene delivery [29] – *i.e.*, polymer-DNA complex; (iii) dextrin is a natural biodegradable polymer used to make up polymer-drug conjugates – *i.e.*, dextrin-doxorubicin

conjugate [30], where doxorubicin is an anti-cancer drug. Examples of polymer-protein conjugates commercially available are PEG-L-asparaginase (Oncaspar® [31]) for the treatment of acute lymphoblastic leukemia, PEG-adenosine deaminase (Adagen® [32]) for the treatment of severe combined immunodeficiency disease, and PEG-interferon-α conjugates (PEGASYS® [33] and PEG-INTRON® [34]) as treatments for hepatitis C.

Therefore, the behaviour of these polymers towards the mucin molecules is of fundamental importance when looking at the delivery of therapeutics through the mucosal barrier.

5.2. Results

5.2.1. SANS results

The scattering of mucin 5 wt% in the presence of a series of polymers has been investigated to quantify any perturbation in that structure induced by the addition of the second 'probe' polymer. Characteristics of all polymers used can be found in Table 3.1 in Chapter 3. The 'probe' polymers considered have been divided into three main groups: (i) uncharged polymers, which includes PEGs and dextrin; (ii) positively charged polymers, comprising PAMAM dendrimers G2.0 and G4.0 (with amine terminal groups) and PEI; (iii) negatively charged polymers such as PAMAM dendrimers G3.5 and G5.5 (with carboxyl terminal groups). In the mucin-'probe' polymer solutions, the concentration of the mucin and of the 'probe' polymers have been kept constant: 5 wt% for the mucin and 0.5 wt% for the 'probe' polymer.

5.2.1.1. Uncharged polymers

The scattering from 5wt% PGM solutions (37 °C) in the presence of 0.5wt% l-PEG 10K g mol^{-1}, b-PEG 20K g mol^{-1}, l-PEG 100K g mol^{-1} and dextrin 50K g mol^{-1} data are presented in Figure 5.2, 5.3, 5.4, 5.5, respectively.

To satisfy the so-called 'contrast variation' condition (explained in the Appendix B), a deuterated l-PEG10K was used to minimize the scattering observed from the polymer when added to mucin solutions. Figure 5.1 shows the scattering from 0.5 wt% l-PEG10K in the hydrogenated (h) and deuterated (d) form in D$_2$O: both the hydrogenated and deuterated l-PEG10K exhibited a very low scattering. This means that, at the concentration of 0.5 wt%, the scattering from an hydrogenated polymer in the mixture mucin-'probe' polymer solutions can be ignored. Therefore, hydrogenated forms were used for the other polymers when performing scattering experiments on the mixture mucin-'probe' polymer solutions: the concentration of the polymers was too low to detect measurable scattering.

The scattering from mucin shows its typical profile – as already seen on Figure 4.1 in Chapter 4 – characterized by pronounced maxima against a slowly decaying background signal. The scattering experiments were performed in the mucin-'probe' polymer solutions at two different pHs which were physiologically relevant, *viz* pH 2 and 7. The same observations were made for all pHs examined.

SANS data were analyzed according to the model discussed in section 4.2.1 in Chapter 4. For each SANS data set, the radius of the globule of the mucin molecule and the volume fraction were obtained from the fitting of the $I(Q)_{globule}$ scattering term in the Equation Eq.4.2; parameters fitted by the $I(Q)_{globule}$ scattering term are expressed in the Equation Eq. 4.4. Zimm plots in the low-Q region for the scattering from mucin 5 wt% in

the presence of these 'probe' polymers were analyzed to derive the correlation length ξ and radius of gyration R_g.

Table 5.1 shows all the parameters obtained from the model and the Zimm plots for each mucin 5 wt% sample in the absence and in the presence of the uncharged 'probe' polymer at the pHs considered (pH 2 and 7). The values for the radius of gyration, correlation length, radius of the globule and the distance between the globules for the mucin molecule in the presence of the 'probe' polymer at pH 2 and 7 are not affected and resulted comparables to the values obtained for the mucin at the same pHs.

Clearly, the presence of the 'probe' polymers in mucin solutions showed no significant differences from the scattering from the 5 wt% PGM solution at the pHs studied. The simplest interpretation of this observation is the lack of an interaction between the mucin and the various PEGs and dextrin, at least to a degree that induces a structural perturbation in the mucin.
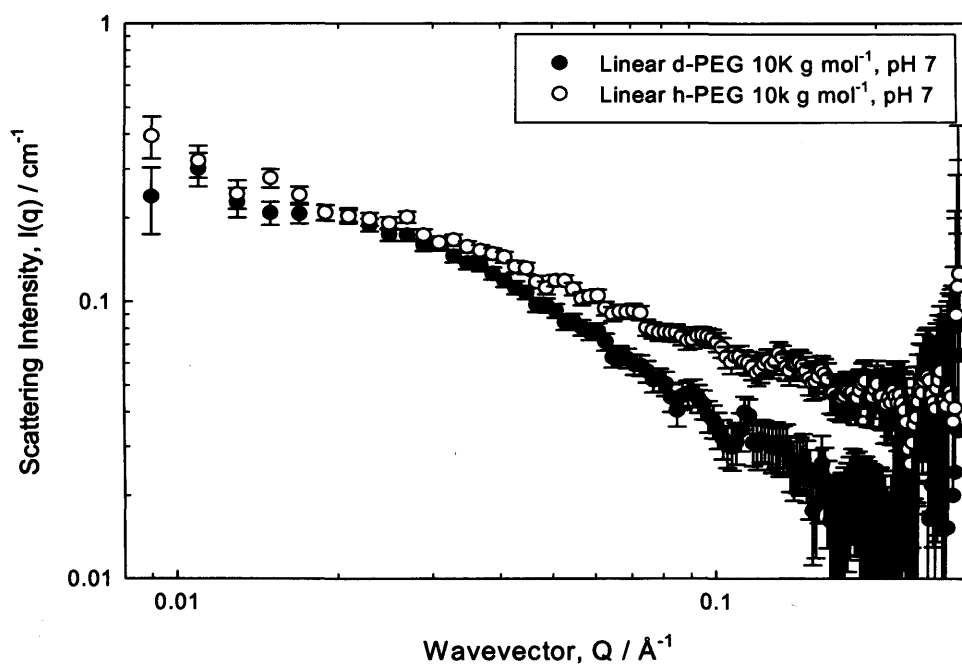
Figure 5.1 Scattering (symbols) from 0.5 wt% l-PEG 10K g mol^{-1} in the hydrogenated (h) and deuterated (d) form in D$_2$O at pH 7.

Figure 5.2 Scattering (symbols) and fit (solid lines) from 5 wt% mucin in the absence and in the presence of 0.5 wt% deuterated l-PEG 10K g mol^{-1} at pH 7 (top) and pH 2 (bottom).

Figure 5.3 Scattering (symbols) and fit (solid lines) from 5 wt% mucin in the absence and in the presence of 0.5 wt% b-PEG 20K g mol^{-1} at pH 7.

Figure 5.4 *Scattering (symbols) and fit (solid lines) from 5 wt% mucin in the absence and in the presence of 0.5 wt% l-PEG 100K g mol⁻¹ at pH 7 (top) and pH 2 (bottom).*
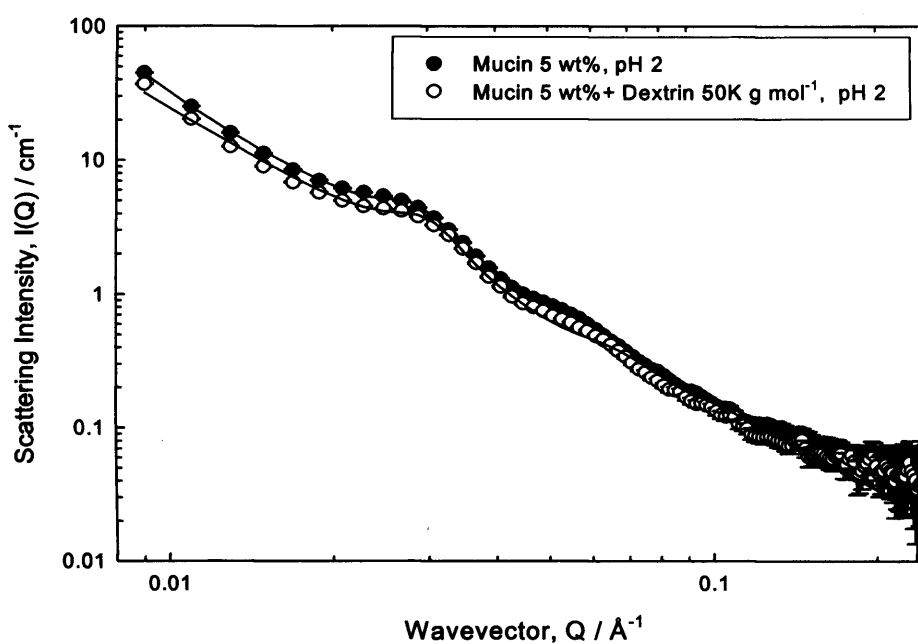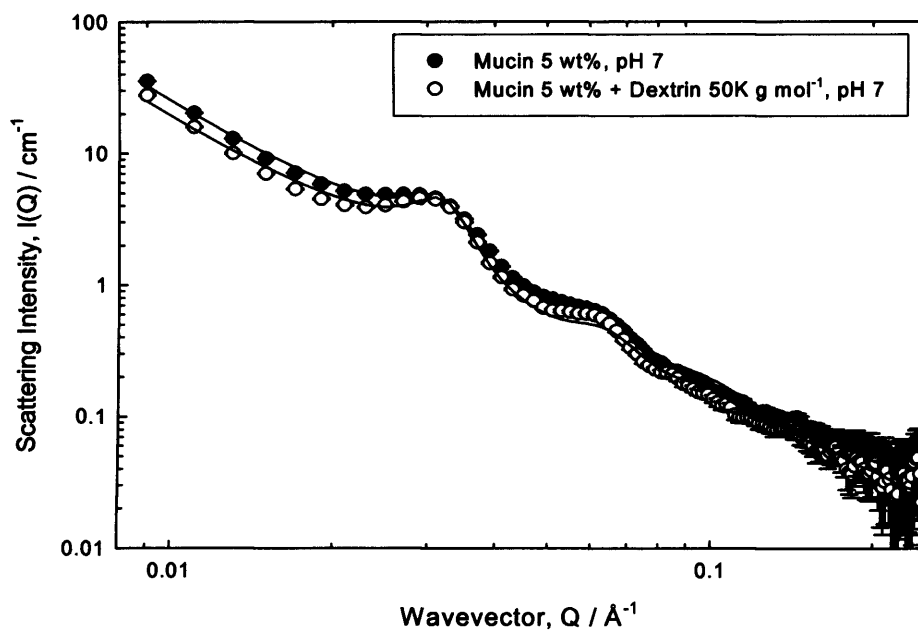
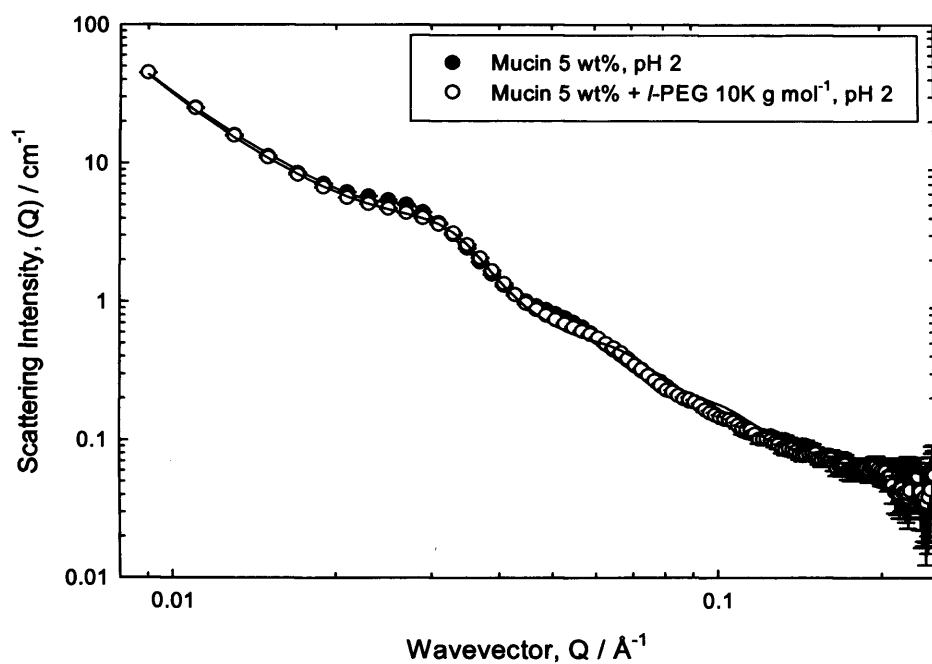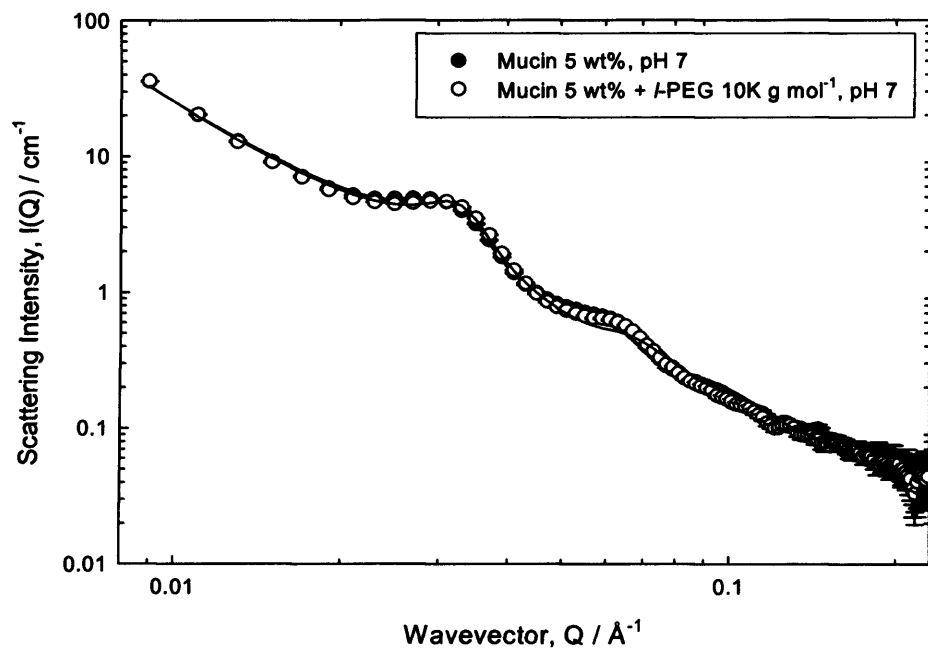**Figure 5.5** *Scattering (symbols) and fit (solid lines) from 5 wt% mucin in the absence and in the presence of 0.5 wt% dextrin 50K g mol^{-1} at pH 7 (top) and pH 2 (bottom).*
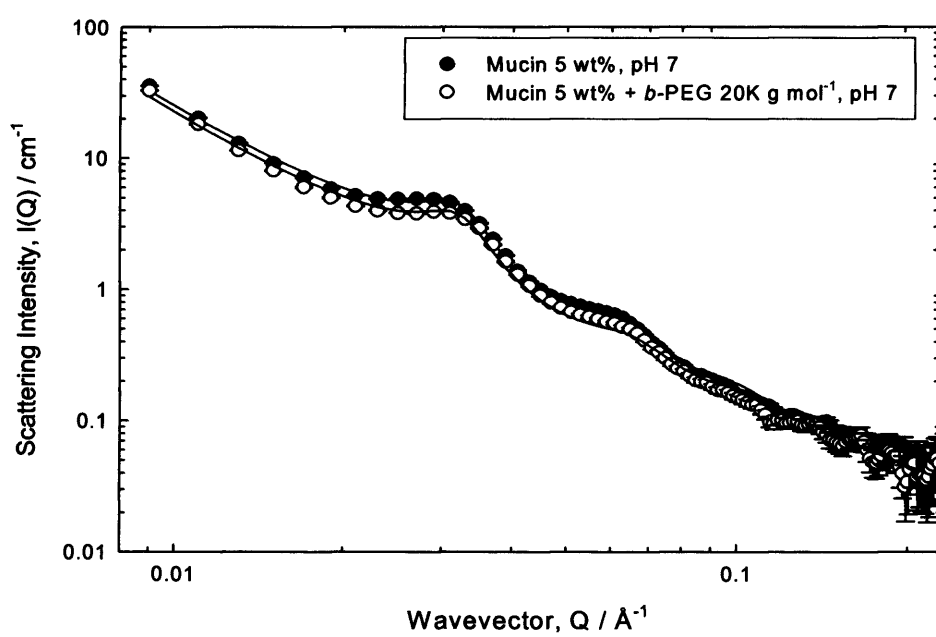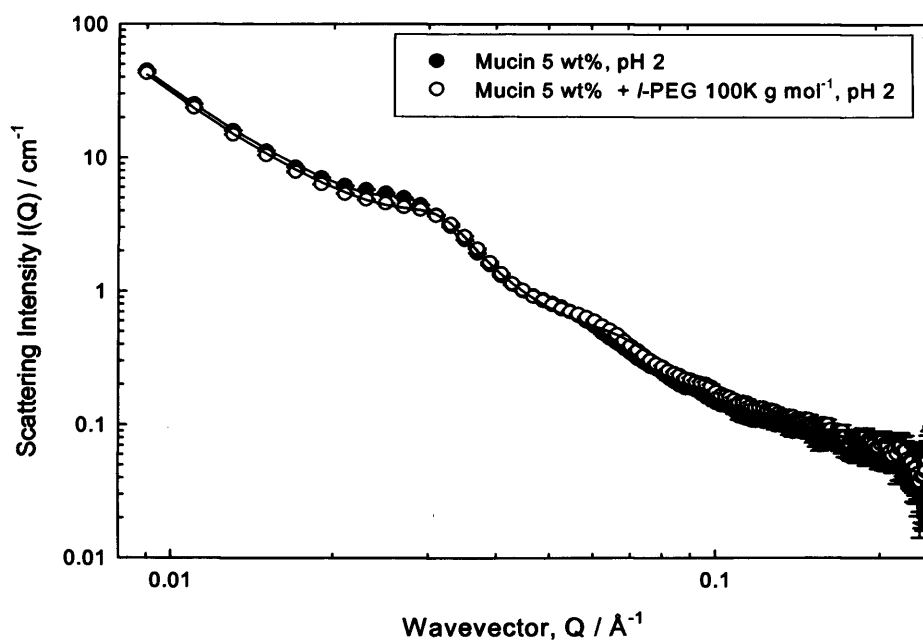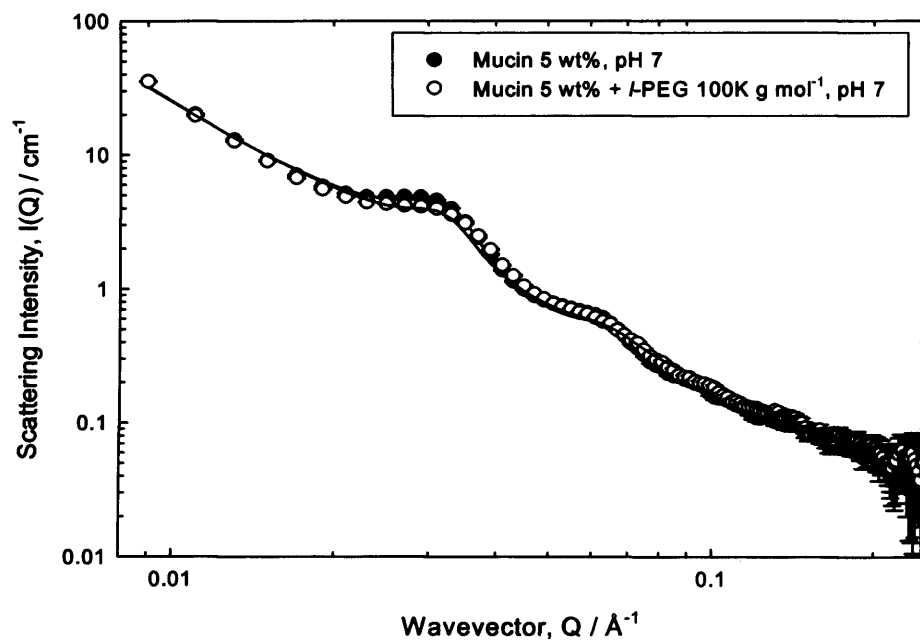
Polymer added to mucin 5 wt%	Radius of gyration, R_g (nm)	Correlation length, ξ (nm)	Radius of the globule, R (nm)	Volume fraction, ϕ	Distance between the globule centres, L (nm)
none pH 7	41.0 ± 2.0	23.5 ± 1.2	9.0 ± 0.5	0.37 ± 0.02	80.0 ± 18.3
none pH 2	71.0 ± 3.5	41.0 ± 2.0	7.0 ± 0.3	0.34 ± 0.02	141.0 ± 32.4
l-PEG 10K pH 7	40.0 ± 2.0	23.0 ± 1.2	8.5 ± 0.4	0.38 ± 0.02	78.0 ± 17.9
l-PEG 10K pH 2	72.0 ± 3.6	41.5 ± 2.1	6.8 ± 0.3	0.35 ± 0.02	143.0 ± 32.9
b-PEG 20K pH 7	44.0 ± 2.2	25.0 ± 1.3	9.0 ± 0.5	0.37 ± 0.02	85.0 ± 19.5
l-PEG 100K pH 7	42.0 ± 2.1	24.0 ± 1.2	8.1 ± 0.4	0.37 ± 0.02	82.0 ± 18.9
l-PEG 100K pH 2	73.0 ± 3.7	42.0 ± 2.1	6.6 ± 0.3	0.34 ± 0.02	145.0 ± 33.3
Dextrin 50K pH 7	39.0 ± 2.0	22.5 ± 1.1	9.2 ± 0.5	0.40 ± 0.02	75.5 ± 17.4
Dextrin 50K pH 2	68.0 ± 3.4	39.5 ± 2.0	6.7 ± 0.3	0.35 ± 0.02	136.0 ± 31.3

Table 5.1 *Parameters obtained from the model for the scattering from mucin solution 5 wt% in the absence and in the presence of a range of 0.5 wt% uncharged polymers at pH 2 and 7.*

5.2.1.2. Positively charged polymers

Unlike the effect of the uncharged polymers on the scattering from mucin solutions, the addition of cationic polymers – such as 0.5wt% PAMAM dendrimers amino terminated G2.0 and G4.0, PEI – to 5wt% mucin solutions did induce changes in the mucin scattering. Any contribution from the PAMAM dendrimers and PEI to the scattering from mucin solutions has been ignored as there was no measurable scattering from these 'probe' polymers in the absence of the mucin, as shown from Figure 5.6.

The presence of 0.5 wt% PAMAM dendrimer G2.0 in 5 wt% mucin did not show any major change in the scattering from mucin solutions at pH 2 and pH 9, while a perturbation in the scattering from mucin was observed at pH 7, as illustrated in Figure 5.7. The same trend was observed when 0.5 wt% PAMAM dendrimer G4.0 was added to 5 wt% mucin solution (Figure 5.8). The most obvious change at pH 7 is the weakening of the principle maximum on addition of the dendrimer, and the shift of both maxima to lower Q. In particular, the two main maxima are at Q values (Q_{max}) of 0.027 Å^{-1} and 0.053 Å^{-1}, which correspond to distances/sizes of 23.3 nm and 11.8 nm respectively. This indicates that the structure giving rise to these features has increased in size and/or their separation has increased of ~ 15-20% (*i.e.*, become more dilute). Analogous behaviour was observed for the PAMAM dendrimer G4.0 in mucin solutions.

SANS data were analyzed according to the model discussed in section 4.2.1 in Chapter 4, from which information on the radius of the globule of the mucin molecule and the volume fraction were obtained. Zimm plots in the low-Q region for the scattering from mucin 5 wt% in the presence of PAMAM dendrimers G2.0 and G4.0 were analyzed to derive the correlation length ζ and radius of gyration R_g. Table 5.3 shows all the parameters obtained from the model and the Zimm plots for each 5 wt% mucin sample in the absence and in the presence of the PAMAM dendrimers at the pHs considered (pH 2, 7 and 9).

Parameters found at pH 2 and 9 for the mucin 5 wt% in the presence of PAMAM dendrimer G2.0 were analogous to those observed for mucin only solutions at the same pHs. Interestingly, the radius of gyration, the correlation length and the distance between the globules in the system 'mucin + PAMAM dendrimer' at pH 7 were larger compared to those observed for mucin only in solution at the same pH. In particular, when the polymer was added to mucin solutions at pH 7, an increase of ~ 18-20 % on the radius of gyration and the correlation length of the mucin molecule was observed. These results are in agreement with the shift to lower Q of the main peaks observed in the scattering of mucin in the presence of PAMAM dendrimer G2.0 at pH 7. This means that the shift of the main peaks in the scattering profile is related to a change in the radius of gyration, R_g, and the correlation length, ξ, of the mucin molecule: the more they move to lower Q, the larger R_g and ξ are. Same results were obtained for the mucin in the presence of PAMAM dendrimer G4.0.

The changes in the scattering from mucin due to the presence of the positively charged PAMAM dendrimers resulted mainly pH-dependent and clearly indicated an interaction between these 'probe' polymers and mucin.

"Signature" pH effects were also observed when *b*-PEI2K was added to the 5wt% mucin solutions as shown in Figure 5.9. The changes in the perturbations in the scattering were much more pronounced that the dendrimer case: no change in scattering was reported at pH 2 but a much larger difference in scattering was observed at pH 7. The presence of the *b*-PEI2K at pH 7 and pH 9 in mucin solutions caused a noticeable weakening of the main maxima, typical of the scattering from mucin solutions. Furthermore, from the analysis of the Zimm plots and the parameters obtained from the model, significant increase in the correlation length, radius of gyration, distance between the globules and the size of the globules was observed in the system 'mucin + *b*-PEI2K' at pH 7 and 9, as reported in Table 5.3. Therefore, the *b*-PEI2K showed a stronger interaction towards mucin compared to the interaction exhibited by the PAMAM dendrimers with mucin solutions.

The presence of *b*-PEI25K caused flocculation of the mucin solutions and therefore, this system was not studied further but serves to underline the importance of the relative signs and magnitudes of the respective charge in these systems.
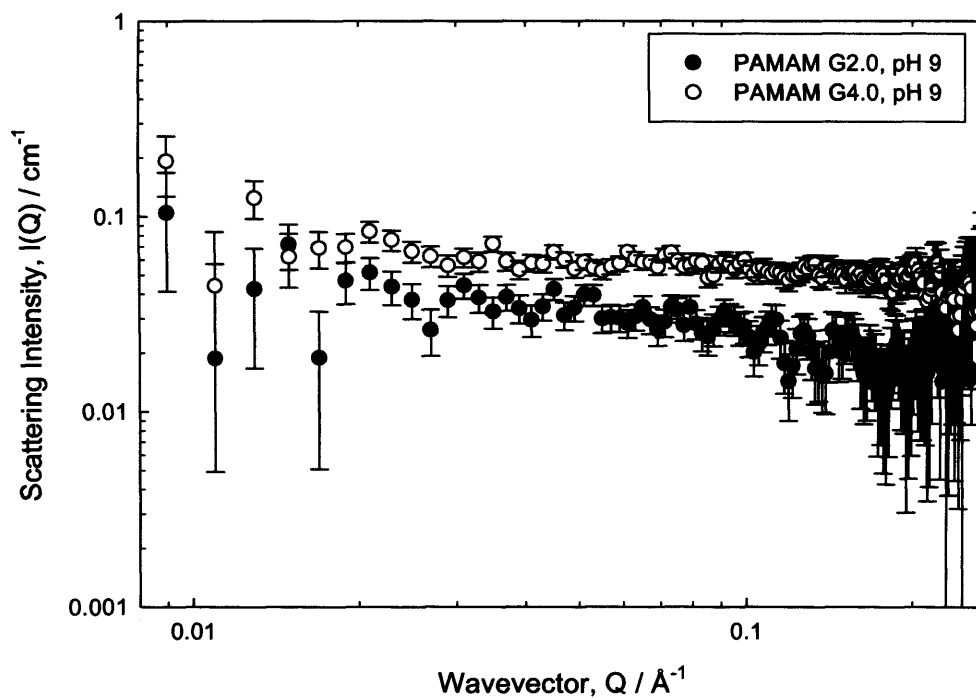
Figure 5.6 Scattering (symbols) from 0.5 wt% PAMAM dendrimers G2.0 and G4.0 in D$_2$O at pH 9.

Figure 5.7 Scattering (symbols) and fit (solid lines) from 5 wt% mucin in the absence and in the presence of 0.5 wt% PAMAM dendrimer G2.0 at pH 2 (top), pH 7(middle) and pH 9 (bottom).

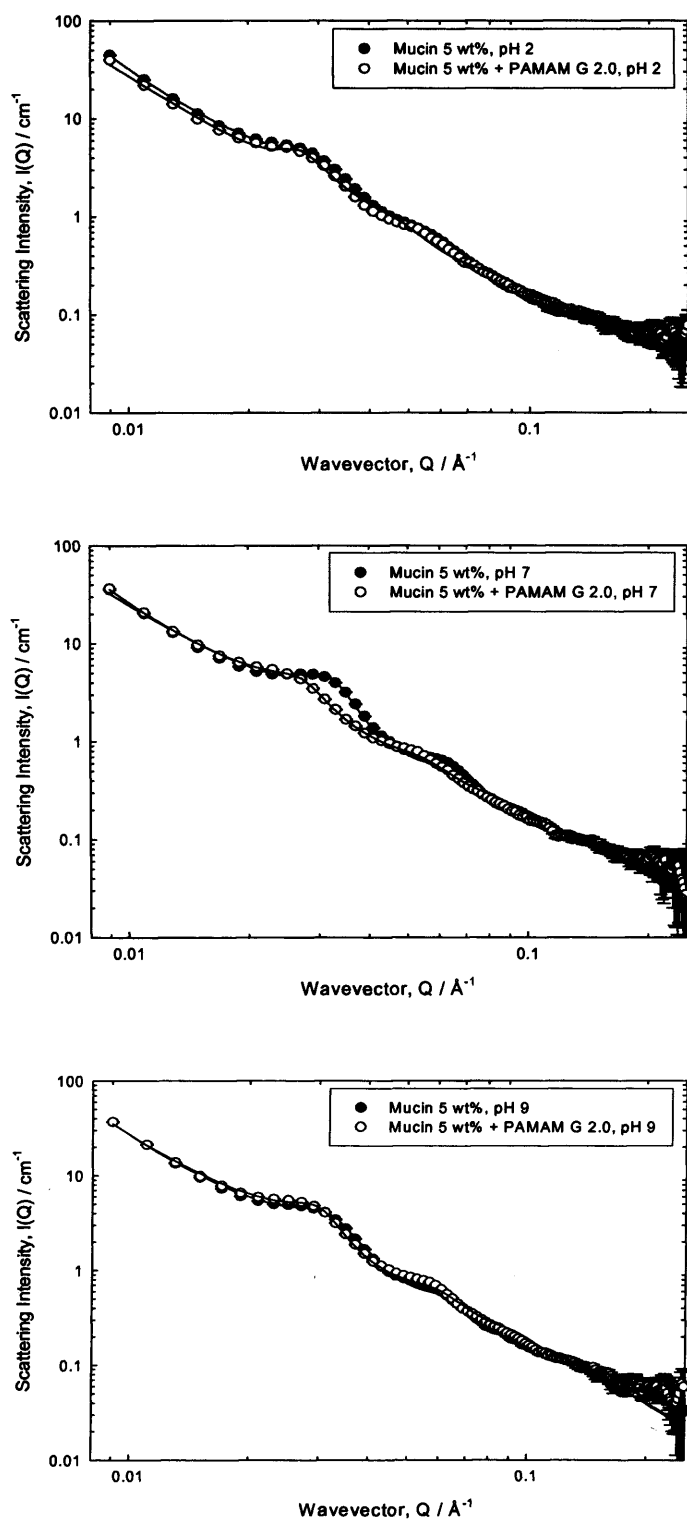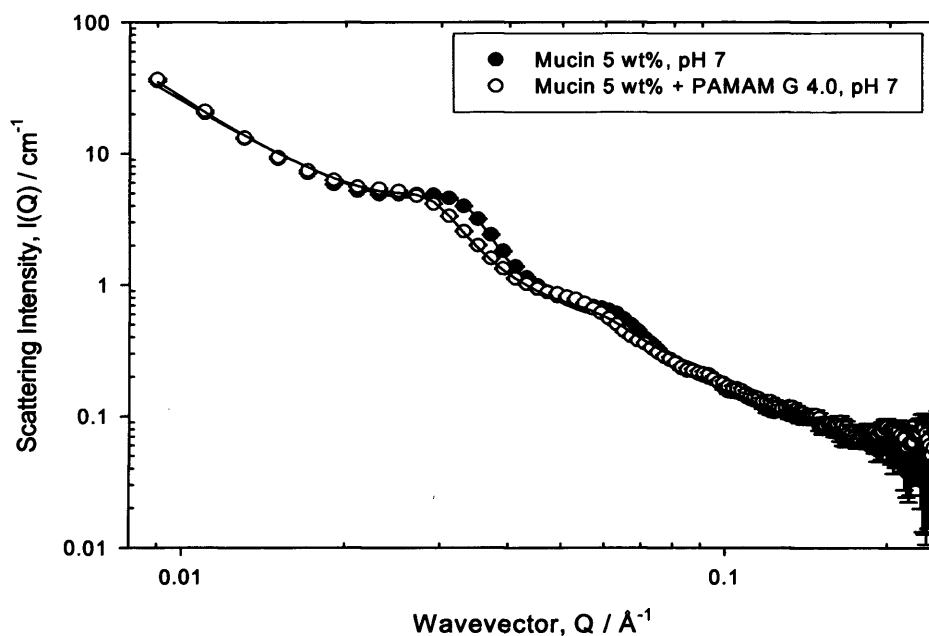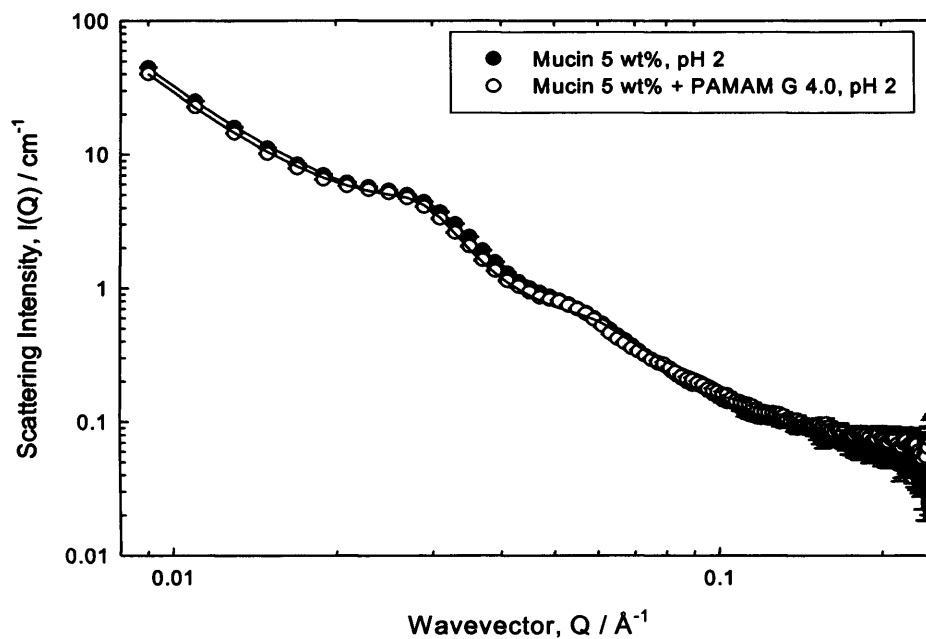*Figure 5.8 Scattering (symbols) and fit (solid lines) from 5 wt% mucin in the absence and in the presence of 0.5 wt% PAMAM dendrimer G4.0 at pH 2 (top) and pH 7 (bottom).*
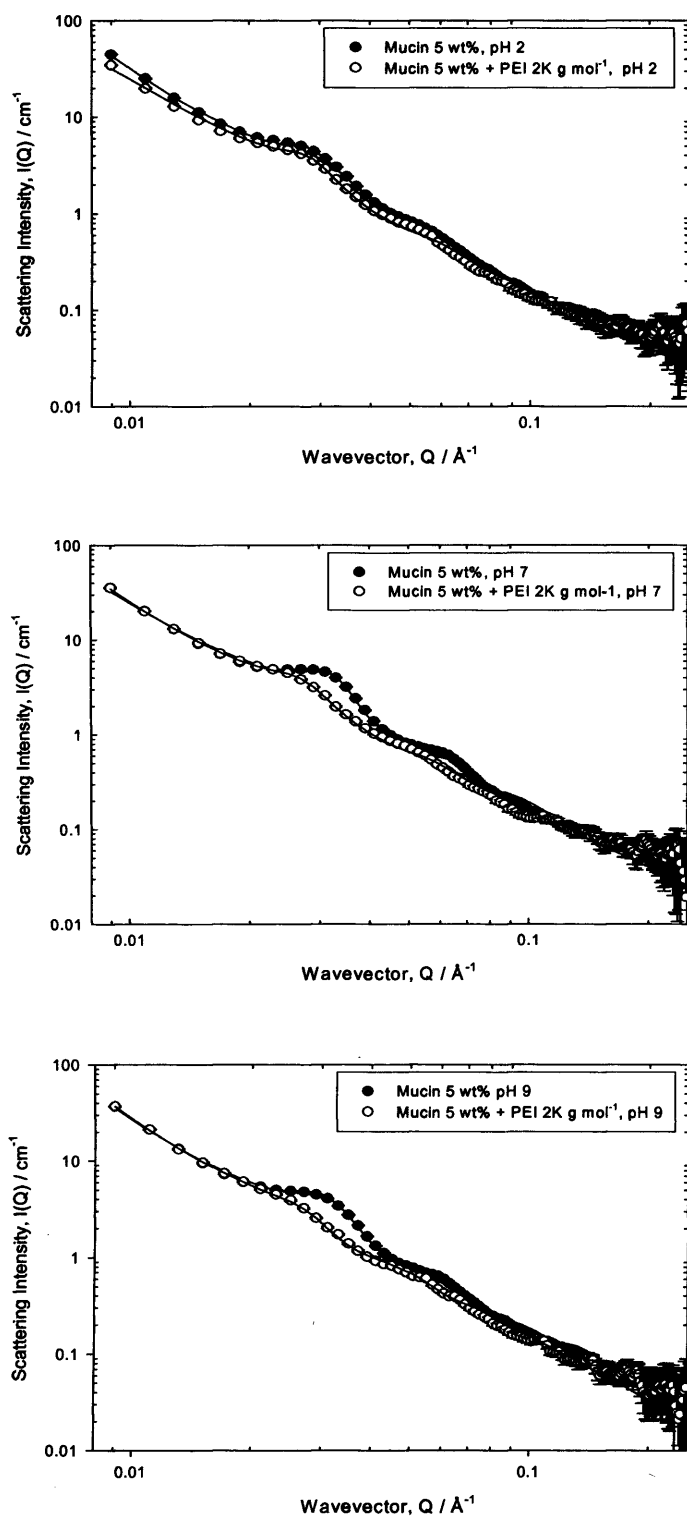
Figure 5.9 *Scattering (symbols) and fit (solid lines) from 5 wt% mucin in the absence and in the presence of 0.5 wt% PEI 2K g mol⁻¹ at pH 2 (top), pH 7 (middle) and pH 9 (bottom).*

Polymer added to mucin 5 wt%	Radius of gyration, R_g (nm)	Correlation length, ξ (nm)	Radius of the globule, R (nm)	Volume fraction, ϕ	Distance between the globule centres, L (nm)
none pH 2	71.0 ± 3.5	41.0 ± 2.0	7.0 ± 0.3	0.34 ± 0.02	141.0 ± 32.4
none pH 7	41.0 ± 2.0	23.5 ± 1.2	9.0 ± 0.5	0.37 ± 0.02	80.0 ± 18.3
none pH 9	43.0 ± 2.2	25.0 ± 1.3	9.0 ± 0.5	0.34 ± 0.02	83.5 ± 19.2
PAMAM G2.0 pH 2	73.0 ± 3.7	42.0 ± 2.1	6.8 ± 0.3	0.38 ± 0.02	144.5 ± 33.2
PAMAM G2.0 pH 7	50.0 ± 2.5	28.0 ± 1.4	9.5 ±0.5	0.36 ± 0.02	98.0 ± 22.5
PAMAM G2.0 pH 9	43.0 ± 2.2	25.0 ± 1.3	9.8 ± 0.5	0.36 ± 0.02	84.5 ± 19.4
PAMAM G4.0 pH 2	71.0 ± 3.5	41.0 ± 2.0	6.7 ± 0.3	0.35 ± 0.02	141.0 ± 32.4
PAMAM G4.0 pH 7	48.5 ± 2.4	28.0 ± 1.4	9.2 ± 0.5	0.35 ± 0.02	95.0 ± 21.8
b-PEI 2K pH 2	73.0 ± 3.6	42.5 ± 2.1	6.6 ± 0.3	0.35 ± 0.02	146.0 ± 33.6
b-PEI 2K pH 7	51.5 ± 2.6	30.0 ± 1,5	10.5 ± 0.5	0.32 ± 0.02	100.5 ± 23.1
b-PEI 2K pH 9	52.0 ± 2.6	30.0 ± 1.5	11.2 ± 0.6	0.31 ± 0.02	102.0 ± 23.5

Table 5.3 Parameters obtained from the model for the scattering from mucin solution 5 wt% in absence and in the presence of a range of 0.5 wt% positively charged polymers at pH 2, 7 and 9.

5.2.1.3. Negatively charged polymers

Compared to the effect of the full generation PAMAM dendrimers G2.0 and G4.0 on the scattering from mucin solutions, the half-generation PAMAM dendrimers G3.5 and G5.5 exhibited a similar modulation of the scattering – as illustrated in Figure 5.10 and 5.11 – but with three notable differences:

(i)   the change in scattering exhibited a rather different pH profile *viz* there was no change induced by the dendrimers at pH 2, but perturbations were evident at pH 7, which became more pronounced at pH 9;

(ii)   the peaks moved in the opposite direction, *i.e.*, towards higher Q values, indicating smaller scatterers and/or a decreasing separation. In the specific case, the position of the main peaks at pH 9 has shifted to 0.035 $Å^{-1}$ and 0.065 $Å^{-1}$, which correspond to distances/sizes of 18.0 nm and 9.7 nm, respectively. This indicates smaller scatterers and/or a decreasing separation of ~ 5-10%;

(iii)   there appears to be slight drop in scattering intensity in the presence of the dendrimer which increases with the strength of the interaction, *i.e.*, it is more pronounced with increasing the pH (no such change was observed in the PAMAM G2.0 and G4.0 cases).

Table 5.3 shows all the parameters obtained from the model and the analysis of the Zimm plots for each mucin 5 wt% sample in the absence and in the presence of the PAMAM dendrimers G3.5 and G5.5 at the pHs considered (pH 2, 7 and 9). While no significant changes in the parameters were recorded for the system 'mucin + PAMAM dendrimer G3.5 (or G5.5)' at pH 2 compared to those observed for the mucin only in solution at the same pH, a strong decrease in the correlation length, radius of gyration and distance between globules was detected when the PAMAM dendrimers were added to the mucin solution at pH 7 and pH 9, as reported in Table 5.3. These alterations, already noticeable at pH 7,

became more pronounced at pH 9. In particular, when the polymers were added to mucin solutions at pH 9, a decrease of ~ 10 % was observed on the radius of gyration and the correlation length of the mucin molecule. These results are in agreement with the shift to higher Q of the main peaks observed in the scattering of mucin in the presence of PAMAM dendrimers G3.5 and G5.5 at pH 9. Again, the shift of the main peaks in the scattering profile is related to a change in the radius of gyration, R_g, and the correlation length, ξ, of the mucin molecule: the more they move to higher Q, the smaller R_g and ξ are.

Therefore, the changes in the scattering from mucin due to the presence of the negatively charged PAMAM dendrimers resulted mainly pH-dependent and clearly indicated an interaction between these 'probe' polymers and mucin.
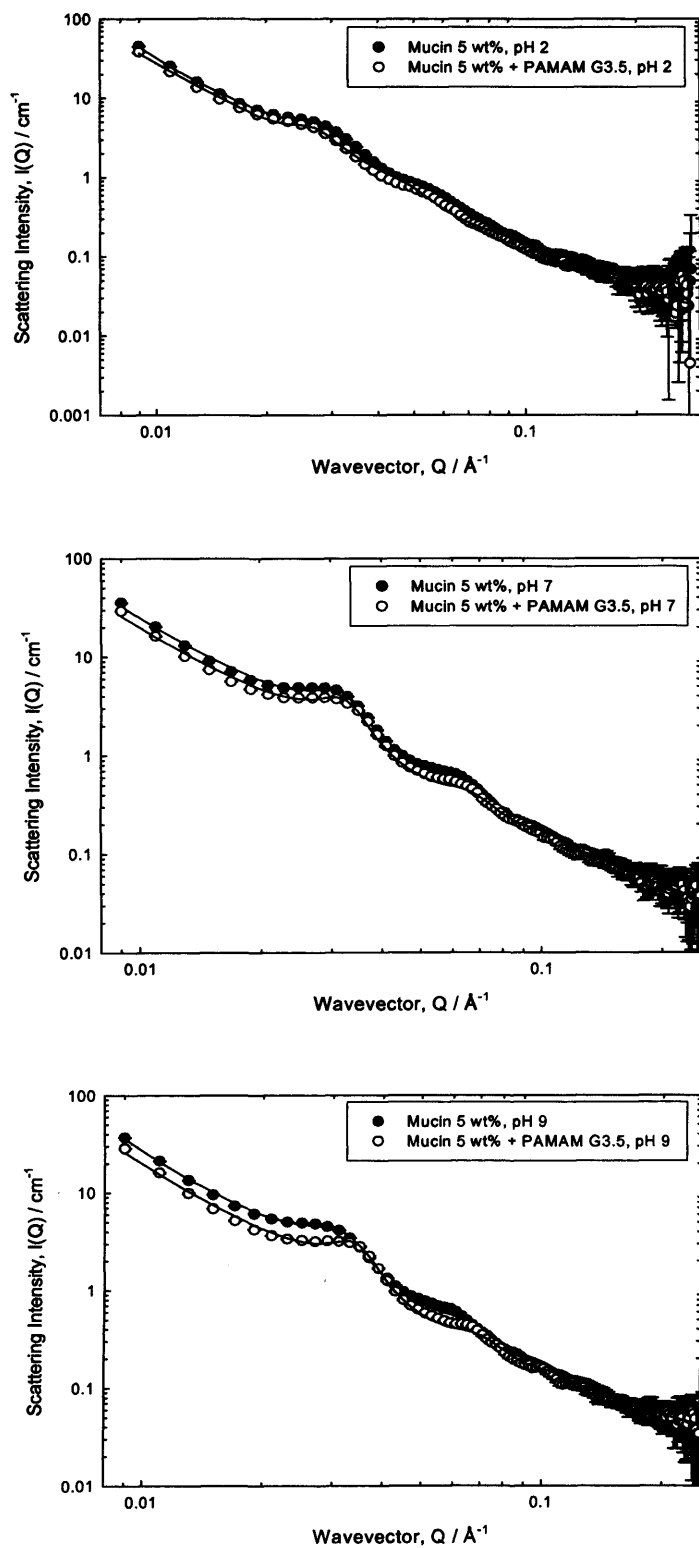
Figure 5.10 *Scattering (symbols) and fit (solid lines) from 5 wt% mucin in the absence and in the presence of 0.5 wt% PAMAM dendrimer G3.5 at pH 2 (top), pH 7 (middle) and pH 9 (bottom).*
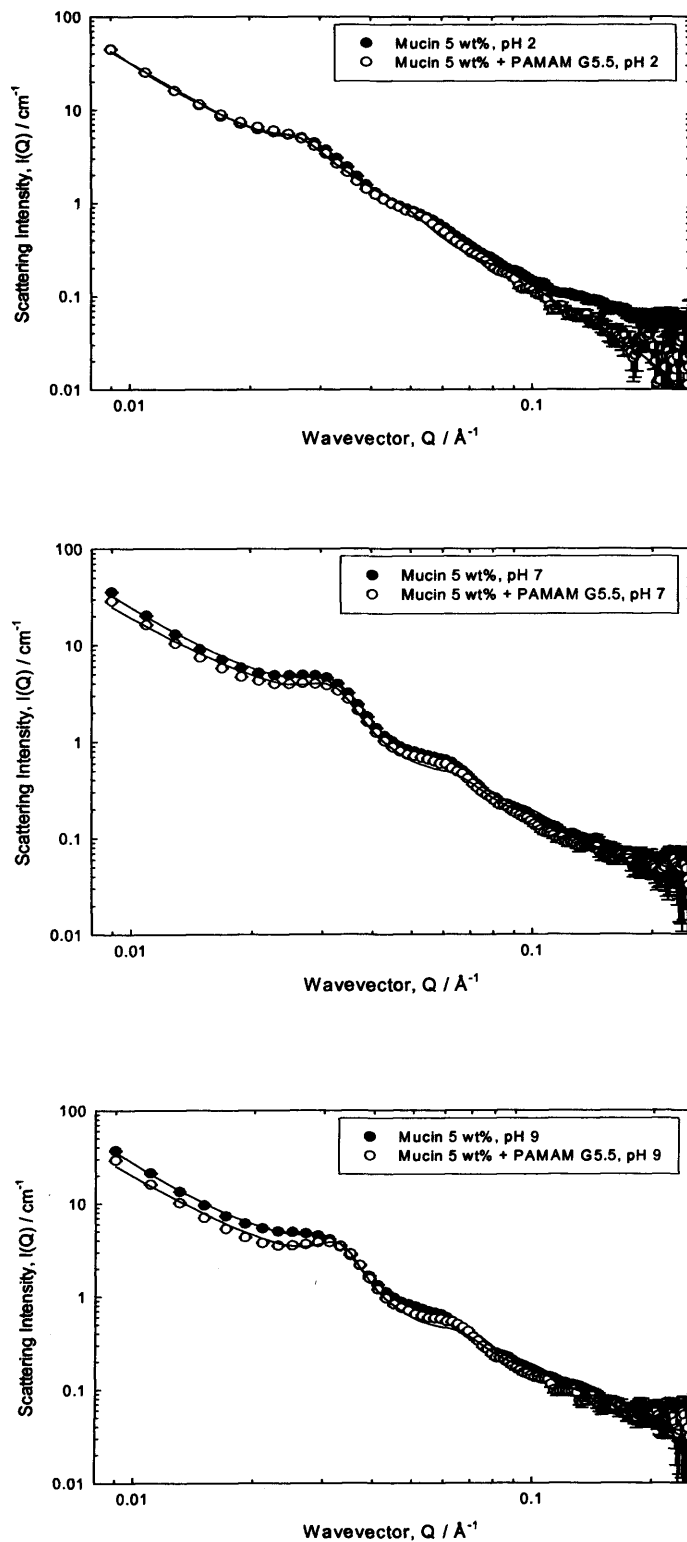
Figure 5.11 Scattering (symbols) and fit (solid lines) from 5 wt% mucin
in the absence and in the presence of 0.5 wt% PAMAM dendrimer G5.5 at
pH 2 (top), pH 7 (middle) and pH 9 (bottom).

Polymer added to mucin 5 wt%	Radius of gyration, R_g (nm)	Correlation length, Ξ (nm)	Radius of the globule, R (nm)	Volume fraction, ϕ	Distance between the globule centres, L (nm)
none pH 2	71.0 ± 3.5	41.0 ± 2.0	7.0 ± 0.3	0.34 ± 0.02	141.0 ± 32.4
none pH 7	41.0 ± 2.0	23.5 ± 1.2	9.0 ± 0.5	0.37 ± 0.02	80.0 ± 18.3
none pH 9	43.0 ± 2.2	25.0 ± 1.3	9.0 ± 0.5	0.34 ± 0.02	83.5 ± 19.2
PAMAM G3.5 pH 2	71.5 ± 3.6	41.0 ± 2.0	6.6 ± 0.3	0.36 ± 0.02	142.0 ± 32.7
PAMAM G3.5 pH 7	38.0 ± 2.0	22.0 ± 1.1	8.9 ± 0.4	0.38 ± 0.02	74.0 ± 17.0
PAMAM G3.5 pH 9	36.0 ± 1.8	21.0 ± 1.1	8.9 ± 0.4	0.38 ± 0.02	70.0 ± 16.1
PAMAM G5.5 pH 2	71.0 ± 3.5	41.0 ± 2.0	6.6 ± 0.3	0.34 ± 0.02	141.0 ± 32.4
PAMAM G5.5 pH 7	38.0 ± 2.0	22.0 ± 1.1	8.9 ± 0.4	0.37 ± 0.02	74.0 ± 17.0
PAMAM G5.5 pH 9	37.0 ± 1.8	21.0 ± 1.1	8.7 ± 0.4	0.40 ± 0.02	71.5 ± 16.4

Table 5.3 *Parameters obtained from the model for the scattering from mucin solution 5 wt% in the absence and in the presence of a range of 0.5 wt% negatively charged polymers at pH 2, 7 and 9.*

127

5.2.2. PGSE-NMR results

The same 'probe' polymers tested in mucin solutions by SANS have been investigated by PGSE-NMR. Diffusion NMR provided a complementary indication of any interaction via the mobility of the 'probe' polymers within the mucin solution. The diffusion of these polymers (at fixed polymer concentration, 0.5wt%) has been examined in a range of mucin solutions (0 ≤ [mucin] ≤ 5wt%) at 37 °C.

All polymers showed a decrease in the diffusion rate with increasing mucin concentration. Therefore, it is important to separate the effects of any specific interactions (*e.g.*, binding) from that arising due to simple obstruction, namely that the 'probe' polymers have to diffuse around the mucin and there is the associated increase in diffusion path-length. Additionally, there is the complication that the 'probe' polymers are inherently of different molecular weights and this will also affect their absolute diffusion rates.

5.2.2.1. Uncharged polymers

The diffusion of a series of uncharged 'probe' polymers – including PEGs with different molecular weights and structure, dextrin – in mucin solutions has been studied.

Diffusion data of *l*-PEG10K and *l*-PEG100K in mucin solutions are presented in Figure 5.12: the top graph shows the absolute self-diffusion coefficients of these polymers in mucin solutions; the same data normalized to the measured self-diffusion coefficient of the PEGs in free solution (*i.e.*, when [mucin] = 0 wt%) are illustrated in the bottom graph. The normalized self-diffusion coefficient, $\dfrac{D_s}{D_0}$, corresponds to the ratio between the self-diffusion coefficient of the polymer in mucin solution (at the specific mucin concentration), D_s, over the self-diffusion coefficient of the polymer in free solution, D_0.

The diffusion of both *l*-PEG10K and *l*-PEG100K decrease with increasing mucin concentration. Since the self-diffusion coefficient D_s is proportional to the inverse of the radius of gyration R_g, $D_s \propto \dfrac{1}{R_g}$, and the radius of gyration is proportional to the inverse of the root squared of the molecular weight M_w, $R_g \propto \dfrac{1}{\sqrt{M_w}}$, for [mucin] = 0, $D_s^{(10K)} > D_s^{(100K)}$ of a factor of 3.5, which is consistent with the 10x decrease in molecular weight. The normalized diffusion data should, at least to a first approximation, remove the inherent effect of molecular weight and permit a comparison of the retardation induced by the mucin.

The normalized self-diffusion coefficients of *b*-PEG20K, *l*-PEG50K and dextrin 50K are displayed in Figure 5.13. Although the difference in molecular weight, the diffusion behaviour of the *b*-PEG20K and *l*-PEG50K in mucin solution looks similar: the reason could be due to the different architecture of the two 'probe' polymers – branched for the PEG20K and linear for the PEG50K – which slows down the diffusion of the *b*-PEG20K in mucin to a degree comparable to the diffusion of the *l*-PEG50K in mucin.

In contrast, even if the *l*-PEG50K and the dextrin 50K have the same molecular weight, the bulkier and more rigid structure of the dextrin together with its glycosydic chemical composition (which could lead to some affinity to the glycosydic chain of the mucin molecule) makes the dextrin diffusing in mucin to a lower rate compared to the *l*-PEG50K because more sterically hindered.
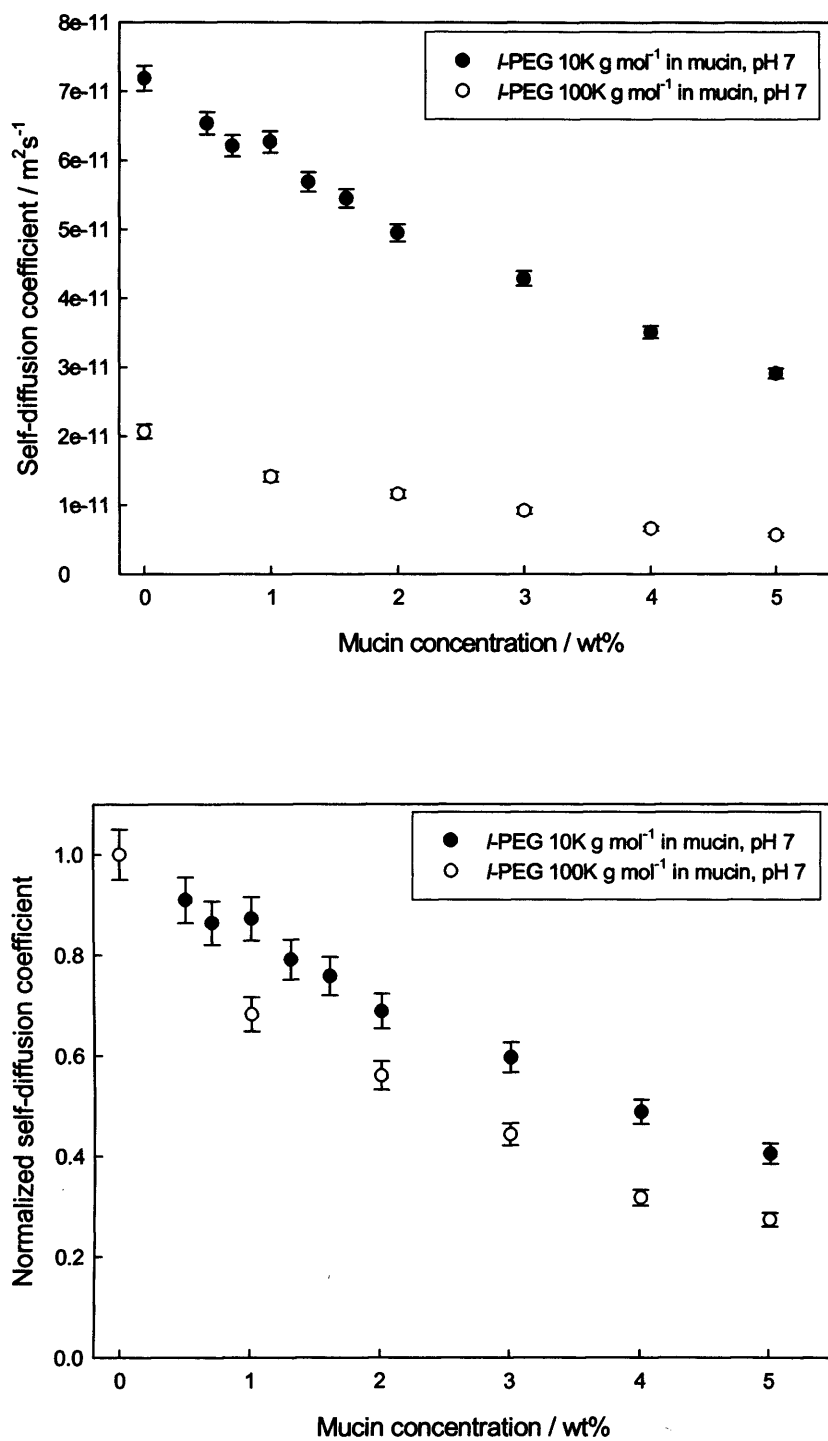
Figure 5.12 *Absolute (top) and normalized (to [mucin] = 0) (bottom) self-diffusion coefficients of l-PEG 10K g mol⁻¹ and l-PEG 100K g mol⁻¹ in mucin solutions at pH 7.*
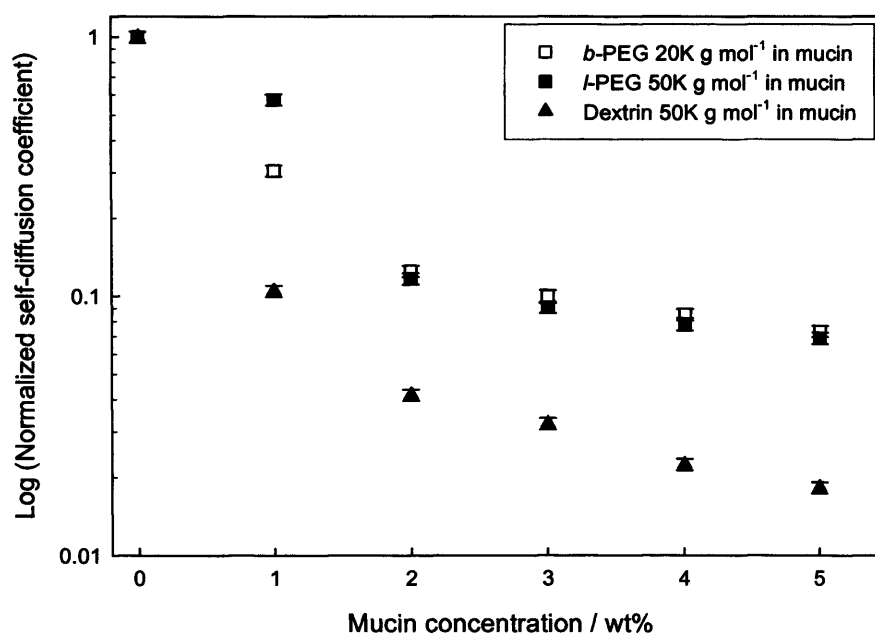
Figure 5.13 *Normalized (to [mucin] = 0) self-diffusion coefficients of l-PEG 50K g mol^1, b-PEG 20K g mol^1 and dextrin 50K g mol^1 in mucin solutions at pH 7.*

5.2.2.2. Positively charged polymers

Compared to the diffusion of the PEGs in mucin where a more linear trend could be identified (Figure 5.12), the diffusion of the PAMAM dendrimers (Figure 5.14) as well as of the *b*-PEI2K (Figure 5.15) in mucin solution showed a rapid decrease in rate when increasing the mucin concentration until a plateau is reached, suggesting a retardation of the 'probe' polymer from the mucin network.

Moreover, the normalized diffusion data of PAMAM G2.0 and G4.0 in mucin solutions showed a complex pH-dependence, in a fashion reminiscent of the characteristic profile observed in the SANS experiment. In particular, the data revealed a higher diffusion rate in mucin solutions at pH 9 (Figure 5.14, top graph) when compared to the diffusion of these probe polymers in mucin at pH 7 (Figure 5.14, bottom graph), suggesting that the same complex pH-dependent interaction between the dendrimers and the mucin is observable in the diffusion data. Therefore, supporting the SANS data, from the diffusion data is clear that a strong interaction between the PAMAM G2.0 and G4.0 and the mucin takes place at pH 7 and no relevant interaction can be considered at pH 9.

Further, the diffusion of *b*-PEI2K was strongly retarded in mucin, interpreted as a strong interaction between the PEI and the mucin (Figure 5.15). A manifestation of this strength of interaction was the short "shelf-life" of *b*-PEI25K/mucin samples, which phase separated after just a few hours.

Figure 5.14 Normalized self-diffusion coefficients of PAMAM dendrimer G2.0 and G4.0 at pH 9 (top) and pH 7 (bottom) in mucin solutions.
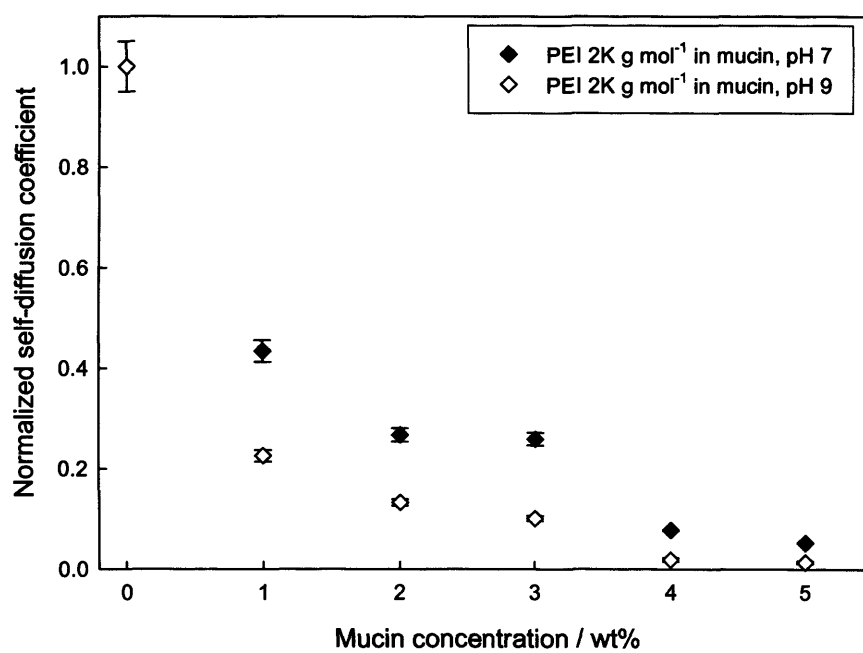
Figure 5.15 Normalized self-diffusion coefficients of b-PEI 2K g mol^{-1} at pH 9 and pH 7 in mucin solutions.
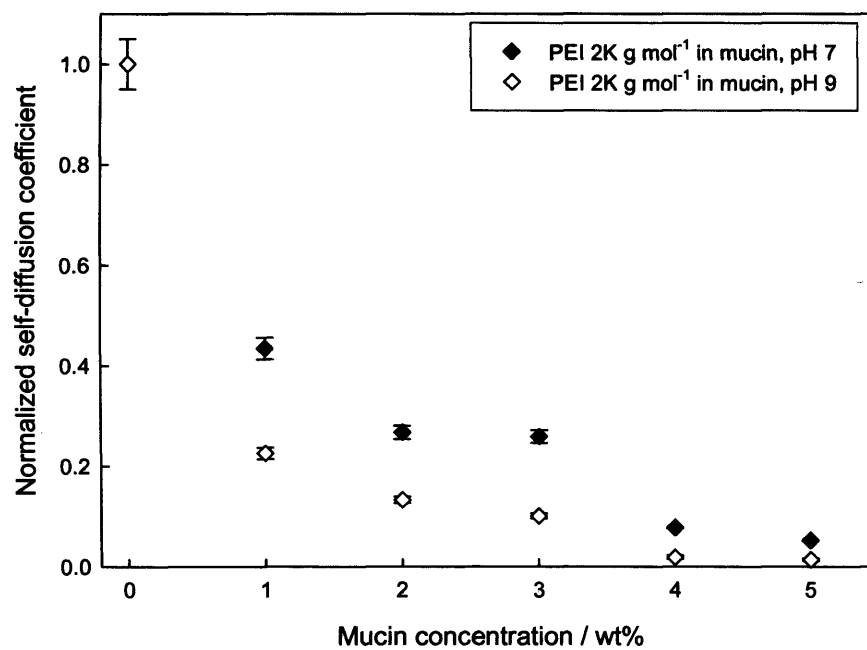
Figure 5.15 *Normalized self-diffusion coefficients of b-PEI 2K g mol-1 at pH 9 and pH 7 in mucin solutions.*

5.2.2.3. Negatively charged polymers

The normalized diffusion data of the half-generation PAMAM dendrimers G3.5 and G5.5 in mucin solutions exhibit a rapid decrease while increasing the mucin concentration, after which a very slow decrease correspond to an increase in mucin concentration (Figure 5.16). The diffusion data of these 'probe' polymers in mucin solutions revealed a pH-dependent behaviour similar to the one observed for the SANS experiment: in fact, the diffusion of the half-generation PAMAM dendrimers showed a higher rate at pH 7 (Figure 5.16, bottom graph) than at pH 9 (Figure 5.16, top graph). Supported by the SANS experiment, the diffusion data suggested that an interaction between the PAMAM dendrimers occurs and that it is stronger at pH 9 than at pH 7.
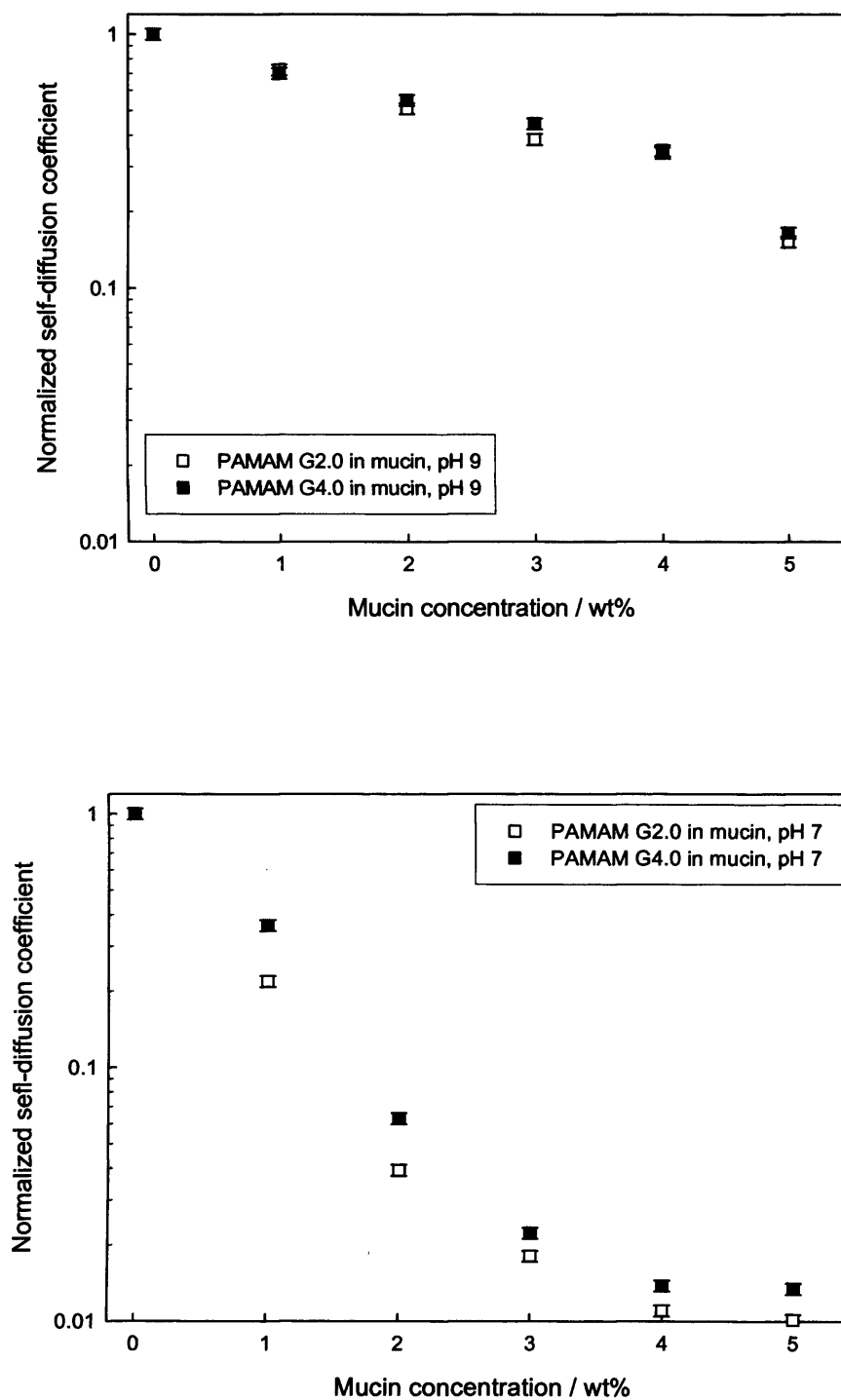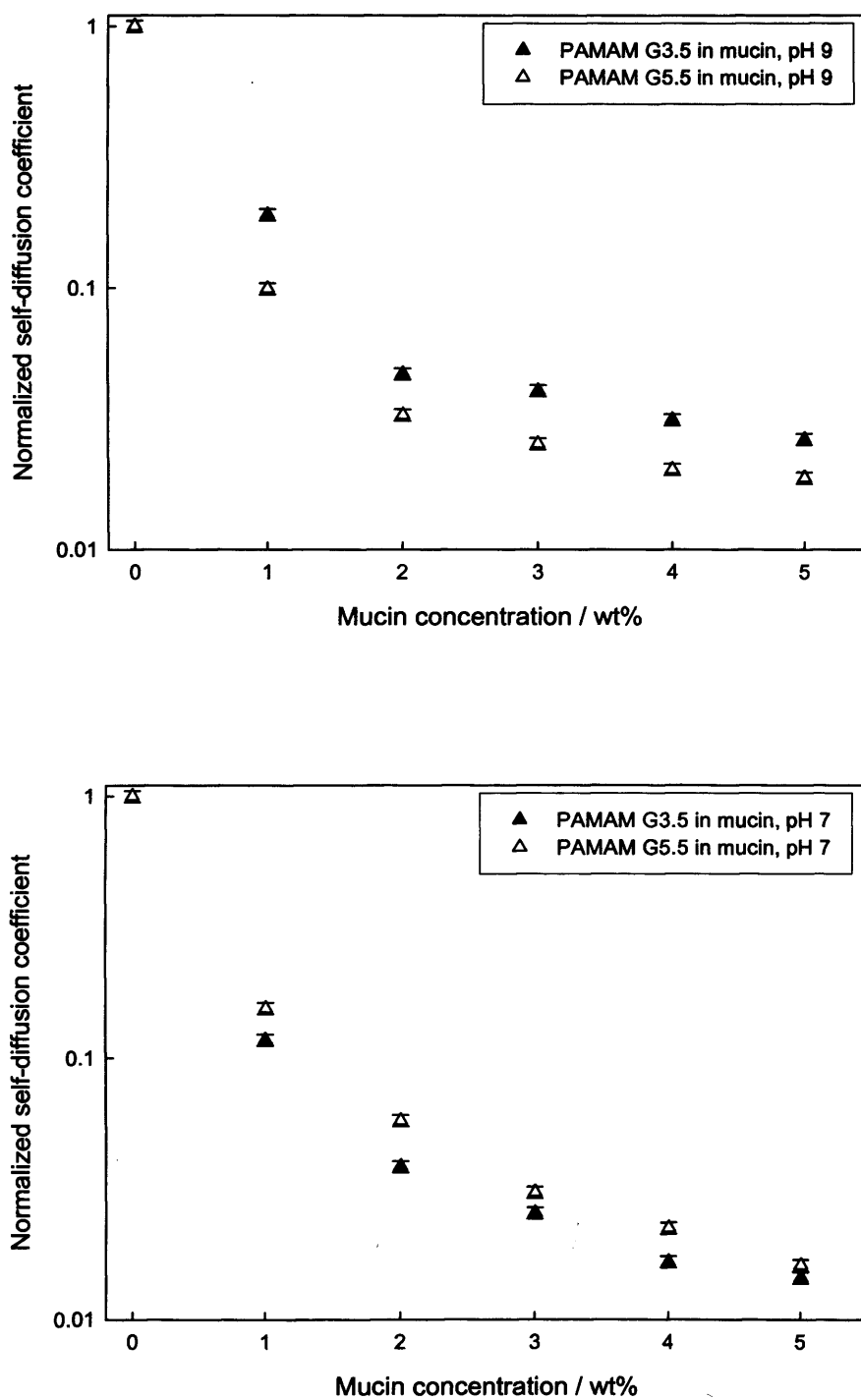
Figure 5.16 Normalized self-diffusion coefficients of PAMAM dendrimer
G3.5 and G5.5 at pH 9 (top) and pH 7 (bottom) in mucin solutions.

5.2.3. Viscosity results

Together with SANS and PGSE-NMR, measuring the viscosity of mucin-'probe' polymer solutions can provide further information on the behaviour of these polymers within mucin solutions.

The viscosity data of mucin solutions over a range of concentration, 0.1 wt% ≤ [Mucin] ≤ 5 wt%, in the presence and in the absence of 0.5 wt% *l*-PEG 10K g mol^{-1} and 0.5 wt% PAMAM dendrimer G2.0 at pH 7 and 9 are showed in Figure 5.17.

However, a clearer view of the mucin-'probe' polymer solutions viscosity behaviour is given by the relative viscosity values, $\frac{\eta_{mucin+'probe'polymer}}{\eta_{mucin}}$: in fact, the relative viscosity reflects the effect of the 'probe' polymer on the viscosity of mucin without taking into account the increase in viscosity due to the increase of mucin concentration.

The relative viscosity from mucin solutions (0.1 wt% ≤ [mucin] ≤ 5 wt%) on the addition of the 0.5 wt% *l*-PEG 10K g mol^{-1}, $\frac{\eta_{mucin+PEG}}{\eta_{mucin}}$, showed no relevant changes as illustrated in Figure 5.18. The relative viscosity values resulted equal to $\frac{\eta_{mucin+PEG}}{\eta_{mucin}} = 1.04 \pm 0.03$ over the entire mucin concentration range, indicating that the 'probe' polymer contribution to the viscosity of mucin was irrelevant.

In contrast, the pH-dependent interaction showed by the PAMAM dendrimers G2.0 with mucin solutions was confirmed by the relative viscosity data as illustrated in Figure 5.19. The relative viscosity from mucin solutions (0.1 wt% ≤ [mucin] ≤ 5 wt%) on the addition of the 0.5 wt% PAMAM dendrimer G2.0, $\frac{\eta_{mucin+PAMAMG2.0}}{\eta_{mucin}}$, exhibited an interesting trend when solutions were measured at pH 7 (Figure 5.19, top graph): the relative viscosity showed an initial rapid decrease followed by a slow

increase. This behaviour can be interpreted as a 'titration' of the fixed concentration of the PAMAM dendrimer (0.5 wt%) with an increasing concentration of mucin solution (0.1 wt% ≤ [mucin] ≤ 5 wt%): initially the concentration of mucin is low (lower than 1 wt%) compared to the concentration of the PAMAM dendrimer (0.5 wt%); therefore, the mucin tends to interact strongly with the PAMAM leading to a rapid decrease in viscosity. When the mucin concentration increases ([mucin] ≥ 1 wt%), a slow increase in viscosity is observed which can be mainly attributed to the increase in mucin concentration: thus, it is like if the PAMAM molecules have been already saturated by mucin molecules when mucin concentration is greater than 1 wt%.

When performing the measurements at pH 9, the relative viscosity showed no relevant changes (Figure 5.19, bottom graph), and the relative viscosity values resulted equal to $\dfrac{\eta_{mucin+PAMAMG2.0}}{\eta_{mucin}} = 0.88 \pm 0.03$ over the entire mucin concentration range.

The viscosity data resulted in agreement with the SANS and PGSE-NMR experiments: in fact, the presence of uncharged polymers such as *l*-PEG 10K did not affect greatly the viscosity of mucin solutions while positively charged polymer like the PAMAM dendrimer G2.0 exhibited a complex pH-dependent behaviour, implying an interaction between the PAMAM and the mucin at pH 7.
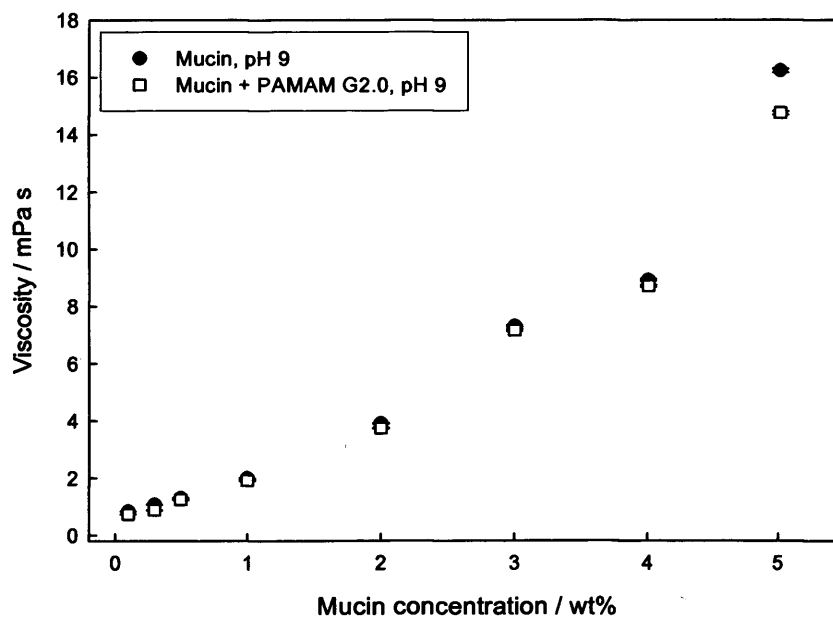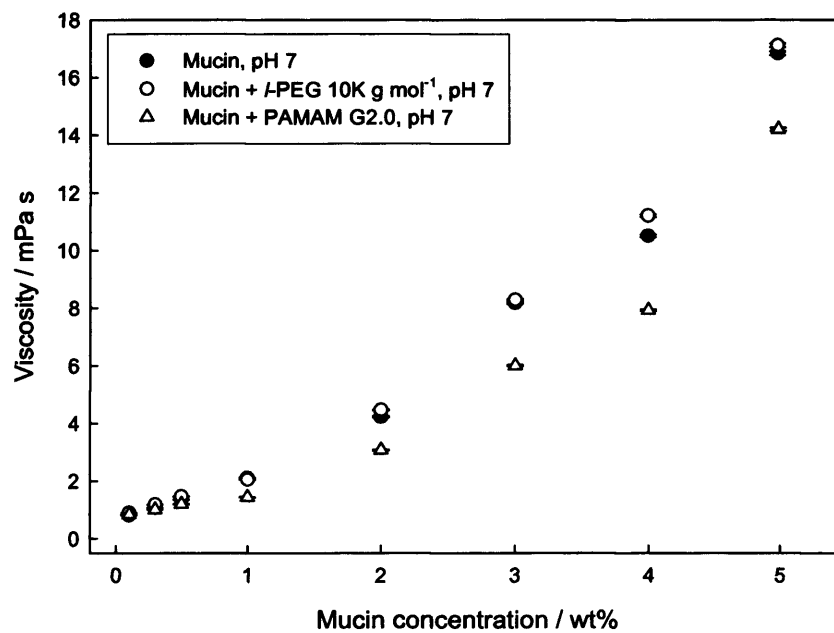
Figure 5.17 *Viscosity of mucin solutions in the presence and absence of 0.5 wt% l-PEG 10K g mol⁻¹ and 0.5 wt% PAMAM dendrimer G2.0 at pH 7 (top) and pH 9 (bottom).*
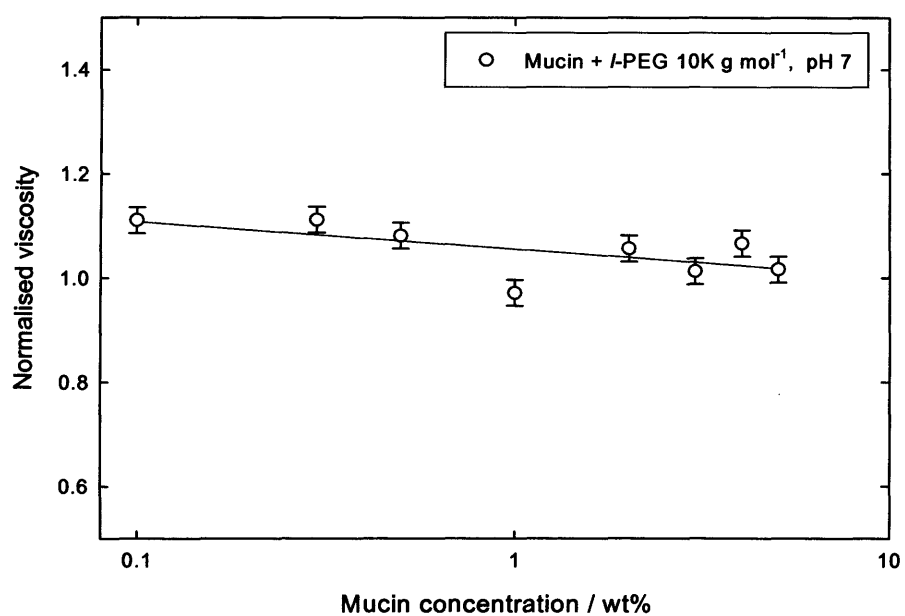
Figure 5.18 *Relative viscosity for mucin solutions in the presence of 0.5 wt% l-PEG 10K g mol⁻¹ at pH 7.*
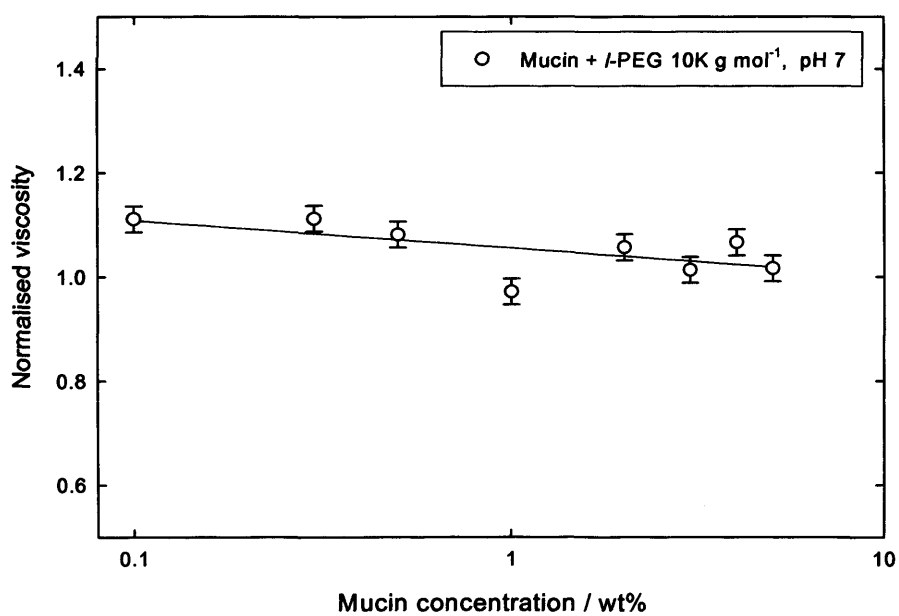
Figure 5.18 *Relative viscosity for mucin solutions in the presence of 0.5 wt% l-PEG 10K g mol⁻¹ at pH 7.*
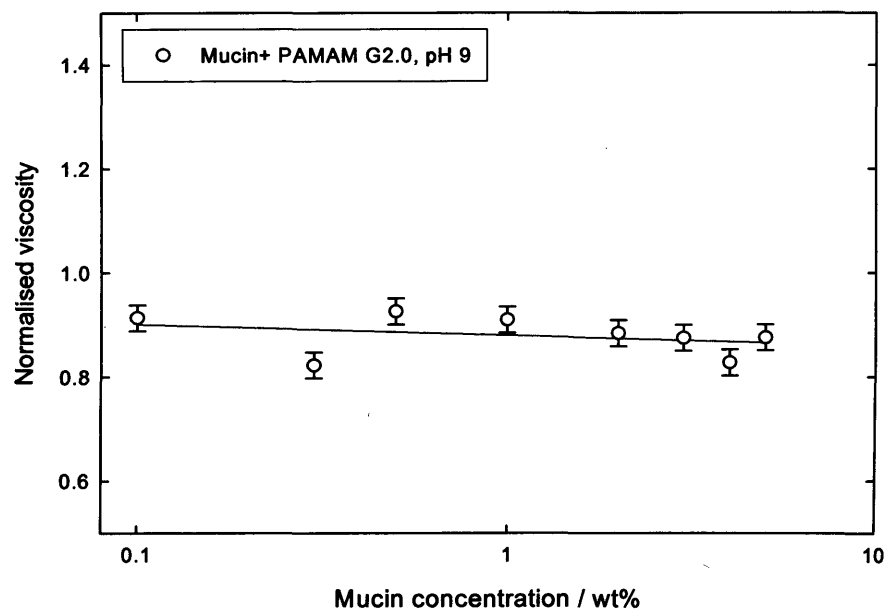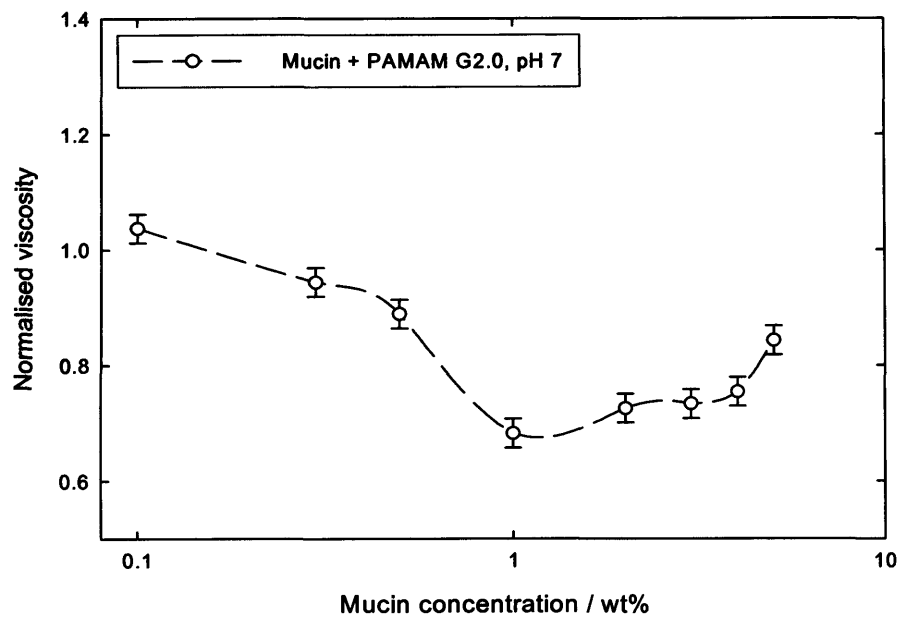
Figure 5.19 *Relative viscosity for mucin solutions in the presence of 0.5 wt% PAMAM dendrimer G2.0 at pH 7 (top) and pH 9 (bottom).*

5.3. Discussion

For all the 'probe' polymer-mucin samples explored, the SANS and PGSE-NMR experiments together with the viscosity measurements gave a complementary insight into the interaction of the probe polymer with the mucin.

The non-ionic polymers (*l*-PEG10K, *l*-PEG100K, *b*-PEG20K, *l*-PEG50K, dextrin 50K) displayed a behaviour consistent with there being no interaction with the mucin: there was no change in the scattering profile and the viscosity of mucin was not affected by the presence of these polymers, in agreement with what found by Huang *et al.* [35]. Therefore, one may conclude that the moderate retardation in the diffusion arises simply due to the obstruction effect, which originates from the fact that the 'probe' polymers have to diffuse around the mucin and there is the concomitant increase in the path-length of the diffusing species[36]. Indeed, the diffusion of probe molecules can be affected by the polymer matrix [37, 38] and, in the specific case, PEG molecules can be retarded by obstruction effects exerted by the mucin matrix. A study by Lafitte *et al.* [8] on the effect of PGM on the diffusion of a series of PEGs as function of pH, ionic strength and temperature demonstrated that pH imparted a stronger impact on the PEGs diffusion rate compared with that due to ionic strength and temperature. The results reflected the underlying changes in mucin network homogeneity, flexibility and viscosity, which enhanced the diffusion of the probes when increasing a pH-dependent flexibility of the mucin network, with the mucin molecules being more flexible at pH 7 than at lower pH.

In analyzing the diffusion of a series of PEGs with different molecular weights, there is the obvious molecular weight dependence to consider when discussing the absolute diffusion rates of the non-ionic 'probe' polymers in mucin, but the normalized diffusion rates suggested no specific molecular weight dependent interaction with mucin. However, a similar study on the self-diffusion of PEGs and dextran in cartilage

conducted by Trampel *et al.* [11] reported that the non-specific obstruction effect of the collagenous network of cartilage together with the molecular weights of the polymers were the main responsible reasons for the restricted diffusion experienced by the polymers.

Despite some studies have shown that PEG can be muchoadhesive, presumably by interpenetrating polymer network (IPN) effects between PEG chains and the mucus mesh [39-44] and/or hydrogen bonding between ether oxygen atoms in PEG and sugars on glycosylated mucins [45-47], Lai *et al.* [48, 49] demonstrated that low molecular weight PEG and high (dense) PEG surface coverage are both required for rapid mucus penetration of PEG-coated particles. Indeed, PEG-coated particles demonstrated a reduced hydrophobic interactions, hydrogen bonding and IPN effects with mucin. However, the hydrogen bonding interactions between the PEG and the mucin discussed by Efremova *et al.* [45] was pH-dependent, with the adhesion being considerably higher at pH 2 than pH 7.

The PAMAM dendrimers experienced a significant retardation in their diffusion within the mucin solutions – sometimes close to an order of magnitude – but under conditions where the PAMAM and mucin bore opposite charge. Concomitantly, there was a movement of the peak in the SANS data to lower Q, related to an increase of ~ 18-20 % on the radius of gyration, R_g, and the correlation length, ξ, of the mucin molecule: clearly, the interaction between the mucin and the PAMAM dendrimers at pH 7 gave rise to a larger feature in which the mucin molecule – mainly the glycosylated spacer – "wraps" around the dendritic polymers, expanding the mucin network. This mechanistic insight observed at pH 7 was supported also by the viscosity data: in fact, a major reduction in the viscosity of mucin due to the addition of the PAMAM dendrimer is observed up to mucin 1 wt%; when increasing the mucin concentration up to 5 wt%, the mucin network is saturated by the PAMAM dendrimers and the small increase in the viscosity can be mainly attributed to the increase of mucin concentration.

Changing the pH (pH 2 and pH 9) to reverse the charge on either mucin or 'probe' polymer, "turned off" the interaction. This effect was visible from: (i) the diffusion data, where the PAMAM dendrimers exhibited a higher diffusion rate in mucin at pH 9 than at pH 7; (ii) the scattering data, where no significant change was observed in the scattering from mucin when the PAMAM dendrimers were added to the mucin solutions; (iii) the viscosity data, since no relevant change in the viscosity of mucin were recorded due to the presence of the PAMAM dendrimers. Therefore, the mechanism of interaction appears to be driven by electrostatic interactions [36].

For the amino terminated PAMAMs (G2.0 and G4.0) at pH = 7, the amine groups are largely protonated (positively charged) [50] while the mucin glycoprotein is deprotonated and negatively charged – *via* the carboxylate acid groups of the protein backbone (pKa ~ 3.9 - 4.1) and the side groups of sialic acid (pKa ~ 2.6) [51], sulfated glucosamine and galactoamines (pKa ~ 1) [52] – leading to the observed strong electrostatic interaction. The peak in the scattering moves to lower Q values, indicating that the separation of the scattering centres has increased of ~15-20%. SANS parameters mainly affected are the radius of gyration, R_g, the correlation length, ξ, and the distance between the globules, L, in the mucin molecule. The addition of PAMAM dendrimer G2.0 to mucin solutions at pH 7 caused an increase of: (i) the radius of gyration from 41.0 nm (mucin only) to 50.0 nm (mucin + PAMAM G2.0); (ii) the correlation length from 23.5 nm to 28.0 nm; (iii) the distance between the globules from 80.0 nm to 98.0 nm. It is hypothesized that the reason of this increase is because the PAMAM binds electrostatically to the oppositely charged mucin monosaccharide side-chains, causing their collapse and perceived dilution (further apart). In Waigh's model [53], this would suggest the glyscoylated spacer had become more extended, pushing the globules further apart. At pH = 2, the amine groups are completely protonated (positively charged) but the mucin is also partially positively charged (IEP = 2 - 3) [54-56], and accordingly, no interaction is observed.

The fact that the scattering from mucin was stronger affected by the *b*-PEI2K than by the PAMAM dendrimers could be due to a charge density that, in the case of PEI2K is one order of magnitude higher compared to the PAMAM dendrimer one.

The effect of positively charged surfactants on proteins such as bovine serum albumin (BSA) has been investigated by Gull *et al.* [23] showing by SANS that the binding of cationic surfactants to proteins disrupt the native structure of the protein. Earlier studies on mucus by scanning electron microscopy [57] and atomic force microscopy [58] demonstrated that the addition of cationic polymers – *i.e.*, poly(vinyl pyridine), chitosan – altered the mucin fiber network caused by electrostatic interactions between the polymer and the mucin molecules, generating a gel with regions of aggregated fibers.

In contrast, for the half generation PAMAMs (G3.5 and G5.5) at pH = 7, the terminating carboxylic acid groups are already moderately deprotonated (*i.e.*, negatively charged) and the mucin is also negatively charged, surprisingly an interaction is still observed. This interaction becomes more pronounced at pH = 9, *i.e.*, where the negative charge on the mucin is further increased. Indeed, at pH 9 the peak in the SANS pattern has moved to higher Q, resulting in a decrease of ~ 10 % on the radius of gyration, R_g, the correlation length, ξ, and the distance between the globules, L, in the mucin molecule: this indicates that the separation of scattering centres has decreased. The addition of PAMAM dendrimer G3.5 to mucin solutions at pH 9 has definitely caused a decrease of: (i) the radius of gyration from 43.0 nm (mucin only) to 36.0 nm (mucin + PAMAM G3.5); (ii) the correlation length from 25.0 nm to 21.0 nm; (iii) the distance between the globules from 83.5 nm to 70.0 nm. Supported by the SANS experiments, also the diffusion data suggested that an interaction between the PAMAM dendrimers 3.5 and 5.5 and mucin occurs: this interaction appears to be stronger at pH 9 rather than at pH 7 since the diffusion of the PAMAM dendrimers 3.5 and 5.5 in mucin are more retarded at pH 9 than at pH 7.

Clearly, a different mechanism is operating in the full and half- generation PAMAMs. The origin of the interaction in the half generation PAMAMs is most likely to be hydrogen bonds between the charged carboxylic acid groups on the PAMAM and the sugar residues on the monosaccharide side-chains. The decrease in the separation may occur via a number of mechanisms – the collapse of the glysosylated spacer in Waigh's model [53] – driven presumably by the PAMAM inducing bridging between adjacent saccharide structures. No interaction is observed at pH 2 where the PAMAM is fully protonated (*i.e.*, no charge is bore) and no hydrogen bonding can take place between the carboxylic acid groups on the PAMAM and the sugar residues on the monosaccharide side-chains. However, Willis *et al.* [57] reported that the presence of anionic polymer such as the poly(acrylic acid) had a little effect on the structure of mucin from a scanning electron microscopy analysis.

A summary of the PGSE-NMR study performed on the wide family of 'probe' polymers with mucin solutions is presented in Figure 5.20. The results of this large study are illustrated in the bar-chart representation, where the normalized self-diffusion coefficients have been tabulated at one representative mucin concentration, 3 wt%. The unshaded bars correspond to those systems for which SANS confirmed the lack of an interaction whereas the shaded bars correspond to the interacting systems. The non-interactive systems demonstrated a reduction in the diffusion of the 'probe' polymer in mucin of 40% when compared to the diffusion of the polymer in free solution (*i.e.*, [mucin] = 0); in the interactive systems the reduction in the diffusion rate resulted of 90%. This relevant difference can be explained considering simply an obstruction effect in limiting the diffusion of the non-interactive 'probe' polymers in the mucin network, while a more specific electrostatic interaction binds the interactive 'probe' polymers to the mucin molecules.
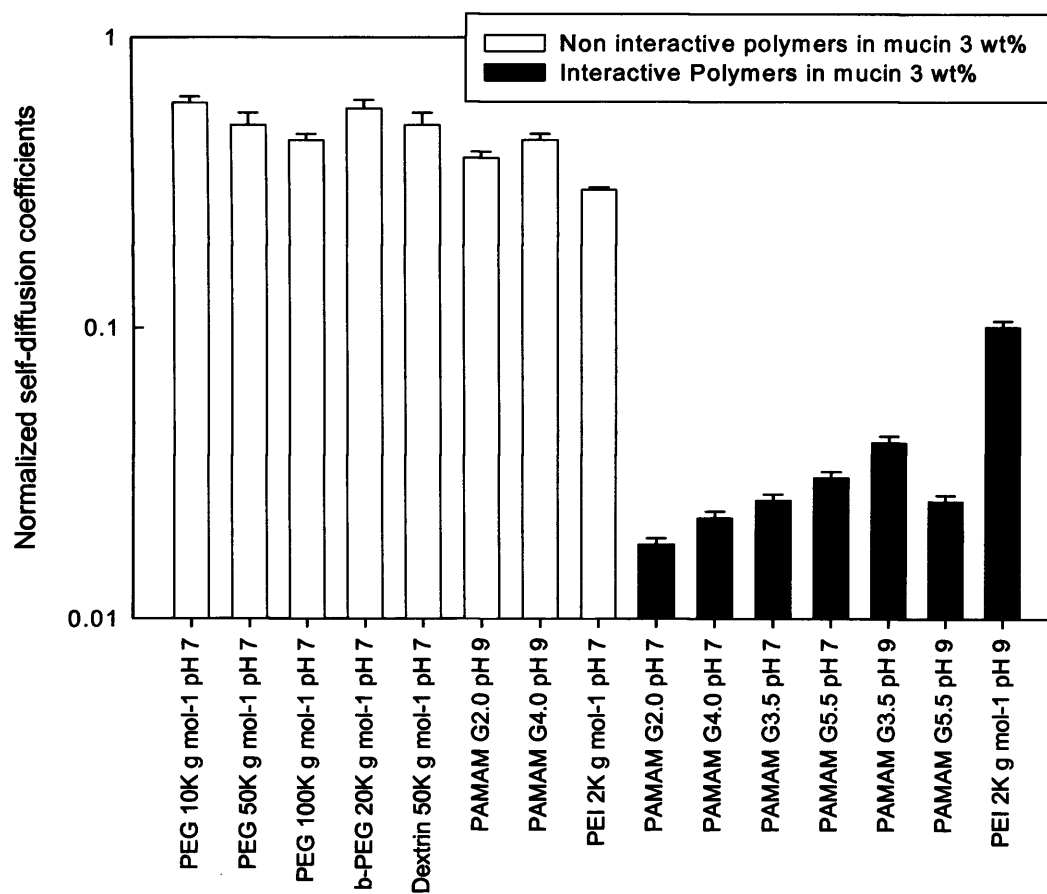
Figure 5.20 *Bar chart of the normalized self-diffusion coefficients of all 'probe' polymers in 3 wt% mucin solutions.*

5.4. Conclusions

A series of polymers-mucin solutions has been investigated to probe the effect of different polymers on the structure of mucin. 'Probe' polymer-mucin solutions have been explored by small-angle neutron scattering (SANS), pulsed-gradient spin-echo NMR (PGSE-NMR) and viscosity measurements. The SANS data provided a simple measure of the occurrence and nature of any interaction between the probe polymer and the mucin. The diffusion data together with the viscosity measurements gave a complementary insight into these systems, trying to differentiate and quantify obstruction effects from specific interactions.

Non-ionic polymers such as *l*-PEG 10K and *l*-PEG100K did not exhibit a specific interaction with the mucin, but suffered a moderate retardation in their diffusion through the mucin, associated to an obstruction effect of the polymer within the mucin gel-network. A pH-dependent interaction was found for a series of PAMAM dendrimers (positively and negatively charged) and PEI, exposing a strong electrostatic interaction. An attractive or repulsive electrostatic interaction was experienced by the polymers depending on the charge bore by both the polymer and the mucin at the specific pH under investigation. This specific interaction resulted in a significant retardation in the diffusion of these polymers in the mucin solution.

This study has shown that it is possible to distinguish and separate the effects of specific interactions between the 'probe' polymer and mucin from simple obstruction effects.

These conclusions should direct the choice of polymer structure to be adopted when designing polymer based delivery systems for the delivery through such mucin-rich environments.

References

1. Momot, K. I.; Kuchel, P. W., Pulsed field gradient nuclear magnetic resonance as a tool for studying drug delivery systems. *Concepts in Magnetic Resonance Part A* **2003**, 19A, 51-64.

2. Price, W. S.; Elwinger, F.; Vigouroux, C.; Stilbs, P., PGSE-WATERGATE, a new tool for NMR diffusion-based studies of ligand-macromolecule binding. *Magnetic Resonance in Chemistry* **2002**, 40, 391-395.

3. Matsukawa, S.; Ando, I., A study of self-diffusion of molecules in polymer gel by pulsed-gradient spin-echo ^{1}H NMR. *Macromolecules* **1996**, 29, 7136-7140.

4. Masaro, L.; Ousalem, M.; Baille, W. E.; Lessard, D.; Zhu, X. X., Self-diffusion studies of water and poly(ethylene glycol) in solutions and gels of selected hydrophilic polymers. *Macromolecules* **1999**, 32, 4375-4382.

5. Walther, B.; Loren, N.; Nyden, M.; Hermanssin, A.-M., Influence of k-carrageenan gel structure on the diffusion of probe molecules determined by transmission electron microscopy and NMR diffusometry. *Langmuir* **2006**, 22, 8221-8228.

6. Nyden, M.; Soderman, O.; Karlstrom, G., A PFG NMR self-diffusion investigation of probe diffusion in an ethyl(hydroxyethyl)cellulose matrix. *Macromolecules* **1999**, 32, 127-135.

7. Kwak, S.; Lafleur, M., NMR self-diffusion of molecular and macromolecular species in dextran solutions and gels. *Macromolecules* **2003**, 36, 3189-3195.

8. Lafitte, G.; Soderman, O.; Thuresson, K.; Davies, J., PFG-NMR diffusometry: a tool for investigating the structure and dynamics of non commercial purified gastric mucin in a wide range of concentrations. *Biopolymers* **2007**, 86, 165-175.

9. Lafitte, G.; Thuresson, K.; Soderman, O., Mixture of mucin and oppositely charged surfactant aggregates with varying charge

density. Phase behaviour, association, and dynamics. *Langmuir* **2005,** 21, 7097-7104.

10. Lafitte, G.; Thuresson, K.; Jarwoll, P.; Nyden, M., Transport properties and aggregation phenomena of polyoxyethylene sorbitane monooleate (polysorbate 80) in pig gastric mucin and mucus. *Langmuir* **2007,** 23, 10933-10939.

11. Trampel, R.; Schiller, J.; Naji, L.; Stallmach, F.; Karger, J.; Arnold, K., Self-diffusion of polymers in cartilage as studied by pulsed field gradient NMR. *Biophysical Chemistry* **2002,** 97, 251-260.

12. Kwak, S.; Lafleur, M., Self-diffusion of macromolecules and macroassemblies in curdlan gels as examined by PFG-SE NMR technique. *Colloids and Surfaces A: Physicochem. Eng. Aspects* **2003,** 221, 231-242.

13. Colsenet, R.; Soderman, O.; Mariette, F., Pulsed Field Gradient NMR Study of Poly(ethylene glycol) Diffusion in Whey Protein Solutions and Gels. *Macromolecules* **2006,** 39, 1053-1059.

14. Le Feunteun, S.; Mariette, F., Impact of casein gel microstructure on self-diffusion coefficient of molecular probes measured by ^{1}H PFG-NMR. *Journal of Agricultural and Food Chemistry* **2007,** 55, 10764-10772.

15. Colsenet, R.; Soderman, O.; Mariette, F., Effects of ionic strength and denaturation time on polyethyleneglycol self-diffusion in whey protein solutions and gels visualized by Nuclear magnetic Resonance. *Journal of Agricultural and Food Chemistry* **2006,** 54, 5105-5112.

16. Colsenet, R.; Soderman, O.; Mariette, F., Effect of casein concentration in suspensions and gels on poly(ethylene glycol)s NMR self-diffusion measurements. *Macromolecules* **2005,** 38, 9171-9179.

17. Davies, J. A.; Griffiths, P. C., A phenomenological approach to separating the effects of obstruction and binding for the diffusion of small molecules in polymer solutions. *Macromolecules* **2003,** 36, 950-952.

18. Duncan, R., Polymer conjugates as anticancer nanomedicines. *Nature Reviews Cancer* **2006,** 6, 688-701.

19. Chen, S. H., Small angle neutron scattering studies of the structure and interaction in micellar and microemulsion systems. *Annual Review in Physical Chemistry* **1986,** 37, 351-399.

20. Urbanc, B.; Cruz, L.; Buldyrev, S. V.; Havlin, S.; Irizarry, M. C.; Stanley, H. E.; Hyman, B. T., Dynamics of plaque formation in Alzheimer's disease. *Biophysical Journal* **1999,** 76, 1330-1334.

21. Boggara, M. B.; Krishnamoorti, R., Small-angle neutron scattering studies of phospholipid-NSAID adducts. *Langmuir* **2009.**

22. Velev, O. D.; Kaler, E. W.; Lenhoff, A. M., Protein interactions in solution characterized by light and neutron scattering: comparison of lysozyme and chymotrypsinogen. *Biophysical Journal* **1998,** 75, 2682-2697.

23. Gull, N.; Chodankar, S.; Aswal, V. K.; Ud-Din, K., Small angle neutron scattering studies on the interaction of cationic surfactants with bovine serum albumin. *Pramana - Journal of Physics* **2008,** 71, 1027-1031.

24. Stradner, A.; Sedgwick, H.; Cardinaux, F.; Poon, W. C. K.; Egelhaaf, S. U.; Schurtenberger, P., Equilibrium cluster formation in concentrated protein solutions and colloids. *Nature* **2004,** 432, 492-495.

25. Mishra, S.; Webster, P.; Davis, M. E., PEGylation significantly affects cellular uptake and intracellular trafficking of non-viral gene delivery particles. *European Journal of Cell Biology* **2004,** 83, 97-111.

26. Gabizon, A.; Martin, F., Polyethylene glycol-coated (pegylated) liposomal doxorubicin. *Drugs* **1997,** 54, 15-21.

27. Katre, N. V., The conjugation of proteins with polyethylene glycol and other polymers: altering properties of proteins to enhancing their therapeutic potential. *Advanced Drug Delivery Reviews* **1993,** 10, 91-114.

28. Hu, J.; Cheng, Y.; Wu, Q.; Zhao, L.; Xu, T., Host-guest chemistry of dendrimer-drug complexes. 2. Effects of molecular properties of guests and surface functionalities of dendrimers. *Journal of Physical Chemistry B* **2009**, 113, 10650-10659.

29. Ahn, C.-H.; Chae, S. Y.; Bae, Y. H.; Kim, S. W., Biodegradable poly(ethylenimine) for plasmid DNA delivery. *Journal of Controlled Release* **2002**, 80, 273-282.

30. Hreczuk-Hirst, D.; Chicco, D.; German, L.; Duncan, R., Dextrins as potential carriers for drug targeting: tailored rates of dextrin degradation by introduction of pendant groups. *International Journal of Pharmaceutics* **2001**, 230, 57-66.

31. Graham, M. L., Pegaspargase: a review of clinical studies. *Advanced Drug Delivery Reviews* **2003**, 55, 1293-1302.

32. Levy, Y.; Hershfield, M. S.; Fernandez-Mejia, C.; Polmar, S. H.; Scudiery, D.; Berger, M.; Sorensen, R. U., Adenosine deaminase deficiency with late onset of recurrent infections: response to treatment with polyethylene glycol-modified adenosine deaminase. *Journal of Pediatrics* **1988**, 113, 312-317.

33. Reddy, K. R.; Modi, M. W.; Pedder, S., Use of peginterferon α-2a (40KD) (PEGASYS) for the treatment of hepatitis C. *Advanced Drug Delivery Reviews* **2002**, 54, 571-586.

34. Wang, Y.-S.; Youngster, S.; Grace, M.; Bausch, J.; Bordens, R.; Wyss, D., F., Structural and biological characterization of pegylated recombinant interferon alpha-2b and its therapeutic implications. *Advanced Drug Delivery Reviews* **2002**, 54, 547-570.

35. Huang, K.; Lee, B. P.; Ingram, D. R.; Messersmith, P. B., Synthesis and characterization of self-assembling block copolymers containing bioadhesive end groups. *Biomacromolecules* **2002**, 3, 397-406.

36. Griffiths, P. C.; Occhipinti, P.; Morris, C.; Heenan, R. K.; King, S. M.; Gumbleton, M., PGSE-NMR and SANS studies of the interaction of model polymer therapeutics with mucin. *Biomacromolecules* **2010**, 11, 120-125.

37. Johansson, L.; Skantze, U.; Lofroth, J.-E., Diffusion and interaction in gels and solutions. 2. Experimental results on the obstruction effect. *Macromolecules* **1991,** 24, 6019-6023.

38. Johansson, L.; Elvingson, C.; Lofroth, J.-E., Diffusion and interaction in gels and solutions. 3. Theoretical results on the obstruction effect. *Macromolecules* **1991,** 24, 6024-6029.

39. Bures, P.; Huang, Y.; Oral, E.; Peppas, N. A., Surface modifications and molecular imprinting of polymers in medical and pharmaceutical applications. *Journal of Controlled Release* **2001,** 72, 25-33.

40. Yoncheva, K.; Gomez, S.; Campanero, M. A.; Gamazo, C.; Irache, J. M., Bioadhesive properties of pegylated nanoparticles. *Expert Opinion in Drug Delivery* **2005,** 2, 205-218.

41. De Ascentiis, A.; deGrazia, J. L.; Bowman, C. N.; Colombo, P.; Peppas, N. A., Mucoadhesion of poly(2-hydroxyethyl methacrylate) is improved when linear poly(ethylene oxide) chains are added to the polymer network. *Journal of Controlled Release* **1995,** 33, 197-201.

42. Sahlin, J. J.; Peppas, N. A., Enhanced hydrogel adhesion by polymer interdiffusion: use of linear poly(ethylene glycol) as an adhesion promoter. *Journal of Biomaterial Science. Polymer Edition* **1997,** 8, 421-436.

43. Huang, Y.; Leobandung, W.; Foss, A.; Peppas, N. A., Molecolar aspects of muco- and bioadhesion: tethered structures and site-specific surfaces. *Journal of Controlled Release* **2000,** 65, 63-71.

44. Serra, L.; Domenech, J.; Peppas, N. A., Design of poly(ethylene glycol)-tethered copolymers as novel mucoadhesive drug delivery systems. *European Journal of Pharmaceutics and Biopharmaceutics* **2006,** 63, 11-18.

45. Efremova, N. V.; Huang, Y.; Peppas, N. A.; Leckband, D. E., Direct measurement of interactions between tethered poly(ethylene glycol) chains and adsorbed mucin layers. *Langmuir* **2002,** 18, 836-845.

46. Lele, B. S.; Hoffman, A. S., Mucoadhesive drug carriers based on complexes of poly(acrylic acid) and PEGylated drugs having

hydrolysable PEG-anhydride-drug linkages. *Journal of Controlled Release* **2000**, 69, 237-248.

47. Shojaei, A. H.; Li, X., Mechanisms of buccal mucoadhesion of novel copolymers of acrylic acid and polyethylene glycol monomethylether monomethacrylate. *Journal of Controlled Release* **1997,** 47, 151-161.

48. Lai, S. K.; O'Hanlon, D. E.; Harrold, S.; Man, S. T.; Wang, Y.-Y.; Cone, R.; Hanes, J., Rapid transport of large polymeric nanoparticles in fresh undiluted human mucus. *PNAS* **2007,** 104, 1482-1487.

49. Wang, Y.-Y.; Lai, S. K.; Suk, J. S.; Pace, A.; Cone, R.; Hanes, J., Addressing the PEG mucoadhesivity paradox to engineer nanoparticles that "slip" through the human mucus barrier. *Angewandte Chemie-International Edition* **2008,** 47, 9726-9729.

50. De Smedt, S. C.; Demeester, J.; Hennink, W. E., Cationic polymer based gene delivery systems. *Pharmaceutical Research* **2000,** 17, 113-126.

51. De Bruyn, P. P. H.; Michelson, S., Changes in the random distribution of sialic acid at the surface of the myeloid sinusoidal endothelium resulting from the presence of diaphragmed fenestrae. *Journal of Cell Biology* **1979,** 82, 708-714.

52. Waigh, T. A.; Papagiannopoulos, A.; Voice, A.; Bansil, R.; Unwin, A. P.; Dewhurst, C. D.; Turner, B.; Afdhal, N., Entanglement coupling in porcine stomach mucin. *Langmuir* **2002,** 18, 7188-7195.

53. Yakubov, G. E.; Papagiannopoulos, A.; Rat, E.; Easton, R. L.; Waigh, T. A., Molecular structure and rheological properties of short-side-chain heavily glycosylated porcine stomach mucin. *Biomacromolecules* **2007,** 8, 3467-3477.

54. Perez, E.; Proust, J. E., Forces between mica surfaces covered with adsorbed mucin across aqueous solution. *Journal of Colloid and Interface Science* **1987,** 118, 182-191.

55. Durrer, C.; Irache, J. M.; Duchene, D.; Ponchel, G., Mucin interactions with functionalized polystyrene latexes. *Journal of Colloid and Interface Science* **1995,** 170, 555-561.

56. Lee, S.; Muller, M.; Rezwan, K.; Spencer, N. D., Porcine gastric mucin (PGM) at the water/poly(dimethylsiloxane) (PDMS) interface: influence of pH and ionic strength on its conformation, adsorption, and aqueous lubrication properties. *Langmuir* **2005**, 21, 8344-8353.

57. Willits, R. K.; Saltzman, M. W., Synthetic polymers alter the structure of cervical mucus. *Biomaterials* **2001**, 22, 445-452.

58. Deacon, M. P.; McGurk, S.; Roberts, C. J.; Williams, P. M.; Tendler, S. J. B.; Davies, M. C.; Davis, S. S.; Harding, S. E., Atomic force microscopy of gastric mucin and chitosan mucoadhesive systems. *Biochemical Journal* **2000**, 348, 557-563.

Chapter 6. Synthesis   and characterization of PEGylated PAMAM dendrimers in mucin solutions

Results presented in this chapter show the effect of PEGylation of full generation polyamidoamine (PAMAM) dendrimers on the interaction with mucin. Because of their unique structure – regularly branched polymers with a well-defined dendritic architecture and several functional groups on their periphery which can be used for the attachment of drugs – PAMAM dendrimers are relevant polymers in polymer-drug delivery systems. PAMAM dendrimers with different degrees of PEGylation were synthesized and characterized. Studies on the PEGylated PAMAM dendrimers in mucin solutions were performed by small-angle neutron scattering (SANS) and pulsed-gradient spin-echo NMR (PGSE-NMR) to investigate whether the PEG coating could reduce the interaction shown by PAMAM dendrimers towards mucin molecules.

6.1. Introduction

6.1.1. The importance of PEGylation of proteins and peptides

PEGylation consists on a simple modification of a molecule – *i.e.*, a protein, peptide or non-peptide molecule – by the covalently linking of one or more poly(ethylene glycol) (PEG) chains which is able to improve the pharmacological properties of a drug, especially for peptide and protein therapeutics [1-3]. Indeed, PEG is a non-toxic, non-immunogenic, non-antigenic, water-soluble polymer. Thanks to these properties, PEG is widely used as a modifying polymer to decrease the immunogenicity and antigenicity as well as to increase the body-residence time and stability of proteins, enzymes, organic molecules. Furthermore, the Food and Drug Administration (FDA, USA) has approved the use of PEG in foods, cosmetics and pharmaceuticals, in different types of formulations – including injectable, topical, rectal and nasal. Examples of PEG

conjugates commercially available are: (i) PEG-L-asparaginase (Oncaspar[®] [4]), for the treatment of acute lymphoblastic leukemia; (ii) PEG-adenosine deaminase (Adagen[®] [5]), for the treatment of severe combined immunodeficiency disease; (iii) PEG-interferon-α conjugates (Pegasys[®] [6] and PEG-Intron[®] [7]), used to remove hepatic and extra-hepatic hepatitis C virus infection.

PEGylation was firstly described in the late 1970s by Davis [8] and Abuchowsky [9, 10] who reported a chemical modification *via* covalent attachment of poly(ethylene glycol) chains to proteins (*i.e.*, albumin) and enzymes (*i.e.*, catalase). At that time, modifying chemically a protein or an enzyme was innovative since proteins were considered delicate molecules able to stand only few gentle alterations. Their study revealed unexpected findings, showing that PEGylation not only protects proteins from destruction during drug delivery, but also improves the pharmacokinetics (*i.e.*, mobility of the drugs throughout the body) and pharmacodynamics (*i.e.*, changes in measureable clinical parameters related to a drug, such as increase in antitumor activity, decrease in nausea) properties of polypeptide drugs by increasing water solubility, reducing renal clearance and limiting toxicity.

Thereafter, PEGylation became a very common method for the modification of molecules, not only proteins [11] with the purpose to overcome the limitations – such as inadequate water solubility and poor pharmacokinetic profile – of some therapeutic agents.

Before reacting with a polypeptide, the PEG needs to be activated. A variety of chemical modifications are used to synthesize an active PEG derivative with an electrophilic functional group – such as active carbonate, active ester, aldehyde, as illustrated in Figure 6.1 – which can be easily coupled to a specific site (*e.g.*, amine, sulphydryl group or other nucleophile) on the therapeutic molecule. The PEG molecule can be made monofunctional by the use of methoxy-PEG (m-PEG), since this PEG form possesses only one hydroxyl group for activation and the methoxy group is inert to standard chemical processes [12].

One of the sites which is frequently used for PEG conjugation is the amino group since it is the most common group in proteins and is usually well-exposed to the solvent and, therefore, can be easily modified. However, PEGylating site-specifically can reduce the loss of biological activity and reduce immunogenicity of the protein. For instance, because cysteines are rarely present in peptides, PEGylation of the thiol groups of cysteines not involved in disulphide bridges is ideal for specific modifications.

PEG derivatives suitable for amine modification include *N*-hydroxysuccinimidyl-activated esters (generating an amide linkage), PEG-epoxide (amine linkage), PEG-carbonyl imidazole (urethane linkage), PEG-tresylate (amine linkage) and PEG-aldehyde (amine linkage). Thiol groups can be modified by use of PEG-maleimide and vinyl sulfone [13-15].
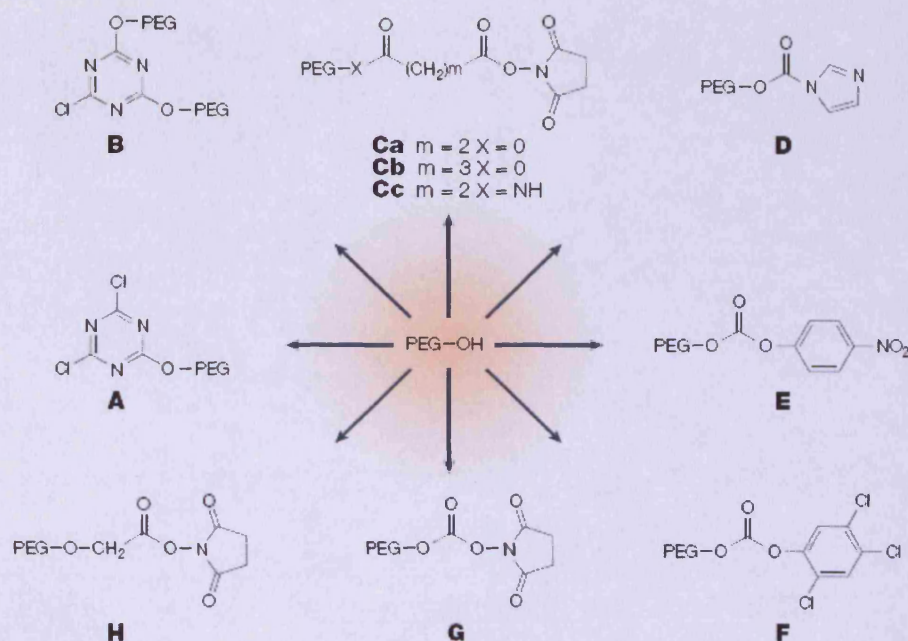
Figure 6.1 *Method for the activation of PEG molecles. (A) Cyanuric chloride method; (B) A variation on the cyanuric chloride method; (Ca) PEG-succinimidyl succinate method; (Cb) Substitution of the succinate residue by glutarate; (Cc) Substitution of the aliphatic ester in (Ca) by an amide bond; (D) Imidazoyl formate method; (E) and (F) Variations using phenylcarbonates of PEG; (G) Succinimidyl carbonates of PEG; (H) Succinimydyl active ester of PEG. Taken from Harris J. M.* [2].

Obviously there are some limitations in the use of PEG. First of all, PEG is a synthetic polymer which means that can be polydisperse: in the conjugation of the PEG with protein or drugs, this leads to a population of protein or drug conjugates which might have different biological properties. Nowadays, the limitation of the polydispersity can be easily overcome considering all the new methods of synthesis and purification which bring on the market low polydisperse PEGs.

Another problem for the use of PEG refers to its elimination from the body. If PEGs can be usually eliminated through urine or feces, high molecular weight PEGs can accumulate in the liver. Therefore, a

molecular weight of 30 KDa was calculated as a threshold for renal clearance [1]. However, enzymes such as cytochrome P450 [16] or alcohol dehydrogenase [17] can break down branched PEG chains. Therefore, the higher PEG molecular weight used in protein conjugation is 40 KDa in the branched form [18].

6.1.2. Other applications of PEGylation

PEGylation has found several applications including the modification of drug delivery systems such as liposomal carriers, nanoparticles and polymeric carriers.

Liposomes (*i.e.*, bilayer vesicles) have been widely used as carriers for the delivery of encapsulated agents. However, liposomal delivery presents a number of limitations. Liposomes are often retained by the liver, kidneys, spleen and the liposomal systems tend to 'leak' drug while in circulation. Many of these limitations can be improved by PEGylation [19, 20]. Indeed, PEGylated liposomes demonstrated an increased half-life, a decreased plasma clearance together with the liposomal system being less likely to leak drug while in circulation. PEG is incorporated into the lipid bilayer of the liposome, forming a hydrated shell that protects it from plasma proteins and lipoproteins, bringing an eight-fold increase in plasma half-life of the liposome compared to an unmodified liposome [21].

Recent studies on the encapsulation of thrombolytic agent into PEGylated liposomes reported a prolonged circulation lifetimes of the therapeutic agent by five-fold compared with the drug lifetime encapsulated into the unPEGylated liposome [22].

Liposome technologies have been applied also for the treatment of metastasis breast cancer and ovarian cancer. Several studies revealed that PEGylated liposomal doxorubicin (with doxorubicin being an anticancer drug for the treatment of solid tumors) – CAELYX®/DOXIL® – showed significantly reduced cardiotoxicity, vomiting and alopecia in the treatment of metastatic breast cancer when compared to the treatment with conventional doxorubicin [23-27]. Also for the treatment of ovarian cancer,

the use of PEGylated liposomal doxorubicin improved the delivery of the therapeutic agent to the target tumor tissue, allowing enhanced uptake by cancer cells, together with a lower toxicity profile [28-30].

Surface-modification of delivery vehicles with PEG has been reported also as a promising method to improve the stability and performance of some non-viral and gene vectors [31-37]. Diffusivity measurements of PEGylated nanoparticles demonstrated how the PEG-surface-modification improved greatly the diffusivity of the nanoparticles compared to unPEGylated nanoparticles as well as reduced adhesive interactions of the nanoparticles with intracellular components. Furthermore, PEGylation has shown to improve particle transport through biological barriers, such as mucus from healthy volunteers [38] or patients with cystic fibrosis [39] since PEG coating can reduce the adhesion and, therefore, enhance the mobility of particles in the mucus gel-network.

Because of their unique structure – highly branched polymers with a well-defined dendritic architecture and many reactive surface groups which can be used for the attachment of drugs – polymers like poly(amidoamine) dendrimers are widely used in biomedical and pharmaceutical applications (*i.e.*, drug and gene delivery vehicles [40-45]) but – especially the PAMAM dendrimers bearing amino terminal groups – show cytotoxicity (*i.e.*, being toxic to cells) and hemolytic properties (*i.e.*, destroying red blood cells). Conjugation of the PAMAM dendrimers with PEG chains has been considered as a method to improve their biocompatibility and reduce the toxicity [46].

Several studies [47-52] indeed demonstrated that PEGylation of the surface of the PAMAM dendrimer can considerably increase the drug carrier cytocompatibility. In addition, the optimized degree of PEGylation for the PAMAM dendrimers would still allow an high drug payload on the dendrimer [49]. However, studies on partly PEGylated PAMAM dendrimers used as carriers for the anticancer drug doxorubicin revealed that the antitumor activity of the conjugates increased with increasing the

PEGylation degree [48, 50]. The PEGylation of PAMAM dendrimers resulted to have increased their drug-loading capacity, reduce their drug release rate and haemolytic toxicity when PEGylated PAMAM dendrimers were used as drug delivery systems for antitubercular drug (*i.e.*, rifampicin) [53], as DNA delivery systems [51] and for pulmonary delivery of heparin [54].

Considering all the positive effects showed by the PEGylation techonology, the idea of the study here presented is to investigate whether the PEGylation of the amino terminated PAMAM dendrimers studied in Chapter 5 can 'turn off' the interaction showed by these polymers in mucin solutions. Furthermore, having synthesized the PEG-PAMAM conjugates with different degrees of PEGylation, the critical degree of PEGylation of PAMAM dendrimers needed to reduce the interaction with mucin was explored. The effects of PEG-PAMAM dendrimer conjugates on mucin solutions have been investigated by SANS and PGSE-NMR.

6.2. Results

6.2.1. Synthesis and characterization of PEG-PAMAM dendrimer conjugates

In order to study the effect of PEGylation on PAMAM dendrimers, a series of PEG-PAMAM dendrimer conjugates – 10%, 50% and 100% PEGylated PAMAM dendrimers G2.0 and G4.0 – were synthesised following the method explained in section 3.2.2 in Chapter 3.

The PEG-PAMAM dendrimer conjugates were characterized by ^{1}H-NMR [55].

^{1}H-NMR spectrum of the 100% PEGylated PAMAM dendrimers G2.0 in D_2O is illustrated in Figure 6.1. The ^{1}H NMR chemical shifts (ppm) of the signals from the PEG-PAMAM dendrimer are as follow: δ_{PAMAM} 2.31 (br, $-NCH_2CH_2CO-$), δ_{PAMAM} 2.42 (m, $-CONHCH_2N-$ and $-NCH_2CH_2N-$), δ_{PAMAM} 2.53 (br, $-CONHCH_2CH_2N-$), δ_{PAMAM} 2.71 (br, $-NCH_2CH_2CO-$), δ_{PAMAM} 3.21 (m, $-ONHCH_2CH_2N-$), δ_{PEG} 3.28 (s, $-OCH_3$), δ_{PEG} 3.52 (m, - $OCH_2CH_2OCH_3$), δ_{PEG} 3.59 (b, $-OCH_2CH_2O-$), δ_{PEG} 3.67 (m, -

NHCOOCH$_2$-). ^{1}H-NMR spectra of the 50% and 10% PEGylated PAMAM dendrimers G2.0 in D$_2$O are reported in Figure 6.3 and 6.4 respectively.

^{1}H-NMR spectrum of the 100% PEGylated PAMAM dendrimers G4.0 in D$_2$O is presented in Figure 6.5. The ^{1}H NMR chemical shifts (ppm) of the signals from the PEG-PAMAM dendrimer are as follow: δ_{PAMAM} 2.32 (br, -NCH$_2$CH$_2$CO-), δ_{PAMAM} 2.43 (m, -CONHCH$_2$N- and -NCH$_2$CH$_2$N-), δ_{PAMAM} 2.53 (br, -CONHCH$_2$CH$_2$N-), δ_{PAMAM} 2.71 (br, -NCH$_2$CH$_2$CO-), δ_{PAMAM} 3.21 (m, -ONHCH$_2$CH$_2$N-), δ_{PEG} 3.28 (s, -OCH$_3$), δ_{PEG} 3.53 (m, -OCH$_2$CH$_2$OCH$_3$), δ_{PEG} 3.60 (b, -OCH$_2$CH$_2$O-), δ_{PEG} 3.68 (m, -NHCOOCH$_2$-). ^{1}H-NMR spectra of the 50% and 10% PEGylated PAMAM dendrimers G4.0 in D$_2$O are shown in Figure 6.6 and 6.7, respectively.

Integration of the NMR peaks belonging to the PEG, PAMAM dendrimer G2.0 and PAMAM dendrimer G4.0 provided an estimation of number of conjugated PEG molecules per dendrimer for each PEG-PAMAM conjugate, as illustrated in Table 6.1. The degrees of PEGylation (10%, 50% and 100%) for the PEG-PAMAM conjugates reported good yields, laying between 87.5% and 100%.

Figure 6.2 *¹H-NMR spectrum of the PEG-PAMAM G2.0 conjugate 100%*
PEGylated, full (top) and zoomed in (bottom), in D₂O.
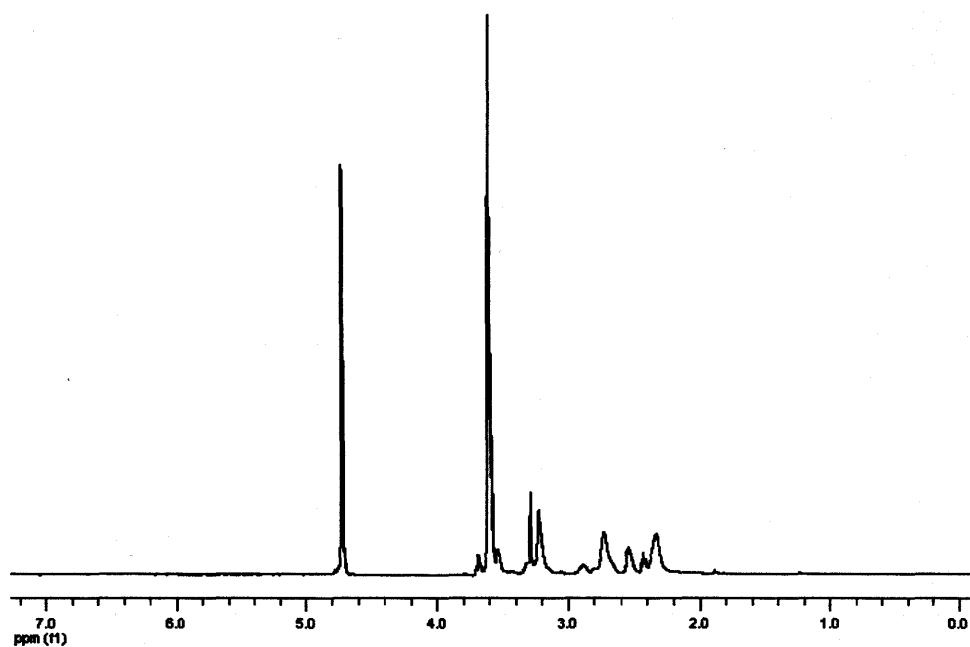
Figure 6.3 ^{1}H-NMR *spectrum of the PEG-PAMAM G2.0 conjugate 50% PEGylated, full (top) and zoomed in (bottom).*
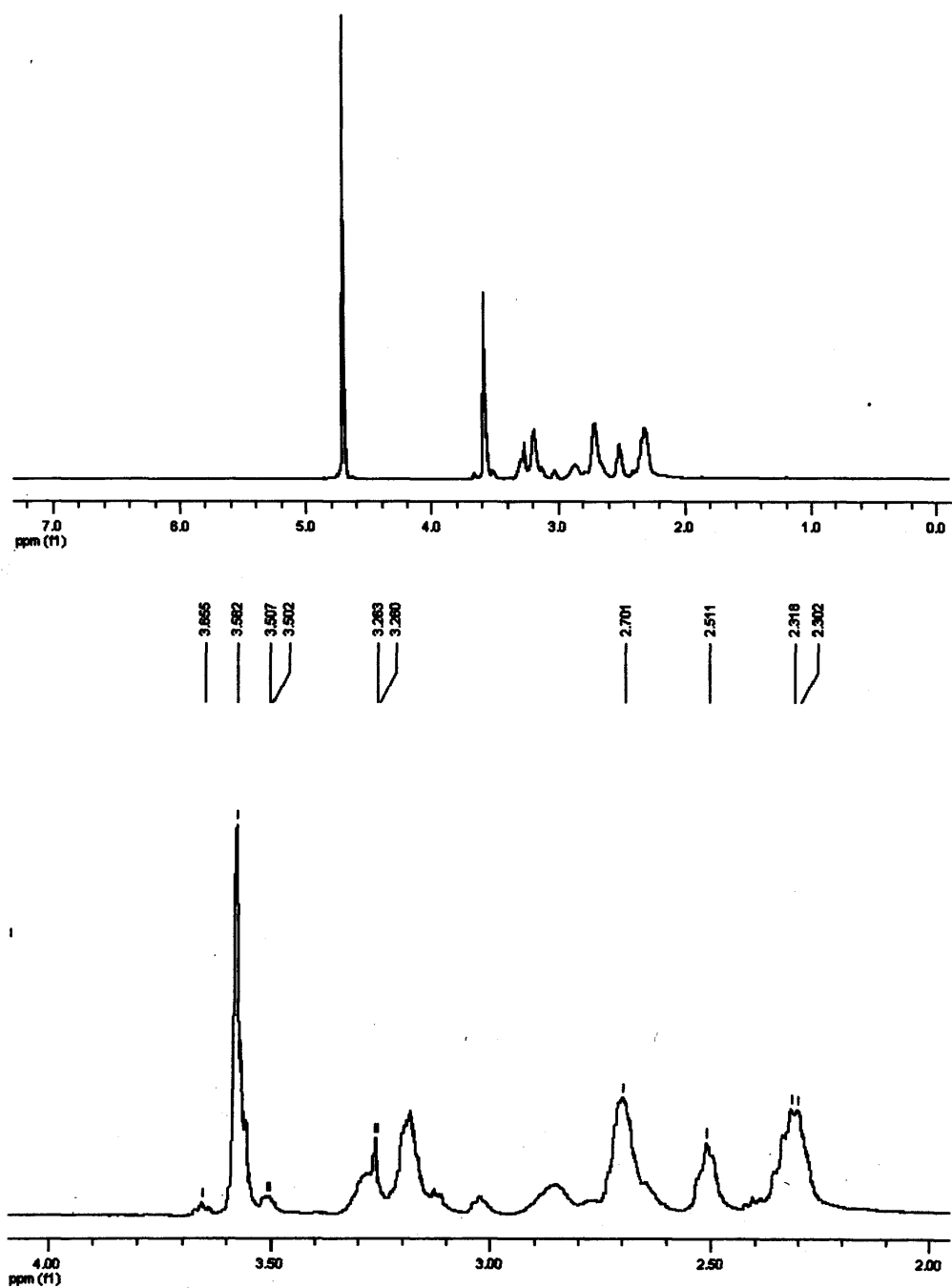
Figure 6.4 *H-NMR spectrum of the PEG-PAMAM G2.0 conjugate 10% PEGylated, full (top) and zoomed in (bottom).*
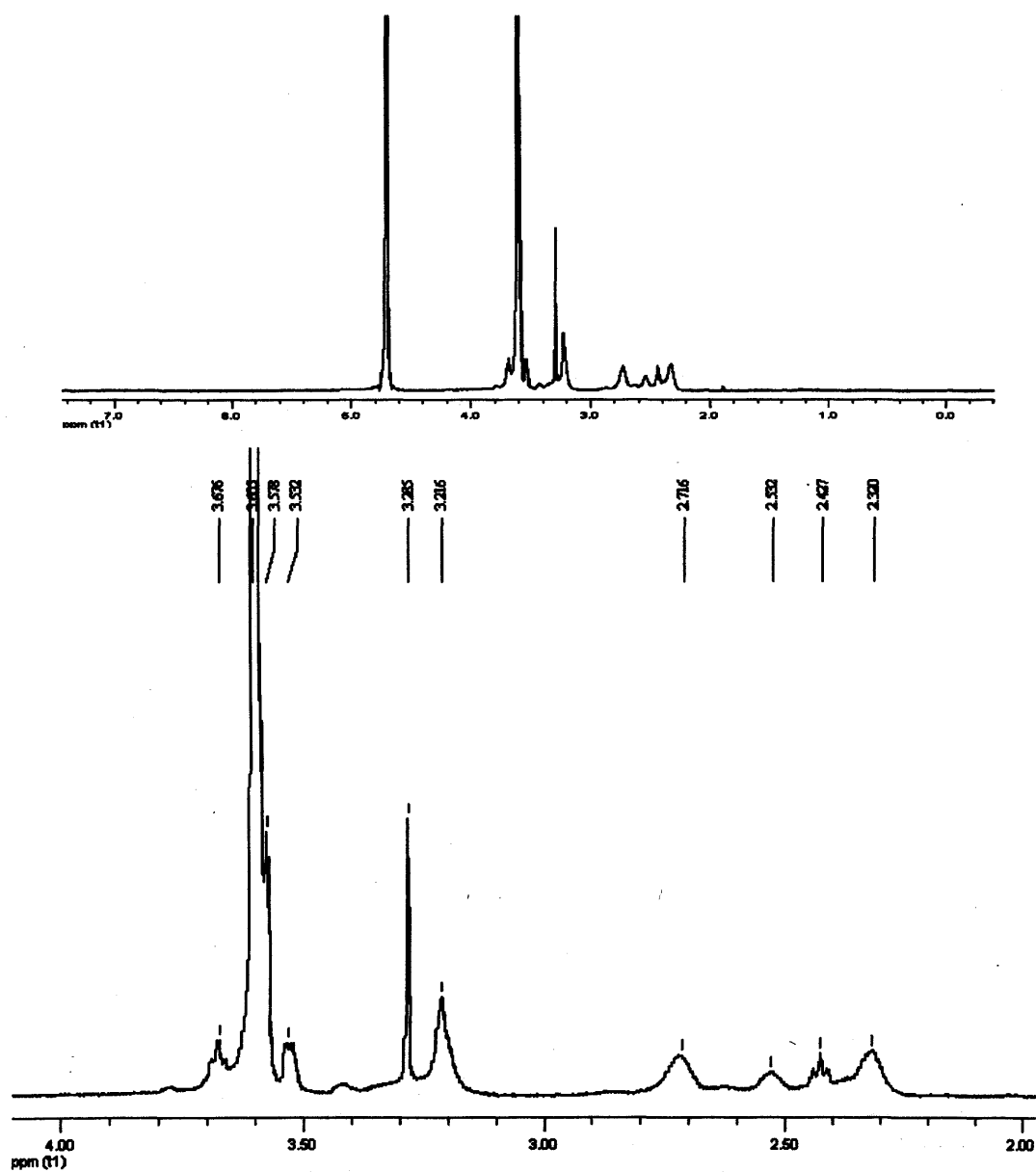
Figure 6.5 ^{1}*H-NMR spectrum of the PEG-PAMAM G4.0 conjugate 100%*
PEGylated, full (top) and zoomed in (bottom), in D_2O.
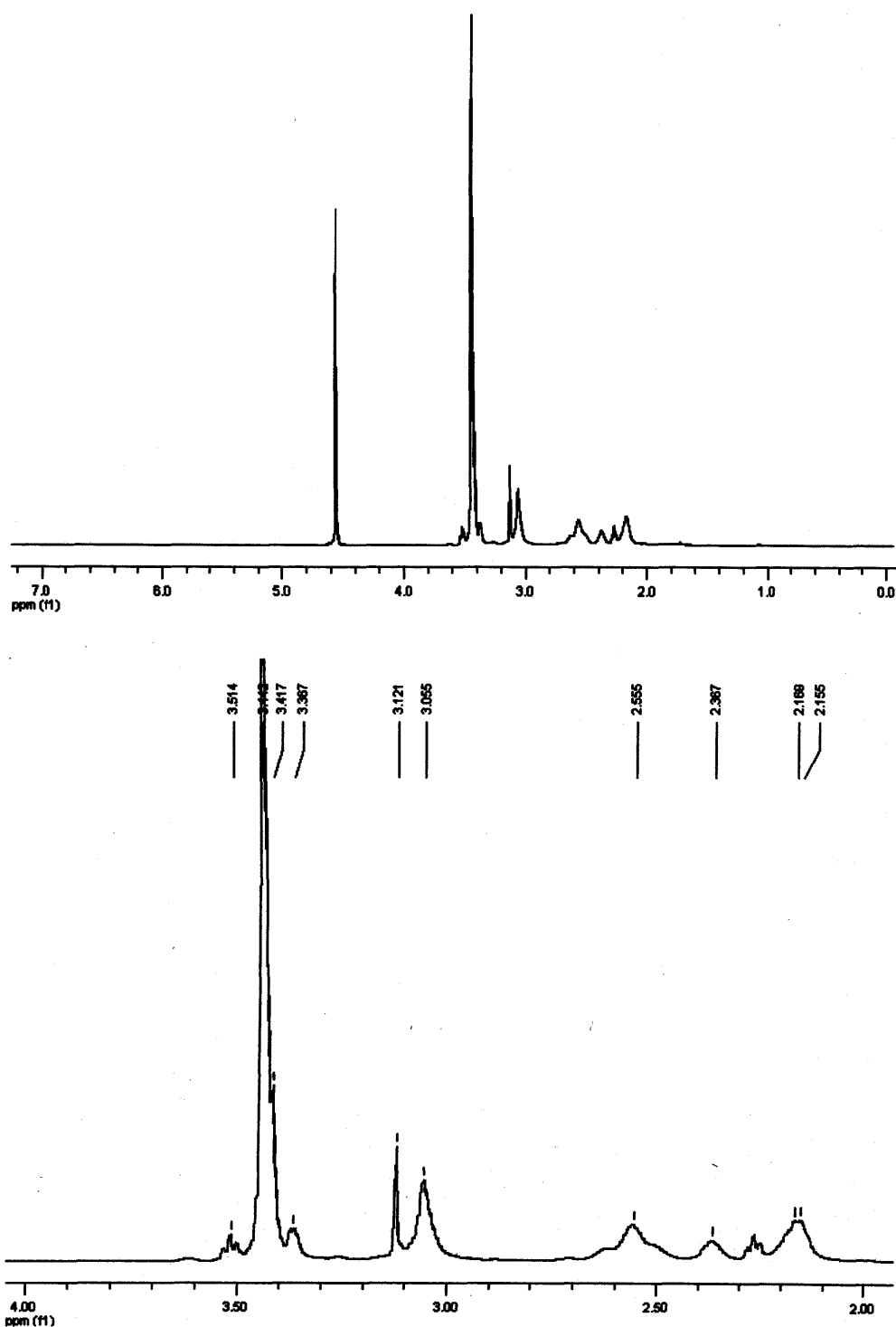
Figure 6.6 ^{1}H-NMR spectrum of the PEG-PAMAM G4.0 conjugate 50% PEGylated, full (top) and zoomed in (bottom), in D$_2$O.

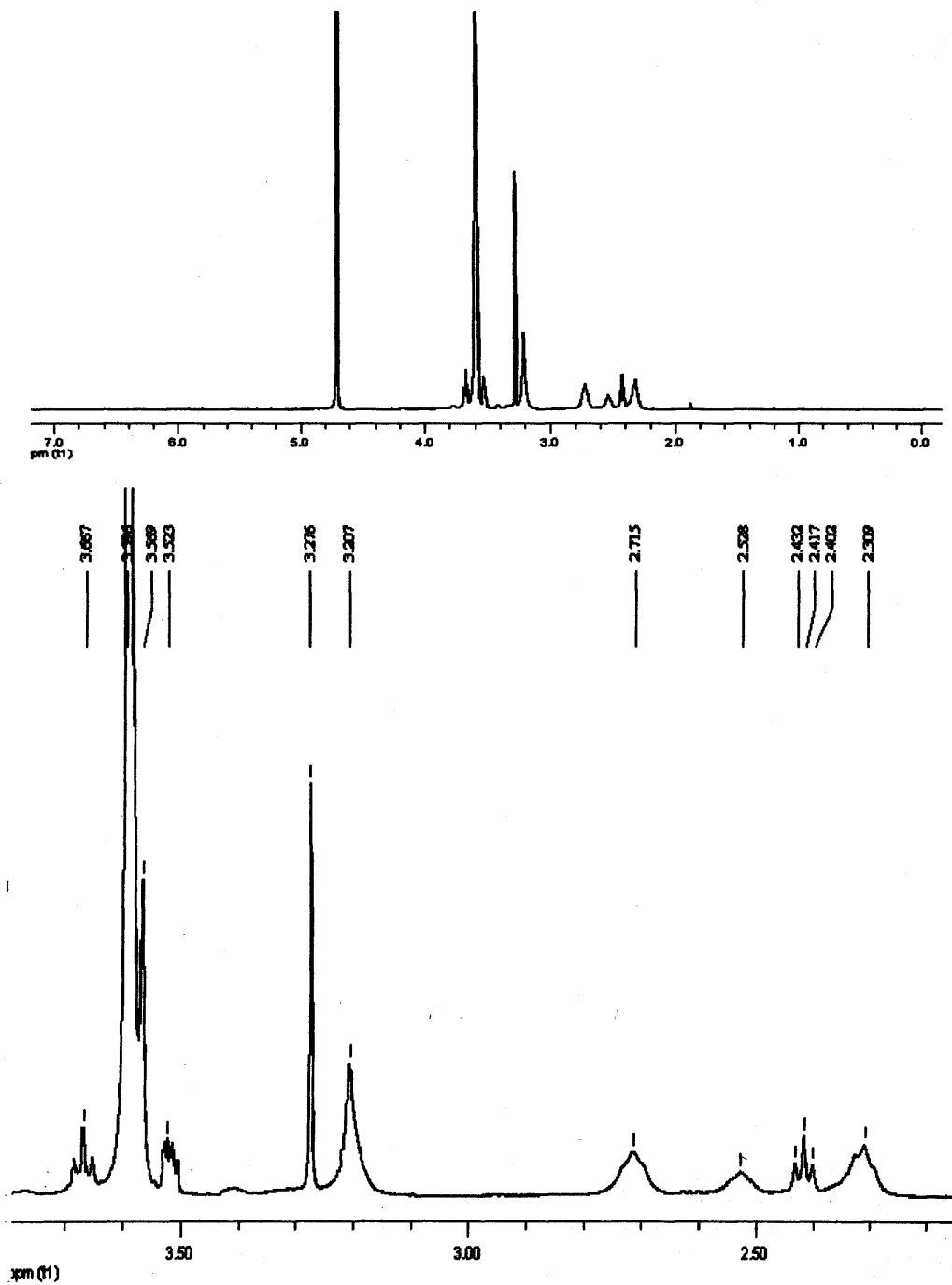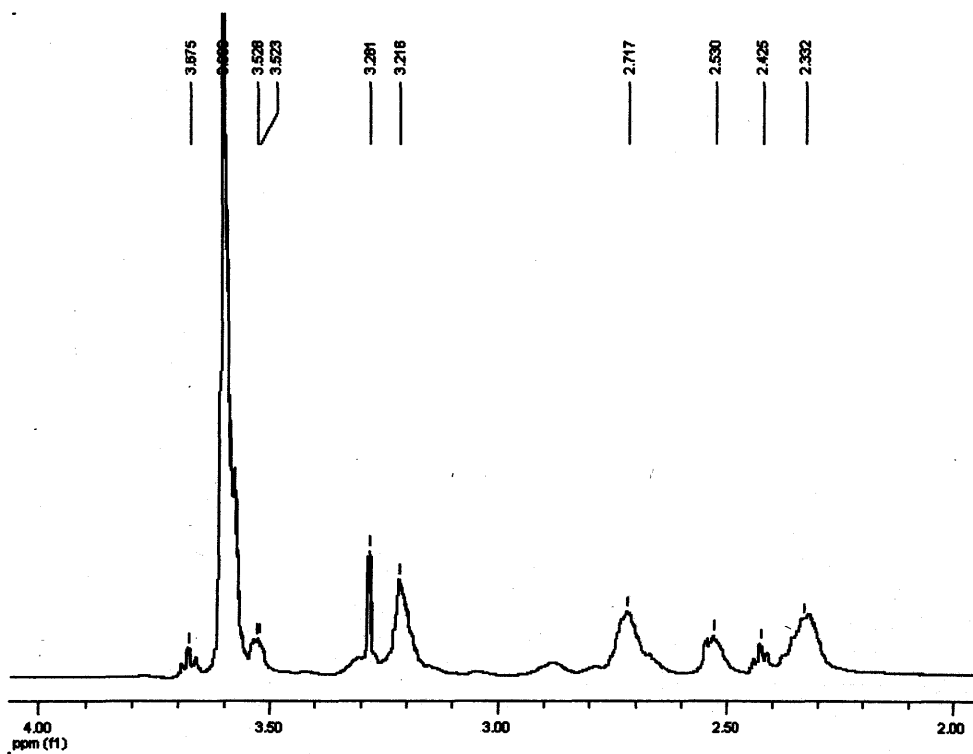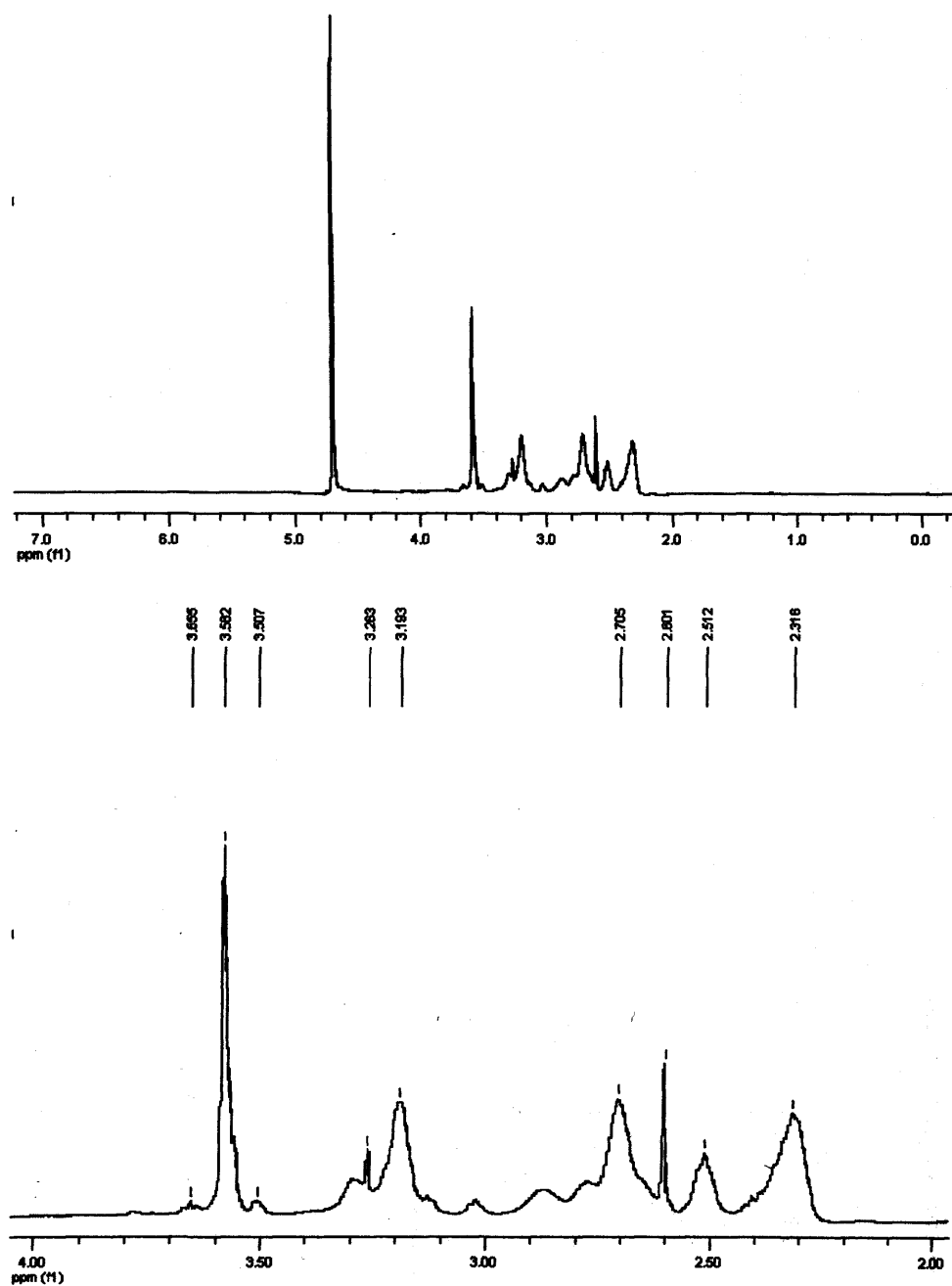*Figure 6.7* ^{1}*H-NMR spectrum of the PEG-PAMAM G4.0 conjugate 10%*
PEGylated, full (top) and zoomed in (bottom), in D$_2$O.

Conjugate	Feed ratio PEG:PAMAM (by mole)	No. of –NH₂ groups	No. of conjugated PEG (expected values)	No. of conjugated PEG (by ^{1}H-NMR)	Degree of PEGylation (%)	Yield (%)	Molecular weight (g mol⁻¹)
PAMAM dendrimer G2.0	-	16	-	-	-	-	3260
PAMAM G2.0 10% PEGylated	1.6	14.4	1.6	1.4	10	87.5	4492
PAMAM G2.0 50% PEGylated	8	8	8	8.0	50	100	7946
PAMAM G2.0 100% PEGylated	16	0	16	16.0	100	100	12650
PAMAM dendrimer G4.0	-	64	-	-	-	-	14210
PAMAM G4.0 10% PEGylated	6.4	57.6	6.4	6.1	10	95	17953
PAMAM G4.0 50% PEGylated	32	32	32	32.0	50	100	32953
PAMAM G4.0 100% PEGylated	64	0	64	61.1	100	95.5	51760

Table 6.1 Characteristics of PAMAM dendrimers and PEG-PAMAM dendrimer conjugates.

6.2.2. SANS results

As previously discussed in Chapter 5, the addition of either PAMAM G2.0 or G4.0 dendrimers to mucin solutions demonstrated a pH-dependent specific electrostatic interaction occurred between the dendrimer and the mucin, which appeared to be significant at pH 7. Here, the effect of PEGylation of the PAMAM dendrimers on mucin solutions is investigated by SANS.

The scattering from 5 wt% mucin solutions in the presence of 0.5 wt% PEG-PAMAM G2.0 and G4.0 conjugates 100% PEGylated at pH 7 is shown in Figure 6.8. The concentration of the conjugates was too low to detect measurable scattering: therefore, it is possible to ignore their contribution to the scattering of mucin when performing scattering experiments on the mixture mucin/PEG-PAMAM conjugates solutions. As illustrated in Figure 6.8, whereas the presence of the PAMAM dendrimer G2.0 or G4.0 clearly perturbed the scattering from mucin at pH 7, no significant changes were observed in the scattering from mucin when the PEG-PAMAM G2.0 and G4.0 conjugates 100% PEGylated were added to mucin solutions.

When the degree of PEGylation of the PAMAM dendrimers was lowered from 100% to 50% and 10% the scattering from mucin was slightly affected by the presence of the partly PEGylated PAMAMs, as showed in Figure 6.9. The effect exhibited by the partly PEGylated PAMAMs in mucin solutions was not as strong as the one showed by the unPEGylated PAMAM dendrimers. This indicates that the partly PEGylated PAMAMs exhibited a small residual electrostatic interaction with the mucin molecules due to the free amino groups which have not been PEG coated.

Parameters obtained from the model and from analysis of the Zimm plots are shown in Table 6.2 (for the PEG-PAMAM G2.0 conjugates) and Table 6.3 (for the PEG-PAMAM G4.0 conjugates). The values obtained for the addition of 100% PEGylated PAMAM G2.0 and G4.0 conjugates

to mucin solutions do not report great difference compared to the ones observed for mucin only in solution at pH 7, indicating a non-interactive system.

For the 50% and 10% PEGylated PAMAM G2.0 and G4.0 conjugates in mucin solutions, parameters such as the radius of gyration, the correlation length and the distance between the globules of the mucin molecules reported slightly larger values than the ones observed for the mucin only samples. This is related to the small electrostatic interaction exhibited by the partly PEGylated PAMAM conjugates with the mucin molecules.

Overall, PEG chains generated a 'shell' able to mask the positively charged surface of the PAMAM dendrimers which indeed 'turned off' the electrostatic interaction between the dendrimer and the mucin glycoprotein. The interaction was completely removed when the degree of PEGylation of the PAMAM was equal to 100%. A degree of PEGylation lower than 100% was, however, able to reduce the strong interaction between the PAMAM and the mucin.
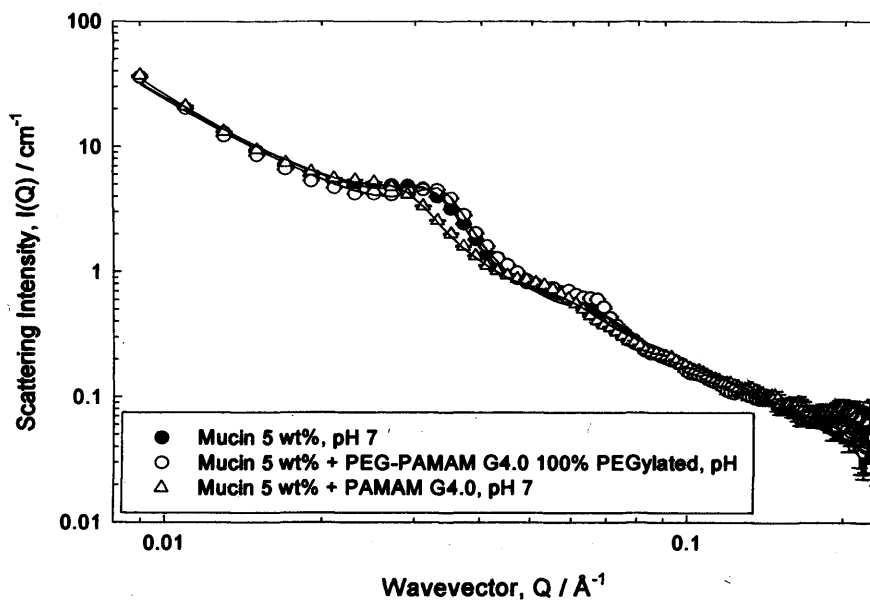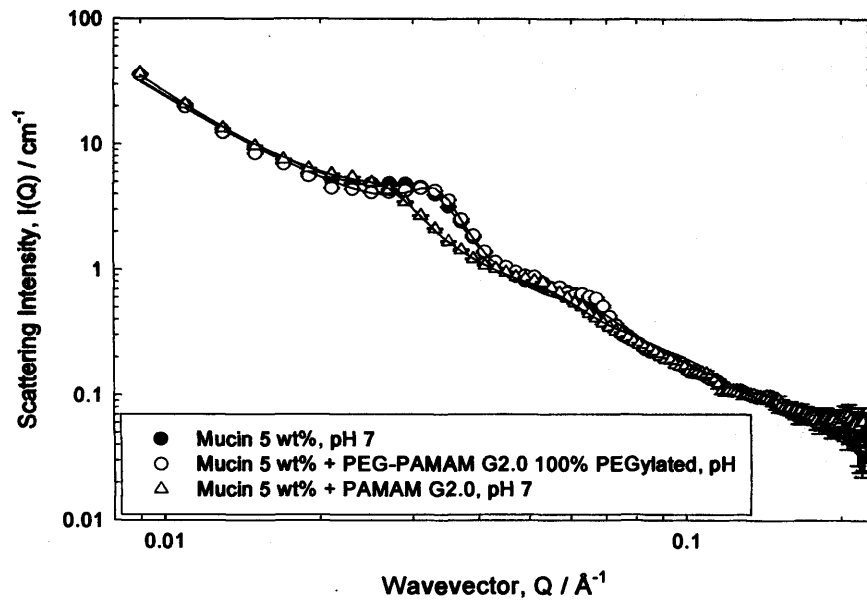
Figure 6.8 Scattering from 5 wt% mucin in the absence and in the presence of: 0.5 wt% PEG-PAMAM dendrimer G2.0 conjugate 100% PEGylated and 0.5 wt% PAMAM dendrimer G2.0 (top); PEG-PAMAM dendrimer G4.0 conjugate 100% PEGylated and 0.5 wt% PAMAM dendrimer G4.0 (bottom).
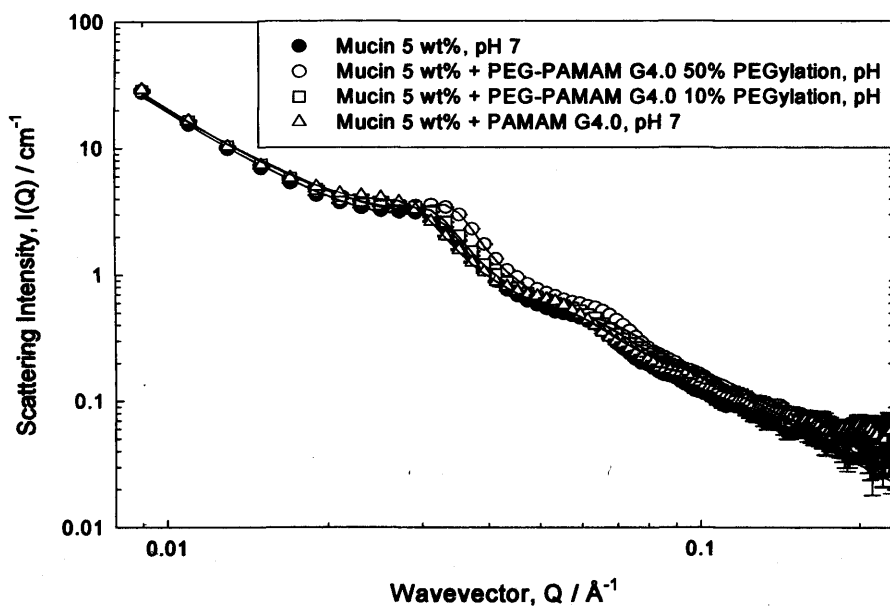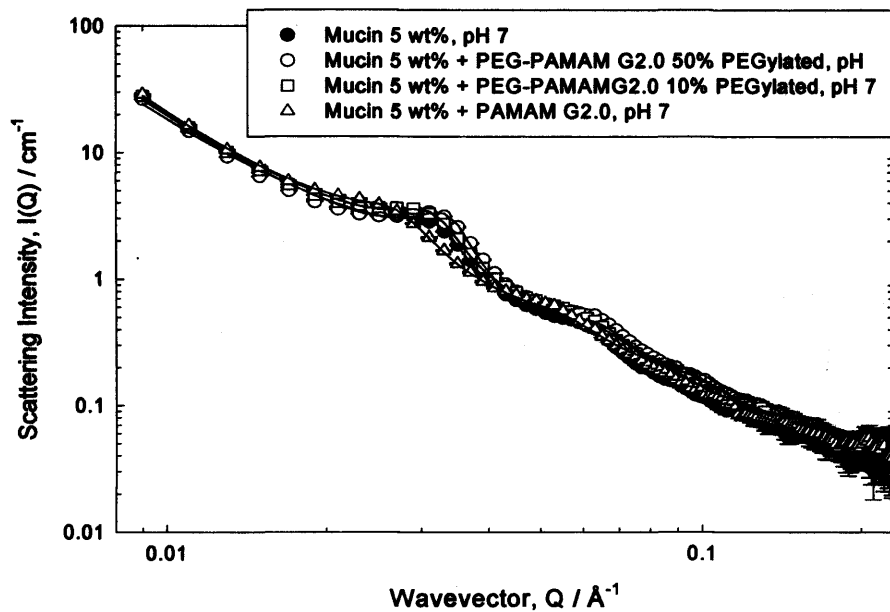
Figure 6.9 Scattering from 5 wt% mucin in the absence and in the presence of: 0.5 wt% PEG-PAMAM dendrimer conjugate 50% PEGylated, 0.5 wt% PEG-PAMAM dendrimer conjugate 10% PEGylated and 0.5 wt% PAMAM dendrimer. The top graph presents the situation for the PEG-PAMAM G2.0 conjugate in mucin 5 wt% while the bottom graph illustrates the state for the PEG-PAMAM G4.0 conjugate.

PEG-PAMAM conjugate added to mucin 5 wt%	Radius of gyration, R_g (nm)	Correlation length, ζ (nm)	Radius of the globule, R (nm)	Volume fraction, ϕ	Distance between the globule centres, L (nm)
none pH 7 (mucin only)	41.0 ± 2.0	23.5 ± 1.2	9.0 ± 0.5	0.37 ± 0.02	80.0 ± 18.3
PAMAM G2.0 0% PEGylation pH 7	50.0 ± 2.5	27.5 ± 1.4	9.5 ± 0.5	0.36 ± 0.02	98.0 ± 22.5
PEG-PAMAM G2.0 10% PEGylation	44.0 ± 2.2	25.5 ± 1.3	9.2 ± 0.5	0.38 ± 0.02	86.5 ± 19.9
PEG-PAMAM G2.0 50% PEGylation	42.0 ± 2.1	24.0 ± 1.2	9.4 ± 0.5	0.39 ± 0.02	82.0 ± 18.9
PEG-PAMAM G2.0 100% PEGylation	40.5 ± 2.0	23.5 ± 1.2	8.9 ± 0.4	0.37 ± 0.02	79.5 ± 18.3

Table 6.2 Parameters obtained from the model for the scattering from mucin solution 5 wt% in the presence and absence of PEG-PAMAM G2.0 conjugates with different degrees of PEGylation and PAMAM dendrimer G2.0 at pH 7.

PEG-PAMAM conjugate added to mucin 5 wt%	Radius of gyration, R_g (nm)	Correlation length, ξ (nm)	Radius of the globule, R (nm)	Volume fraction, ϕ	Distance between the globule centres, L (nm)
none pH 7 (mucin only)	41.0 ± 2.0	23.5 ± 1.2	9.0 ± 0.5	0.37 ± 0.02	80.0 ± 18.3
PAMAM G4.0 0% PEGylation pH 7	48.5 ± 2.4	28.0 ± 1.4	9.2 ± 0.5	0.35 ± 0.02	95.0 ± 21.8
PEG-PAMAM G4.0 10% PEGylation	44.5 ± 2.2	25.5 ± 1.3	9.2 ± 0.5	0.37 ± 0.02	87.0 ± 20.0
PEG-PAMAM G4.0 50% PEGylation	42.5 ± 2.1	24.5 ± 1.2	8.7 ± 0.4	0.40 ± 0.02	83.0 ± 19.1
PEG-PAMAM G4.0 100% PEGylation	40.5 ± 2.0	23.5 ± 1.2	9.0 ± 0.5	0.38 ± 0.02	79.0 ± 18.2

Table 6.3 Parameters obtained from the model for the scattering from mucin solution 5 wt% in the presence and absence of PEG-PAMAM G4.0 conjugates with different degrees of PEGylation and PAMAM dendrimer G4.0 at pH 7.

6.2.3. PGSE-NMR results

As already discussed in Chapter 5, the diffusion of PAMAM dendrimers in mucin solutions was greatly slowed compared to the diffusion of the dendrimer in free solution (*i.e.*, [mucin] = 0). In addition, the reduced mobility of the PAMAM dendrimers within mucin solutions resulted to be pH-dependent with pH 7 being the pH at which the dendrimers exhibited the strongest interaction towards the mucin.

Following the PEGylation, the PEG-PAMAM G2.0 conjugate full PEGylated has increased in size – having a bulkier shape, as idealized in Figure 6.10 – as well as in molecular weight compared to the original PAMAM dendrimer G2.0, from 3,260 g mol^{-1} (Mw of the PAMAM dendrimer G2.0) to 12,650 g mol^{-1} (Mw of the PEG-PAMAM G2.0 conjugate 100% PEGylated). A comparison of the normalized diffusion data of the PAMAM dendrimer G2.0 and PEG-PAMAM G2.0 dendrimer 100% PEGylated in mucin solutions are presented in Figure 6.11. The first thing that is evident is that the diffusion of the PEG-PAMAM G2.0 dendrimer 100% PEGylated in mucin solutions was greatly enhanced compared with the diffusion of the much smaller PAMAM G2.0 dendrimer. Because of their similarity in molecular weight, the normalized diffusion data from the PEG-PAMAM G2.0 in mucin solutions were compared with the normalized diffusion data from the *l*-PEG 10K g mol^{-1} in mucin solutions, as illustrated in Figure 6.11. Despite their different shape (random coil for the *l*-PEG and spherical for the PEG-PAMAM G2.0 conjugate), the diffusion data of the two polymers follow a similar linear trend. Whereas the PAMAM dendrimer G2.0 showed more adhesion than diffusion when increasing the mucin concentration, the full PEGylation of the dendrimer demonstrated a lack of significant interaction with the mucin.

Similarly, the diffusion NMR study of the PEG-PAMAM G4.0 full PEGylated in mucin solutions showed a significant increase in the diffusion rate of the conjugate when compared with the parent PAMAM

dendrimer G4.0, as illustrated in Figure 6.12. After the PEGylation, the size and the molecular weight of the PEG-PAMAM G4.0 conjugate has increased from 14,210 g mol^{-1} (Mw of the PAMAM dendrimer G4.0) to 51,760 g mol^{-1} (Mw of the PEG-PAMAM G4.0 conjugate 100% PEGylated). Considering the similarity in molecular weight with the *l*-PEG 50K g mol^{-1} (but still a different shape: random coil for the *l*-PEG and a more spherical shape for the PEG-PAMAM conjugate), the normalized diffusion data of the PEG-PAMAM G4.0 conjugate full PEGylated in mucin solutions were compared to the normalized diffusion data from the *l*-PEG 50K g mol^{-1} in mucin solutions (Figure 6.12). Even though the normalized diffusion data of the two polymers in mucin solutions exhibited a similar linear trend, the large spherical-shaped PEG-PAMAM G4.0 conjugate demonstrated a higher mobility in mucin solution compared to the random coiled *l*-PEG. As already seen for the PEG-PAMAM G2.0 conjugate, also the PEG-PAMAM G4.0 conjugate demonstrated a lack of significant interaction with the mucin when compared to the relative parent PAMAM dendrimers.
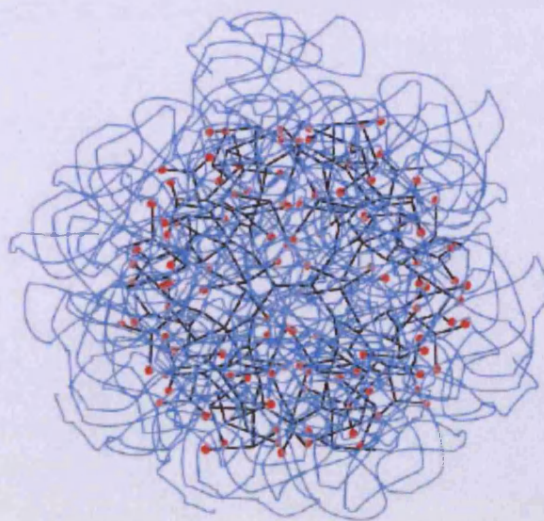
Figure 6.10 Schematic representation of a PEG-PAMAM dendrimer 100% PEGylated. The PAMAM core is black and the PEG chains are blue. Red circles indicate primary amine sites on the PAMAM. Taken from Luo D. [51].
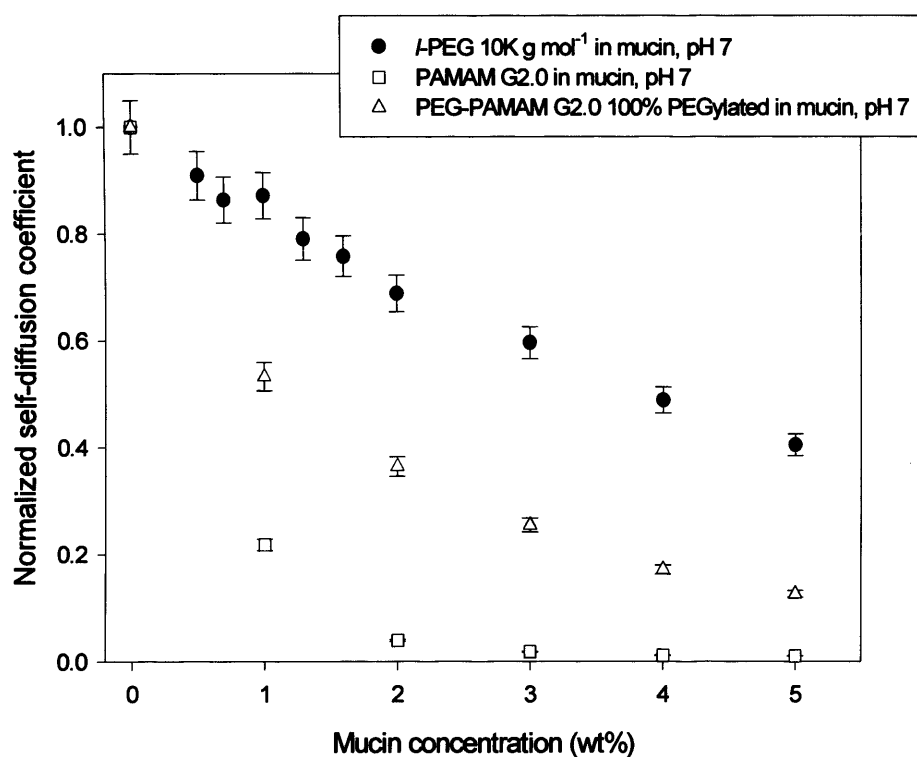
Figure 6.11 Normalized (to [mucin] = 0) self-diffusion coefficients of l-PEG 10K g mol⁻¹, PAMAM dendrimer G2.0 and PEG-PAMAM G2.0 100% PEGylated at pH 7.
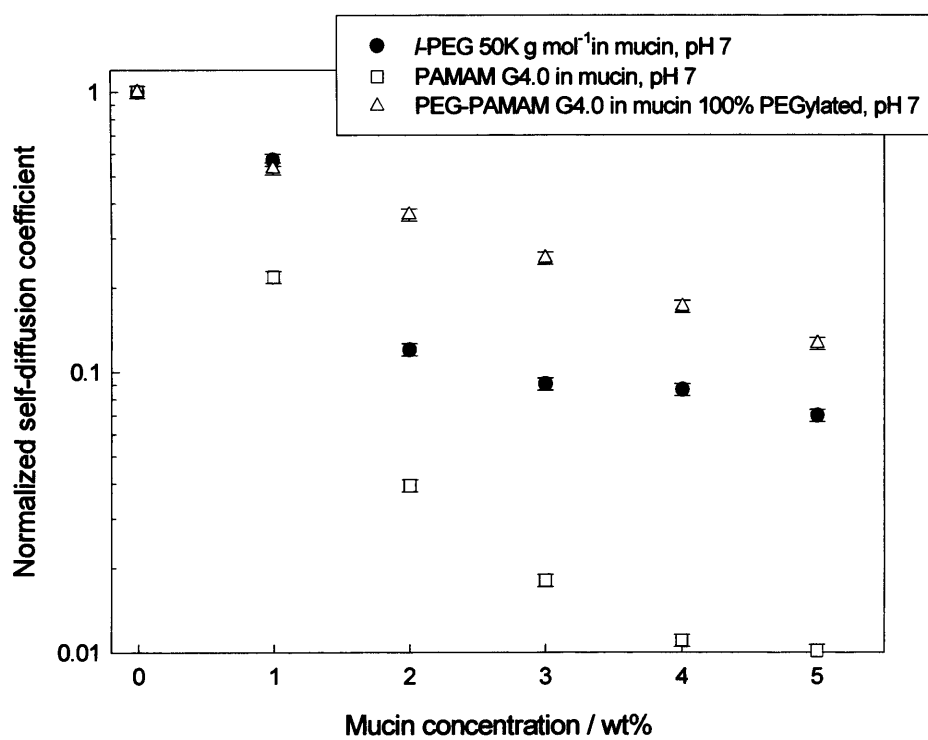
Figure 6.12 *Normalized (to [mucin] = 0) self-diffusion coefficients of l-PEG 50K g mol⁻¹, PAMAM dendrimer G4.0 and PEG-PAMAM G4.0 100% PEGylated at pH 7.*

6.3. Discussion

In the study here presented, the behaviour of partly and fully PEGylated PAMAM dendrimers as potential polymeric carriers for therapeutics in the mucin gel network has been explored. The synthesis of total (100%) or partial (10% and 50%) PEGylated PAMAM dendrimers G2.0 and G4.0 was carried out to mask fully or partly the amino terminal surfaces of these polymers, main responsible of the specific interaction exhibited by the dendrimers towards the mucin. The effect of PEGylation on PAMAM dendrimers in terms of interaction with the mucin has been evaluated by SANS and PGSE-NMR.

The SANS study revealed that the presence of the PEGylated PAMAM dendrimers G2.0 and G4.0 reduced the specific electrostatic interaction exhibited by the PAMAM dendrimers towards mucin molecules.
100% PEGylated PAMAM dendrimer conjugates did not show significant change in the scattering from mucin solutions, at least to a degree that induces a structural perturbation in the mucin. These results could be interpreted as an evidence of a lack of an interaction between the 100% PEGylated conjugates and the mucin. Indeed, the fully PEG modified dendrimers appear like bulky, spherical molecules coated by a dense layer of inert PEG chains which cover the amino surfaces of the PAMAM, as idealized in Figure 6.10: therefore, a shielding of the positive charge on the dendrimer surface is played by the attached PEG chains. For this reason, the PEG-PAMAM conjugates did not exhibit any relevant change in the scattering from mucin since they were behaving as neutral molecules.
From the diffusion NMR study performed on the fully PEGylated PAMAM dendrimers G2.0 and G4.0, fundamental findings were obtained. The PEG-PAMAM conjugates demonstrated an enhanced diffusion in mucin solutions compared with the unPEGylated PAMAM denrimers. Although an almost four-fold increase in molecular weight is observed in the 100% PEGylated PAMAM conjugates compared with the parent PAMAM dendrimers, the conjugates exhibited a higher diffusion rate in

mucin solutions thanks to their non interactive properties given by the PEG coating.

50% and 10% PEGylated PAMAM dendrimer conjugates exhibited a small electrostatic interaction with mucin molecules due to the residual positively charged amino groups which have not been PEGylated. However, the scattering from mucin in the presence of the partly PEGylated PAMAM conjugates was not significantly affected by the presence of the conjugates when compared to the perturbation on the scattering from mucin caused by the unPEGylated PAMAM dendrimers. The fact that changing the degree of modification of the PEG-PAMAM conjugates did not affect greatly the interaction with mucin is in agreement with the findings from Yang *et al.* [49] who demonstrated that PEGylation degree on low generation PAMAM dendrimers could be reduced dramatically while maintaining the drug carrier cytocompatibility.

PGSE-NMR data, together with the scattering data, can be considered an evidence of a less interactive behaviour between the PEGylated conjugates and the mucin. The achievement obtained after PEG modification of the PAMAM was in agreement with the results reported by Lai *et al.* [38] who demonstrated how the PEG-coating process increased the transport of nanoparticles through mucus. Also, the effect of PEG modification on PAMAM dendrimers towards the mucin resulted in accordance with studies reporting a less toxicity of the PEG-PAMAM conjugates compared to the unPEGylated PAMAM [47-52]. As the cytotoxicity of cationic PAMAM dendrimers is thought to be the result of the interaction between positively charged dendrimers and negatively charged cell surfaces, in the same way the interaction between the PAMAM and mucin is driven by an electrostatic interaction between the positively charged dendrimers and the negatively charged mucin glycoprotein. In both cases, PEGylation is able to reduce this electrostatic interaction.

Moreover, the PEG modification of PAMAM dendrimers allow these polymers to maintain their unique structure and, at the same time, to show

less specific interaction towards mucin molecules as well as to show reduced cytotoxicity and haemolytic activity. Therefore, PEG-PAMAM conjugates can potentially be used as polymeric carriers for therapeutic molecules which can be either entrapped/encapsulated in the dendritic cavities of the modified dendrimers [54, 56] or covalently linked to the modified branch of the polymer [48].

6.4. *Conclusions*

Despite their unique structure and the ability to carry high drug payload, PAMAM dendrimers exhibited a strong interaction towards mucin, as findings on Chapter 5 demonstrated. Therefore, the study here presented has arisen from the possibility to keep the structural characteristics typical of the PAMAMs and to reduce their interaction with mucin by building up a PEG-coating shell around the PAMAM dendrimers, known the inert properties of the PEG.

A series of PEG-PAMAM conjugates (PAMAM dendrimers G2.0 and G4.0) with different degree of PEGylation (10%, 50% and 100%) has been synthesized. Their behaviour in mucin solutions has been investigated by SANS and diffusion NMR. The PEG-PAMAM conjugates were much less interacting with the mucin network compared to the unPEGylated PAMAM dendrimers, thanks to the PEG chains that provide them an inert shell. The degree of PEGylation did not influence significantly the system mucin-conjugate, even though the 100% PEGylated PAMAM dendrimers conjugates were the less interactive. Also the self-diffusion of the conjugates in mucin resulted greatly improved compared to the self-diffusion of the parent PAMAM dendrimers in mucin, merit of the PEG modification which reduced any specific interaction of the PAMAM dendrimers with the mucin glycoprotein.

The study presented here was further confirmation on the effect of PEGylation on PAMAM dendrimers: in fact, the PEG chains modification of these polymers not only makes these polymeric carriers less toxic but also decreases greatly the interaction with the mucosal barrier. Therefore, PEG-PAMAM conjugates could be positively considered as potential polymeric carriers for the delivery of therapeutics – encapsulated in the dendritic cavities or covalently bound to the modified branches of the polymer – through organs bearing a mucus gel layer (*i.e.*, gastrointestinal, pulmonary, oral, nasal and genital tracts).

Furthermore, PEGylation technology could be extended also to the half-generation PAMAM dendrimers. Although they have showed to be less cytotoxic and hemolytic compared to the full generation PAMAM dendrimers [57], PEG chains conjugation to the half-generation dendrimers could definitely improve their behaviour as potential polymeric carriers for therapeutic molecules.

Based on the initial hypothesis of the positively effects of PEGylation on PAMAM dendrimers, it can be concluded that PEGylation experiments have produced the expected effects, removing or significantly reducing the interaction of the PAMAM dendrimers with mucin.

References

1. Veronese, F. M.; Pasut, G., PEGylation, successful approach to drug delivery. *Drug Discovery Today* **2005**, 21, 1451-1458.

2. Harris, J. M.; Chess, R. B., Effect of PEGylation on pharmaceuticals. *Nature Reviews Drug Discovery* **2003**, 2, 214-221.

3. Harris, J. M.; Martin, N. E.; Modi, M., PEGylation: a novel process for modifying pharmacokinetics. *Clinical Pharmacokinetics* **2001**, 40, 539-551.

4. Graham, L. M., PEGASPARAGINASE: a review of clinical studies. *Advanced Drug Delivery Reviews* **2003**, 55, 1293-1302.

5. Levy, Y.; Hershfield, M. S.; Fernandez-Mejia, C.; Polmar, S. H.; Scudiery, D.; Berger, M.; Sorensen, R. U., Adenosine deaminase deficiency with late onset of recurrent infections: response to treatment with polyethylene glycol-modified adenosine deaminase. *Journal of Pediatrics* **1988**, 113, 312-317.

6. Reddy, K. R.; Modi, M. W.; Pedder, S., Use of peginterferon α-2a (40KD) (PEGASYS) for the treatment of hepatitis C. *Advanced Drug Delivery Reviews* **2002**, 54, 571-586.

7. Wang, Y.-S.; Youngster, S.; Grace, M.; Bausch, J.; Bordens, R.; Wyss, D., F., Structural and biological characterization of pegylated recombinant interferon alpha-2b and its therapeutic implications. *Advanced Drug Delivery Reviews* **2002**, 54, 547-570.

8. Davis, F. F., Enzyme-polyethylene glycol adducts: modified enzymes with unique properties. *Enzyme Engineering* **1978**, 4, 169-173.

9. Abuchowsky, A.; van Es, T.; Palczuk, N. C.; Davis, F. F., Alteration of immunological properties of bovine serum albumin by covalent attachment of polyethylene glycol. *Journal of Biological Chemistry* **1977**, 252, 3578-3581.

10. Abuchowsky, A.; McCoy, J. R.; Palczuk, N. C.; van Es, T.; Davis, F. F., Effect of covalent attachment of polyethylene glycol on

immunogenicity and circulating life of bovine liver catalase. *Journal of Biological Chemistry* **1977**, 252, 3582-3586.

11. Pasut, G.; Guiotto, A.; Veronese, F. M., Protein, peptide and non-peptide drug PEGylation for therapeutic application. *Expert Opinion on Therapeutic Patents* **2004**, 14, 859-894.

12. Katre, N. V., The conjugation of proteins with polyethylene glycol and other polymers: altering properties of proteins to enhancing their therapeutic potential. *Advanced Drug Delivery Reviews* **1993**, 10, 91-114.

13. Bailon, P.; Berthold, W., Polyethylene glycol-conjugated pharmaceutical proteins. *Pharmaceutical Science & Technology Today* **1998**, 1, 352-356.

14. Fung, W.-J.; Porter, J. E.; Bailon, P., Strategies for the preparation and characterization of polyethylene glycol (PEG) conjugated pharmaceutical proteins. *Polymer Preprint* **1997**, 38, 565-566.

15. Morpurgo, M.; Veronese, F. M.; Kachensky, D.; Harris, J. M., Preparation and characterization of polyethylene glycol vinyl sulfone. *Bioconjugate Chemistry* **1996**, 7, 363-368.

16. Friman, S.; Egestad, B., Hepatic excretion and metabolism of polyethylene glycols and mannitol in the cat. *Journal of Hepatitology* **1993**, 17, 48-55.

17. Kawai, F., Microbial degradation of polyethers. *Applied Microbiology and Biotechnology* **2002**, 58, 30-38.

18. Bailon, P.; Palleroni, A.; Schaffer, C. A.; Spence, C. L.; Fung, W.-J.; Porter, J. E.; Ehrlich, G. K.; Pan, W.; Xu, Z.-X.; Modi, M. W.; Farid, A.; Berthold, W.; Graves, M., Rational design of a potent, long lasting form of interferon: a 40 KDa branched polyethylene glycol-conjugated interferon alpha-2a for the treatment of hepatitis C. *Bioconjugate Chemistry* **2001**, 12, 195-202.

19. Gabizon, A.; Martin, F., Polyethylene glycol-coated (pegylated) liposomal doxorubicin. *Drugs* **1997**, 54, 15-21.

20. Allen, T. M., Liposomes: opportunities in drug development. *Drugs* **1997**, 54, 8-14.

21. Stewart, S.; Jablonowski, H.; Goebel, F. D.; Arasteh, K.; Spittle, M.; Rios, A.; Aboulafia, D.; Galleshaw, J.; Dezube, B. J., Randomized comparative trial of pegylated liposomal doxorubicin versus bleomycin and vincristine in the treatment of AIDS-related Kapoi's sarcoma. International pegylated liposomal doxorubicin study group. *Journal of Clinical Oncology* **1998**, 16, 683-691.

22. Kim, J. Y.; Kim, J. K.; Park, J. S.; Byun, Y.; Kim, C. K., The use of PEGylated liposomes to prolong circulation lifetimes of tissue plasminogen activator. *Biomaterials* **2009**, 30, 5751-5756.

23. O'Brien, M. E. R.; Wingler, N.; Inbar, M.; Rosso, R.; Griscke, E.; Santoro, A.; Catane, R.; Kieback, D. G.; Tomczak, P.; Ackland, S. P.; Orlandi, F.; Mellars, L.; Alland, L.; Tendler, C., Reduced cardiotoxicity and comparable efficacy in a phase III trial of pegylated liposomal doxorubicin HCl (CAELYX ᵀᴹ/Doxil) versusconventional doxorubicin for first-line treatment of metastatic breast cancer *Annals of Oncology* **2004**, 15, 440-449.

24. Verma, S.; Dent, S.; Chow, B. J.; Rayson, D.; Safra, T., Metastatic breast cancer: the role of pegylated liposomal daxorubicin after conventional anthracyclines. *Cancer Treatment Reviews* **2008**, 34, 391-406.

25. O'Brien, M. E. R., Single-agent treatment with pegylated liposomal doxorubicin for metastatic breast cancer. *Anti-Cancer Drugs* **2008**, 19, 1-7.

26. Salzberg, M.; Thurlimann, B.; Hasler, U.; Delmore, G.; von Rohr, A.; Thurlimann, A.; Ruhstaller, T.; Stopatschinskaja, S.; von Moos, R., Pegylated liposomal doxorubicin (caelyx) in metastatic breast cancer: a community-based observation study. *Oncology* **2007**, 72, 147-151.

27. Al-Batran, S.-E.; Bischoff, J.; von Minckwitz, G.; Atmaca, A.; Kleeberg, U.; Meuthen, I.; Morack, G.; Lerbs, W.; Hecker, D.; Sehouli, J.; Knuth, A.; Jager, E., The clinical benefit of pegylated liposomal doxorubicin in patients with metastatic breast cancer

previously treated with conventional anthracyclines: a multicentre phase II trial *British Journal of Cancer* **2006**, 94, 1615-1620.

28. Strother, R.; Matei, D., Pegylated liposomal doxorubicin in ovarian cancer. *Journal of Therapeutics and Clinical Risk Management* **2009**, 5, 639-650.

29. Green, A. E.; Rose, P. G., Pegylated liposomal doxorubicin in ovarian cancer. *International Journal of Nanomedicine* **2006**, 1, 229-239.

30. Thigpen, J. T.; Aghajanian, C. A.; Alberts, D. S.; Campos, S. M.; Gordon, A. N.; Markman, M.; McMeekin, D. S.; Monk, B. J.; Rose, P. G., Role of pegylated liposomal doxorubicin in ovarian cancer. *Gynecologic Oncology* **2005**, 96, 10-18.

31. Sanders, N. N.; De Smedt, S. C.; Cheng, S. H.; Demeester, J., Pegylated GL67 lipoplexes retain their gene transfection activity after exposure to component of CF mucus. *Gene Therapy* **2002**, 9, 363-371.

32. Ogris, M.; Walker, G.; Blessing, T.; Kircheis, R.; Wolscher, M.; Wagner, E., Tumor-targeted gene therapy: strategies for the preparation of ligand-polyethylene glycol-polyethylenimine/DNA complexes. *Journal of Controlled Release* **2003**, 91, 173-181.

33. Lenter, M. C.; Garidel, P.; Pelisek, J.; Wagner, E.; Ogris, M., Stabilized non viral formulations for the delivery of MCP-1 gene into cells of the vasculoendothelial system. *Pharmaceutical Research* **2004**, 21, 683-691.

34. Mishra, S.; Webster, P.; Davis, M. E., PEGylation significantly affects cellular uptake and intracellular trafficking of non-viral gene delivery particles. *European Journal of Cell Biology* **2004**, 83, 97-111.

35. Pun, S. H.; Tack, F.; Bellocq, N. C.; Cheng, G. J.; Grubbs, B. H.; Jensen, G. S.; Davis, M. E.; Brewster, M.; M., J.; Janssens, B.; Floren, W.; Bakker, A., Targeted delivery of RNA-cleaving DNA enzyme (DNAzyme) to tumor tissue by transferrin-modified,

cyclodextrin-based particles. *Cancer Biology and Therapy* **2004**, 3, 641-650.

36. Sun, X.; Rossin, R.; Turner, J. L.; Becker, M. L.; Joralemon, M. J.; Welch, M. J.; Wooley, K. L., An assessment of the effects of shell cross-linked nanoparticle size, core composition, and surface PEGylation on in vivo biodistribution. *Biomacromolecules* **2005**, 6, 2541-2544.

37. Zahr, A. S.; de Villiers, M.; Pishko, M. V., Encapsulation of drug nanoparticles in self-assembled macromolecular nanoshells. *Langmuir* **2005**, 21, 403-410.

38. Lai, S. K.; O'Hanlon, D. E.; Harrold, S.; Man, S. T.; Wang, Y.-Y.; Cone, R.; Hanes, J., Rapid transport of large polymeric nanoparticles in fresh undiluted human mucus. *Proceedings of the National Academy of Sciences of the United States of America* **2007**, 104, 1482-1487.

39. Hanes, J.; Dawson, M. R.; Wirtz, D.; Fu, J.; Krauland, E. M. Drugs and gene carrier particles that rapidly move through mucous barriers. 2005.

40. Kolhe, P.; Khandare, J.; Pillai, O.; Kannan, S.; Lieh-Lai, M.; Kannan, R. M., Preparation, cellular transport, and activity of polyamidoamine-based dendritic nanodevices with a high drug payload. *Biomaterials* **2006**, 27, 660-669.

41. Kukowska-Latallo, J. F.; Bielinska, A. U.; Johnson, J. J.; Spindler, R.; Tomalia, D. A.; Baker, J. R. J., Efficient transfer of genetic material into mammalian cells using Starbust polyamidoamine dendrimers. *Proceedings of the National Academy of Sciences of the United States of America* **1996**, 93, 4897-4902.

42. Agarwal, A.; Saraf, S.; Asthana, A.; Gupta, U.; Gajbhiye, V.; Jain, N. K., Ligand based dendritic systems for tumor targeting. *International Journal of Pharmaceutics* **2008**, 350, 3-13.

43. Costantino, L.; Gandolfi, F.; Bossy-Nobs, L.; Tosi, G.; Gurny, R.; Rivasi, F.; Vandelli, M. A.; Forni, F., Nanoparticulate drug carriers

based on hybrid poly(D,L-lactide-co-glycolide)-dendron structures. *Biomaterials* **2006,** 27, 4635-4645.

44. Esfand, R.; Tomalia, D. A., Poly(amidoamine) (PAMAM) dendrimers: from biomimicry to drug delivery and biomedical applications. *Drug Discovery Today* **2001,** 6, 427-436.

45. Ke, W.; Zhao, Y.; Huang, R.; Jiang, C.; Pei, Y., Enhanced oral bioavailability of daxorubicin in a dendrimer drug delivery system. *Journal of Pharmaceutical Science* **2008,** 97, 2208-2216.

46. Guillaudeu, S. J.; Fox, M. E.; Haidar, Y. M.; Dy, E. E.; Szoka, F. C.; Frechet, J. M. J., PEGylated dendrimers with core functionality for biological applications. *Bioconjugate Chemistry* **2008,** 19, 461-469.

47. Wang, W.; Xiong, W.; Wan, J.; Sun, X.; Xu, H.; Yang, X., The decrease of PAMAM dendrimer-induced cytotoxicity by PEGylation via attenuation of oxidative stress. *Nanotechnology* **2009,** 20, 1-7.

48. Zhu, S.; Hong, M.; Tang, G.; Qian, L.; Lin, J.; Jiang, Y.; Pei, Y., Partly PEGylated polyamidoamine dendrimer for tumor-selective targeting of doxorubicin: the effects of PEGylation degree and drug conjugation style. *Biomaterials* **2010,** 31, 1360-1371.

49. Yang, H.; Lopina, S. T.; DiPersio, L. P.; Schmidt, S. P., Stealth dendrimers for drug delivery: correlation between PEGylation, cytocompatibility, and drug payload. *Journal of Material science: Materials in Medicine* **2008,** 19, 1991-1997.

50. Zhu, S.; Hong, M.; Zhang, L.; Tang, G.; Jiang, Y.; Pei, Y., PEGylated PAMAM dendrimer-daxorubicin conjugates: in vitro evaluation and in vivo tumor accumulation. *Pharmaceutical Research* **2010,** 27, 161-174.

51. Luo, D.; Haverstick, K.; Belcheva, N.; Han, E.; Saltzman, W. M., Poly(ethylene glycol)-conjugated PAMAM dendrimer for biocompatible, high-efficiency DNA delivery. *Macromolecules* **2002,** 35, 3456-3462.

52. Jevprasephant, R.; Penny, J.; Jalal, R.; Attwood, D.; McKeown, N. B.; D'Emanuele, A., The influence of surface modification on the

cytotoxicity of PAMAM dendrimers. *International Journal of Pharmaceutics* **2003,** 252, 263-266.

53. Kumar, P. V.; Agashe, H.; Dutta, T.; Jain, N. K., PEGylated dendritic architecture for development of a prolonged drug delivery system for an antitubercular drug. *Current Drug Delivery* **2007,** 4, 11-19.

54. Bai, S.; Ahsan, F., Synthesis and evaluation of PEGylated dendrimeric nanocarrier for pulmonary delivery of low molecular weight heparin. *Pharmaceutical Research* **2009,** 26, 539-548.

55. Kojima, C.; Kono, K.; Maruyama, K.; Takagishi, T., Synthesis od polyamidoamine dendrimers having poly(ethylene glycol) grafts and their ability to encapsulate anticancer drugs. *Bioconjugate Chemistry* **2000,** 11, 910-917.

56. Bhadra, D.; Bhafra, S.; Jain, S.; Jain, N. K., A PEGylated dendritic nanoparticulate carrier of fluorouracil. *International Journal of Pharmaceutics* **2003,** 257, 111-124.

57. Wiwattanapatapee, R.; Carreno-Gomez, B.; Malik, N.; Duncan, R., Anionic PAMAM dendrimers rapidly cross adult rat intestine in vitro: a potential oral delivery system? *Pharmaceutical Research* **2000,** 17, 991-998.

Chapter 7.   Towards a more realistic mucus model

In this chapter, the study focuses on investigating more complex mucin solutions, which are closer to a more realistic mucus. Mucin solutions have been enriched with phospholipids and proteins, these being the main constituents in mucus. These more complex systems have been examined by small-angle neutron scattering (SANS).

7.1.   Introduction

7.1.1.   The importance of the presence of phospholipids and proteins in mucus

Although the main organic component in mucus is represented by the mucin [1,2] (as already extensively discussed in Chapter 1), mucus is rich in lipids (free fatty acids, phospholipids), surfactants and proteins [3] (see composition of mucus in Table 1.1 in Chapter 1).

Phospholipids, the major lipid components of mucus, are amphiphilic molecules containing a polar head group and a non-polar hydrocarbon (fatty acid) tails. The major classes of phospholipids include phosphatidylcholine (PC), phosphatidylethanolamine (PE), phosphatidylinositol (PI), and phosphatidylserine (PS). Their chemical structures are illustrated in Figure 7.1.

The phospholipids composition of the mucus which covers epithelial surfaces can vary depending on its location and role [4,5]. The major surface active component of lung surfactant is the dipalmitoyl phosphatidylcholine (DPPC), which contains two saturated fatty acids, palmitic acid (DPPC 16:0/16:0); whereas for the gastric mucus the main phospholipids are phosphatidylcholine (PC) species – containing one saturated (palmitic acid 16:0 or stearic acid 18:0) and one unsaturated (oleic acid 18:1 or linoleic acid 18:2) fatty acid – and phosphatidylethanolamine (PE) [6]. A phospholipid composition of gastric mucus is presented in Table 7.1.

Phosphatidylcholine
(PC)

Phosphatidylethanolamine
(PE)

Phosphatidylinositol
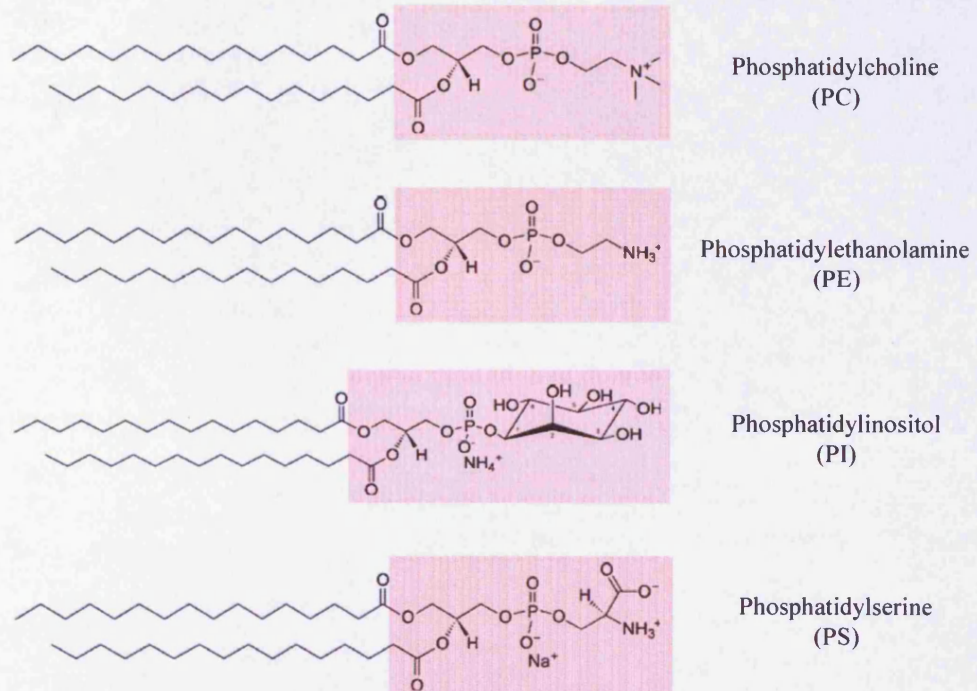(PI)

Phosphatidylserine
(PS)

Figure 7.1 Chemical structures of the phosphatidylcholine (PC), phosphatidylethanolamine (PE), phosphatidylinositol (PI), and phosphatidylserine (PS) (highlighted in the pink boxes). Each one is attached to two palmitic acid (16:0/16:0) chains.

Phospholipid	Mean percentage (%)
Phosphatidylcholine (PC)	33.1 ± 0.72
Phosphatidylethanolamine (PE)	29.6 ± 0.48
Phosphatidylinositol (PI)	23.2 ± 0.57
Phosphatidylserine (PS)	2.1 ± 0.12

Table 7.1 *Phospholipid composition in human gastric mucus* [7].

The role of pulmonary surfactant is to maintain alveolar function in mammalian lungs. The high resistance to compression of the dipalmitoyl phospatidylcholine opposes surface tension forces in the alveolus, generating a very high surface pressure, which prevents alveolar collapse at end expiration. These functions are critical for efficient respiration [8, 9]. Also, surfactant posses anti-inflammatory properties [10], facilitates mucus clearance [11], plays a role in preventing pulmonary infection [10]. Respiratory diseases, such as cystic fibrosis (CF), asthma, and chronic bronchitis, are usually associated with excessive insoluble accumulation of secretory material in the airways which may be responsible for the airway obstruction leading to cough and sputum production. Surfactant composition and function are chemically and physically altered in patients with cystic fibrosis and asthma. The surface activity of surfactant was markedly repressed and a deficiency in quantity and composition of the phospholipids – in particular a decrease in phosphatidylcholine and phosphatidylglycerol content [12] – was observed in CF and asthma patients than in controls: some of these changes have been associated with increases in mucus rigidity or increased mucus adherence to the respiratory mucosa [13, 14]. To help the surfactant deficiency in patients with

chronic respiratory problems, the exogenous administration of synthetic surfactant preparation seemed to be promising to improve mucus clearance [15-17], even though a surfactant replacement therapy remains still a clinical challenge [18].

In contrast, gastric surfactant – synthesized and secreted from cells of the gastric mucosa – is fundamental to form a barrier to avoid back-diffusion of hydrogen ions and following damage to mucosal surfaces in the stomach [4, 19]. The 'hydrophobic gastric mucosal barrier' is a complex and dynamic defence system for the gastric mucosa to resist the corrosive effects of peptic hydrochloric acid secretion and the surface active phospholipids have been reported to play a key part in the gastric cytoprotection [20-27]. Therefore, a defective mucosa with a variation in the phospholipid composition may result in the development of gastritis or ulcerative colitis: in particular, quantitatively less phosphatidylcholine and lysophosphatidylcholine were reported from mucus of patients with ulcerative colitis than from healthy controls, even though it is not completely clear whether this is due to a reduced biosynthesis and/or increased breakdown of these phospholipids [28]. For this reason, a treatment with phosphocholine rich phospolipids for reinforcing the mucus hydrophobic barrier was thought as therapeutic approach for ulcerative colitis, considering also the promising results [29].

Together with the lipids, another component contributing to the complexity of the mucus is represented by the non-mucin proteins. Proteins such as IgA, lysozyme, lactoferrin and lactoperoxidase, which all have protective functions against bacterial infections, have been identified in mucous secretions [30, 31].

Studies performed on different types of mucus – pulmonary [32-34], gastro-intestinal [35, 36], cervical [37] – reported that some common proteins present in the mucus are related to serum proteins such as albumin. Serum albumin is also one of the most abundant plasma proteins and one of its main role is the maintenance of the colloid osmotic pressure (COP) – *i.e.*, a form of

osmotic pressure exerted by proteins that usually tends to pull water into the system.

Considering the complexity of the mucus composition, in this Chapter the attention was focused on the analysis of a more realistic mucus, investigating the contribution, binding, interaction of phospholipids and proteins towards the mucin. Bovine serum albumin (BSA), 1,2-dihexanoyl-*sn*-glycero-3-phosphocoline (DHPC) and 1,2-dipalmitoyl-*sn*-glycero-3-phosphocholine (DPPC) were chosen as main representative components for serum protein, 'short-chain' lipid and 'long-chain' lipid to enrich mucin solutions and create a more realistic mucus. Their effects on mucin solutions were analyzed by SANS.

7.2. Results

The addition of bovine serum albumin (BSA), 1,2-dihexanoyl-*sn*-glycero-3-phosphocoline (DHPC) and 1,2-dipalmitoyl-*sn*-glycero-3-phosphocholine (DPPC) on mucin solutions was investigated by SANS. Effects of each single component were first studied on mucin solutions (binary mixtures); afterwards, the mixture of more than one component with mucin solutions was investigated (ternary mixtures).

The scattering from 5 mM DPPC vesicles in D_2O was also studied.

7.2.1. SANS study on DPPC vesicles

DPPC vesicles were prepared according to the procedure described in Section 3.2.3 in Chapter 3. Therefore, unilamellar DPPC vesicles were obtained after the extrusion process.

The scattering from 5 mM h-DPPC vesicles in D_2O is presented in Figure 7.1. The scattering data were modelled to a polydisperse shell sphere describing the DPPC bilayer divided into three concentric shells corresponding to two polar headgroups region (one on each side of the bilayer) and the bilayer center spanning hydrocarbon region, as idealized in Scheme 7.1.

For dispersions of monodisperse centrosymmetric particles, the scattered intensity is given by Eq. 7.1:

$$I(Q) = N_p |F(Q)|^2 S(Q)$$
Eq. 7.1

where Q is the scattering vector $Q = \dfrac{4\pi \sin\theta}{\lambda}$, N_p the number density of particles, $|F(Q)|^2$ their form factor $- |F(Q)|^2 = P(Q)$ - and $S(Q)$ the interparticle structure factor. The interparticle structure factor $S(Q)$ is approximately equal to 1 for dilute and weakly interacting particles, which is a good approximation for unilamellar vesicles at phospholipid concentration lower than 2 wt% [38, 39].

The form factor $|F(Q)|^2 = P(Q)$ is the Fourier transform of the contrast $\Delta\rho(r)$ between the coherent neutron-scattering length density (SLD) of the bilayer and the solvent. For unilamellar vesicles bilayer model represented in the Scheme 7.1, $F(Q)$ is given by Eq. 7.2:

$$F(Q) = 4\pi \sum_{i=1}^{3} \int_{R_{i-1}}^{R_i} \Delta\rho_i \frac{\sin(Qr)}{Qr} r^2 dr$$
Eq. 7.2

where $\Delta\rho_i(r)$ is the SLD contrast and $\Delta d_i = R_i - R_{i-1}$ is the thickness of the ith strip [40].

As illustrated in Scheme 7.1, the radii $- R_1$, R_2, R_3 and $R_4 -$ measure the distance from the center of the spherical vesicles to the border of the ith concentric shell: the values of the radii for a 5 mM DPPC vesicle are reported in Table 7.1. The DDPC vesicle has a radius (R_4) of $\sim$ 830 Å, which is consistent with the DPPC vesicles extruded through 100 nm membrane filter. The thickness of the polar region (R_2-R_1 and R_4-R_3) of the DPPC bilayer can be deduced from the data of other authors as well [41-45]. A constrained value of 9 Å was considered as thickness of the headgroups layer (R_2-R_1 and R_4-R_3). The calculated thickness of the phospolipid bilayer (R_4-R_1) resulted of 56 Å, which is in agreement with the data from Nagle *et al.* [44].
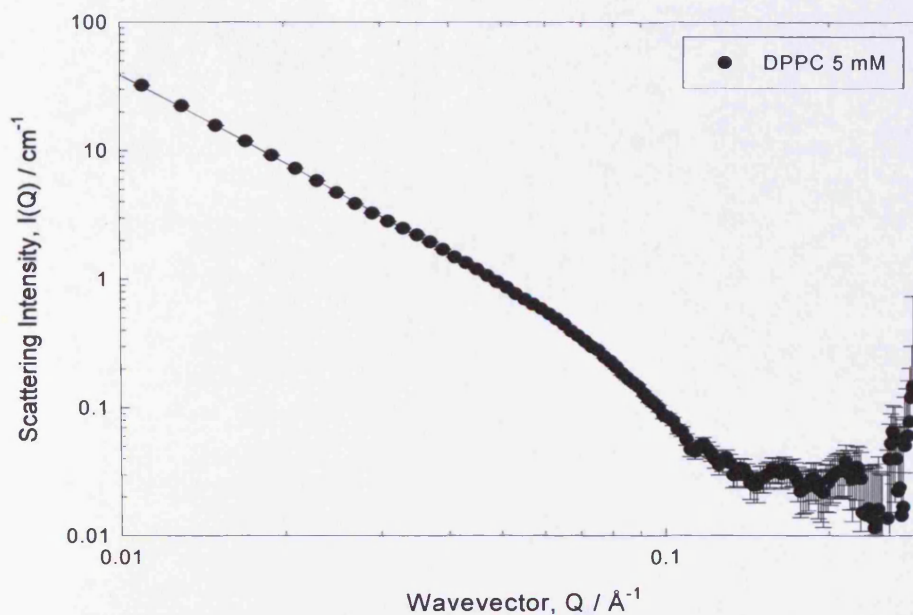
Figure 7.1 *Scattering (symbols) and fit (solid lines) from 5 mM (h) DPPC vesicles in D_2O.*
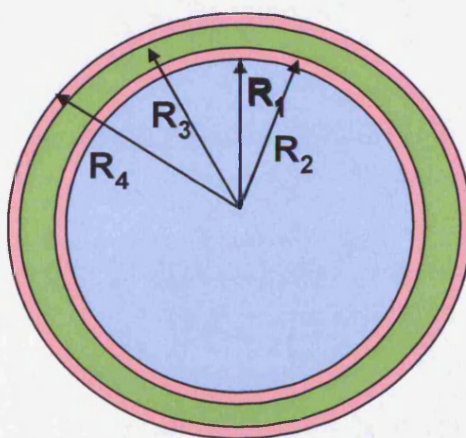
Scheme 7.1 *Representation of the DPPC vesicle: the pink circle represents the headgroups thickness; the green circle is the phospholipid bilayer; the blue circle symbolizes the inside aqueous compartment.*

R_1 (nm)	R_2 (nm)	R_3 (nm)	R_4 (nm)
77.1 ± 3.8	78.0 ± 3.9	81.8 ± 4.1	82.7 ± 4.1

Table 7.1 *Values for the radii of the DPPC vesicle sketched in Scheme 7.1.*

7.2.2. SANS study on binary mixtures

Scattering from 5 wt% mucin solutions was studied in the presence of one of each added component: (i) 500 ppm and 5000 ppm BSA; (ii) h- and d-DHPC 5 mM; and (iii) h- and d-DPPC vesicles 5 mM. The BSA concentrations used are in agreement with the albumin concentration present in the respiratory tract as reported by Rennard *et al.* [46]. Since the surfactant concentration in the lungs is above 2-3 mg/ml [47] – values for neonatal lungs which tend to diminish to adult level – the phospholipids concentrations used were selected accordingly.

The scattering from 5 wt% mucin solutions after the addition of BSA at a concentration of 500 and 5000 ppm are presented in Figure 7.2. The presence of the bovine serum protein perturbed the scattering from mucin shifting the maxima to lower Q, corresponding an increase in size/distance of ~ 15 %. Increasing the BSA concentration to 5000 ppm did not induce any further changes to the scattering from mucin. The changes in the scattering from mucin could be attributed to a possible protein-protein interaction between the bovine serum albumin and the mucin glycoprotein.

The effects of the addition of 5 mM DHPC on 5 wt% mucin solutions is shown in Figure 7.3. Whether the phospholipid was added in the hydrogenated or deuterated form made no significant difference to the scattering from mucin solutions as both forms induced a similar change, which means that the scattering from h-DHPC 5 mM could be assumed to be insignificant. The addition of DHPC 5 mM to 5 wt% mucin solutions caused the movement of the position of the main maxima to lower Q (0.027 Å^{-1} and 0.059 Å^{-1}), comparable to the BSA case: also in this case, it indicates the formation of some larger structures due to a possible DHPC-mucin aggregation.

All the parameters obtained from the model and the analysis of the Zimm plots for each mucin 5 wt% sample in the presence of BSA and DHPC are presented in Table 7.2. When the protein or phospholipid were added to mucin solutions at pH 7, an increase of ~ 15 % on the radius of

gyration and the correlation length of the mucin molecule was observed when compared to the values obtained for 5 wt% mucin only solutions at pH 7. These results are in agreement with the shift to lower Q of the main peaks observed in the scattering of mucin in the presence of BSA and DHPC.
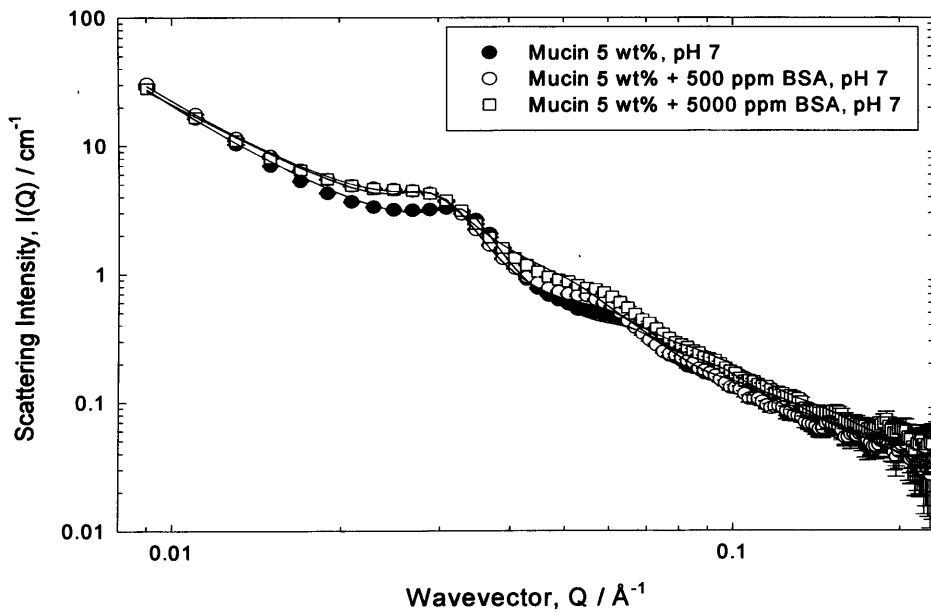

Figure 7.2 Scattering (symbols) and fit (solid lines) from 5 wt% mucin in the absence and in the presence of BSA 500 ppm and BSA 5000 ppm at pH 7.
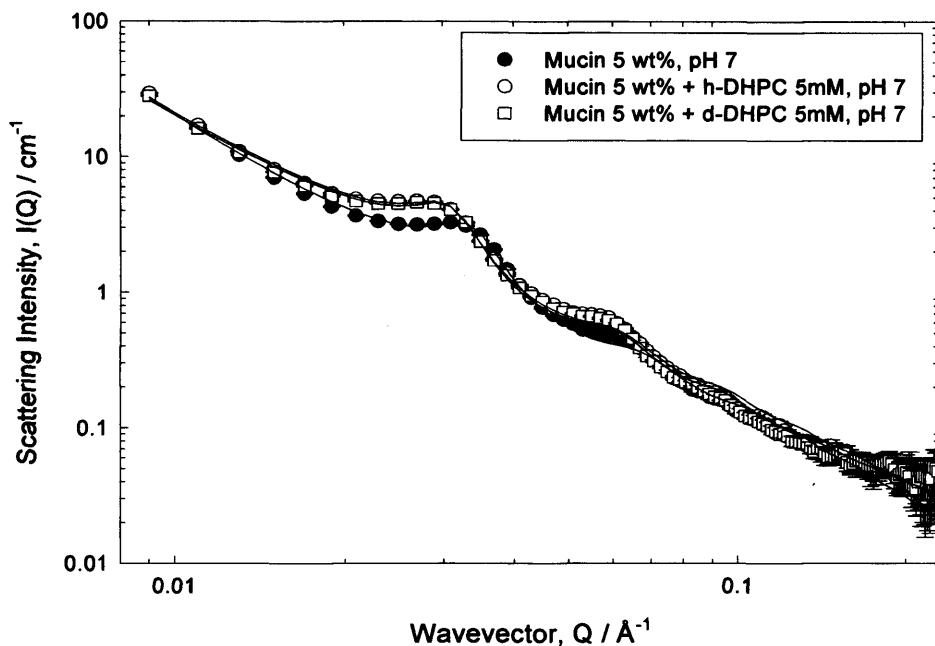
Figure 7.3 *Scattering (symbols) and fit (solid lines) from 5 wt% mucin in the absence and in the presence of 5 mM hydrogenated h-DHPC and deuterated d-DHPC at pH 7 .*

Protein or phospholipid added to mucin 5 wt%	Radius of gyration , R_g (nm)	Correlation length, Ξ (nm)	Radius of the globule, R (nm)	Volume fraction, ϕ	Distance between the globule centres, L (nm)
none pH 7	41.0 ± 2.0	23.5 ± 1.2	9.0 ± 0.5	0.37 ± 0.02	80.0 ± 18.3
BSA 500 ppm	46.5 ± 2.3	27.0 ± 1.3	9.7 ± 0.5	0.35 ± 0.02	91.0 ± 20.9
BSA 5000 ppm	47.0 ± 2.3	27.0 ± 1.3	9.5 ± 0.5	0.37 ± 0.02	92.0 ± 21.2
h-DHPC 5 mM	47.0 ± 2.3	27.0 ± 1.3	9.5 ± 0.5	0.38 ± 0.02	91.5 ± 21.0
d-DHPC 5 mM	47.5 ± 2.4	27.5 ± 1.4	9.6 ± 0.5	0.38 ± 0.02	92.5 ± 21.3

Table 7.2 Parameters obtained from the model for the scattering from mucin solution 5 wt% in the presence and in the absence of BSA or DHPC at pH 7.

The effect of h- and d-DPPC vesicles on 5 wt% mucin solution is illustrated in Figure 7.4. For the h-DPPC/mucin system, two different h-DPPC vesicles concentrations were considered: 2.75 mM and 5 mM. In the case of d-DPPC vesicles in mucin solutions, only 5 mM d-DPPC vesicles concentration was studied.

All DPPC vesicles investigated in mucin solutions were prepared according to the procedure described in Section 3.2.3 in Chapter 3. Therefore, unilamellar DPPC vesicles were obtained after the extrusion process.

In the binary mixtures h-DPPC/mucin, the position of both maxima are shifted at lower Q: the two main maxima are now located to a Q values of 0.025 Å^{-1} and 0.059 Å^{-1}, which correspond to a distance/size of 25.1 nm and 10.6 nm, respectively. These values indicate that the presence of the phospholipid has given rise to some features with an increased size. Furthermore, the scattering profile presents a Bragg peak at $Q = 0.089$Å^{-1}, corresponding to a distance of ~70 Å which is consistent with a regular stacking of lipid bilayers [44, 48-50]. Due to the presence of this Bragg peak, the fit of the scattering profile from mucin 5 wt% in the presence of h-DPPC 5 mM and 2.75 mM was not possible: for this system, only the scattering data are presented in Figure 7.4.

The scattering experiment was repeated in the presence of deuterated d-DPPC 5 mM. If in the mixture h-DPPC/mucin the scattering profile was given by the contribution of both the h-DPPC and the mucin glycoprotein (open circles in Figure 7.4), in the d-DPPC/mucin mixture the 'contrast variation' condition (explained in the Appendix B) is satisfied and the scattering profile belongs only to the mucin and reflects the effect of the DPPC on mucin (open squares in Figure 7.4). The position of both maxima has moved to higher Q and they can be found at 0.033 Å^{-1} and 0.067 Å^{-1}: these Q values correspond to sizes of 19.0 nm and 9.5 nm, respectively. This indicated that the presence of h-DPPC in mucin gives rise to some features (probably h-DPPC/mucin aggregates) with a larger size but the presence of d-DPPC in mucin clarifies that the mucin

molecules are affected by a reduction in size/distance of ~ 20% when the phospholipid is added.

All the parameters obtained from the model and the analysis of the Zimm plots for each mucin 5 wt% sample in the presence of d-DPPC are presented in Table 7.3. When the phospholipid was added to mucin solutions at pH 7, a decrease of ~ 18 % on the radius of gyration and the correlation length of the mucin molecule was observed when compared to the values obtained for 5 wt% mucin only solutions at pH 7. These results are in agreement with the shift to higher Q of the main peaks observed in the scattering of mucin in the presence of d-DPPC.

Moreover, it is possible to clearly observe the disappearance of the Bragg peak, indicating a feature related more to the DPPC itself than to any particular structure born from the adhesion/binding of the DPPC with the mucin. Considering that the scattering from 5 mM DPPC vesicles in D_2O (Figure 7.1) showed the typical scattering from unilamellar vesicles and did not exhibit any interaction peak characteristic of multilamellar structures, the Bragg peak might indicate that the presence of the mucin can induce a re-organization of the DPPC lipid bilayers into one-dimensional periodic lattice of periodicity d ~ 70 Å.

If in the unilamellar structure the structure factor $S(Q) = 1$, the structure factor in the multilamellar structure – which gives rise to the characteristic interaction peak – can be approximated by Gaussian distribution function as the following:

$$S(Q) = 1 + k \exp\left[-\frac{(Q - Q_0)^2}{2\sigma^2} \right]$$

Eq. 7.3

where σ is the width of the interference peak, and Q_0 is the position of its center, which is inversely related to the distance between bilayers –

$Q_{peak} = \dfrac{2\pi}{d_{bilayerspacing}}$. The coefficient k corresponds to the amount of

multilamellar structures [49].

Figure 7.4 Scattering (symbols) and fit (solid lines) from 5 wt% mucin in the absence and in the presence of 5 mM and 2.75 mM hydrogenated h-DPPC and 5 mM deuterated d-DPPC at pH 7 .

Phospholipid added to mucin 5 wt%	Radius of gyration , R_g (nm)	Correlation length, ζ (nm)	Radius of the globule, R (nm)	Volume fraction, ϕ	Distance between the globule centres, L (nm)
none pH 7	41.0 ± 2.0	23.5 ± 1.2	9.0 ± 0.5	0.37 ± 0.02	80.0 ± 18.3
d-DPPC 5 mM	33.0 ± 1.6	19.0 ± 1.0	9.2 ± 0.5	0.37 ± 0.02	64.0 ± 14.7

Table 7.3 Parameters obtained from the model for the scattering from mucin solution 5 wt% in the presence and in the absence of DPPC at pH 7.

7.2.3. SANS study on ternary mixtures

As a preliminary exposition of the complexity of these mixtures, a ternary mixture comprising 5 wt% mucin / DHPC 5 mM / BSA 5000 ppm was examined as illustrated in Figure 7.5.

When all the three components considered (mucin, DHPC and BSA) are in the hydrogenated form, the scattering observed is a contribution from all of them (open circles in Figure 7.5): the scattering profile exhibits a shift to lower Q compared to the mucin-only case (closed circles). This shift corresponds to an increase of ~15 % in the characteristic dimension giving rise to the peak. This change in the peak position is consistent with the contribution of the single extra components – h-DHPC and BSA – to the scattering from mucin since both of them individually caused a shift to lower Q of the main peak when added to the mucin solutions (open squares in Figure 7.2 and open circles in Figure 7.3). The parameters obtained from the model and the analysis of the Zimm plots for mucin 5 wt% in the presence of BSA 5000 ppm and h-DHPC 5 mM are presented in Table 7.4. The addition of the BSA and h-DHPC both together to a 5 wt% mucin solution caused an increase of ~ 15 % on the radius of gyration and the correlation length of the mucin molecule, which is in agreement with the shift at lower Q observed in the scattering profile.

However, the scattering profile changes when one of the component, d-DHPC, is added in the deuterated form. In this case, the scattering profile comes from the contribution of the mucin and the BSA in the presence of the deuterated DHPC (closed squares in Figure 7.5). This time a shift to higher Q of the peak is observed which corresponds to a contraction in dimension of ~ 15 %: in fact, parameters reported in Table 7.4 show a reduction of ~ 15 % on the radius of gyration and the correlation length of the mucin molecule when the BSA 5000 ppm and d-DHPC are both added together to the mucin 5 wt% solution. This could be interpreted as if, in the presence of d-DHPC, the mucin and the serum albumin give rise to collapsed structure with a reduced dimension.

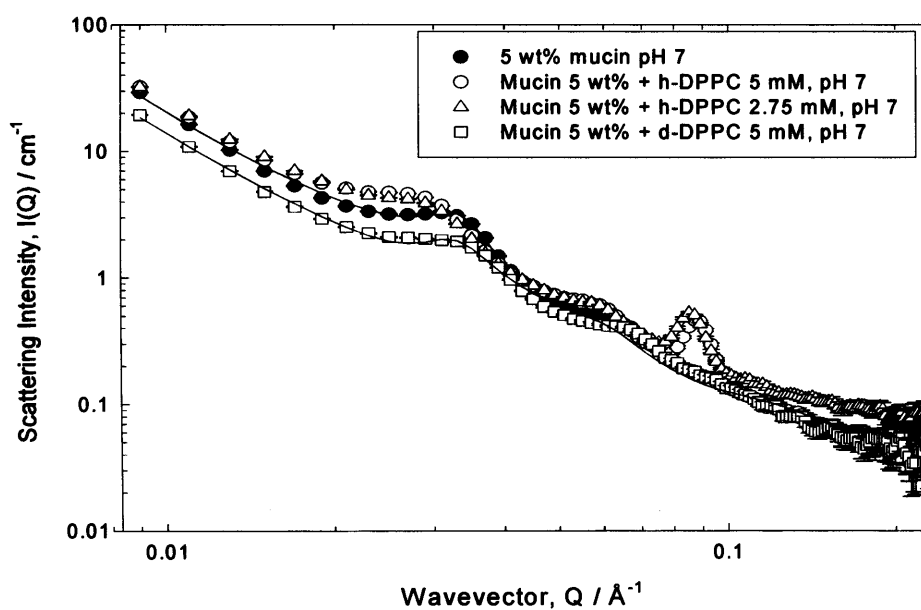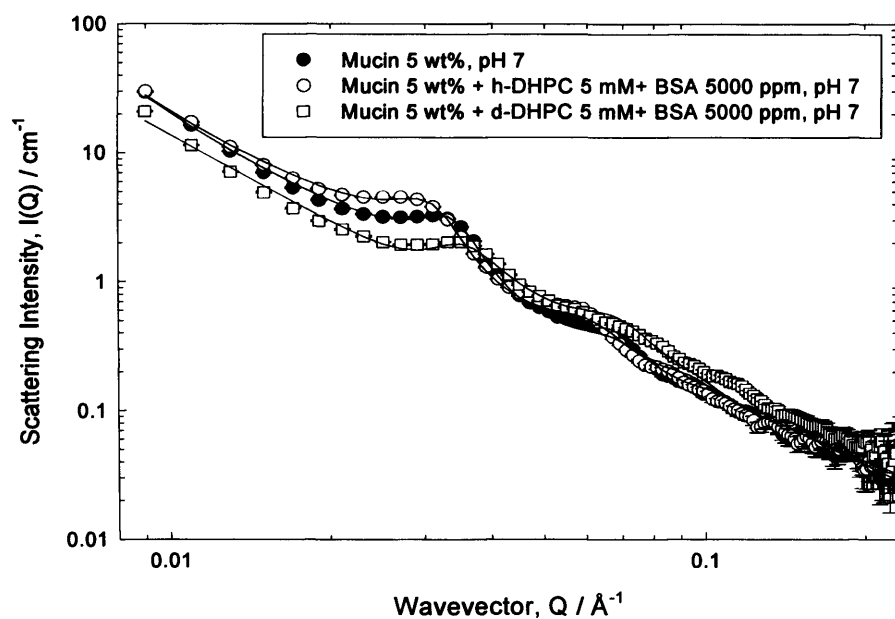**Figure 7.5** *Scattering (symbols) and fit (solid lines) from 5 wt% mucin in the absence and in the presence of hydrogenated h-DHPC 5mM + BSA 5000 ppm and deuterated d-DHPC 5 mM + BSA 5000 ppm at pH 7.*

Protein and phospholipid added to mucin 5 wt%	Radius of gyration, R_g (nm)	Correlation length, ζ (nm)	Radius of the globule, R (nm)	Volume fraction, ϕ	Distance between the globule centres, L (nm)
none pH 7	41.0 ± 2.0	23.5 ± 1.2	9.0 ± 0.5	0.37 ± 0.02	80.0 ± 18.3
BSA 5000 ppm + h-DPPC 5 mM	47.5 ± 2.4	27.5 ± 1.4	9.7 ± 0.5	0.37 ± 0.02	92.5 ± 21.3
BSA 5000 ppm+ d-DPPC 5 mM	36.0 ± 1.8	21.0 ± 1.0	9.2 ± 0.5	0.35 ± 0.02	70.0 ± 16.1

Table 7.4 *Parameters obtained from the model for the scattering from mucin solution 5 wt% in the presence and in the absence of BSA and DHPC at pH 7.*

7.3. Discussion

BSA, as serum protein, DHPC and DPPC, as phospholipids, were used to enrich mucin solutions and simulate a more realistic mucosal system. The effects of these compounds were tested on mucin solutions by SANS. The addition of BSA – and similarly the addition of DHPC – on mucin solutions exhibited a perturbation on the scattering profile causing a shift to lower Q of the main peaks: this resulted in an increase on the radius of gyration, correlation length and distance between the globule centres in the mucin molecule when compared to the values obtained for 5 wt% mucin only solutions. These changes might be related to the formation of larger structures that could be associated to a protein-protein interaction (in the case of the bovine serum albumin) or lipid- protein interaction (in the case of the DHPC) of the mucin towards these compounds. Indeed, mucin molecules contain a large number of binding sites for hydrophobic ligands. These hydrophobic binding domains are situated in the unglycosylated portion of the peptide and are involved in the binding of biliary lipids [51].

Particularly interesting resulted the behaviour of DPPC in mucin solutions which, together with a shift to lower Q of the maxima, gave rise to a Bragg peak. Once more, the movement in the position of the main peaks is related to a possible lipid-protein aggregation between the DPPC and the mucin. The Bragg-peak present in the scattering of mucin with the addition of the hydrogenated h-DPPC, suddenly disappears when the h-DPPC is substituted with the deuterated form of the phospholipid, d-DPPC. The Bragg-peak at $Q = 0.089\text{Å}^{-1}$, corresponding to a distance of ~70 Å, is related to a regular stacking of bilayers of DPPC. Therefore, it looks like if the mucin enhances the piling of DPPC bilayers.

The system was made further complex by the addition of two extra components to the mucin solutions: BSA and DHPC were added together to mucin solutions. Again, the main peaks moved to lower Q implying that larger structures are formed due to the association of BSA / DHPC /

mucin. This result was in agreement with the contribution that the BSA and DHPC individually gave to the scattering from mucin: in fact, both of them independently caused a shift to lower Q of the scattering from mucin.

Early rheological investigation by List *et al.* [52] showed clear evidence of increased viscosity of pig gastric mucin with addition of serum albumin. Interestingly, similar findings were not obtained with α-casein, haemoglobin, collagen or immunoglobulin G, suggesting that there was some specificity for albumin from the mucin. The mucin-albumin association appeared to involve non-covalent hydrophobic interactions which were enhanced by heating but not significantly weakened by the increase of pH or ionic strength. Murty *et al.* [25] demonstrated that also lipids have the effect to increase the viscosity of mucin.

More recent studies performed by Feiler *et al.* [53] reported that the BSA associates with the mucin layer via hydrophobic interactions, causing stiffening. Moreover, it is thought that the BSA molecules swell the mucin-albumin complex, which would be in agreement with our SANS findings relative to the mucin-BSA mixture.

Several studies have denoted the affinity of mucin for lipids and hydrophobic molecules [3, 51, 54-56]. In particular, it has been reported that the non-covalent hydrophobic binding properties of the mucin are related to the hydrophobic domain of the mucin glycoprotein, presumably on the non-glycosylated polypeptide core. However, the mucin-lipid aggregation did not report any disruption of the mucin network. Instead, the mucin-associated lipid resulted to enhance the protective effect as hydrophobic mucosal barrier against oxygen radicals [57] as well as its acid-resistant properties. Therefore, the binding of phospholipids to gastric mucin may be potentially important in the formation and maintenance of the gastric mucosal barrier in various gastric ulcers [20, 23, 26].

7.4. Conclusions

Changes induced by the addition of a second material (BSA, DHPC, DPPC) in the position and intensity of the maxima observed in the SANS from mucin solutions are an indication of the perturbation caused to the structure of the mucin molecules. The effects of 500 ppm BSA, 5000 ppm BSA and 5 mM DHPC on mucin solutions consisted in an increase of the parameters characterizing the size of the mucin molecule (increased R_g, ξ, L). On the other hand the mixture DPPC/mucin did cause a significant impact on the scattering profile of mucin, introducing a degree of higher order not seen in any of the other systems. However, all the systems studied (binary and ternary mixtures) reported binding/aggregating phenomena of the single components with mucin giving rise to larger structures.

The protein-protein interaction exhibited in the system mucin-BSA mixture could be relevant in the field of biomaterial: in fact the ability of the albumin to alter and tune the physical properties of the mucin can have important implications for biomaterial coating strategies, for example in the area of contact lens coating. The use of mucin and albumin is also particularly significant to the area of biolubrificant.

The hydrophobic interaction in the mucin-lipid mixture could be positively considered as an enhancing factor for the protective role of the gastric mucosal barrier.

The study of the interaction/binding/adhesion of mucus components with mucin should be carefully evaluated for the understanding of the mucus as a protective barrier and in the improvement of any treatment for the reinforcement of the mucosal barrier. However, further work is needed to better resolve the precise structure in this complex system.

References

1.   Bansil, R.; Turner, B. S., Mucin structure, aggregation, physiological functions and biomedical applications. *Current Opinion in Colloid and Interface Science* **2006**, 11, 164-170.

2.   Khanvilkar, K.; Donovan, M. D.; Flanagan, D. R., Drug transfer through mucus. *Advanced Drug Delivery Reviews* **2001**, 48, 173-193.

3.   Witas, H.; Sarosiek, J.; Aono, M.; Murty, V. L. N.; Slomiany, A.; Slomiany, B. L., Lipids associated with rat small-intestinal mucus glycoproteins. *Carbohydrate Research* **1983**, 120, 67-76.

4.   Hills, B. A., Gastric surfactant and the hydrophobic mucosal barrier. *Gut* **1996**, 39, 621-624.

5.   Ethell, M. T.; Hodgson, D. R.; Hills, B. A., Ultrastructure of the hydrophobic gastric surfactant barrier in the dog. *Australian Veterinary Journal* **1999**, 77, 240-244.

6.   Bernhard, W.; Postle, A. D.; Linck, M.; Sewing, K.-F., Composition of phospholipid classes and phospatidylcholine molecular species of gastric mucosa and mucus. *Biochimica et Biophysica Acta* **1995**, 1255, 99-104.

7.   Nardone, G.; Laccetti, P.; Civiletti, C.; Budillon, G., Phospholipid composition of human gastric mucosa: a study of endoscopic biopsy specimens. *Gut* **1993**, 34, 456-460.

8.   Bernhard, W.; Postle, A. D.; Rau, G. A.; Freihorst, J., Pulmonary and gastric surfactants. A comparison of the effect of surface requirements on function and phospholipid composition. *Comparative Biochemistry and Physiology Part A* **2001**, 129, 173-182.

9.   Hills, B. A., The role of lung surfactant. *British Journal of Anaesthesia* **1990**, 65, 13-29.

10. Wright, J. R., Immunomodulatory functions of surfactant. *Physiological Reviews* **1997**, 77, 931-962.

11. Morgenroth, K.; Bolz, J., Morphological features of interactions between mucus and surfactant on the bronchial mucosa. *Respiration* **1985,** 47, 225-231.

12. Griese, M.; Birrer, P.; Demirsoy, A., Pulmonary surfactant in cystic fibrosis. *European Respiratory Journal* **1997,** 10, 1983-1988.

13. Girod, S.; Galabert, C.; Lecuire, A.; Zahm, J. M.; Puchelle, E., Phospholipid composition and surface-active properties of tracheobronchial secretions from patients with cystic fibrosis and chronic obstructive pulmonary diseases. *Pediatric Pulmonology* **1992,** 13, 22-27.

14. Meyer, K. C.; Sharma, A.; Brown, R.; Weatherly, M.; Moya, F. R.; Lewandoski, J.; Zimmerman, J. J., Function and composition of pulmonary surfactant and surfactant-derived fatty acid profiles are altered in young adults with cystic fibrosis. *Chest* **2000,** 118, 164-174.

15. Rubin, B. K.; Ramirez, O.; King, M., Mucus rheology and transport in neonatal respiratory distress syndrome and the effect of surfactant therapy. *Chest* **1992,** 101, 1080-1085.

16. Bissinger, R. L.; Carlson, C. A., Surfactant. *Newborn and Infant Nursing Reviews* **2006,** 6, 87-93.

17. Lewis, J. F.; Veldhuizen, R., The role of exogenous surfactant in the treatment of acute lung injury. *Annual Reviews in Physiology* **2003,** 65, 613-642.

18. Westphal, M.; Traber, D. L., Exogenous surfactant in acute lung injury: no longer a question? *Critical Care Medicine* **2005,** 33, 2431-2433.

19. Lichtenberger, L. M., The hydrophobic barrier properties of gastrointestinal mucus. *Annual Reviews in Physiology* **1995,** 57, 565-583.

20. Lichtenberger, L. M.; Graziani, L. A.; Dial, E. J.; Butler, B. P.; Hills, B. A., Role of surface-active phospholipids in gastric cytoprotection. *Science* **1983,** 219, 1327-1329.

21. Schmitz, M. G. J.; Renooij, J. W., Phospholipid from rat, human, and canine gastric mucosa. Composition and metabolism of molecular classes of phosphatidylcholine. *Gastroenterology* **1990**, 99, 1292-1296.

22. Butler, B. P.; Lichtenberger, L. M.; Hills, B. A., Distribution of surfactants in the canine gastrointestinal tract and their ability to lubrificate. *American Journal of Physiology: Gastrointestinal and Liver Physiology* **1983**, 244, G645-G651.

23. Lichtenberger, L. M.; Richards, J. E.; Hills, B. A., Effects of 16,16-dimethyl prostaglandin E2 on the surface hydrophobicity of aspirin-treated canine gastric mucosa. *Gastroenterology* **1985**, 88, 308-314.

24. Kiviluoto, T.; Paimela, H.; Mustonen, H.; Kivilaakso, E., Exogenous surface-active phospholipid protects Necturus gastric mucosa against luminal acid and barrier breaking agents. *Gastroenterology* **1991**, 100, 38-46.

25. Murty, V. L. N.; Sarosiek, J.; Slomiany, A.; Slomiany, B. L., Effect of lipids and proteins on the viscosity of gastric mucus glycoprotein. *Biochemical and Biophysical Research Communications* **1984**, 21, 521-529.

26. Hills, B. A.; Lichtenberger, L. M., Gastric mucosal barrier: hydrophobicity of stretched stomach lining. *American Journal of Physiology: Gastrointestinal and Liver Physiology* **1985**, 248, G643-G647.

27. Goddar, P. J.; Hills, B. A.; Lichtenberger, L. M., Does aspirin damage canine gastric mucosa by reducing its surface hydrophobicity? *American Journal of Physiology: Gastrointestinal and Liver Physiology* **1987**, 252, G421-G430.

28. Ehehalt, R.; Wagenblast, J.; Erben, G.; Lehmann, W. D.; Hinz, U.; Merle, U.; Stremmel, W., Phosphatidylcholine and lysophosphatidylcholine in intestinal mucus of ulcerative colitis patients. A qualitative approach by nanoelectrospray tandem mass spectroscopy. *Scandinavian Journal of Gastroenterology* **2004**, 39, 737-742.

29. Gibson, P. R.; Muir, J. G., Reinforcing the mucus: a new therapeutic approach for ulcerative colitis? *Gut* **2005,** 54, 900-903.

30. Clamp, J. R.; Creeth, J. M., Some non-mucin components of mucus and their possible biological roles. *Ciba Foundation Symposium* **1984,** 109, 121-136.

31. Salathe, M.; Forteza, R.; Conner, G. E., Post-secretory fate of host defence components in mucus. In *Mucus Hypersecretion in Respiratory Disease*, John Wiley & Sons: Chichester, UK, 2002; pp 20-37.

32. Ryley, H. C.; Brogan, T. D., Quantitative immunoelectrophoretic analysis of the plasma proteins in the sol phase sputum from patients with chronic bronchitis. *Journal of Clinical Pathology* **1973,** 26, 852-856.

33. Brogan, T. D.; Ryley, H. C.; Neale, L.; Yassa, J., Soluble proteins of bronchopulmonary secretions from patients with cystic fibrosis, asthma, and chronic bronchitis. *Thorax* **1975,** 30, 72-79.

34. Ryley, H. C., An immunoelectrophoretic study of the soluble secretory proteins in sputum *Biochimica et Biophysica Acta* **1972,** 271, 300-309.

35. Larhed, A. W.; Artursson, P.; Bjork, E., The influence of intestinal mucus components on the diffusion of drugs. *Pharmaceutical Research* **1998,** 15, 66-71.

36. Lukie, B. E., Serum protein content of rat small-intestinal mucus. *Digestive diseases and Sciences* **1986,** 31, 73-78.

37. Elstein, M.; Pollard, A. C., Proteins of Cervical Mucus. *Nature* **1968,** 219, 612-613.

38. Knoll, W.; Haas, J.; Stuhrmann, H. B.; Fuldner, H. H.; Vogel, H.; Sackmann, E., Small-angle neutron scattering of aqueous dispersions of lipids and lipid mixtures. A contrast variation study. *Journal of Applied Crystallography* **1981,** 14, 191-202.

39. Nawroth, T.; Conrad, H.; Dose, K., Neutron small angle scattering of liposomes in the presence of detergents. *Physica B: Condensed Matter* **1989,** 156-157, 477-480.

40. Kucerka, N.; Nagle, J. F., Models to analyze small-angle neutron scattering from unilamellar lipid vesicles. *Physical Review E* **2004**, 69, (051903), 1-9.

41. Pabst, G.; Rappolt, M.; Amenitsch, H.; Laggner, P., Structural information from multilamellar liposomes at full hydration: full q-range fitting with high quality x-ray data. *Physical Review E* **2000**, 62, 4000-4009.

42. Buldt, G.; Gally, H. U.; Seelig, J.; Zaccai, G., Neutron diffraction studies on phospatidylcholine model membranes: I. Head group conformation. *Journal of Molecular Biology* **1979**, 134, 673-691.

43. Zaccai, G.; Buldt, G.; Seelig, A.; Seelig, J., Neutron diffraction studies on phosphatidylcholine model membranes: II. Chain conformation and segmental disorder. *Journal of Molecular Biology* **1979**, 134, 693-706.

44. Nagle, J. F.; Tristram-Nagle, S., Structure of lipid bilayers. *Biochimica et Biophysica Acta* **2000**, 1496, 159-195.

45. Petrache, H. I.; Tristram-Nagle, S.; Harries, D.; Kucerka, N.; Nagle, J. F.; Parsegian, V. A., Swelling of phospholipids by monovalent salt. *Journal of Lipid Research* **2006**, 47, 302-309.

46. Rennard, S. I.; Basset, G.; Lecossier, D.; O'Donnell, K. M.; Pinkston, P.; Martin, P. G.; Crystal, R. G., Estimation of volume of epithelial lining fluid recovered by lavage using urea as marker of dilution. *Journal of Applied Physiology* **1986**, 60, 532-538.

47. Sun, B., Surfactant and inhaled nitric oxide in acute lung injury. *Hong Kong Journal of Pediatrics* **2000**, 5, 121-124.

48. Seto, H.; Nobutou, H.; Yamada, N. L.; Takeda, T.; Ihara, D.; Nagao, M.; Inoue, K., A swollen gel phase of DPPC aqueous solution with small amount of ethanol observed at moderate pressure and temperature. *Journal of Applied Crystallography* **2003**, 36, 607-611.

49. Uhrikova, D.; Teixeira, J.; Lengyel, A.; Almasy, L.; Balgavy, P., Formation of unilamellar dipalmitoyl phosphatidylcholine vesicles by Ca^{2+}: a small-angle neutron scattering study. *Spectroscopy* **2007**, 21, 43-52.

50. Uhrikova, D.; Lengyel, A.; Hanulova, M.; Funari, S. S.; Balgavy, P., The structural diversity of DNA-neutral phospholipids-divalent metal cations aggregates: a small-angle synchrotron X-ray diffraction study. *European Biophysics Journal* **2007**, 36, 363-375.

51. Smith, B. F.; LaMont, J. T., Hydrophobic binding properties of bovine gallbladder mucin. *Journal of Biological Chemistry* **1984**, 259, 12170-12177.

52. List, S. J.; Findlay, B. P.; Forstner, G. G.; Forstner, J. F., Enhancement of the viscosity of mucin by serum albumin. *Biochemical Journal* **1978**, 175, 565-571.

53. Feiler, A. A.; Sahlholm, A.; Sandberg, T.; Caldwell, K. D., Adsorption and viscoelastic properties of fractionated mucin (BSM) and bovine serum albumin (BSA) studied with quartz crystal microbalance (QCM-D). *Journal of Colloid and Interface Science* **2007**, 315, 475-481.

54. Kim, K. C.; Opaskar-Hincman, H.; Bhaskar, K. R., Secretions from primary hamster tracheal surface epithelial cells in culture: mucin-like glycoproteins, proteoglycans, and lipids. *Experimental Lung Research* **1989**, 15, 299-314.

55. Sachdev, G. P.; Zodrow, J. M.; Carubelli, R., Hydrophobic interaction of flyorescent probes with fetuin, ovine submaxillary mucin and canine tracheal mucins. *Biochimica et Biophysica Acta: Protein Structure* **1979**, 580, 85-90.

56. Slomiany, A.; Murty, V. L. N.; Aono, M.; Snyder, C. E.; Herp, A.; Slomiany, B. L., Lipid composition of tracheobronchial secretions from normal individuals and patients with cystic fibrosis. *Biochimica et Biophysica Acta: Lipids and Lipid Metabolism* **1982**, 710, 106-111.

57. Gong, D.; Turner, B.; Bhaskar, K. R.; LaMont, J. T., Lipid binding to gastric mucin: protective effect against oxygen radicals. *American Journal of Physiology: Gastrointestinal and Liver Physiology* **1990**, 259, G681-G686.

Chapter 8. General conclusions

The overall aim of this thesis was to understand and improve the potential efficiency of drug delivery through mucus by analyzing the limiting factors in the transport of potential drug carriers through mucus and evaluating how these limitations could be overcome. Studies presented in this thesis showed how technologies such as small-angle neutron scattering (SANS) and pulsed-gradient spin-echo nuclear magnetic resonance (PGSE-NMR) can be applied as non-invasive techniques to study delicate bio-materials like mucin and to reveal physicochemical interaction of mucin with polymer-based drug delivery systems (DDS).

In first instance, the conformation of mucin in solution was investigated by SANS and the analysis of the complex scattering profile from mucin solutions was believed to most appropriate model a dispersion of hydrophobic globules – described as a dispersion of uncharged polydisperse spheres – connected by the glycosylated peptide backbone. Mucin molecules in solution were described by a the radius of the globule, R, of 9.0 nm, a volume fraction, ϕ, of 0.37, a radius of gyration, R_g, of the mucin of 41.0 nm, a correlation length, ξ, of 23.5 nm and distance between the two globules, L, of 80.0 nm. Conformation of mucin in solution together with its behaviour upon alteration of some external conditions (concentration, pH, ionic strength, temperature, the presence of a mucolytic agent) was further studied by SANS and viscosity measurements.

The results achieved at this stage were very important since they put the bases for undertaking any further and deeper SANS studies on the conformation of mucin in solution.

A series of 'probe' polymers-mucin solutions was investigated to evaluate the effect of different polymers on the structure of mucin. Understanding the mobility through, and interactions with, mucin

solutions of model polymer DDS is fundamental when designing polymer based delivery systems for the delivery through such mucin-rich environments. The SANS data supported by the diffusion study and the viscosity measurements allow to differentiate and quantify obstruction effects from specific interactions experienced by the 'probe' polymers in mucin solutions.

Non-ionic polymers such as *l*-PEG 10K and *l*-PEG100K did not exhibit a specific interaction with the mucin, but suffered a moderate retardation in their diffusion through the mucin, associated to an obstruction effect of the polymer within the mucin gel-network. A pH-dependent interaction was found for a series of PAMAM dendrimers (positively and negatively charged) and PEI, exposing a strong electrostatic interaction towards mucin molecules. An attractive or repulsive electrostatic interaction was experienced by the polymers depending on the charge bore by both the polymer and the mucin at the specific pH under investigation. This specific interaction resulted in a significant retardation in the diffusion of these polymers in mucin solution.

However, thanks to their unique structure, PAMAM dendrimers are considered of relevant importance in the field of polymer-drug delivery systems. To reduce the specific interaction exhibited by PAMAM dendrimers towards mucin, a series of PEG-PAMAM conjugates with different degree of PEGylation were synthesized. SANS and PGSE-NMR data demonstrated that PEG-PAMAM conjugates were much less interacting with the mucin network compared to the unPEGylated PAMAM dendrimers, thanks to the PEG chains that provide them an inert shell. The degree of PEGylation did not influence significantly the system mucin-conjugate, even though the 100% PEGylated PAMAM dendrimers conjugates were the less interactive. Also, the self-diffusion of the PEG-PAMAM conjugates in mucin resulted greatly improved compared to the self-diffusion of the parent PAMAM dendrimers in mucin, merit of the PEG modification which reduced any specific interaction of the PAMAM dendrimers with the mucin glycoprotein.

Therefore, PEG chains modification of these polymers is able not only to make these polymeric carriers less toxic but also to decrease greatly the interaction with the mucosal barrier: thus, PEG-PAMAM conjugates could be positively considered as potential polymeric carriers for the delivery of therapeutics through organs bearing a mucus gel layer (*i.e.,* gastrointestinal, pulmonary, oral, nasal and genital tracts).

The findings related to the studies of 'probe' polymers with mucin solutions were of fundamental importance in the field of drug delivery through mucus: in fact, they can direct the choice of a polymer structure to be adopted when designing polymer based delivery systems for the delivery through such mucin-rich environments depending on the purpose that wanted to be achieved (i.e.: increase the mobility of the drug delivery device or enhance the mucoadhesion). Furthermore, the PEG-coating of the PAMAM dendrimers represented one of the biggest achievement since a PEG shell was able to turn these polymers from being strongly interactive polymers into potential polymeric carriers.

Finally, a more complex mucin solution, closer to a more realistic mucus, was studied. Mucin solutions enriched with phospholipids (DHPC, DPPC) and serum albumin (BSA) were investigated by SANS. The addition of a second material (BSA, DHPC, DPPC) to mucin solutions caused some changes in the scattering profile of mucin, which can be related to some binding/aggregating phenomena of the single components with mucin giving rise to larger structures. Of particular interest was the mixture DPPC/mucin where the DPPC in mucin cause a significant impact on the scattering profile mucin, introducing a degree of higher order not seen in any of the other systems.

The hydrophobic interaction/binding/adhesion of mucus components with mucin could be positively considered as an enhancing factor for the protective role of the gastric mucosal barrier. Also, the ability of mucus components to alter and tune the physical properties of the mucin can have important implications for biomaterial coating strategies, for example in the area of contact lens coating, or in the area of biolubrificant. However,

further work is needed to better resolve the precise structure in these complex systems.

All the studies performed in this thesis have been evaluated and optimized on commercial mucin samples, as good representative of the 'real' mucus. Useful and important results have been achieved in the field of the transport of macromolecules/drug delivery systems through mucin, which could be applied to a more fresh 'real' mucus. Therefore, as future studies, it would be of interest looking at the mobility and/or interaction of the 'probe' polymers investigated within fresh 'real' mucus.

Appendix A

Basics of NMR

Nuclear spin

Nuclear magnetic resonance (NMR) is based on the magnetic property possessed by the atomic nuclei, which have an intrinsic angular momentum known as spin. The spin angular momentum I is a vector and its magnitude is defined by $[I(I+1)]^{1/2}\dfrac{h}{2\pi}$, where h is the Planck's constant and I the spin quantum number, which can take values of 0, ½, 1, $^3/_2$, 2, etc. (depending on the number of unpaired protons and neutrons). For a spin of a given quantum number I, there are $2I+1$ possible projections onto an arbitrarily chosen axis: for an hydrogen nucleus ^{1}H, $I =$ ½ and there are two possible projections. When applying a magnetic field along the z-axis, the magnitude of the angular momentum I is equal to $I_z = \dfrac{mh}{2\pi}$, with m being the magnetic quantum number which can take $2I+1$ values laying between -I and +I: for an hydrogen nucleus ^{1}H, $I =$ ½ and m can take two values ranging between -½ and +½. In the absence of an external magnetic field, all the $2I+1$ orientations posses the same energy level. Therefore, the spins can orientate randomly. However, in the presence of an external magnetic field, energy levels are split and spins take well-defined states. In a field B_0, these energy levels are equal to $E = -m\gamma B_0 h/2\pi$, being γ the gyromagnetic ratio of the nucleus. In the case of an hydrogen nucleus ^{1}H ($I =$ ½), the energy levels are shown in Figure 1A (left panel).

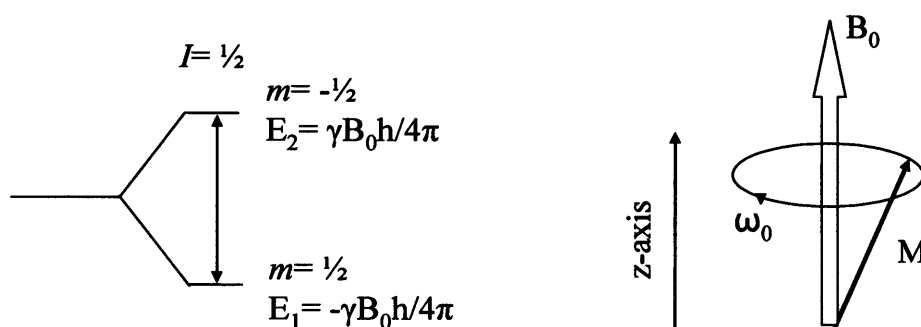*Figure 1A Energy levels allowed for a nucleus of spin I= ½ - i.e., proton - (left panel) and the precession of the macroscopic magnetic moment, M, around B_0 at the Larmor frequency ω_0 (right panel).*

Since macroscopic samples contain a large number of nuclei, a vector sum of the individual magnetic moments is considered, which is known as the macroscopic magnetic moment **M**. When applying a magnetic field, B_0, to a particle with a magnetic moment, nuclei adsorb energy and their spins move from a lower energy level to an higher one: spins are said to be in resonance. The nuclei precess (*i.e.*, change the orientation of their rotation axis) with Larmor frequency, ω_0, equal to the resonance frequency (Figure 1A, right panel). The Larmor frequency, ω_0, for a nucleus with a gyromagnetic ratio γ and in the presence of a constant magnetic field B_0 is expressed by Eq. 1a:

$$\omega_0 = \gamma B_0 \qquad\qquad \textbf{Eq. 1a}$$

The resonance condition depends on the nucleus itself, on the external magnetic field B_0 and also on the environment the nucleus experiences in the molecule [1]. The resonance frequency is expressed by the following equation:

$$\omega_0 = \gamma B_0 (1 - \sigma) \qquad\qquad \textbf{Eq. 2a}$$

where σ is the so-called shielding constant. The shielding effect is the perturbation of the applied magnetic field B_0 by a secondary 'induced'

magnetic field as effect of the surrounding electrons on the nucleus in a molecule.

The chemical shift describes the dependence of nuclear magnetic energy levels on the electronic environment in a molecule. The chemical shift δ is usually expressed in part per million (ppm) and for the ith nucleus it is calculated with the following equation:

$$\delta = \frac{\omega_i - \omega_{TMS}}{\omega_{Spectrometer}}$$

Eq. 3a

where ω_i is the resonance frequency of the ith nucleus, ω_{TMS} is the resonance frequency for the tetramethylsilane (TMS) - which is usually used as internal standard for calibrating the chemical shift for other nuclei - and $\omega_{Spectrometer}$ is the frequency of the NMR spectrometer. The chemical shift of the singlet of TMS is assigned as δ=0.0 ppm.

Relaxation process

Since a small perturbation in the magnetic field can have a large effect on the frequency of a nucleus, the application of a short intense pulse of radiofrequency radiation to a sample causes **M** to precess. When a $\pi/2$ pulse is applied along the x-axis, it causes the rotation of the magnetization **M** towards the y-axis. Afterwards, the spins return to their equilibrium state through a relaxation process where an energy exchange between themselves and their surroundings occurs. Two relaxation processes can take place: the spin-spin relaxation and the spin-lattice relaxation. A schematic representation of the two relaxation processes is showed in Figure 2A.
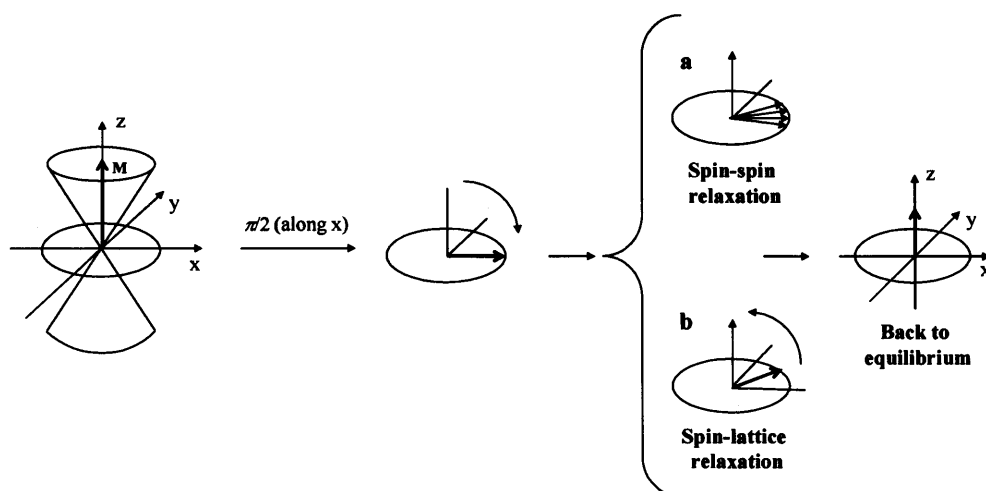
Figure 2A *Schematic representation of the relaxation processes of the magnetization M following a π/2 pulse along the x-axis: (a) Spin-spin relaxation and (b) Spin-lattice relaxation.*

In the spin-spin relaxation, the magnetization **M**, decays in the *xy*-plane (that is why it is also know as transverse relaxation) with a relaxation time, T_2. The spin-lattice (or longitudinal) relaxation occurs along the *z*-axis with a characteristic time T_1. Both relaxation processes take place at the same time and both relaxation times, T_1 and T_2, can be measured by NMR. Usually T_1 is the longer of the two relaxation times and its knowledge provides information on the molecular environment of the nucleus.

Pulse programmes

Spin-echo (SE) concept

The inhomogeneity of the magnetic field affects the frequency of a nucleus, ω_{eff}, causes a dephasing of the transverse magnetization following a π/2 (90°) pulse along the *x*-axis. The pioneering work of Hahn in the 50's [2] revealed that this loss of phase coherence can be reversible.

A π/2 (90°) pulse rotates the magnetization along the *z*-axis into the *x-y* plane and creates phase coherence. After a time τ, spins dephase due to the inhomogeneity of the magnetic field. A π (180°) pulse applied after the delay time τ inverts the dephasing effect and spins refocus after another

delay time τ along the x-axis. Therefore, after a time of 2τ all spins have refocused and the signal observed and recorded is called spin-echo or Hahn spin-echo. An illustration of the Hahn spin-echo sequence is given in Figure 3A.
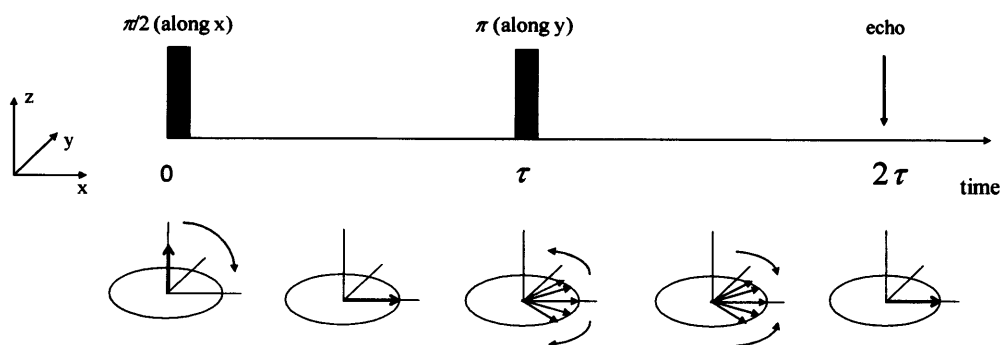

Figure 3A Schematic representation of the Hahn spin-echo pulse sequence.

However, a complete refocusing of the echo signal can only be observed if the precession frequency of every spin has been constant during the time interval 2τ. If the nuclei have experienced a displacement from their original positions in the inhomogeneous field, their frequency will vary and the spin-echo signal will result attenuated. Therefore, in the case of the self-diffusion displacement, the refocusing of the spin vectors will be incomplete at the time of the echo [3]. The concept is illustrated in Figure 4A: the nuclei e and f in the figure are the only ones which experienced a self-diffusion displacement, leading to an incomplete refocusing of their spins at the time of the echo.
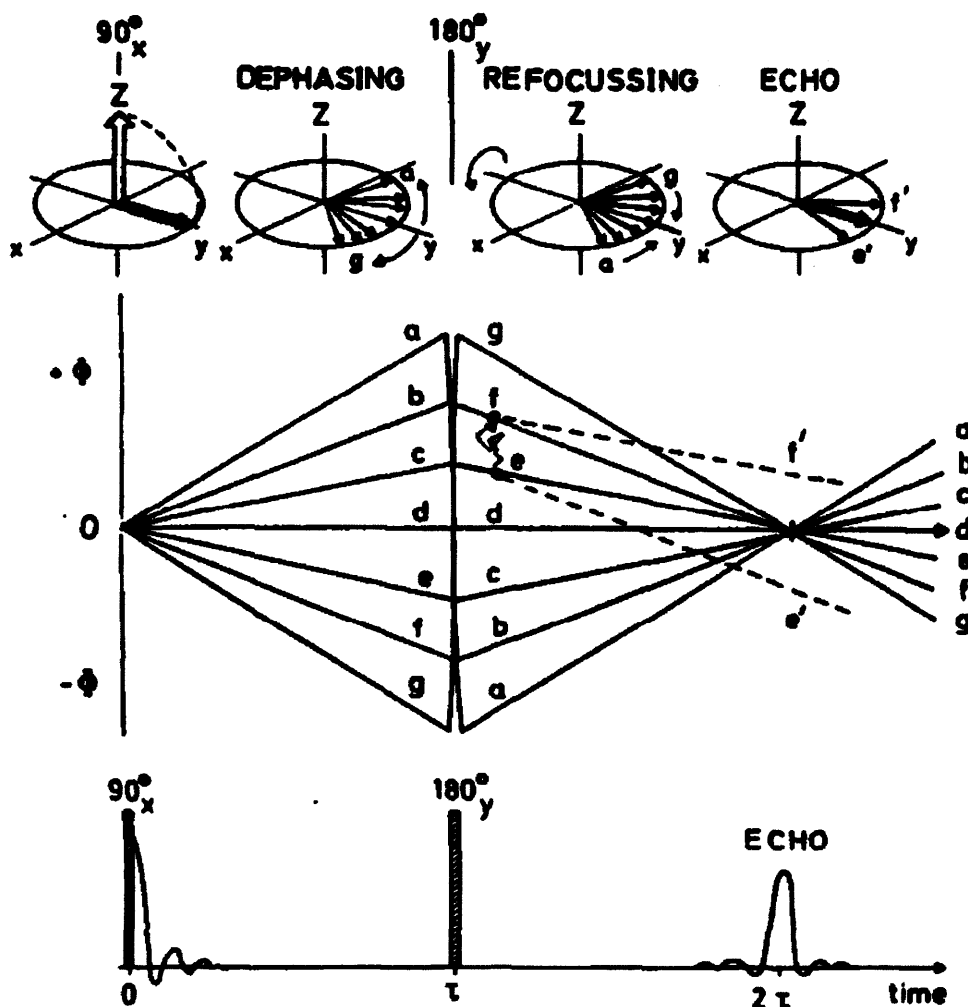
Figure 4A Illustration of the basic concept of diffusion measurements through the spin-echo (SE) technique. Taken from Stilbs P.[3].

Stejskal-Tanner sequence

The spin-echo effect noted by Hahn was significantly improved by Stejskal and Tanner [4] with the introduction of pulsed field gradients, leading to the PGSE-NMR technique and its related applications. Pulsed-gradients of magnitude g, duration δ and separated by a time Δ are applied to the spin-echo sequence. Figure 2.6 represents a schematic illustration of the Stejskal-Tanner pulse sequence.

A first $\pi/2$ gradient pulse sets the spin positions in the direction of the gradient, creating phase shifts. A second π pulse, together with the radiofrequency pulse, refocuses the phase shifts and generates an echo signal, indicating whether the spins have experienced any translational motion in the direction of the gradient during the time Δ. The echo attenuation, as described in the Figure 5A, is given by the following equation:

$$A = A_0 \exp\left[-\frac{2\tau}{T_2} - \gamma^2 D_s g^2 \delta^2 \tau^3 / 3\right]$$

Eq. 4a

where A_0 is the initial amplitude at $\tau = 0$. In Eq. 2.12, the first exponential term, $\exp\left[-\frac{2\tau}{T_2}\right]$, is related to the spin-spin relaxation time, T_2, while the second term, $\exp\left[-\gamma^2 D_s g^2 \delta^2 \tau^3 / 3\right]$, is associated to the attenuation due to the diffusion. Therefore, diffusion measurements become extremely difficult for systems where T_2 is short, γ is low or D_s is small.
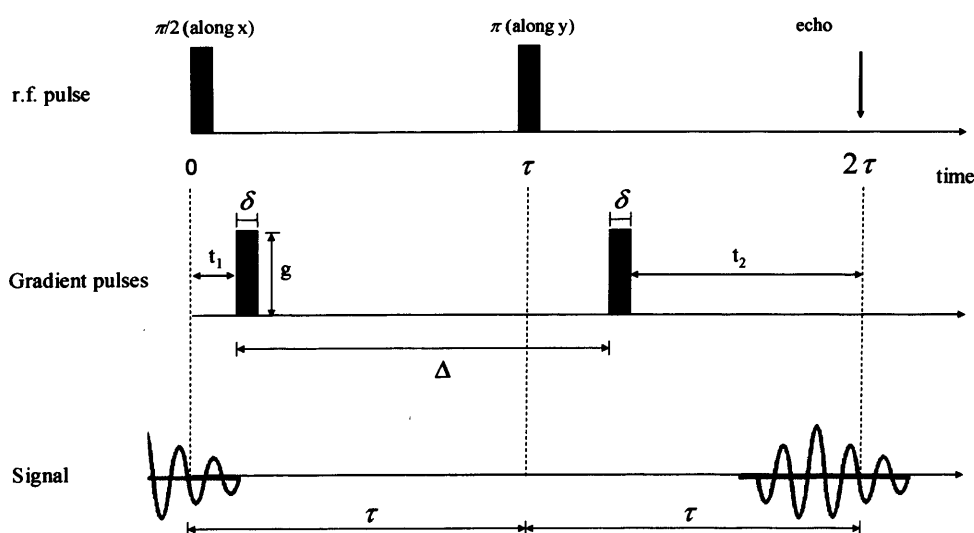

Figure 5A The Stejskal-Tanner pulse sequence.

Stimulated echo pulse sequence

In the Eq. 4a, the main limiting factor in measuring slow diffusion is actually the associated short T_2 times [5]. The application of a three pulses or multi-pulses sequences to generate stimulated echoes attempts to overcome this limitation by storing the magnetization to prevent spin-spin relaxation. In particular, a stimulated echo pulse sequence consisting of three 90° pulses is often used. In this case, it was shown that the limiting factor then becomes spin-lattice relaxation time T_1. Therefore, for polymers where often T_1 is much larger than T_2, the use of the stimulated echo pulse sequence is an advantage.

The stimulated pulse echo sequence is shown in Figure 6A where a first 90° pulse rotates the magnetization from the z-axis into the xy-plane and the spins start dephasing. After a delay time τ_1, the second 90° pulse is applied which stores the memory of the current phase shifts in the z-direction. Usually those are not affected by the field gradient and relax in the longitudinal direction. After a time τ_2, the third 90° pulse restores the phase shifts with a reversed sign and the spins form an echo recorded at time $\tau = \tau_1 + \tau_2$.

The application of a three pulse sequence generates five echoes: a primary echo (PE) at $2\tau_1$, the stimulated echo (STE) at $\tau_1 + \tau_2$, and three secondary echoes that are usually not of interest. A phase cycling is usually required to remove the other echoes.

Three pre-pulses are applied before each sequence. The current pulses used in the pulsed gradient experiments can produce heat, mechanical forces and minor currents. For a pulse to be reproducible, the use of pre-pulses allows the system to reach a state close to the one experienced during the PGSE sequence.

By properly setting the values of the diffusion time Δ, the ramp time σ, the amplitude δ and the magnitude g of the gradient pulse, a wide range of self-diffusion coefficients can be investigated.
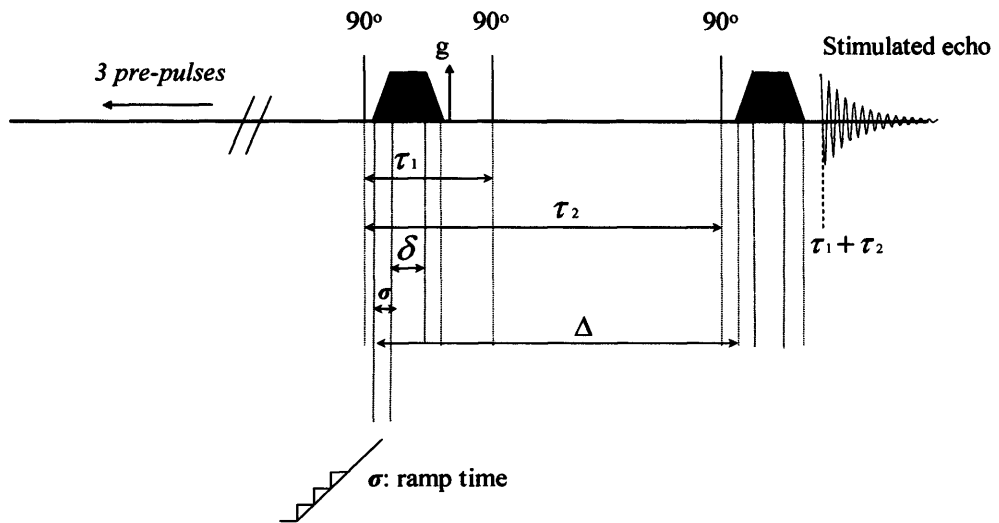
Figure 6A *The stimulated echo pulse sequence.*

Appendix B

Neutrons and their production

Neutrons

The first description of neutrons was given in 1932 by James Chadwick (Cavendish Laboratory, Cambridge), when he first discovered a new radiation form made of uncharged particles bearing a similar mass to that of a proton [6]. The neutron is an uncharged particle with a mass of 1.6749×10^{-24} g. The neutron is slightly heavier than a proton (the proton mass being 1.6726×10^{-24} g) and 1839 fold greater than an electron (the electron mass being 9.1094×10^{-28} g). It has a spin of ½ and possesses a magnetic moment. The half life of a neutron is 894 seconds, decaying into a proton, an electron and an antineutrino. Since the interaction of a neutron with the matter are rare, it usually penetrates well through the matter, making it a unique probe for investigating bulk condensed matter.

Production

Neutrons can be produced to perform scattering experiments either via a nuclear reactor or through a spallation neutron source. A nuclear reactor is used for neutrons production at the Institute Laue Langevin (ILL, in Grenoble, France). A spallation neutron source operates at ISIS in Rutherford Appleton Laboratories (Didcot, U.K.).

Nuclear reactor

In a nuclear reactor, neutrons are produced by the fission of Uranium-235. Each fission results in the release of two to three neutrons, one of which is used to sustain the chain reaction (Figure 1B). Wavelength selection is obtained by Bragg scattering from a crystal monochromator or by selecting the neutron velocity with a mechanical chopper. The nuclear reactor at the ILL is a 57 MW HFR (High-Flux Reactor). Figure 2B shows a schematic representation of the D11 instrument at ILL.
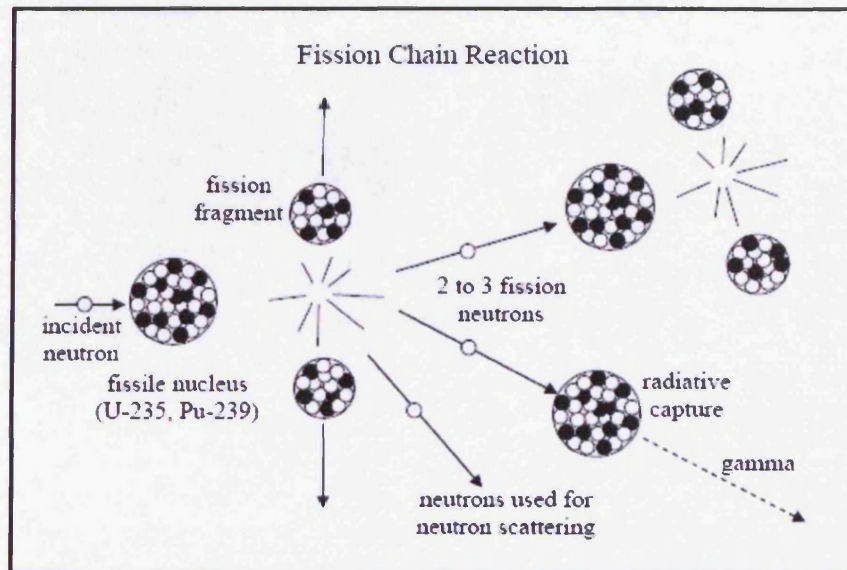
Figure 1B *Typical fission chain reaction for a reactor-based neutron source.* *Taken from Hammouda B., from* *www.ncnr.nist.gov/staff/hammouda/the_sans_toolbox.pdf*.
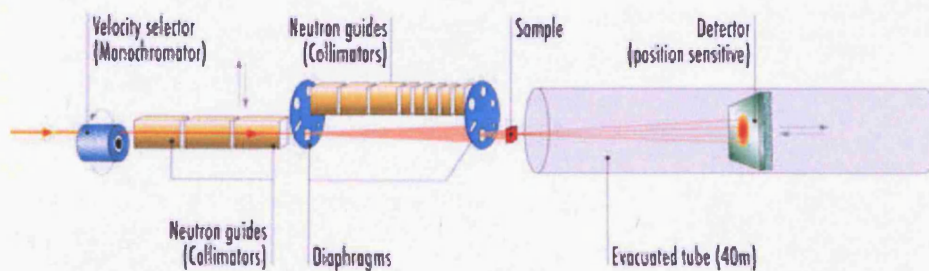

Figure 2B *Schematic layout of the D11 instrument at ILL. Taken from ILL website,* *www.ill.eu/instruments-support/instruments-groups/instruments/d11/*.

231

Spallation neutron source

This method is an accelerator-based pulsed neutron source. High energy proton beams obtained via acceleration in a synchrotron are used to bombard a heavy-metal (neutron rich) target (*e.g.*: U, Ta, W) and release pulses of neutrons with a range of wavelengths (Figure 3B) [7]. Direct determination of the energy and wavelength of each neutron is achieved by using time-of-flight (TOF) techniques on the polychromatic 'white' neutron beam.

At ISIS, the spallation neutron source is based around a 200 μA (800 MeV) proton synchrotron operating at 50 Hz, the heavy metal target is made of tantalum (Ta), and about 15 neutrons are produced per incident proton. A schematic representation of the spallation neutron source at ISIS is showed in Figure 4B.
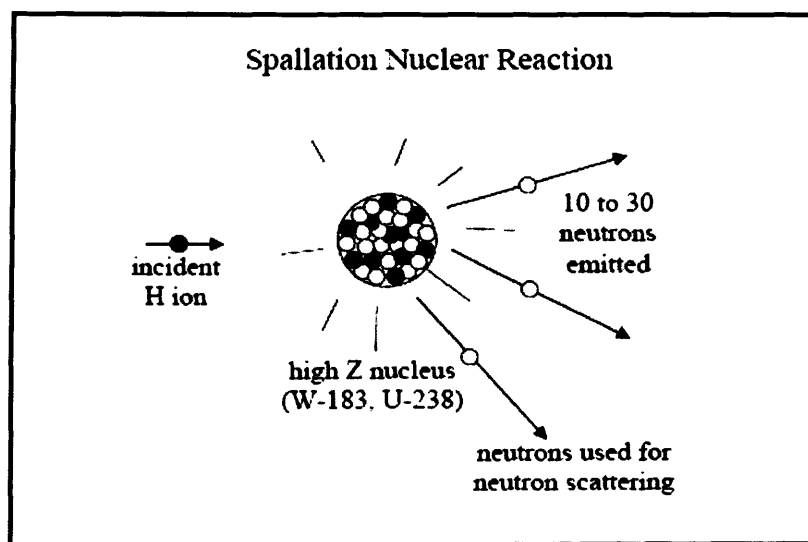

Figure 3B *Spallation nuclear reaction for a accelerator-based pulsed neutron source. Taken from Hammouda B., from* www.ncnr.nist.gov/staff/hammouda/the_sans_toolbox.pdf
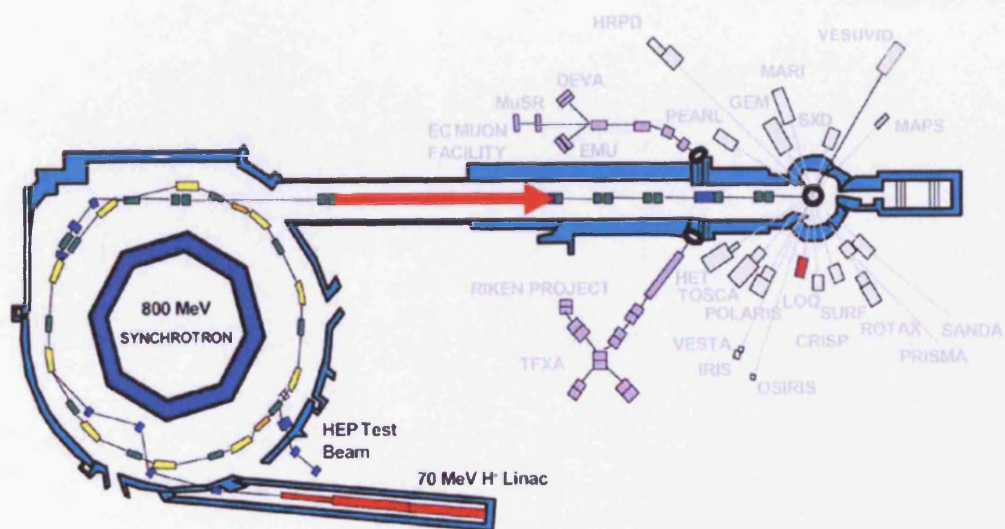
Figure 4B *Schematic layout of the spallation neutron source and instrument facilities at ISIS. Taken from ISIS website, www.isis.rl.ac.uk/ISIS99/introduction/ISIS_pla.JPG.*

It is easy to understand that the use of neutron radiation and the scattering experiments are not simple laboratory 'benchtop' techniques. These facilities are high costly and they are financially supported and operated by several countries at governmental level. The neutron beam time is allocated on a competitive proposal based system.

Scattering theory

The radiation-matter interactions can generate scattering events where the neutron beam can be scattered in different modes: elastic or inelastic, but also coherent or incoherent.

In an elastic scattering – *i.e.*, when scattered neutrons have the same energy than the incident neutrons – information from the spatial organization of nuclei to 'large-scale' structures (*e.g.*: polymers, aggregates) can be obtained. When some of the energy is lost (or gained)

by the neutron interacting with the matter – *i.e.*, inelastic scattering – data related to the dynamic behaviour of the sample can be achieved.

Coherent scattering can generate patterns of constructive and destructive interference bearing structural information of the colloidal arrangement. In contrast, incoherent scattering arises from random events (*e.g.*: thermal motion) and carries no information about the structure of the sample, but about its dynamics.

However, in a SANS experiment, only the coherent elastic scattering is taken into account. The incoherent scattering, appearing as a background, can be easily measured and subtracted from the total scattering [7].

The scattering vector Q

Scattering data are usually presented as plots of the intensity of the scattered neutron beam, I(Q), versus the scattering vector, Q. The scattering vector Q is proportional to the scattering angle, θ, and is the modulus of the resultant between the incident and the scattered wavevectors, k_i and k_s. For coherent elastic scattering Eq. 1b can be applied:

$$k_i = k_s = \frac{2\pi n}{\lambda}$$
Eq. 1b

Since

$$\frac{Q}{2} = k_s \sin\frac{\theta}{2}$$
Eq. 2b

combining Eq. 1b and Eq. 2b, we can obtain

$$Q = \left|\vec{Q}\right| = \left|\vec{k}_s - \vec{k}_i\right| = \frac{4\pi n}{\lambda}\sin\frac{\theta}{2}$$
Eq. 3b

where the refractive index, *n*, is equal to 1 for neutrons and λ is the neutron wavelength. Figure 5B illustrates the geometrical correlation involved in Eq. 3b.
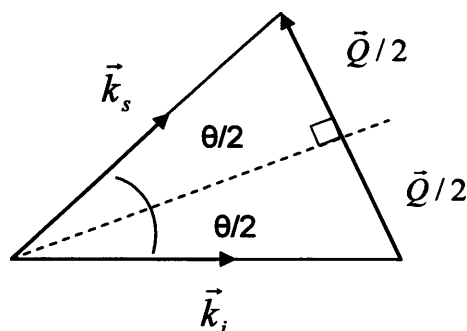
Figure 5b *Geometrical relationship for the determination of the scattering vector Q.*

Considering Bragg's law of diffraction (Eq. 4b) which correlates the angle of diffraction, θ, of a radiation of wavelength λ, for planes separated by a distance d

$$\lambda = 2d \sin\frac{\theta}{2}$$ **Eq. 4b**

Combining together the Eq. 3b and the Bragg's law (Eq. 4b), the following relationship is obtained

$$d = \frac{2\pi}{Q}$$ **Eq. 5b**

where Q values are proportional to the inverse of a distance d.

Q has the dimensions of $(length)^{-1}$ and is usually expressed as $Å^{-1}$. High Q values can probe small scale structures, and vice versa.

The scattering vector Q, therefore, depends on both the angle and the neutron wavelength. This highlights the two different approaches in SANS:

> ➤ On a reactor-based neutron source (ILL), a monochromatic neutron beam is scattered by the sample. For a constant wavelength, the scattering intensity must be measured at different angles. In order to

achieve that, the sample-detector distance is varied using a moveable detector.

> On a spallation neutron source (ISIS), the neutron wavelength varies and is determined by time-of-flight (TOF) method, therefore the position of the detector is fixed.

Contrast variation

The contrast term can be described as the squared difference in scattering length densities between the solute, ρ_p, and the solvent, ρ_s: $(\Delta\rho)^2 = (\rho_p - \rho_s)^2$. If both the solute and the solvent have the same scattering length densities, the contrast term is equal to zero, which means there will be no measurable scattering and therefore no structural information can be obtained. In this case, solute and solvent are said to be contrast matched.

However, as mentioned above, the large difference in the scattering lengths between hydrogen and deuterium is employed in SANS experiments to highlight details of the structure and composition of the sample under investigation. This can be obtained by exchanging hydrogen with deuterium, either in the solvent or the solute, or even in some specific part of the solute. Figure 6B illustrates the contrast variation principle in a simple diagrammatic way. While none of the elements could be differentiated in panel A, by matching the background to one of the elements, the red lobes and the yellow core can be probed (panel B), then the blue lobes and the yellow core (panel C), and even both red lobes and blue lobes by matching the yellow centre (panel D).

This concept could be applied in a more realistic case of a core shell particle – *i.e.*, a microemulsion droplet – where the core, the shell and the solvent can be selectively hydrogenated or deuterated to study different parts of the same colloidal system.
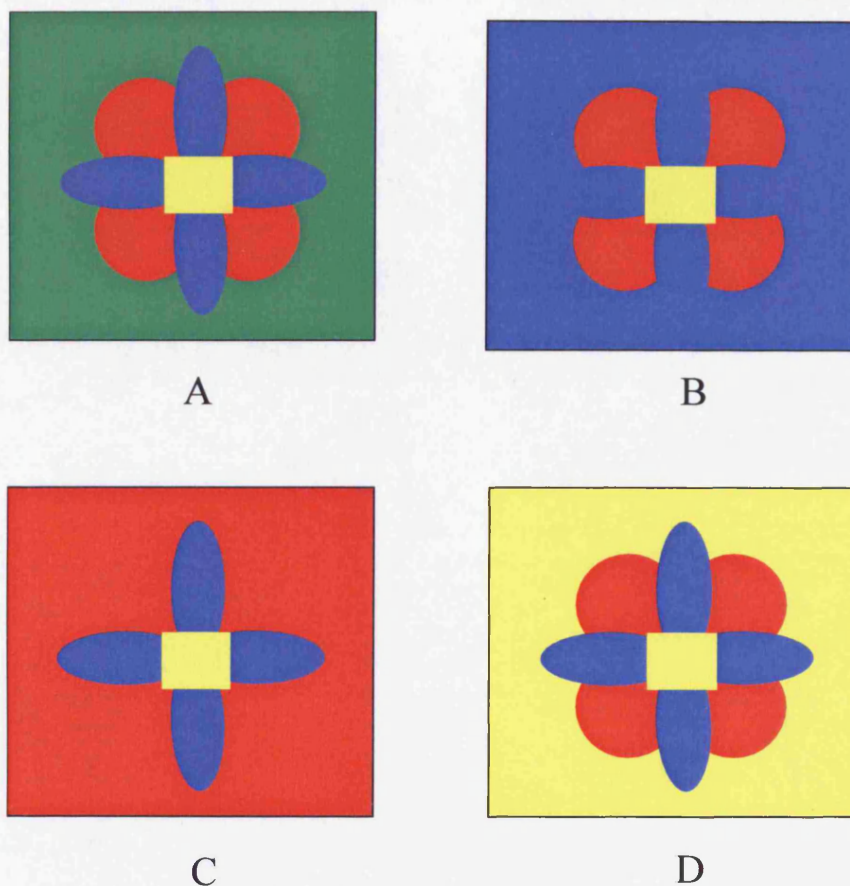
Figure 6B *Diagrammatic illustration of the contrast variation principle.*

<u>*Additional measurements required*</u>

The measurement of the scattering intensity of the sample under investigation requires several other measurements to be taken into account. Specifically, the scattering intensity and the transmission of (i) the empty beam, (ii) the cell, (iii) the background solvent of the sample, (iv) a calibration sample and (v) the investigated sample. The SANS raw data are corrected using Eq. 6b

$$I_s(Q) = \frac{\left(I_{s+c}(Q) - I_b\right)}{T_{s+c}} - \frac{\left(I_c(Q) - I_b\right)}{T_c} \qquad \textbf{Eq. 6b}$$

where $I_s(Q)$ is the scattering intensity from the sample, $I_{s+c}(Q)$ is the scattering intensity from the sample + cell, $I_c(Q)$ is the scattering intensity from the empty cell, $I_b(Q)$ is the scattering with the empty beam, T_{s+c} is the transmission for the sample inside the cell and T_c is the empty cell transmission. Note that $T_{s+c} = T_s \cdot T_c$.

The 2D corrected data are radially averaged to produce 1D data (*i.e.*, scattering pattern I(Q) vs. Q). The data are then reduced considering the type of instrument used.

SANS approximations

Guiner approximation

The Guiner approximation relates the low Q part of the scattering profile (Guiner regime) to the characteristic dimension R of the scattering particle. It can be used to probe disc, spheres and cylindrical shapes and it is expressed as follows:

$$I(Q) \propto Q^{-D} \exp\left(-\frac{Q^2 R^2}{K}\right)$$
Eq. 7b

where D is equal to 1, 0 and 2 and K to 4, 5 and 12 for cylinders, spheres and discs respectively. However, Eq. 2.28 is valid for non-interacting particles (*i.e.*, $S(Q) \rightarrow 1$) only, and over a restricted Q-range.

By plotting different quantities against Q^2, the characteristic dimension R of the particle can be obtained (*i.e.*, the disc thickness, the sphere radius or the cylinder radius). Table 1B shows the different Guiner representations for these shapes.

Shape	Guiner Plot	Characteristic dimension R
Disc	$Ln[I(Q) \cdot Q^2]$ vs. Q^2	$Thickness = \sqrt{slope \times 12}$
Sphere	$Ln[I(Q)]$ vs. Q^2	$Radius = \sqrt{slope \times 5}$
Cylinder	$Ln[I(Q) \cdot Q]$ vs. Q^2	$Radius = \sqrt{slope \times 3}$

Table 1B *Guiner plots and extracted characteristic dimensions for a disc, a sphere and a cylinder shape.*

The curve giving a linear decay over the low Q values will give the most probable particle shape. One restriction applies to the Guiner plot for a spherical shape, for which the product Q·R must be smaller than 1 [8].

Porod approximation

At high Q values, the Porod approximation can be used. In this region, the scattering intensity I(Q) is more sensitive to the scattering arising from local surfaces and can be related to the total interfacial area by the following equation:

$$I(Q) = 2\pi(\Delta\rho)^2 \left(\frac{S}{V}\right) Q^{-4} \qquad \textbf{Eq. 8b}$$

where S/V is the total interfacial area per unit volume of sample, in cm^{-1}. The Porod approximation is limited to smooth interfaces, in a Q range much greater than the reciprocal characteristic dimension (*i.e.*, for Q $\gg$ 1/R) [8].

References

1. Horne, P. J., *Nuclear Magnetic Resonance*. Oxford University Press: New York, 1995; Vol. 32.

2. Hahn, E. L., Nuclear induction due to free Larmor precession. *Physical Reviews* **1950**, 77, 297-298.

3. Stilbs, P., Fourier transform pulsed-gradient spin echo studies of molecular diffusion. *Progress in Nuclear Magnetic Resonance Spectroscopy* **1987**, 19, 1-45.

4. Stejskal, E. O.; Tanner, J. E., Spin diffusion measurements: spin echoes in the presence of a time-dependent field gradient. *Journal of Chemical Physics* **1965**, 42, 288-292.

5. Weingartner, H.; Holz, M., NMR studies of self-diffusion in liquids. *Annual Reports on the Progress of Chemistry Section C* **2002**, 98, 121-155.

6. Chadwick, J., Possible existence of a neutron. *Nature* **1932**, 129, 312.

7. Higgins, J. S.; Benoit, H. C., *Polymers and Neutron Scattering*. Oxford University Press: 1996.

8. Eastoe, J., *Surfactant Chemistry*. (Book arising from a series of advanced lectures given in October 2002 at the China Research Institute for Daily Chemical Industry (RIDCI) TaiYuan), 2003.

ELSEVIER

Quantifying diffusion in mucosal systems by pulsed-gradient spin-echo NMR

Paola Occhipinti [a,b], Peter C. Griffiths [a,*]

[a] School of Chemistry, Cardiff University, Main Building, Park Place, Cardiff CF10 3AT, UK
[b] Welsh School of Pharmacy, Redwood Building, King Edward VII Avenue, Cardiff CF10 3XT, UK

ARTICLE INFO

ABSTRACT

Mucus, a thick and slimy secretion produced by submucosal cells, covers many epithelial surfaces in mammalian organs and prevents foreign particles that enter the body from accessing cells. However, the mucus layer also represents a potential barrier to the efficient delivery of nano-sized drug delivery systems (polyplexes, lipoplexes, particles) to the underlying mucosal epithelium. Many studies have considered the ability of nano-sized particles and polymers to diffuse within the mucosal network using a range of different techniques, including multiple-particle tracking (MPT), diffusion chamber studies and fluorescence recovery after photobleaching (FRAP). This review highlights the current understanding of the interaction of the diffusion of nano-sized structures within mucosal networks. Moreover, this article presents an introduction to pulsed-gradient spin-echo NMR (PGSE-NMR), a potential new tool to investigate the mobility of molecular species through mucosal networks and related biological gels.

© 2008 Elsevier B.V. All rights reserved.

Contents

1. Introduction

A successful drug delivery system should be able to traverse several biological barriers en-route to the site of action and to give a sufficiently high uptake of the active therapeutic. Low molecular weight molecules can usually traverse bio-membranes whilst nano-sized drug delivery constructs (liposomes, nanoparticles, macromolecular drugs, polymer therapeutics) must cross the cells to have access to the body. Nevertheless, there are still several physicochemical and biological barriers to be overcome to ensure an adequate bioavailability [1]. One barrier that has been frequently investigated is the cell plasma membrane. However, prior to encountering the cell membrane, the mucus layer which covers several epithelial surfaces in mammalian organs (e.g. respiratory tract, gastrointestinal and reproductive tract)

* Corresponding author.
  E-mail address: griffithspc@cf.ac.uk (P.C. Griffiths).

must be overcome. This mucus coating has a fundamental role in limiting the exposure of human tissues to external particles and as such mucus potentially represents a significant barrier to the efficient delivery of nano-sized drug delivery constructs to the epithelium and beyond [2–5]. The thickness of the mucus layer which ranges from 7–70 μm in the airways [6,7], 50–500 μm in the stomach [3,8] and 15–150 μm in the colon [9–12], combined with its inherent viscoelasticity, are important factors which affect the pharmacokinetics of the therapeutic agent [13,14]. This situation is exacerbated by the presence of any disease that causes an overproduction of mucus (e.g. cystic fibrosis (CF), ulcerative colitis).

Mucoadhesive drug delivery systems require an interaction between mucus and the polymeric drug carriers, chitosan [15,16] and the thiol group containing polymers polycarbophil-cysteine conjugates have been employed [17]. The interaction of the polymers with the mucosal layer results in: (i) a prolonged residence time of the delivery device, (ii) a localization of the delivery system at a specific target site, and (iii) an increase in the drug concentration gradient [9,18,19]. Despite the value of bio-adhesion in promoting localised delivery, the focus of this article is on quantifying the permeability and diffusion of nano-sized drug delivery constructs through the mucosal layer and to develop an understanding of how molecular interactions affect the pharmacokinetics. Accordingly, this review presents an overview of the techniques currently available to investigate the mobility of nano-sized drug delivery constructs in bio-gels, focusing in particular on the ability of pulsed-gradient spin-echo NMR (PGSE-NMR) to provide a unique insight into this challenging discipline.

2. Composition and structure of the mucus

2.1. Mucus

Mucus is a water-rich bio-gel, the main components being water (up to 95%), mucin (generally no more than 5%), inorganic salts (about 1%), carbohydrates and lipids. The composition differs slightly depending on the site of secretion (e.g. ocular mucus: protein 29% w/w [of dry solids], carbohydrate 53% w/w, lipid 12% w/w; submaxillary gland mucus: protein 31% w/w, carbohydrate 58% w/w,
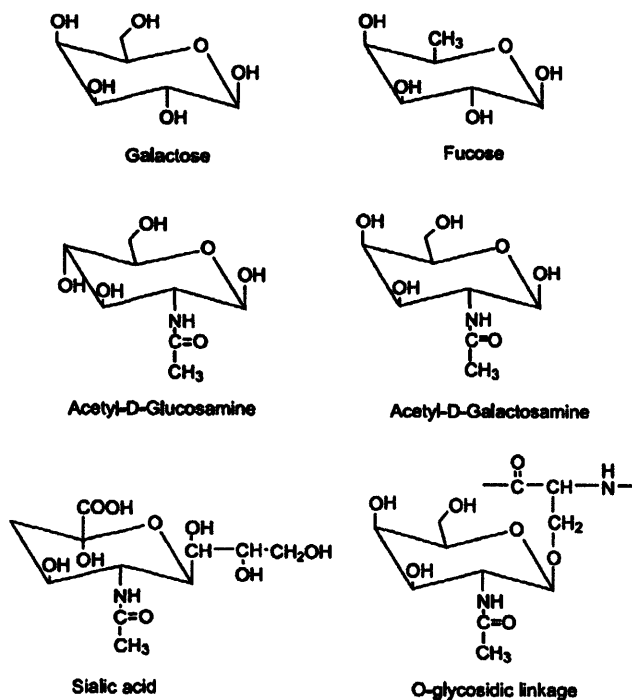

Fig. 1. Chemical structures of the sugar units generally found in mucin (Reprinted from Advanced Drug Delivery Reviews, 56, Peppas, N. A. et al., Nanoscale technology of muchoadhesive interactions, 1657–1687, Copyright 2004, with permission from Elsevier [18]).

lipid 11% w/w), the physiological role of the mucus layer and the presence of any disease.
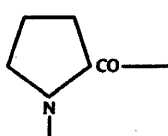
2.2. Mucin

Mucin consists of high molecular weight (ranging from 0.5 to 20 M g mol^{-1}) O-linked glycoproteins. It represents 80% of the organic component of mucus and controls its rheological character [20,21]. Mucin is a high ordered molecule, whose assemblies yield structures exhibiting length scales from a few hundred nanometers up to several microns [22,23]. Mucin monomers comprise glycosylated and non-glycosylated peptide blocks linked by intra-molecular disulphide bridges. The smallest molecular components in mucin are a small number of amino acids (Table 1) that form the protein backbone and sugar residues, largely galactose, fucose, N-acetylglucosamine, N-acetylgalactosamine and sialic acid (Fig. 1) that form the oligosaccharide chains. The presence of the sialic acid, together with the sulphide residues, gives the mucin molecule a negative charge at physiological pH (IEP ~ 5). Interestingly, whereas different members of the mucin family might differ greatly in molecular weight, the composition of the glycoprotein domains does not greatly vary [24,25].

Mucin is a rod-shaped molecule with a central linear polypeptide core of 100,000<Mw<250,000 g mol^{-1} with radial oligosaccharide side chains, consisting of 2 to 12 monosaccharide residues, attached to the serine and threonine residues by O-glycosidic linkages, Fig. 2 [26,27]. The high degree of mucin glycosylation provides for resistance to proteolysis by rendering the peptide core less accessible to enzymatic hydrolysis and afford a protective role for the mucus layer in mammalian organs [4,28].

Mucins are extremely large molecules, with radii of gyration Rg as measured by light-scattering, in the of between 150 and 200 nm [30]. Rg values of this magnitude imply that at the low mucin concentrations used in these studies, typically 1–2 mg ml^{-1}, the polymer molecules start to physically overlap. It has been proposed that at

Table 1
Amino acid composition of gastrointestinal mucin

-CO-CH-NH- (R)	-R	% in small intestine	% in stomach
Thr	-CH-OH (CH₃)	16.8%	25.3%
Ser	-CH₂-OH	10.5%	14.2%
Pro	(ring) CO—	9.8%	17.8%
Glu	-CH₂-CH₂-COOH	8.7%	4.7%
Asp	-CH₂-COOH	8.1%	2.4%
Ala	-CH₃	6.5%	10.8%
Gly	-H	7.4%	6.7%
Arg	-(CH₂)₃-NH-C-NH₂ (NH)	3.1%	2.1%
Lys	-(CH2)₄-NH₂	3.3%	4.8%
Cys	-CH₂-SH	1.5%	–

Polypeptide backbone

Polysaccharide side chain

N- and C- terminal end

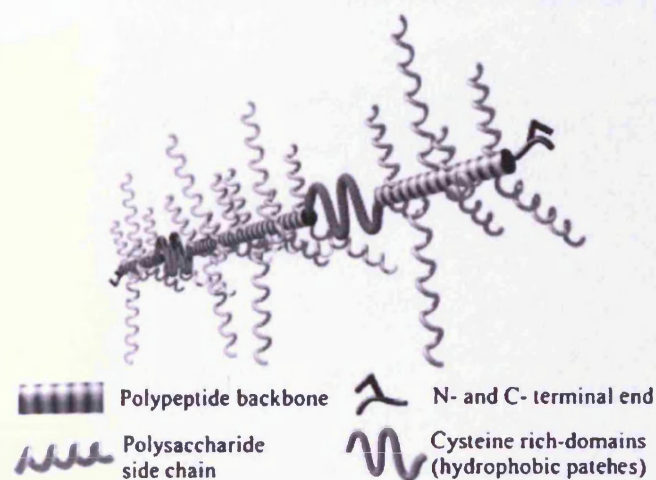Cysteine rich-domains (hydrophobic patches)

Fig. 2. Schematic representation of the mucin molecule (Fig. reproduced, with permission, from Lafitte et al. [29]).

physiological concentrations of 10–50 mg ml^{-1}, the overlap is likely to be extensive and the mucus layer forms an entangled network [28].

2.3. Mucin aggregation

One of the most important physicochemical properties of mucus is its viscoelasticity. Mucin molecules aggregate at low concentrations, thereby forming viscous solutions or viscoelastic gels [31,32]. Bhaskar et al. [33] reported viscometry, analytical ultracentrifugation and dynamic light scattering (DLS) studies that showed a noticeable increase in the viscosity and aggregation of mucin in vitro when the pH was lowered from 7 to 2. Similarly, Hong et al. [34] used atomic force microscopy (AFM) to show that mucin aggregates at low pH forming clusters of 10 or fewer molecules at pH 2, suggesting that

oligosaccharide side chains are not directly involved in the aggregation process. DLS, turbidity and rheo-small angle light scattering (rheo-SALS) methods have also shown that mucin solutions tend to aggregate at pH 2, where the polymer becomes weakly charged [35].

The aggregation/gelation behaviour of mucin is essential for the protection of the stomach from auto-digestion, at a physiological gastric pH of 2. Cao et al. [26,36,37] studied the pH-dependent conformational change of gastric mucin by DLS and showed that mucin undergoes a reversible conformational change from a random coil at pH>4 to an extended conformation at pH<4, interpreted as a sol-gel transition. At low pH, the extended conformation exposes the hydrophobic regions of the mucin polymer, leading to a more accessible protein-protein interaction, which increases the viscosity. Pig gastric mucin (PGM) gelatination involves interactions between acidic Asp or Glu residues (pKa~4) from the non-glycosylated side chains of the molecule, such as. At pH>4, salt bridges between negatively charged carboxylate side chains and positively charged amine groups in the non-glycosylated regions induces a random coil that results in the hydrophobic domains becoming folded and hidden. At pH<4, the carboxylate groups of the salt bridges become protonated and mucin unfolds, exposing the hydrophobic and promoting a more extended conformation results [20]. In summary, high mucin concentration and low pH lead to gel formation due to interplay of hydrophobic and electrostatic interactions between those parts of the mucin molecule that have little or no glycosylation, Fig. 3.

3. Diffusion and permeability of nanoparticles through mucus

3.1. Network characteristics of mucosal systems

The thickness of the mucus layer is a key factor for determining the mobility of a drug species through it. The thickness, as described previously, differs depending on the organ bearing the mucus coating.

Scanning electron microscopy (SEM) of dried mucin has been used to quantify the structure and physical characteristics of the mucin fiber network and to explore the effect of synthetic polymers on these
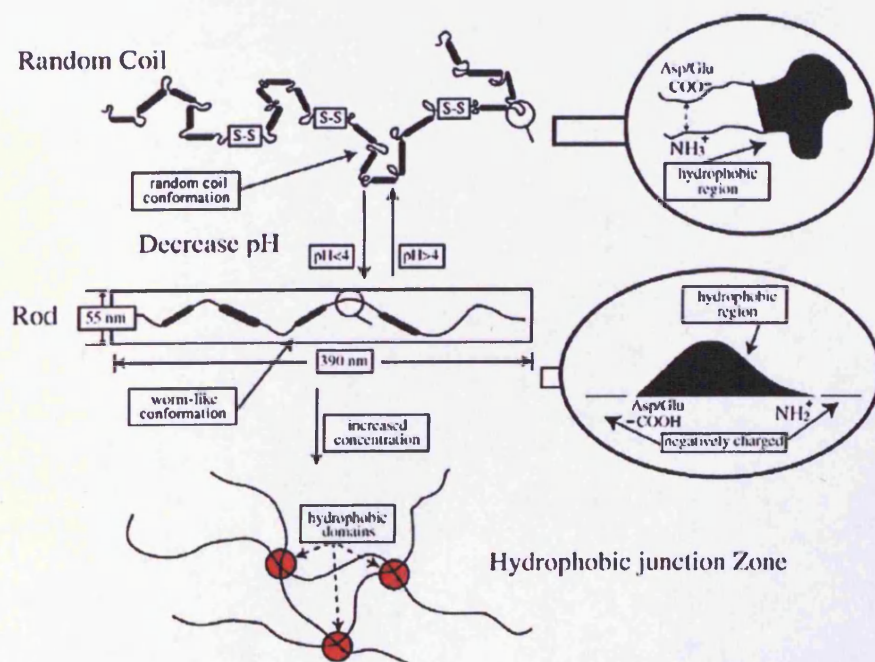

Fig. 3. A model showing how the electrostatic interactions at pH<4 can produce a conformational change from a random coil to a rod, leading to gelation (Reprinted from Current Opinion in Colloid & Interface Science, 11, Bansil R. et al., Mucin structure, aggregation, physiological functions and biomedical applications, 164–170, Copyright 2005, with permission with Elsevier [20]).
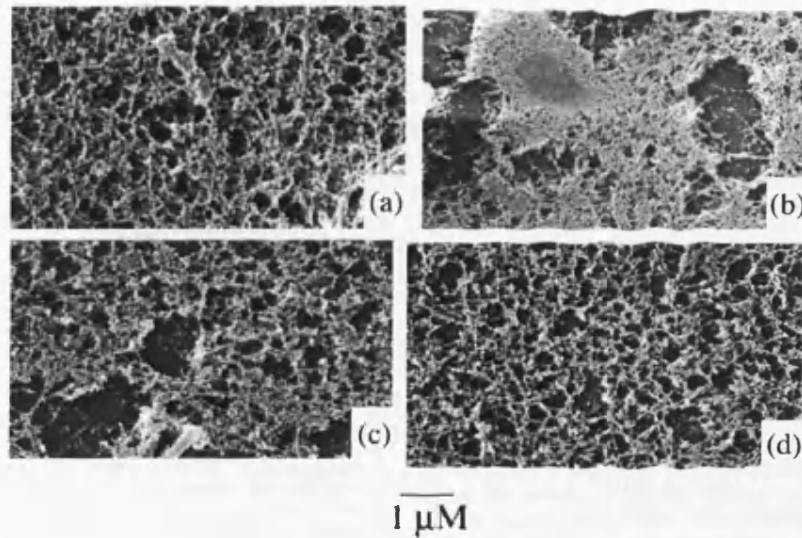
Fig. 4. Scanning electron microscophs of human cervical mucus (a) un-treated, (b) treated with PEG-33 0.001% v/v, (c) PVP-400 0.001% v/v and (d) PAA-3000 0.001% v/v (Reprinted from Biomaterials, 22, Willits R. et al., Synthetic polymers alter the structure of cervical mucus, 445–452, Copyright 2001, with permission from Elsevier [38]).

mucin fibers. Mucin possesses an inter-fiber spacing between 80 and 400 nm and a fiber network mesh size of 1 μm [38,39]. As mentioned above, mucus is made of high molecular weight negatively charged glycoproteins: hence the ionic character, as well as the hydrophobicity/hydrophilicity of the delivery device are significant factors [18,40,41].

Willits et al. [38] revealed that addition of the non-ionic poly (ethylene glycol) (PEG), the cationic poly(vinyl pyridine) (PVPy) at a buffered pH of 7.4 altered the mucin fiber network, while the anionic poly(acrylic acid) (PAA) had little effect on the structure. It was postulated that PEG-mucin interaction occurs through hydrogen bonding of the ether oxygen with the acid moieties in mucin, forming fiber patches in the mucin gel, on the other hand, PVPy interacts with mucin via an electrostatic interaction forming a gel with regions of aggregated fibers, Fig. 4.

Larhed et al. [42] quantified the diffusion of lipophilic low molecular weight drugs such as metoprolol, propranolol, hydrocortisone and testosterone in native mucus and in solutions made from purified mucin. Different mucus components were identified and separated by density gradient centrifugation. Analysis of the self-diffusion coefficients of these drugs in the different components using a tracer technique at a pH between 6.4 and 6.9 showed that it was the

lipid and cholesterol components that retard drug diffusion in native mucus, rather than mucin glycoprotein component of mucin.

3.2. Quantifying diffusion through mucus

3.2.1. Multiple-particle tracking

Multiple-particle tracking (MPT) technology can be used to study the diffusion of particles through biological environments. In this method, the microscopic motion of hundreds of particles is recorded by video microscopy. Both quantitative information (diffusion coefficients) and qualitative information (direction and transport mode) are extracted from an analysis of time-resolved particle trajectories. Therefore, data thus obtained can give direct and indirect information about particle-environment interactions and is easily applied to study the effects of intracellular (e.g. cell cytoplasm) [43] and extra-cellular media (e.g. mucus) [44].

MPT has been applied to study the diffusion of uniform polystyrene (PS) particles of various diameters (100, 200 and 500 nm) in cystic fibrosis mucus. Smaller particles showed a greater transport rate compared with larger particles, revealing their more facile mobility within pores formed in the cystic fibrosis mucus network [14,45]. Similarly, Lai et al. [46] found that larger polystyrene
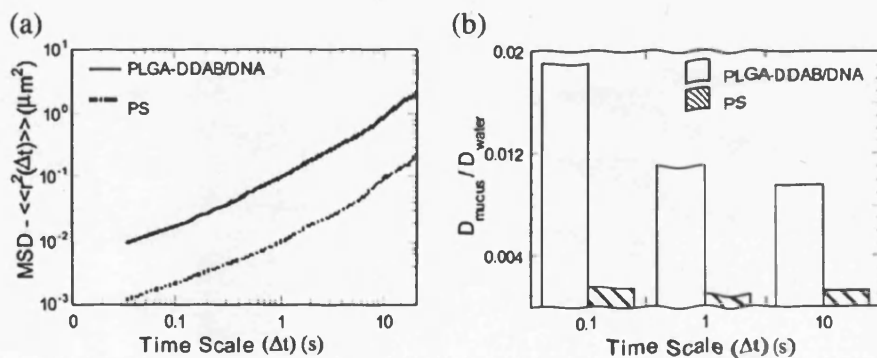

Fig. 5. (a) Mean square displacement (MSD) of PLGA-DDAB/DNA and PS nanoparticles in PGM. (b) The normalized diffusion coefficients of PS and PLGA- DDAB/DNA (Reprinted from Advanced Drug Delivery Reviews, 57, Dawson, M. et al., Real-time multiple-particle tracking: applications to drug and gene delivery, 63–78, Copyright 2004, with permission from Elsevier [47]).
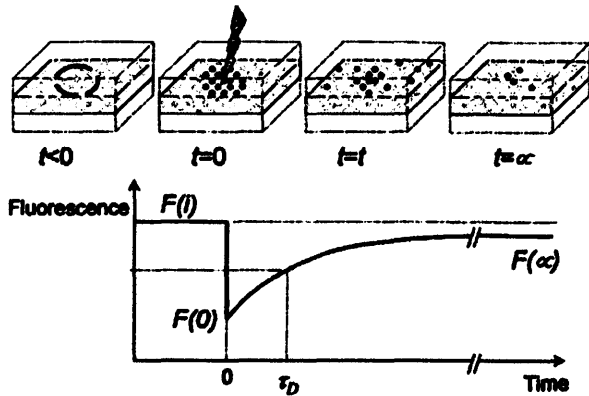
Fig. 6. Schematic representation of a FRAP experiment. Before bleaching, the initial fluorescence is recorded as F(i). At t=0, a high intensity light beam bleaches the molecules causing a drop in fluorescence to F(0). Due to the random motion/diffusion, the bleached molecules will exchange their position in the bleached area with non-bleached fluorescent molecules from the surrounding. This results in a recovery of the observed fluorescence. The characteristic diffusion time (τD) is indicated as the time at which half of the fluorescence has recovered (Figure reproduced, with permission, from Meyvis et al. [54]).

nanoparticles (500 and 200 nm in diameter), when coated with poly (ethylene glycol), diffuse faster through cervico-vaginal mucus compared to smaller 100 nm coated particles. This study showed that PEGylation not only reduced obstruction for larger PEG-PS (200 and 500 nm) but also increased the homogeneity of transport compared with similar sized PS particles.

Furthermore, Dawson et al. [47] investigated the transport rates in mucus of cationic nanoparticles made from poly(D,L-lactic-co-glycolic) acid (PLGA) and the cationic surfactant dimethyldioctadecylammonium bromide (DDAB) coated with DNA (PLGA-DDAB/DNA) as potential nanoparticle gene carriers. Their results showed that transport rates of PLGA-DDAB/DNA nanoparticles in mucus were higher than that of the slightly smaller PS nanoparticles because the DNA coating makes the PLGA-DDAB/DNA nanoparticles moderately hydrophilic when compared to PS nanoparticles, allowing a greater mobility within the relatively hydrophobic mucus media, Fig. 5.

3.2.2. Diffusion chamber studies

The diffusion chamber is somewhat dated but is still used to study diffusion of particles through bio-gels. It involves the vertical mounting of two chambers, one donor and one receiver, either side of a mucus or gel solution. The donor compartment is filled with the drug delivery system, while the receiver is filled with the buffer solution. Diffusion rates through the mucus are calculated by measuring the change in drug concentration in serial samples removed from donor, receiver or both compartments as a function of time. The advantages of this method are its simplicity and the fact that the mucus composition can be changed or altered, simulating several disease states or physiological situations. Disadvantages include the need for lengthy experiments (usually several hours) and that during this period, native mucus with its endogenous proteolytic enzymes can degrade the mucus glycoproteins [2,21].

Sanders et al. [13,48] studied the transport of fluorescently labelled polystyrene particles (with size comparable to that of some transfection systems for cystic fibrosis gene therapy) through a 220 μm thick cystic fibrosis mucus layer with a vertical diffusion chamber system. It was found that the largest PS nanospheres (560 nm) were sterically obstructed by the mucus network, while the smaller nanospheres (124 nm) were retarded only by a factor of 1.3 when compared with buffer.
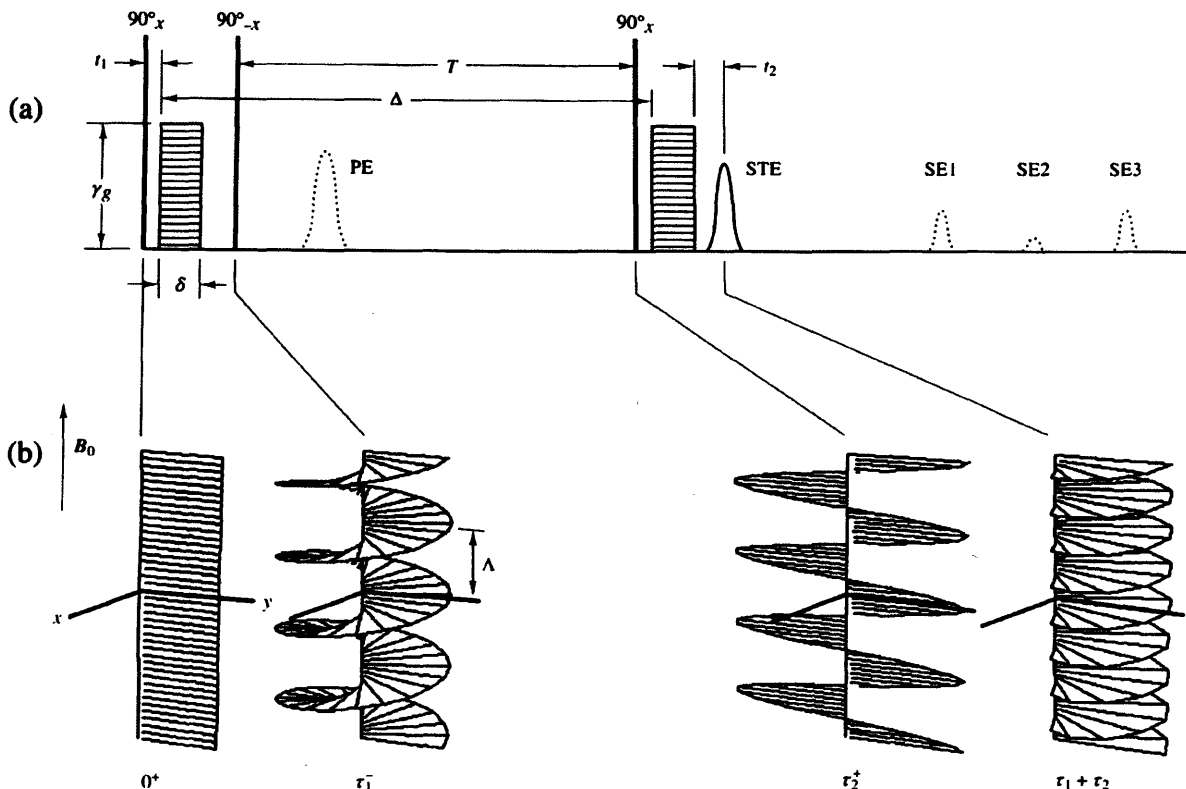

Fig. 7. Stimulated echo sequence showing the rf and field gradient pulses and the helix induced in the phase isochromats (Figure reproduced, with permission, from Johnson [62]).
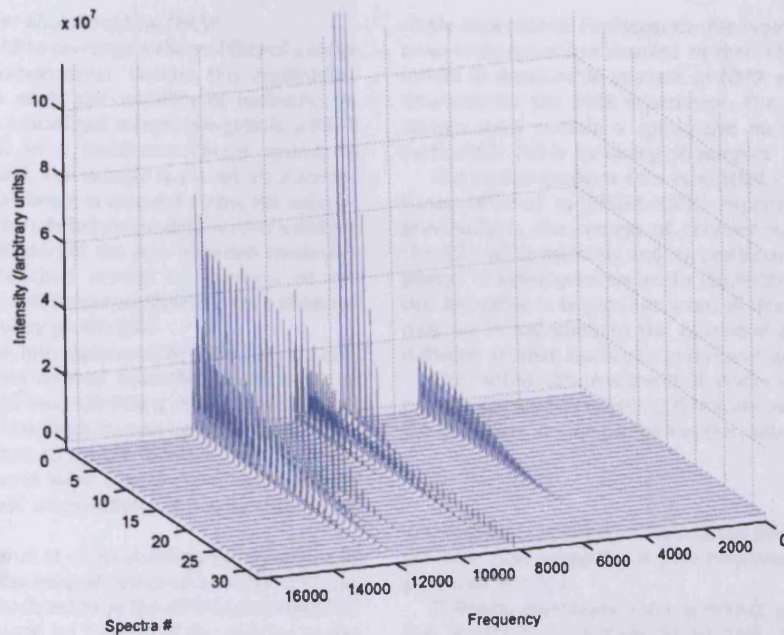
Fig. 8. Typical presentation of a pseudo-2D diffusion dataset; sample is an oil in water (D$_2$O) emulsion.

The diffusion of a selection of drugs, such as isoniazid, pentamidine, rifampicin, p-aminosalicylic acid and pyrazinamide (which can be all potentially delivered as pulmonary aerosols) through mucin has been carried out by Bhat et al. [49,50]. They showed that the mucus layer presented an additional diffusional barrier to the drugs of 50–57% of the total observed resistance, the latter due to a combination of factors including protein binding, viscosity and physical obstruction. When the mucus was replaced with different cystic fibrosis mucus solutions, there was a 28–75% decrease in drug permeability [51], indicating that significant decreases in drug transport rate occur when crossing cystic fibrosis mucus and that these could play an important role in reduced pulmonary bioavailability.

Similarly, Desai et al. [52,53] investigated the diffusion through mucus gel of a range of solutes with various molecular weights (126<Mw<14,400 g mol^{-1}) and physical properties, including phloroglucinol, 5-hydroxy-L-tryptophan, β-nicotinamide adenine dinucleotide (NAD) and ribonucleic acid (RNA). This study showed, for all solutes studied, a retardation of solute flux in mucus by a factor of at least two when compared to the diffusion of the same solute in aqueous solutions. The limitations of the diffusion chamber methodology centre on the risk of artefacts arising from practical difficulties, principally the inability to control the layer of bio-gel and its propensity to obstruct the filters, reducing the apparent diffusion coefficient.
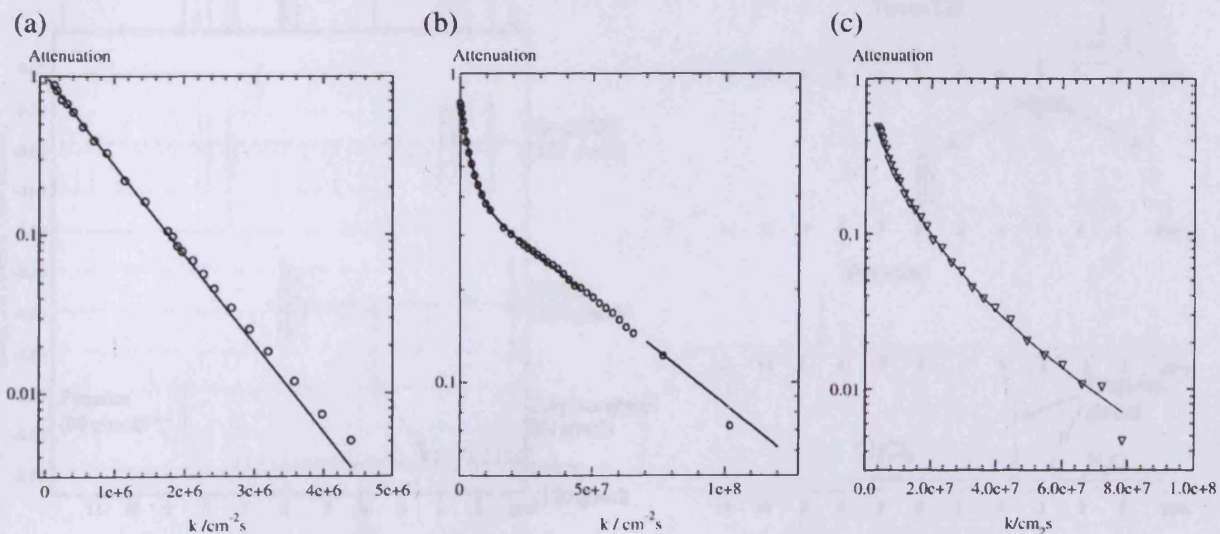

Fig. 9. Attenuation functions arising from the integral of a simple polymer in solution and in a polymer blend showing (a) monodisperse, (b) bi-exponential and (c) polydisperse behaviour.

3.2.3. Fluorescence recovery after photobleaching (FRAP)

Many studies have used FRAP to investigate the mobility of a range of solutes in sub-cellular compartments. Besides this application, FRAP has also been used to study the mobility of molecules in extracellular matrices such as mucus and related bio-gels. In a FRAP experiment, one component in a multi-component system is selectively fluorescently labelled. The sample is placed on a microscope and a high intensity laser beam is rastered across the sample, bleaching the fluorescence of the labeled molecules, causing a drop in the fluorescence intensity. Diffusion of the non-bleached molecules into the area previously bleached results in recovery of the fluorescence intensity, Fig. 6. The diffusion coefficient is then obtained by fitting the curve of the recovery profile [54].

The diffusion of polystyrene microspheres (59–1000 nm) viruses, and artificial virus-like particles derived from the capsid layers of human papilloma virus HPV (55 nm, ~20,000 g mol^{-1}) and Norwalk virus (38 nm, ~10,000 g mol^{-1}) in fresh human cervical mucus were quantified using FRAP [55]. When compared to virus-like particles of similar size, the PS microspheres were bound more tightly to the mucin fibers. Even the smallest microspheres (59 nm) showed no detectable diffusion by FRAP.

FRAP was also used by Afdhal et al. to examine the influence of mucin in the aggregation of cholesterol enriched vesicles [56]. An increase in the vesicle size (calculated from the diffusion coefficients measured by FRAP) was explained by binding of the vesicles to the mucin, suggesting that both glycosylated and non-glycosylated domains of the mucin are involved in the interaction even though the effect is reversible in the absence of non-glycosylated domains.

4. Pulsed-gradient spin-echo NMR (PGSE-NMR)

4.1. Theoretical considerations

Like all nuclear magnetic resonance (NMR) techniques, PGSE-NMR offers a numbers of advantages when applied to multi-component or heterogeneous systems - it is non-invasive, non-destructive but most importantly the chemical specificity of NMR enables the behaviour of each component within the mixture to be identified and analysed in a

single experiment. Furthermore, the typical length scales present in nano-scale structures coupled to their characteristic diffusion rates results in measurable changes in NMR signal over the appropriate timescale for the NMR experiment. The only drawback is that the sample must contain a spin-active nucleus, but 1H and 19F are particularly viable for biological samples.

The pulsed-gradient spin-echo NMR [57–77] (PGSE-NMR, sometimes referred to PFGSE-NMR) experiment has been reviewed previously in the context of polymer solutions [60,68,78,79], gels [80–83], self-associating and supramolecular systems [77,84–88] and porous or heterogeneous media [58,86,89–101]. A full description of this technique is beyond the scope of this article so here we provide only an introduction to the technique and its application to the diffusion of small molecules in mucosal systems.

The central feature of the PGSE-NMR experiment is the application of magnetic field-gradients $G(r)$ that encodes into the NMR signal (via the frequency, ω) the position of the molecule, r;

$$B(r) = B_0 + \gamma\,G(r) \tag{1}$$

where $B(r)$ is the effective field in the presence of field gradients, B_0 the static field strength and γ the magnetogyric ratio, a constant for a particular nucleus.

Diffusion experiments are generally pseudo-2D experiments, in that a series of typically 16–64 high resolution 1D spectra are recorded, following an evolution period during which diffusion leads to a displacement of the molecules. The field-gradients are pulsed at the start and end of the evolution time to encode and decode respectively, the NMR signal with the spatial information. The diffusion period is a very useful experimental parameter in itself and may be used to test for the presence of and subsequently "size" any boundaries present within the system.

Many pulse sequences have been written in order to quantify the diffusion for a range of different sample circumstances (strong signals, solvent suppression, convection compensation, the presence of background gradients, etc) [67,68,71,72,102–132] but arguably the most commonly used are the Stejskal-Tanner, stimulated echo and longitudinal echo decay sequences. Central to all pulse sequences are a set

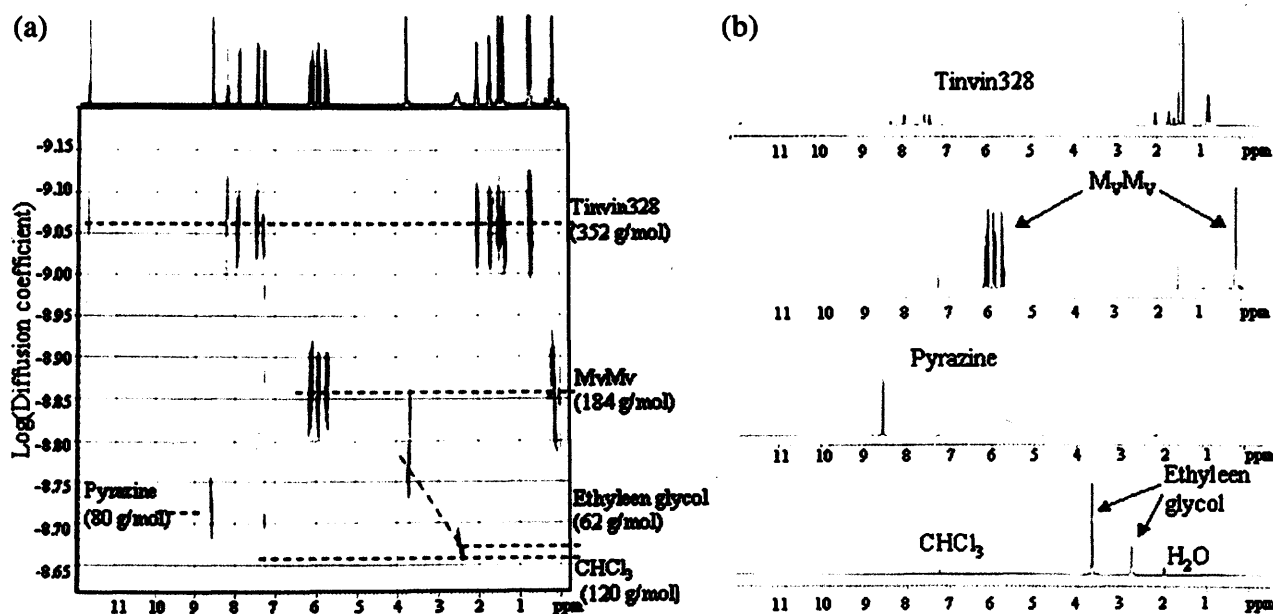Fig. 10. Typical DOSY plot for different components in a chemical mixture: (a) the DOSY spectrum of the experimental data and (b) the corresponding pure spectra (Reprinted from Journal of Magnetic Resonance, 169, Huo, R. et al., Improved DOSY NMR data processing by data enhancement and combination of multivariate curve resolution with non-linear square fitting, 257–269, Copyright 2004, with permission from Elsevier [133]).

of matched field gradient pulses that perform the encoding and decoding of the spatial information. The stimulated echo sequence is depicted in Fig. 7.

The first of the 90 degree pulses tips the magnetization into the xy plane where its precessional frequency is determined by the applied field gradient pulse, accordingly to Eq. (1). A second 90 degree pulse minimises the effects of spin-spin relaxation by storing the magnetization in the longitudinal plane, particularly useful for materials such as polymers where $T_1 \gg T_2$ values. After the evolution time, the final 90 degree pulse tips in magnetization back into the xy plane where the second field gradient pulse quantifies changes in the precessional frequency induced by diffusion of the molecules leading to a different effective field being sensed, Fig. 7.

A typical raw 2D dataset is presented in Fig. 8 where the normal 1H NMR spectrum runs left to right and the spectra decrease in intensity with increasing field gradient duration (fixed magnitude) running back to front. It is clear that various peaks decay – attenuate – at different rates, corresponding to different diffusion coefficients.

4.2. Calculating diffusion coefficients

There are various analysis protocols for quantifying the diffusion coefficient; the simplest involves measuring the integral of a characteristic peak arising from the molecule of interest and fitting the exponential attenuation of this signal, Fig. 9(a). If the molecule of interest is monodisperse , the diffusion behaviour should give a simple exponential decay. Polydispersity or slow exchange – where the molecule exists in two discrete dynamic environments that are not averaged on the NMR timescale – lead to non-exponential behaviour that often presents a challenge to interpret but is nonetheless a valuable insight. Non-exponential behaviour may also arise from the attenuation of a signal arising from similar functional groups in two of the components i.e. where there is significant "spectral overlap". In these cases, fitting to a bi- or sum of exponentials may still provide a valid insight, Fig. 9(b), (c).

More elaborate protocols also exist where *a priori* information is used to further refine the analysis by constraining input parameters to

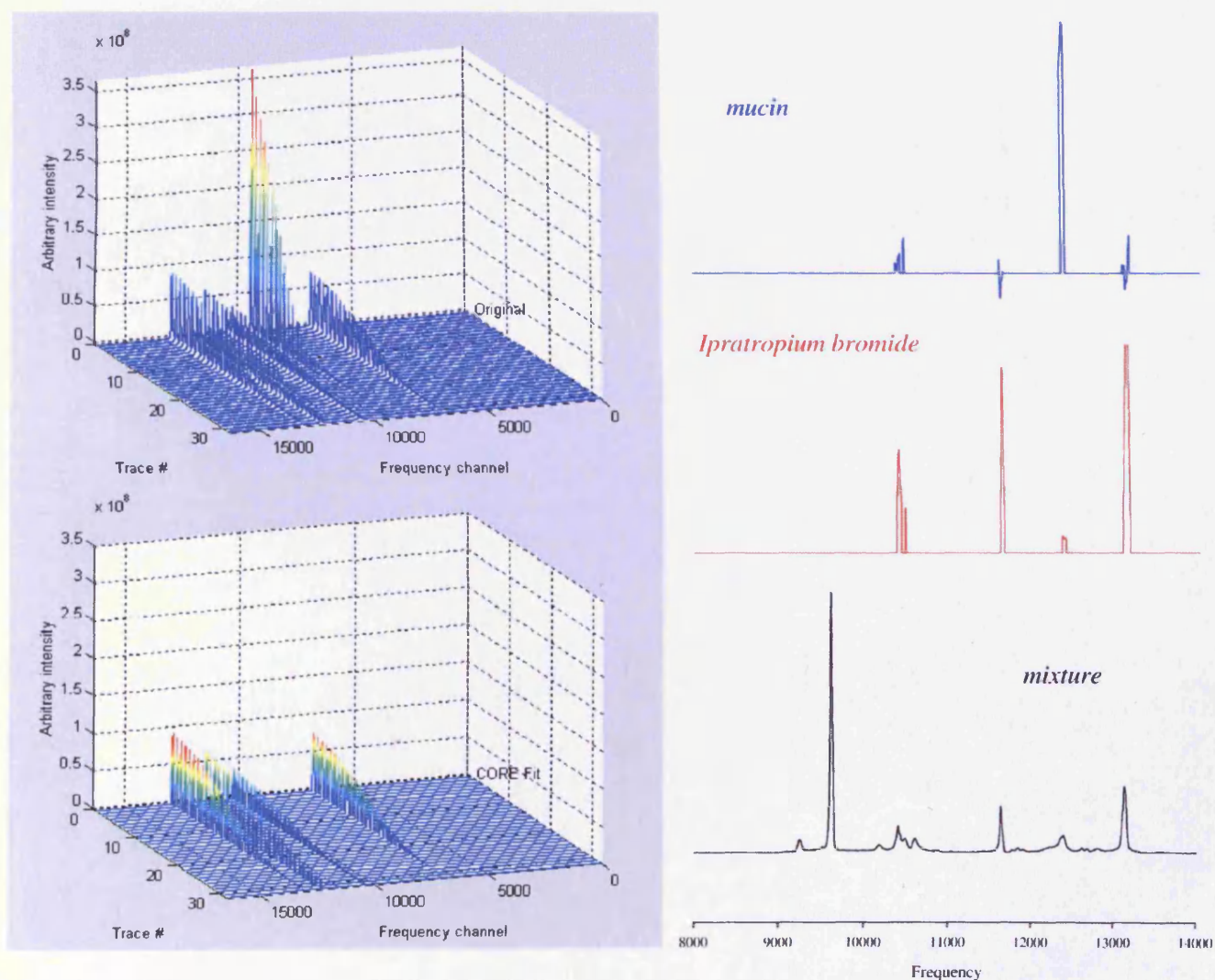Fig. 11. COmponent REsolved (CORE) analysis of the diffusion of ipratropium bromide in mucin, at 37 °C. The attenuation of the spectra arise from three diffusing species, drug, mucin and HOD. The HOD has been "edited out" of the analysis protocol, leading just two components, drug and mucin. The extracted 1D spectra are also accessible permitting the unequivocal identification of each particular component.

known spectra or to the known number of diffusion coefficients, this latter approach particularly useful if one needs to identify an unknown species in a mixture. Arguably the most commonly employed protocol, which is not without drawbacks, is the DOSY (Diffusion Ordered SpectroscopY) NMR approach in which an inversion of the attenuation function for each point in the spectrum leads to a 2D representation of the diffusion coefficient vs. spectral characteristic, Fig. 10. This is a particularly powerful approach if one is interested in editing or resolving spectra based on diffusion rates, Fig. 11.

The diffusion coefficients thus determined contains dynamical and structural information defined by the size and shape of the diffusing species and the solution within which it is dispersed. Diffusion coefficients decrease with increasing molecular size and as a reflection of any binding or obstruction the diffusing specie experiences within the solution. In dilute solutions, hydrodynamic radii are most frequently calculated from diffusion coefficients via the Stokes–Einstein relationship, notwithstanding its limitations.

Associations and other interactions (such as binding) between diffusing species leads to a reduction in diffusion rate, commensurate with the increased size of the aggregate, modulated by the lifetime and concentration of the aggregate. For the situation where the aggregate is long-lived compared to the NMR timescale, two discrete populations are manifest, sometimes giving rise to two discrete NMR signals. More commonly, fast exchange occurs and the effective diffusion coefficient is a population weighted average of the two discrete environments, the faster rate associated with the non-aggregated species and the slower rate associated with aggregates;

$$D_s^{average} = \frac{C_{non-aggregated}D_s^{fast} + C_{aggregated}D_s^{sloe}}{C_{total}} \qquad (2)$$

In the case of small, rapidly diffusing molecules interacting with large, slowly diffusing structures, there is a significant sensitivity to the concentration of the non-aggregated fraction of the small molecule, and thus NMR diffusion measurements are highly useful for the study of weak interactions.

4.3. Application of PGSE-NMR to bio-gel systems

Several classes of vehicles employed for drug delivery systems are now available including (i) liposomes, (ii) surfactant micelles, (iii) micro-emulsions, and (iv) polymers [134]. As a non-invasive technique, PGSE-NMR can be used to quantify the diffusion of micro- and nano-sized drug delivery constructs [135] in colloidal systems [136–140] and bio-gels such as mucin glycoprotein solutions [29,141,142], cartilage [143], curdlan gels [144], whey and casein protein gels [145–148].

Diffusion measurements of PEG polymers with different molecular weights (1080, 8500, 82,250 g mol^{-1}) in whey protein solutions and gels were carried out by Colsenet et al. [145]. Their studies revealed that PEG diffusion in both whey solutions and gels was strongly related to the probe polymer size i.e. an increase in the size of the PEG resulted in a reduction in its diffusion coefficient. This effect was more pronounced with increasing protein concentration. Thermal-aggregation of the whey protein caused structural changes in the protein, leading to an increase in inter-particle distances, enhancing the diffusion of all PEGs. Similarly, a diffusion study of PEGs in curdlan gels [144] showed a dependence on the polysaccharide concentration, the size of the PEG and the temperature.

Lafitte et al. [29] studied the effect of pig gastric mucin on the diffusion of PEGs spanning a molecular weight range 1020 g mol^{-1}<Mw<716,500 g mol^{-1} in 5 wt.% mucin gels (equivalent to the normal human physiological concentration in the stomach) as functions of pH, ionic strength and temperature. They concluded that the structure of the mucin molecules revealed a stronger dependency on the PEG diffusion as a result of changes in the pH compared with changes in ionic strength and temperature. In fact, it was found that intermediate molecular weight PEG that displayed a slower diffusion at pH 4 compared to pH 1 and 7, Fig. 12. The increase in diffusion between pH 1 and 4 was due to the mucin network being less homogeneous at pH 1 compared with pH 4. More surprising was the fact that the diffusion of the PEGs was faster at pH 7 than at pH 4, explained by the decrease in flexibility of the PGM molecules within the network induced by stronger hydrophobic interactions as a result of the decreasing pH. These interactions facilitate the diffusion of PEGs of intermediate but not the largest PEGs which are too sterically hindered.

The same research group investigated the transport in mucin and mucus of polysorbate 80 (PS-80), a non-ionic surfactant commonly used as an excipient in many pharmaceutical formulations [142]. The PGSE-NMR attenuation functions for PS-80 in mucin solution and mucus showed a bi-exponential nature (see Fig. 13). This is explained by the existence of two populations of PS-80 molecules within a single sample: a non-surface-active fraction that can move freely in the system (PS-80free) and a surface-active fraction that forms micellar structures resulting in a slower diffusion in the bio-gel (PS-80mic). However, the reduced transport rate of PS-80 in mucin is not due to a specific interaction with mucin but to a simple interaction of the PS-80 with the mucin network. PS-80 consists of and fatty acid chains and long ethylene oxide chains and as such, they are expected to behave in a similar fashion to PEG, showing steric hindrance on diffusion processes in the mucin network. When the excipient is mixed with mucus in solution, the PS-80 experiences a greater decrease in its diffusion coefficient. The abundant lipids
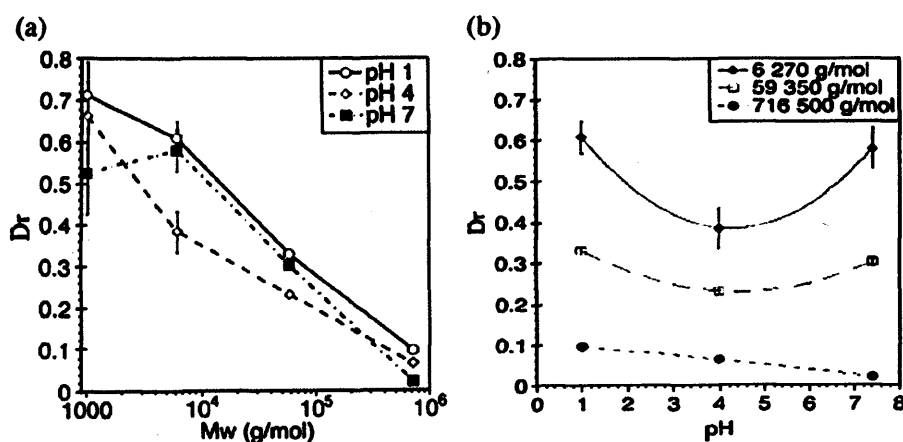
(a)   **(b)**

Fig. 12. Relative diffusion coefficients of PEG probe molecules in PGM solutions at 5 wt.% reported as function of the Mw of the polymers (a) and as function of the pH (b) (Figure reproduced, with permission, from [29]).
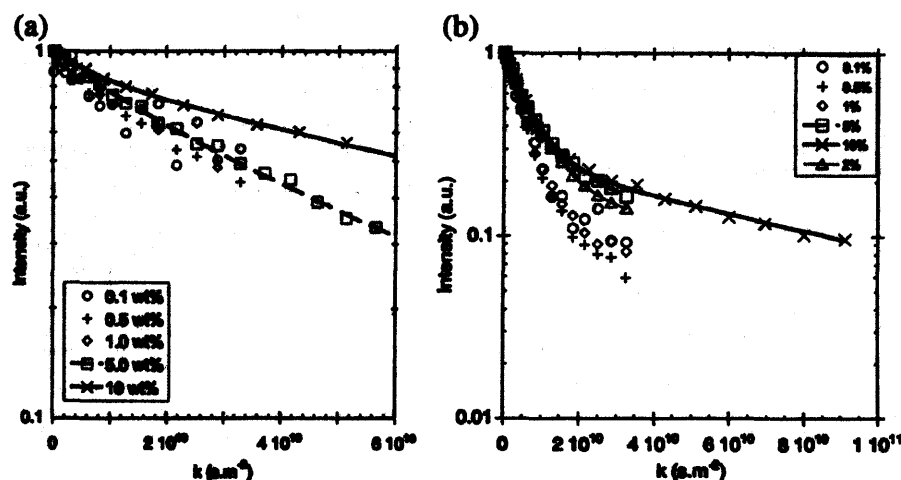
(a)

(b)

Fig. 13. Echo-decays obtained by PGSE-NMR for different concentrations of PS-80 in the presence of 5 wt.% mucin (a) and 5 wt.% mucus (b) (Figure reproduced, with permission, from [149]).

contribute most to reduce the diffusion of drugs in native mucus [42], acting as adsorption sites for amphiphile molecules through hydrophobic interactions.

Upon addition of the cationic surfactant tetradecyltrimethylammonium chloride (TTAC) to the mixture of mucin and PS-80, the formation of mixed micelles between PS-80 and TTAC occurred [141]. Depending on the composition of the mixture, complex-formation led to precipitation. PGSE-NMR measurements demonstrated that at low concentrations of PS-80, mixed PS-80, TTAC and mucin aggregates were formed, but an increase in PS-80 concentration caused the dissolution of the precipitate, limiting the interactions between the mixed micelles and the mucin. Our interest focuses on "polymer therapeutics" [150,151], polymeric carriers conjugated via a covalent (often cleavable) bond to the therapeutic moiety. The polymeric carrier confers aqueous solubility, biocompatibility or biodegradability and improves the pharmacokinetics of the therapeutic agent. The bioavailability of the therapeutic agent is closely coupled to its ability to be transported to the site of action. Therefore, a key aspect in defining structure-activity relationships for polymer therapeutics derived from polymer diffusion data is the requirement to separate the effects of obstruction – the reduction in polymer mobility due to

the increased diffusion path-length associated with the polymer having to diffuse around the mucin molecules – from the effects of binding against the backdrop of inherently varying molecular weight and chemical structures of the range of polymers being examined. One approach to achieve this is to examine the diffusion coefficient of the polymer as a function of mucin concentration. By normalising such diffusion data to the diffusion rate observed at infinite dilution in terms of the mucin concentration $\frac{D^{mucin}}{D^{infinite}}$, one may to a first approximation remove the effects of molecular weight, Fig. 14.

It is clear from Fig. 14 that the relative diffusion coefficients vary significantly with mucin concentration, being substantially slower in the presence of physiological amounts of mucin. These data also show a complex relationship with molecular weight – there is the expected decrease in diffusion rate for the two PEGs (10 K and 10 K g mol^{-1}) but there is a negligible difference in the relative G2 and G4 diffusion rates given their rather different molecular weights (3256 g mol^{-1} and 14,215 g mol^{-1} respectively). Further, the mucin retards the diffusion of the two PAMAMs to a comparable degree to the larger PEG, notwithstanding its much greater size. The greatest reduction is shown by the highly branched poly(ethylene imine) 25 K g mol^{-1} sample. These data reflect the complex interplay between obstruction-only behaviour (PEG, e.g. the basis of PEGylation [152]) and obstruction plus binding to the mucin (PAMAM, PEI) where additional retardation arises due to the molecular characteristics of the polymer and the mucin.

5. Outlook and future perspectives

This article has surveyed the range of techniques commonly used to measure the diffusion of particles, polymers and self-assembled structures through mucosal systems. Some interesting and unexpected behaviour has been highlighted, for example a non-monotonic behaviour of diffusion rate on particle size, requiring further study. The PGSE-NMR technique has been discussed in some detail as it offers an as-yet unexploited approach to studying the diffusion of both small molecules such as drugs and larger polymer-based drug delivery systems in mucin. Considerable effort is required to separate the effects of specific interactions between the species of interest and the mucin from simple obstruction effects, in order to define the underlying structure-activity relationships.
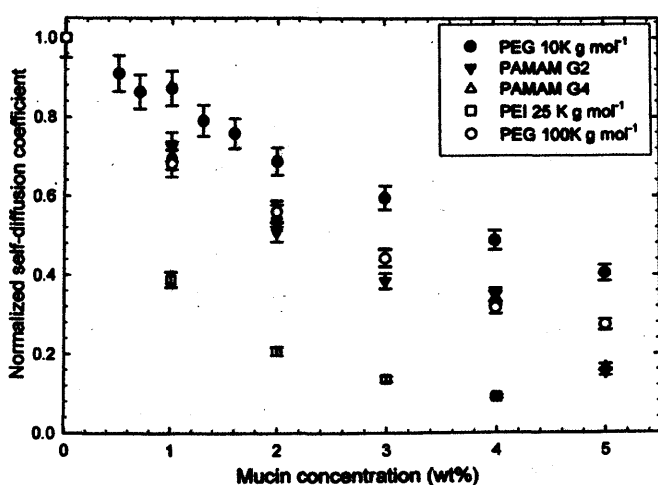
Acknowledgements

Fig. 14. Relative self-diffusion coefficients measured by PGSE-NMR for a series of polymers in different concentrations of mucin. poly(ethylene glycol) 10 K g mol^{-1} and 100 K g mol $^{-1}$; PAMAM dendrimers generation 2 and 4 and poly(ethylene imine) 25 K g mol^{-1}.

References

[1] R. Duncan, Targeting and intracellular delivery of drugs, in: R.A. Meyers (Ed.), Encyclopedia of Molecular Cell Biology and Molecular Medicine, Weinhem, Germany, 2005, pp. 163–204.

[2] N.N. Sanders, S.C. De Smedt, J. Demeester, The physical properties of biogels and their permeability for macromolecular drugs and colloidal drug carriers, Journal of Pharmaceutical Sciences 89 (2000) 835–849.

[3] D.A. Norris, N. Puri, P.J. Sinko, The effect of physical barriers and properties on the oral absorption of particulates, Advanced Drug Delivery Reviews 34 (1998) 135–154.

[4] S.K. Linden, P. Sutton, N.G. Karlsson, V. Korolik, M.A. McGuckin, Mucins in the mucosal barrier to infection, Mucosal Immunology 1 (2008) 183–197.

[5] P.G. Bhat, D.R. Flanagan, P.D. Donovan, Drug binding to gastric mucus glycoproteins, International Journal of Pharmaceutics 134 (1996) 15–25.

[6] H. Rahmoune, K.L. Shephard, State of airway surface liquid on guinea-pig trachea, Journal of Applied Physiology 78 (1995) 2020–2024.

[7] D.E. Sims, M.M. Horne, Heterogeneity of the composition and thickness of tracheal mucus in rats, American Journal of Physiology-Lung Cellular and Molecular Physiology 273 (1997) L1036–L1041.

[8] M.R. Neutra, J.F. Forstner, Gastrointestinal mucus: synthesis, secretion, and function, in: L.R. Johnson (Ed.), Physiology of the Gastrointestinal Tract, New York, 1986, pp. 975–1009.

[9] G. Ponchel, J.M. Irache, Specific and non-specific bioadhesive particulate systems for oral delivery to the gastrointestinal tract, Advanced Drug Delivery Reviews 34 (1998) 191–219.

[10] S. Kerss, A. Allen, A. Garner, A simple method for measuring thickness of the mucus gel layer adherent to rat, frog and human gastric-mucosa — influence of feeding, prostaglandin, n-acetylcysteine and other agents, Clinical Science 63 (1982) 187–195.

[11] T. Sakata, W. Vonengelhardt, Luminal mucin in the large-intestine of mice, rats and guinea-pigs, Cell and Tissue Research 219 (1981) 629–635.

[12] L.A. Sellers, A. Allen, E.R. Morris, S.B. Rossmurphy, Mechanical characterization and properties of gastrointestinal mucus gel, Biorheology 24 (1987) 615–623.

[13] N.N. Sanders, S.C. De Smedt, E. Van Rompaey, P. Simoens, F. De Baets, J. Demeester, Cystic fibrosis sputum — a barrier to the transport of nanospheres, American Journal of Respiratory and Critical Care Medicine 162 (2000) 1905–1911.

[14] M. Dawson, D. Wirtz, J. Hanes, Enhanced viscoelasticity of human cystic fibrotic sputum correlates with increasing microheterogeneity in particle transport, Journal of Biological Chemistry 278 (2003) 50393–50401.

[15] I. Fiebrig, K.M. Varum, S.E. Harding, S.S. Davis, B.T. Stokke, Colloidal gold and colloidal gold labelled wheat germ agglutinin as molecular probes for identification in mucin/chitosan complexes, Carbohydrate Polymers 33 (1997) 91–99.

[16] I. Genta, M. Costantini, A. Asti, B. Conti, L. Montanari, Influence of glutaraldehyde on drug release and mucoadhesive properties of chitosan microspheres, Carbohydrate Polymers 36 (1998) 81–88.

[17] A. Bernkop-Schnurch, V. Schwarz, S. Steininger, Polymers with thiol groups: a new generation of mucoadhesive polymers? Pharmaceutical Research 16 (1999) 876–881.

[18] N.A. Peppas, Y.B. Huang, Nanoscale technology of mucoadhesive interactions, Advanced Drug Delivery Reviews 56 (2004) 1675–1687.

[19] N.A. Peppas, J.J. Sahlin, Hydrogels as mucoadhesive and bioadhesive materials: a review, Biomaterials 17 (1996) 1553–1561.

[20] R. Bansil, B.S. Turner, Mucin structure, aggregation, physiological functions and biomedical applications, Current Opinion in Colloid & Interface Science 11 (2006) 164–170.

[21] K. Khanvilkar, M.D. Donovan, D.R. Flanagan, Drug transfer through mucus, Advanced Drug Delivery Reviews 48 (2001) 173–193.

[22] T.J. McMaster, M. Berry, A.P. Corfield, M.J. Miles, Atomic force microscopy of the submolecular architecture of hydrated ocular mucins, Biophysical Journal 77 (1999) 533–541.

[23] M.D.G. Oates, A.C. Rosbottom, J. Schrager, Further investigations into structure of human gastric mucin — structural configuration of oligosaccharide chains, Carbohydrate Research 34 (1974) 115–137.

[24] J. Perez-Vilar, R.L. Hill, The structure and assembly of secreted mucins, Journal of Biological Chemistry 274 (1999) 31751–31754.

[25] J.K. Sheehan, K. Oates, I. Carlstedt, Electron-microscopy of cervical, gastric and bronchial mucus glycoproteins, Biochemical Journal 239 (1986) 147–153.

[26] R. Bansil, X.X. Cao, N.H. Afdhal, N. Niu, K.R. Bhaskar, J.T. Lamont, Mucin — aggregation and colloidal interactions of relevance to some biomedical problems, Nuovo Cimento Della Societa Italiana Di Fisica D-Condensed Matter Atomic Molecular and Chemical Physics Fluids Plasmas Biophysics 16 (1994) 1411–1418.

[27] R. Bansil, E. Stanley, J.T. Lamont, Mucin biophysics, Annual Review of Physiology 57 (1995) 635–657.

[28] N. Jentoft, Why are proteins o-glycosylated, Trends in Biochemical Sciences 15 (1990) 291–294.

[29] G. Lafitte, O. Soderman, K. Thuresson, J. Davies, PFG-NMR diffusometry: a tool for investigating the structure and dynamics of noncommercial purified pig gastric mucin in a wide range of concentrations, Biopolymers 86 (2007) 165–175.

[30] R.L. Shogren, A.M. Jamieson, J. Blackwell, N. Jentoft, conformation of mucous glycoproteins in aqueous solvents, Biopolymers 25 (1986) 1505–1517.

[31] M.C. Rose, Mucins — structure, function, and role in pulmonary-diseases, American Journal of Physiology 263 (1992) L413–L429.

[32] J. Celli, B. Gregor, B. Turner, N.H. Afdhal, R. Bansil, S. Erramilli, Viscoelastic properties and dynamics of porcine gastric mucin, Biomacromolecules 6 (2005) 1329–1333.

[33] K.R. Bhaskar, D. Gong, R. Bansil, S. Pajevic, J.A. Hamilton, B.S. Turner, J.T. Lamont, Profound increase in viscosity and aggregation of pig gastric mucin at low pH, American Journal of Physiology 261 (1991) G827–G833.

[34] Z.N. Hong, B. Chasan, R. Bansil, B.S. Turner, K.R. Bhaskar, N.H. Afdhal, Atomic force microscopy reveals aggregation of gastric mucin at low pH, Biomacromolecules 6 (2005) 3458–3466.

[35] A. Maleki, G. Lafitte, A.L. Kjoniksen, K. Thuresson, B. Nystrom, Effect of pH on the association behavior in aqueous solutions of pig gastric mucin, Carbohydrate Research 343 (2008) 328–340.

[36] X.X. Cao, R. Bansil, K.R. Bhaskar, B.S. Turner, J.T. LaMont, N. Niu, N.H. Afdhal, pH-dependent conformational change of gastric mucin leads to sol-gel transition, Biophysical Journal 76 (1999) 1250–1258.

[37] R. Bansil, X.X. Cao, K.R. Bhaskar, J.T. LaMont, Gelation and aggregation of mucin in relation to the stomach's protective barrier, Macromolecular Symposia 109 (1996) 105–113.

[38] R.K. Willits, W.M. Saltzman, Synthetic polymers alter the structure of cervical mucus, Biomaterials 22 (2001) 445–452.

[39] W.M. Saltzman, M.L. Radomsky, K.J. Whaley, R.A. Cone, Antibody diffusion in human cervical-mucus, Biophysical Journal 66 (1994) 508–515.

[40] D.A. Norris, P.J. Sinko, Effect of size, surface charge, and hydrophobicity on the translocation of polystyrene microspheres through gastrointestinal mucin, Journal of Applied Polymer Science 63 (1997) 1481–1492.

[41] C. Durrer, J.M. Irache, D. Duchene, G. Ponchel, Study of the interactions between nanoparticles and intestinal mucosa, Trends in Colloid and Interface Science Viii 97 (1994) 275–280.

[42] A.W. Larhed, P. Artursson, E. Bjork, The influence of intestinal mucus components on the diffusion of drugs, Pharmaceutical Research 15 (1998) 66–71.

[43] J.H. Suh, D. Wirtz, J. Hanes, Real-time intracellular transport of gene nano-carriers studied by multiple particle tracking, Biotechnology Progress 20 (2004) 598–602.

[44] M. Dawson, D. Wirtz, J. Hanes, Real-time tracking of nanoparticle gene carriers in gastrointestinal mucus, Biophysical Journal 86 (2004) 598A.

[45] J. Suh, M. Dawson, J. Hanes, Real-time multiple-particle tracking: applications to drug and gene delivery, Advanced Drug Delivery Reviews 57 (2005) 63–78.

[46] S.K. Lai, D.E. O'Hanlon, S. Harrold, S.T. Man, Y.Y. Wang, R. Cone, J. Hanes, Rapid transport of large polymeric nanoparticles in fresh undiluted human mucus, Proceedings of the National Academy of Sciences of the United States of America 104 (2007) 1482–1487.

[47] M. Dawson, E. Krauland, D. Wirtz, J. Hanes, Transport of polymeric nanoparticle gene carriers in gastric mucus, Biotechnology Progress 20 (2004) 851–857.

[48] N.N. Sanders, S.C. De Smedt, J. Demeester, Mobility and stability of gene complexes in biogels, Journal of Controlled Release 87 (2003) 117–129.

[49] P.G. Bhat, D.R. Flanagan, M.D. Donovan, The limiting role of mucus in drug absorption: Drug permeation through mucus solution, International Journal of Pharmaceutics 126 (1995) 179–187.

[50] P.G. Bhat, D.R. Flanagan, M.D. Donovan, Drug-permeation studies through cystic fibrotic mucus solution, Pharmaceutical Research (New York) 12 (1995) S244.

[51] P.G. Bhat, D.R. Flanagan, M.D. Donovan, Drug diffusion through cystic fibrotic mucus: Steady-state permeation, rheologic properties, and glycoprotein morphology, Journal of Pharmaceutical Sciences 85 (1996) 624–630.

[52] M.A. Desai, P. Vadgama, Estimation of effective diffusion-coefficients of model solutes through gastric mucus — assessment of a diffusion chamber technique based on spectrophotometric analysis, Analyst 116 (1991) 1113–1116.

[53] M.A. Desai, M. Mutlu, P. Vadgama, A study of macromolecular diffusion through native porcine mucus, Experientia 48 (1992) 22–26.

[54] T.K.L. Meyvis, S.C. De Smedt, P. Van Oostveldt, J. Demeester, Fluorescence recovery after photobleaching: a versatile tool for mobility and interaction measurements in pharmaceutical research, Pharmaceutical Research 16 (1999) 1153–1162.

[55] S.S. Olmsted, J.L. Padgett, A.I. Yudin, K.J. Whaley, T.R. Moench, R.A. Cone, Diffusion of macromolecules and virus-like particles in human cervical mucus, Biophysical Journal 81 (2001) 1930–1937.

[56] N.H. Afdhal, X.X. Cao, R. Bansil, Z.N. Hong, C. Thompson, B. Brown, D. Wolf, Interaction of mucin with cholesterol enriched vesicles: role of mucin structural domains, Biomacromolecules 5 (2004) 269–275.

[57] P.T. Callaghan, NMR in polymers using magnetic field gradients: imaging, diffusion and flow, in: R.N. Ibbett (Ed.), NMR Spectrosc. Polym. Blackie, Glasgow, UK, 1993, pp. 308–342.

[58] P.T. Callaghan, Principles of Nuclear Magnetic Resonance Microscopy, Oxford University Press, Oxford, 1991.

[59] D. Canet, M. Decorps, Applications of field gradients in NMR, Dyn. Solutions Fluid Mixtures NMR, Jean-Jacques, 1995, pp. 309–343.

[60] P. Griffiths, P. Stilbs, NMR self-diffusion studies of polymeric surfactants, Current Opinion in Colloid & Interface Science 7 (2002) 249–252.

[61] I. Furo, S.V. Dvinskikh, Field gradient NMR of liquid crystals, in: G.A. (Ed.), Modern magnetic resonance, Springer, Dordrecht, Neth., 2006, pp. 113–118.

[62] C.S. Johnson, Diffusion measurements by magnetic field gradient methods, in: D.M. Grant, R.K. Harris (Eds.), Encyclopedia of Nuclear Magnetic Resonance, Wiley, New York, 1996, pp. 1626–1644.

[63] L.E. Kay, Field gradient techniques in NMR-spectroscopy, Current Opinion in Structural Biology 5 (1995) 674–681.

[64] J. Karger, H. Pfeifer, NMR studies of molecular diffusion, NMR Techniques in Catalysis 55 (1994) 69–137.

[65] J. Karger, H. Pfeifer, Self-diffusion by NMR measurements, Recents Prog. Genie Procedes 5 (1991) 65–70.

[66] J. Keeler, R.T. Clowes, A.L. Davis, E.D. Laue, Pulsed-field gradients — theory and practice, Nuclear Magnetic Resonance Pt C 239 (1994) 145–207.

[67] J.C. Lindon, M.L. Liu, J.K. Nicholson, Diffusion coefficient measurement by high-resolution NMR-spectroscopy — biochemical and pharmaceutical applications, Reviews in Analytical Chemistry 18 (1999) 23–66.

[68] L. Masaro, X.X. Zhu, Pulsed field gradient NMR spectroscopy in the study of self-diffusion in polymer systems, Canadian Journal of Analytical Sciences and Spectroscopy 43 (1998) 81–89.

[69] K.I. Momot, P.W. Kuchel, PFG NMR diffusion experiments for complex systems, Concepts in Magnetic Resonance A 28A (2006) 249–269.

[70] K. Nicolay, K.P.J. Braun, R.A. de Graaf, R.M. Dijkhuizen, M.J. Kruiskamp, Diffusion NMR spectroscopy, NMR in Biomedicine 14 (2001) 94–111.

[71] W.S. Price, Pulsed-field gradient nuclear magnetic resonance as a tool for studying translational diffusion 1. Basic theory, Concepts in Magnetic Resonance 9 (1997) 299–336.

[72] W.S. Price, Pulsed-field gradient nuclear magnetic resonance as a tool for studying translational diffusion: part II. Experimental aspects, Concepts in Magnetic Resonance 10 (1998) 197–237.

[73] W.S. Price, Recent advances in NMR diffusion techniques for studying drug binding, Australian Journal of Chemistry 56 (2003) 855–860.

[74] W.S. Price, Diffusion-based studies of aggregation, binding and conformation of biomolecules: theory and practice, in: D.M. Grant, R.K. Harris (Eds.), Encyclopedia of Nuclear Magnetic Resonance, John Wiley & Sons Ltd, Chichester, UK, 2002, pp. 364–374.

[75] M.E. Smith, J.H. Strange, NMR techniques in materials physics: a review, Measurement Science & Technology 7 (1996) 449–475.

[76] P. Stilbs, Diffusion studied using NMR spectroscopy, in: J.C. Lindon, G.E. Tranter, J. L. Holmes (Eds.), Encyclopedia of Spectroscopy and Spectrometry, Accademic Press, London, 1999, pp. 369–375.

[77] P. Stilbs, Fourier transform pulsed-gradient spin-echo studies of molecular diffusion, Progress in Nuclear Magnetic Resonance Spectroscopy 19 (1987) 1–45.

[78] R. Kimmich, N. Fatkullin, Polymer chain dynamics and NMR, NMR - 3D Analysis - Photopolymerization, vol. 170, 2004, pp. 1–113.

[79] A.G. Palmer, Probing molecular motion by NMR, Current Opinion in Structural Biology 7 (1997) 732–737.

[80] L. Masaro, X.X. Zhu, Physical models of diffusion for polymer solutions, gels and solids, Progress in Polymer Science 24 (1999) 731–775.

[81] S. Matsukawa, H. Yasunaga, C. Zhao, S. Kuroki, H. Kurosu, I. Ando, Diffusion processes in polymer gels as studied by pulsed field-gradient spin-echo NMR spectroscopy, Progress in Polymer Science 24 (1999) 995–1044.

[82] Y. Nakashima, Measurement of H_2O self-diffusion coefficients in clay gels by pulsed-field-gradient Nuclear magnetic Resonance: a review, Nendo Kagaku 42 (2002) 37–50.

[83] Y. Yamane, S. Kanesaka, S. Kim, K. Kamiguchi, M. Matsui, S. Kuroki, I. Ando, Diffusion in soft polymer systems as approached by field-gradient NMR, Annual Reports on NMR Spectroscopy 58 (2006) 51–154.

[84] G. Colafemmina, G. Palazzo, A. Ceglie, L. Ambrosone, G. Cinelli, V. Di Lorenzo, Restricted diffusion: an effective tool to investigate food emulsions, Lipid and Polymer-Lipid Systems 120 (2002) 23–27.

[85] A.A. Pena, G.J. Hirasaki, NMR characterization of emulsions, Surfactant Science Series 132 (2006) 283–309.

[86] O. Soderman, U. Olsson, Dynamics of amphiphilic systems studied using NMR relaxation and pulsed field gradient experiments, Current Opinion in Colloid & Interface Science 2 (1997) 131–136.

[87] O. Soderman, B. Balinov, NMR self-diffusion studies of emulsions, Surfactant Science Series 61 (1996) 369–392.

[88] Y. Cohen, L. Avram, L. Frish, Diffusion NMR spectroscopy in supramolecular and combinatorial chemistry: an old parameter – new insights, Angewandte Chemie-International Edition 44 (2005) 520–554.

[89] P.T. Callaghan, A. Coy, PGSE and molecular translational motion in porous media, in: P. Tycko (Ed.), NMR probes of molecular dynamics, Kluwer Acad. Publishers, Dordrecht, Neth., 1994, pp. 489–523.

[90] D. Candela, A. Ding, X.Y. Yang, Applications of NMR to transport in random systems, Physica B-Condensed Matter 279 (2000) 120–124.

[91] I. Furo, S.V. Dvinskikh, NMR methods applied to anisotropic diffusion, Magnetic Resonance in Chemistry 40 (2002) S3–S14.

[92] L.F. Gladden, Nuclear-magnetic-resonance in chemical-engineering – principles and applications, Chemical Engineering Science 49 (1994) 3339–3408.

[93] M.D. Herbst, J.H. Goldstein, A review of water diffusion measurement by NMR in human red blood-cells, American Journal of Physiology 256 (1989) C1097–C1104.

[94] J. Karger, H. Pfeifer, W. Heink, NMR diffusion studies in zeolites, in: D. Olson, a. Bisio (Eds.), Proc. Int. Zeolite Conf., 6th, Meeting Date 1983, 1984, pp. 184–200.

[95] J. Karger, G. Fleischer, NMR diffusion studies in heterogeneous systems, Trac-Trends in Analytical Chemistry 13 (1994) 145–157.

[96] J. Karger, NMR studies of diffusion in porous solids, NATO ASI Ser. Ser. C 491 (1998) 297–329.

[97] J. Karger, F. Stallmach, S. Vasenkov, Structure-mobility relations of molecular diffusion in nanoporous materials, Magnetic Resonance Imaging 21 (2003) 185–191.

[98] K. Nicolay, A. vanderToorn, R.M. Dijkhuizen, In vivo diffusion spectroscopy. An overview, N MR in Biomedicine 8 (1995) 365–374.

[99] F. Stallmach, J. Karger, The potentials of pulsed field gradient NMR for investigation of porous media, Adsorption-Journal of the International Adsorption Society 5 (1999) 117–133.

[100] D. Topgaard, Probing biological tissue microstructure with magnetic resonance diffusion techniques, Current Opinion in Colloid & Interface Science 11 (2006) 7–12.

[101] P.J. Barrie, Characterization of porous media using NMR methods, Annual Reports on NMR Spectroscopy 41 (2000) 265–316.

[102] I. Ardelean, R. Kimmich, The diversity of B-0 and B-1 gradient NMR diffusometry techniques, Israel Journal of Chemistry 43 (2003) 9–24.

[103] I. Ardelean, R. Kimmich, Diffusion measurements using the nonlinear stimulated echo, Journal of Magnetic Resonance 143 (2000) 101–105.

[104] B.A. Becker, K.F. Morris, C.K. Larive, An improved method for suppressing protein background in PFG NMR experiments to determine ligand diffusion coefficients in the presence of receptor, Journal of Magnetic Resonance 181 (2006) 327–330.

[105] D.M. Cantor, J. Jonas, Automated measurement of self-diffusion coefficients by spin-echo method, Journal of Magnetic Resonance 28 (1977) 157–162.

[106] M. Cercignani, M.A. Horsfield, An optimized pulse sequence for isotropically weighted diffusion imaging, Journal of Magnetic Resonance 140 (1999) 58–68.

[107] J.C. Cobas, M. Martin-Pastor, A homodecoupled diffusion experiment for the analysis of complex mixtures by NMR, Journal of Magnetic Resonance 171 (2004) 20–24.

[108] M.A. Connell, A.L. Davis, A.M. Kenwright, G.A. Morris, NMR measurements of diffusion in concentrated samples: avoiding problems with radiation damping, Analytical and Bioanalytical Chemistry 378 (2004) 1568–1573.

[109] C. Dalvit, J.M. Bohlen, Analysis of biofluids and chemical mixtures in non-deuterated solvents with H-1 diffusion-weighted PFG phase-sensitive double-quantum NMR spectroscopy, Nmr in Biomedicine 10 (1997) 285–291.

[110] N. Esturau, F. Sanchez-Ferrando, J.A. Gavin, C. Roumestand, M.A. Delsuc, T. Parella, The use of sample rotation for minimizing convection effects in self-diffusion NMR measurements, Journal of Magnetic Resonance 153 (2001) 48–55.

[111] W. Heink, J. Karger, H. Pfeifer, A simple pulse sequence to exclude falsification of NMR self-diffusion results by multiphase relaxation, Journal of the Chemical Society-Chemical Communications (1990) 1454–1455.

[112] R. Kimmich, E. Fischer, One-dimensional and 2-dimensional pulse sequences for diffusion experiments in the fringe-field of superconducting magnets, Journal of Magnetic Resonance Series A 106 (1994) 229–235.

[113] M.F. Lin, M.J. Shapiro, Mixture analysis in combinatorial chemistry. Application of diffusion-resolved NMR spectroscopy, Journal of Organic Chemistry 61 (1996) 7617–7619.

[114] B. Manz, Combined relaxation and displacement experiment: a fast method to acquire T-2, diffusion and velocity maps, Journal of Magnetic Resonance 169 (2004) 60–67.

[115] D.C. McCain, The echo-pulse experiment – a new pulse sequence for measuring diffusion along magnetic-field gradients, Journal of Magnetic Resonance Series B 109 (1995) 209–212.

[116] A. Mohoric, A modified PGSE for measuring diffusion in the presence of static magnetic field gradients, Journal of Magnetic Resonance 174 (2005) 223–228.

[117] K.I. Momot, P.W. Kuchel, Convection-compensating PGSE experiment incorporating excitation-sculpting water suppression (CONVEX), Journal of Magnetic Resonance 169 (2004) 92–101.

[118] I.V. Nesmelova, D. Idiyatullin, K.H. Mayo, Measuring protein self-diffusion in protein-protein mixtures using a pulsed gradient spin-echo technique with WATERGATE and isotope filtering, Journal of Magnetic Resonance 166 (2004) 129–133.

[119] M. Nilsson, A.M. Gil, I. Delgadillo, G.A. Morris, Improving pulse sequences for 3D diffusion-ordered NMR spectroscopy: 2DJ-IDOSY, Analytical Chemistry 76 (2004) 5418–5422.

[120] M. Nilsson, G.A. Morris, Improving pulse sequences for 3D DOSY: convection compensation, Journal of Magnetic Resonance 177 (2005) 203–211.

[121] M. Nilsson, A.M. Gil, I. Delagadillo, G.A. Morris, Improving pulse sequences for 3D DOSY: COSY-IDOSY, Chemical Communications (2005) 1737–1739.

[122] W.H. Otto, C.K. Larive, Improved spin-echo-edited NMR diffusion measurements, Journal of Magnetic Resonance 153 (2001) 273–276.

[123] K.D. Park, Y.J. Lee, Slice-selected LED and BPPLED: application of slice selection to DOSY, Magnetic Resonance in Chemistry 44 (2006) 887–891.

[124] W.S. Price, P.W. Kuchel, Effect of nonrectangular field gradient pulses in the Stejskal and Tanner (diffusion) pulse sequence, Journal of Magnetic Resonance 94 (1991) 133–139.

[125] G.H. Sorland, B. Hafskjold, O. Herstad, A stimulated-echo method for diffusion measurements in heterogeneous media using pulsed field gradients, Journal of Magnetic Resonance 124 (1997) 172–176.

[126] J.P. Stamps, B. Ottink, J.M. Visser, J.P.M. van Duynhoven, R. Huist, Difftrain: a novel approach to a true spectroscopic single-scan diffusion measurement, Journal of Magnetic Resonance 151 (2001) 28–31.

[127] M.J. Thrippleton, N.M. Loening, J. Keeler, A fast method for the measurement of diffusion coefficients: one-dimensional DOSY, Magnetic Resonance in Chemistry 41 (2003) 441–447.

[128] E. Tonning, D. Polders, P.T. Callaghan, S.B. Engelsen, A novel improved method for analysis of 2D diffusion-relaxation data-2D PARAFAC-Laplace decomposition, Journal of Magnetic Resonance 188 (2007) 10–23.

[129] D. Topgaard, A. Pines, Self-diffusion measurements with chemical shift resolution in inhomogeneous magnetic fields, Journal of Magnetic Resonance 168 (2004) 31–35.

[130] P. Trautner, K. Woelk, Improved strategies for NMR diffusion measurements with magnetization-grating rotating-frame imaging (MAGROFI), Physical Chemistry Chemical Physics 4 (2002) 5973–5981.

[131] S.S. Velan, N. Chandrakumar, High-resolution NMR measurement of molecular self-diffusion by fast multi-spin-echo diffusion sequences, Journal of Magnetic Resonance Series A 123 (1996) 122–125.

[132] X. Zhang, C.G. Li, C.H. Ye, M.L. Liu, Determination of molecular self-diffusion coefficient using multiple spin-echo NMR spectroscopy with removal of convection and background gradient artifacts, Analytical Chemistry 73 (2001) 3528–3534.

[133] R. Huo, R. Wehrens, L.M.C. Buydens, Improved DOSY NMR data processing by data enhancement and combination of multivariate curve resolution with non-linear least square fitting, Journal of Magnetic Resonance 169 (2004) 257–269.

[134] K.I. Moniot, P.W. Kuchel, Pulsed field gradient nuclear magnetic resonance as a tool for studying drug delivery systems, Concepts in Magnetic Resonance Part A 19A (2003) 51–64.

[135] W.S. Price, F. Elwinger, C. Vigouroux, P. Stilbs, PGSE-WATERGATE, a new tool for NMR diffusion-based studies of ligand-macromolecule binding, Magnetic Resonance in Chemistry 40 (2002) 391–395.

[136] S. Matsukawa, I. Ando, A study of self-diffusion of molecules in polymer gel by pulsed-gradient spin-echo H-1 NMR, Macromolecules 29 (1996) 7136–7140.

[137] L. Masaro, M. Ousalem, W.E. Baille, D. Lessard, X.X. Zhu, Self-diffusion studies of water and poly(ethylene glycol) in solutions and gels of selected hydrophilic polymers, Macromolecules 32 (1999) 4375–4382.

[138] B. Walther, N. Loren, M. Nyden, A.M. Hermansson, Influence of kappa-carrageenan gel structures on the diffusion of probe molecules determined by transmission electron microscopy and NMR diffusometry, Langmuir 22 (2006) 8221–8228.

[139] M. Nyden, O. Soderman, G. Karlstrom, A PFG NMR self-diffusion investigation of probe diffusion in an ethyl(hydroxyethyl)cellulose matrix, Macromolecules 32 (1999) 127–135.

[140] S. Kwak, M. Lafleur, NMR self-diffusion of molecular and macromolecular species in dextran solutions and gels, Macromolecules 36 (2003) 3189–3195.

[141] G. Lafitte, K. Thuresson, O. Soderman, Mixtures of mucin and oppositely charged surfactant aggregates with varying charge density. Phase behavior, association, and dynamics, Langmuir 21 (2005) 7097–7104.

[142] G. Lafitte, K. Thuresson, P. Jarwoll, M. Nyden, Transport properties and aggregation phenomena of polyoxyethylene sorbitane monooleate (polysorbate 80) in pig gastrointestinal mucin and mucus, Langmuir 23 (2007) 10933–10939.

[143] R. Trampel, J. Schiller, L. Naji, F. Stallmach, J. Karger, K. Arnold, Self-diffusion of polymers in cartilage as studied by pulsed field gradient NMR, Biophysical Chemistry 97 (2002) 251–260.

[144] S. Kwak, M. Lafleur, Self-diffusion of macromolecules and macroassemblies in curdlan gels as examined by PFG-SE NMR technique, Colloids and Surfaces A,-Physicochemical and Engineering Aspects 221 (2003) 231–242.

[145] R. Colsenet, O. Soderman, F.O. Mariette, Pulsed field gradient NMR study of poly (ethylene glycol) diffusion in whey protein solutions and gels, Macromolecules 39 (2006) 1053–1059.

[146] S. Le Feunteun, F. Mariette, Impact of casein gel microstructure on self-diffusion coefficient of molecular probes measured by H-1 PFG-NMR, Journal of Agricultural and Food Chemistry 55 (2007) 10764–10772.

[147] R. Colsenet, O. Soderman, F. Mariette, Effects of ionic strength and denaturation time on polyethyleneglycol self-diffusion in whey protein solutions and gels visualized by nuclear magnetic resonance, Journal of Agricultural and Food Chemistry 54 (2006) 5105–5112.

[148] R. Colsenet, O. Soderman, F. Mariette, Effect of casein concentration in suspensions and gels on poly(ethylene glycol)s NMR self-diffusion measurements, Macromolecules 38 (2005) 9171–9179.

[149] G. Lafitte, K. Thuresson, P. Jarwoll, M. Nyden, Transport properties and aggregation phenomena of polyoxyethylene sorbitane monooleate (polysorbate 80) in pig gastric mucin and mucus, Langmuir 23 (2007) 10933–10939.

[150] R. Duncan, The dawning era of polymer therapeutics, Nature Reviews Drug Discovery 2 (2003) 347–360.

[151] R. Duncan, Polymer conjugates as anticancer nanomedicines, Nature Reviews Cancer 6 (2006) 688–701.

[152] F.M. Veronese, G. Pasut, PEGylation, successful approach to drug delivery, Drug Discovery Today 10 (2005) 1451–1458.

Manuscripts

PGSE-NMR and SANS Studies of the Interaction of Model Polymer Therapeutics with Mucin

Peter Charles Griffiths,*,† Paola Occhipinti,†,‡ Christopher Morris,‡ Richard K. Heenan,§ Stephen Michael King,§ and Mark Gumbleton‡

School of Chemistry, Cardiff University, Main Building, Park Place, Cardiff CF10 3AT, United Kingdom, Welsh School of Pharmacy, Cardiff University, Redwood Building, King Edward VII Avenue, Cardiff CF10 3NB, United Kingdom, and ISIS Facility, Science and Technology Facilities Council, Rutherford Appleton Laboratory, Didcot OX11 0QX, United Kingdom

The viscous mucus coating that adheres to the epithelial surfaces of mammalian organs provides protection for the underlying tissues and is an efficient barrier to drug delivery. Pulsed-gradient spin—echo NMR and small-angle neutron scattering have been used to study the aqueous solution interaction of various model polymer therapeutics with mucin, the principle organic component within mucus. Nonionic polymers such as linear and star-branched poly(ethylene oxide) (PEO) and dextrin showed no appreciable interaction with mucin but suffered a moderate retardation in their rate of diffusion through the mucin solution. A strong interaction with mucin was observed for a series of polyamidoamine (PAMAM) dendrimers and hyperbranched poly(ethylene imine) (PEI), which displayed a characteristic pH-dependent profile and led to significant reductions in their rates of diffusion. These observations have implications for the design of optimized polymer therapeutic structures being adopted for the delivery of therapeutic moieties through mucin-rich environments.

Introduction

Significant progress has indeed been made over the past decade in the design and development of polymer-based nanosized hybrid therapeutics with several such delivery systems entering clinical trials but many challenges remain.[1]

Epithelial surfaces in mammalian organs (e.g., conductive airways of the lung and the gastrointestinal and reproductive tract) bear a mucus coating, a complex mixture of glycoprotein, lipid, and electrolytes that provides protection for the underlying cells and, therefore, represents an inherently efficient barrier to drug delivery. The efficacy of this barrier depends on its physicochemical state such as hydration and mucin content, which in turn is defined by its site of secretion and the presence of any disease (e.g., cystic fibrosis), all of which are factors that can affect the absorptive pharmacokinetics of the therapeutic agent.[2]

Mucus is in essence a water-rich biogel, the main components being water (up to 95%), mucin (generally no more than 5%), inorganic salts (about 1%), carbohydrates, and lipids. Mucin consists of high-molecular-weight (ranging from 500 to 20 000 kg mol⁻¹) O-linked glycoproteins (of varying length scales from a few hundred nanometers up to several micrometers) in turn composed of glycosylated and nonglycosylated peptide blocks linked by intramolecular disulfide bridges,[3] calcium ion or peptide cross-linking,[4] carbohydrate—carbohydrate bonds, and hydrophobic associations.[5] Mucins have a low isoelectric point (IEP ≈ 2 to 3) because of the anionic nature of their oligosaccharide side chains (sulfate and sialic acid units).

Several models have been invoked to describe the solution structure of mucin; aggregates of rod-shaped molecules com-

prising a central linear polypeptide core of $100\,000 < M_w < 250\,000$ g mol⁻¹ with radial oligosaccharide side chains of 2 to 12 monosaccharide residues attached to serine and threonine residues by O-glycosidic linkages,[6] a solvated random coil of flexible linear glycoprotein[7] that is either stiffened by the glycosylated fragments[8] or their interaction (the so-called "zipper" or bottle-brush model),[9] liquid crystalline structures,[7] and a double globule comb structure.[10] This complexity is compounded by the tendency of mucin to aggregate at low concentrations (and pH).

The aim of this study is to examine by pulsed-gradient spin—echo NMR (PGSE-NMR), the diffusion of a series of water-soluble polymers intended to represent model polymer therapeutics within mucin solutions and to quantify by small-angle neutron scattering (SANS) changes induced in the structure of mucin by the addition of that second polymer.

Material and Methods

Materials. Dried porcine gastric mucin (PGM) type III was purchased from Sigma Aldrich and used without any further treatment. Over the concentration range 0.5 < [mucin] < 5 wt %, solutions of PGM are viscous (Figure S1 in the Supporting Information) and exhibit a pronounced concentration dependence ($\eta \propto$ [mucin]²) but do not form gels. There is no pronounced sol—gel transition (Figure S2 in the Supporting Information), as has been reported previously for commercial samples of mucin. A series of water-soluble polymers, termed the "probe" polymer, have been examined in the presence of PGM, and these also were not further purified: linear PEO (l-PEG10K) nominal molecular weight M_w = 10 000 g mol⁻¹ (Sigma-Aldrich, U.K.); linear deuterated PEO nominal molecular weight M_w = 10 000 g mol⁻¹ (Polymer Laboratories, U.K.); linear PEO (l-PEG100K) nominal molecular weight M_w = 100 000 g mol⁻¹ (Sigma-Aldrich, U.K.); branched polyethylenimine (b-PEI2K) nominal molecular weight M_w = 2000 g mol⁻¹ (Sigma-Aldrich, U.K.); branched polyethylenimine (b-PEI25K) nominal molecular weight M_w = 25 000 g mol⁻¹ (Sigma

* To whom correspondence should be addressed. Tel: +44-29 20875858. Fax: +44-29 20874030. E-mail: griffithspc@cardiff.ac.uk.
† School of Chemistry, Cardiff University.
‡ Welsh School of Pharmacy, Cardiff University.
§ Rutherford Appleton Laboratory.

Aldrich, U.K.); polyamidoamine dendrimer G2.0 (PAMAM G2.0) nominal molecular weight M_w = 3260 g mol^{-1} (Dendritech); polyamidoamine dendrimer G4.0 (PAMAM G4.0) nominal molecular weight M_w = 14 210 g mol^{-1} (Dendritech); polyamidoamine dendrimer G3.5 (PAMAM G3.5) nominal molecular weight M_w = 12 930 g mol^{-1} (Dendritech); polyamidoamine dendrimer G5.5 (PAMAM G5.5) nominal molecular weight M_w = 52 900 g mol^{-1} (Dendritech); dextrin (type 1, corn) nominal molecular weight M_w = 60 000 g/mol (ML laboratories, Keele, U.K.).

Preparation of Polymer–Mucin Solutions. Solutions were prepared with different mucin concentrations (1 wt % < [mucin] < 5 wt %) and a constant probe polymer concentration (0.5 wt %) by simply dissolving the required masses of polymer in D_2O (99.5 atom % D). Samples were left for at least 2 h but typically overnight at room temperature to allow full dissolution and equilibration. The solutions were not filtered, and the pH was adjusted by the addition of HCl or NaOH.

Small-Angle Neutron Scattering. SANS experiments were performed on the fixed-geometry, time-of flight LOQ diffractometer at the ISIS Spallation Neutron Source, Rutherford Appleton Laboratory, Didcot, U.K. A Q =$(4\pi/\lambda)$ $\sin(\theta/2)$ range between 0.008 and 0.25 Å^{-1} is obtained by using neutron wavelengths (λ) spanning 2.2 to 10 Å with a fixed sample–detector distance of 4.1 m. The samples were contained in 2 mm path length, UV-spectrophotometer grade, quartz cuvettes (Hellma, GmBh) and mounted in aluminum holders on top of an enclosed, computer-controlled, sample chamber. Sample volumes were ~0.6 cm^3. All experiments were conducted at 37 °C (unless otherwise stated). Temperature control was achieved by using a thermostatted circulating bath pumping fluid through the base of the sample chamber, achieving a temperature stability of ±0.2 °C. Experimental measuring times were approximately 30–40 min.

All scattering data were (a) normalized for the sample transmission, (b) background corrected using a quartz cell filled with D_2O, and (c) corrected for the linearity and efficiency of the detector response using the instrument specific software package.

Pulsed-Gradient Spin–Echo NMR (PGSE-NMR). Pulsed-gradient spin–echo NMR experiments were carried out on a Bruker AMX360 NMR spectrometer operating at 360 MHz (^{1}H) and using a stimulated echo sequence, as described elsewhere.[11] For each measurement, a 5 mm diffusion probe and a Bruker gradient spectroscopy accessory unit was used. All experiments were conducted at 37 °C. Temperature stability was maintained by the standard air heating/cooling system of the spectrometer to an accuracy of ±0.3 °C.

Two approaches to analyzing the data were employed; where there is little spectral overlap with the peaks of interest (e.g., PAMAMs in mucin), the diffusion coefficients have been extracted by an analysis of the peak integrals; however, where spectral overlap is pronounced (e.g., PEG in mucin), a more involved component-resolved (CORE) approach (Figure S3 in the Supporting Information) was adopted.[12]

In both cases, the self-diffusion coefficient D_s was extracted from an analysis of the peak amplitudes according to eq 1

$$A(\delta, G, \Delta) = A_o \exp[(-kD_s)] \qquad (1)$$

where A is the peak amplitude in the absence (A_o) or the presence of trapezoidal field gradient pulses of duration δ (400 μs < δ < 2.8 ms), ramp time σ (250 μs) strength G (0.86 T m^{-1}) and separation Δ (140 ms), and k is given by eq 2

$$k = -\gamma^2 G^2 \left(\frac{30\Delta(\delta + \sigma)^2 - (10\delta^3 + 30\sigma\delta^2 + 35\sigma^2\delta + 14\delta^3)}{30} \right) \qquad (2)$$

where γ is the gyromagnetic ratio.

Results

In this current work, PGSE-NMR has been used to quantify the diffusion of model polymer therapeutics (the "probe"
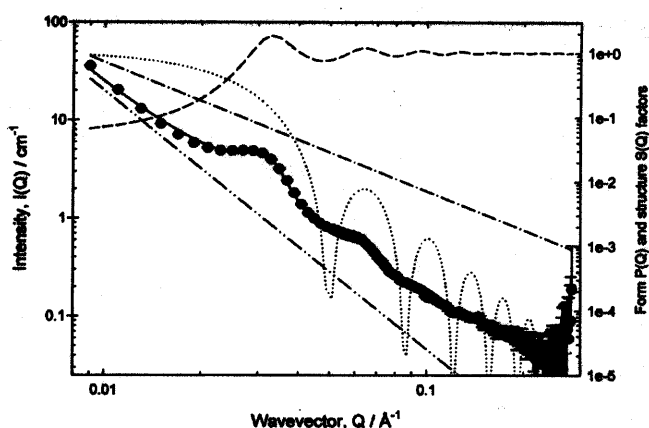

Figure 1. Scattering from mucin 5 wt % (closed circles) at 37 °C, pH 7; fitting to the scattering data (solid line); globule form factor $P(Q)$ (dotted line); globule structure factor $S(Q)$ (dashed line); Q^{-2} (dashed-dotted line); and Q^{-4} (dashed-dotted-dotted line) terms. The final data points have been omitted for clarity.

polymer) within aqueous mucin solutions. SANS has been used to detect any perturbation in the mucin solution structure induced by the addition of the probe polymer and thus to provide a complementary indication of any interaction between the mucin and probe polymer. However, we first present the SANS analysis of simple mucin solutions, subsequently, that from mixtures of mucin–probe polymer, before elaborating on the PGSE-NMR study.

SANS from PGM Solutions. The SANS from 5 wt % (50 mg mL^{-1}) (nonpurified) porcine gastric mucin PGM solutions at 37 °C is presented in Figure 1. As may be seen, there are a number of features in the data, including pronounced maxima against a slowly decaying background signal. The maxima arise as a result of the interference from scattering centers within the solution, implying some level of order. The spacing (ξ) associated with these maxima scale with concentration ($\xi \propto c^{-0.38 \, (\pm 0.03)}$) (over the entire range studied 1 < [mucin] < 5 wt %)) characteristic of liquid-like ordering ($\xi \propto c^{-1/3}$) (Figure S4 in the Supporting Information). These maxima are still present in the scattering, even at concentrations as low as 1 wt % (10 mg mL^{-1}). These features are more pronounced than those in the SANS (and SAXS) studies of Waigh et al.[10,13−16] Interestingly, the peak does not move with increasing ionic strength (ambient < [salt] < 0.1 M NaCl, where on the basis of conductivity measurements the ambient ionic strength is comparable to ~10 mM NaCl), implying that they do not arise as a result of an electrostatic structure factor (Figure S5 in the Supporting Information).

In their early SANS study, Waigh et al.[16] interpreted their data in terms of representing mucin glycoprotein as a homogeneous cylinder, for which a Guiner analysis suggested that the length of the glycosylated regions was ~100 nm with a radius of 24 ± 1 nm. Subsequently, they reanalyzed their SANS data in light of the SAXS study[10] and invoked a dumbbell model in which two globular structures (with dimension 10–20 nm) are connected by a 40–50 nm glycosylated spacer with a thickness of a few nanometers.

A more complex form factor approach has been adopted here that embodies the essence of the dumbbell model, in which the scattering has been analyzed using a model that comprises two main scattering terms

$$I(Q) = I(Q)_{\text{peptidebackbone}} + I(Q)_{\text{globule}} \qquad (3)$$

The first term of eq 3 is the contribution from the glycosylated peptide backbone (Scheme 1), whereas the second term accounts

Scheme 1. Solution Conformation of Mucin Comprising Hydrophobic Globules Connected by a Glycosylated Spacer[a]
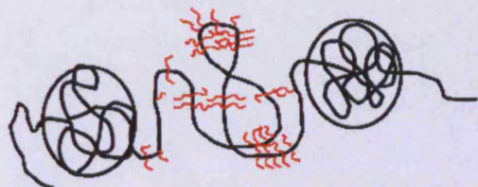
[a] Hydrophobic globules are modeled in terms of a dispersion of polydisperse spheres, whereas the spacer gives rise to a Q^{-2} contribution to the overall scattering (adapted from ref 10).

for the dispersion of hydrophobic globules connected by the glycosylated peptide backbone. The peptide backbone is modeled as

$$I(Q)_{\text{peptidebackbone}} = \frac{I_1}{\xi^2 Q^2} + \frac{I_2}{\zeta^4 Q^4} \qquad (4)$$

where the intensities I_1 and I_2 characterize the contribution to the scattering arising from the peptide backbone with characteristic length scale ξ (where $\xi^2 Q^2 > 1$) and from some larger, ill-defined structure, ζ.

The second term in eq 3, $I(Q)_{\text{globule}}$, is responsible for the scattering from the locally ordered hydrophobic globules, and it was deemed most appropriate to model this structure as a concentrated dispersion of uncharged (polydisperse) spheres given (i) the liquid ordering scaling of the peak positions with concentration and (ii) the fact that no change in scattering is observed as a result of the increase in the ionic strength (Figure S5 in the Supporting Information). Therefore,

$$I(Q)_{\text{globule}} = NV^2(\rho_m - \rho_s)^2 P(Q)S(Q) \qquad (5)$$

where N is the number of scatterers of volume, V, per unit volume and $(\rho_m - \rho_s)^2$ is their contrast against the solvent. The form factor $P(Q)$ is calculated using a distribution of polydisperse spherical scatterers with

$$P(Q) = 3\left[\frac{\sin QR - QR\cos QR}{(QR)^3}\right]^2 \qquad (6)$$

integrated over a modified Schulz distribution

$$n(R) = \left[\frac{(Z+1)}{(\bar{R} - R_1)}\right]^{Z+1} (R - R_1)^Z \frac{\exp\left[\frac{-(Z+1)}{(\bar{R} - R_1)(R - R_1)}\right]}{\Gamma(Z+1)} \qquad (7)$$

with width $\sigma = ((\bar{R} - R_1))/((Z+1)^{1/2})$ to account for variation in size.

This model, idealized in Scheme 1 with the various contributions to the overall fit illustrated in Figure 1, is most sensitive to the position of the peaks, allowing the size, R, and volume fraction, ϕ (= NV), of the globules to be readily parametrized ($R \approx 10-15$ nm, $\phi \approx 0.30$ to 0.40), yielding values that are in very good agreement with those obtained by Waigh et al.[10] The Q^{-2} contribution to the overall fit can be reanalyzed representing the data in a Zimm plot to yield a correlation length of ~13 (± 1) nm (and over the high Q limit, $R_g \approx 9$ (± 1) nm). This observation is consistent with previous reports of a swollen coil, commensurate with the type of structure envisaged by Waigh as a glycosylated spacer. As may be seen, the Q^{-4} term contributes rather weakly to the overall fit; indeed, the fit is dominated by the Q^{-2} and globule terms. Therefore, there is also a resonance of this model with the "bottle brush" and
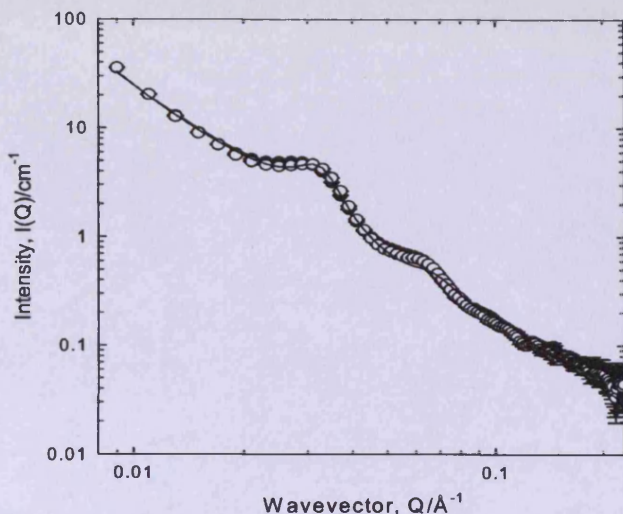

Figure 2. Scattering from 5 wt % mucin in the absence (closed circles) and in the presence of 0.5 wt % deuterated PEG10K g mol^{-1} (open circles) at 37 °C, pH 7. The lines correspond to the fits to the model described in the text.

"zipper" models,[17] which lends support to and gains credence from the aforementioned various models used previously to describe the solution conformation of mucin.

Upon dilution from [mucin] = 5 to 1 wt %, the peak in the data moves to lower Q ($\xi \propto c^{-0.38\,(\pm 0.03)}$). The peak position corresponds to a distance of 21 nm at 5 wt % mucin increasing to 39 nm at 1 wt % mucin. The scattering from 5 wt % mucin solutions over a pH range of 2 < pH< 9 (at 37 °C) (Figure S6 in the Supporting Information) showed identical maxima, indicating that the conformation of the mucin does not change over this pH range, in contradiction to that observed by Cao et al.[18] However, the sample at pH 2 did exhibit slightly different scattering: the intensity of the maxima is slightly reduced, but there is no change in the peak position. This observation confirms what is known about commercial PGM samples: the extraction process disrupts the disulfide bridges, leading to a much weaker sol−gel transition around pH < 4 and the lack of gel formation. The Supporting Information also presents supporting viscosity studies (Figure S2 in the Supporting Information).

SANS from PGM Solutions in the Presence of the Polymers. The scattering from 5 wt % PGM solutions (37 °C) in the presence of 0.5 wt % *l*-PEG10K, *b*-PEG20K, and *l*-PEG100K showed no significant differences from the 5 wt % PGM solution. A typical data set is presented in Figure 2. A deuterated *l*-PEG10K was used, so no scattering is observed from this polymer in D$_2$O, the so-called "contrast match" condition. For the other polymers, the concentration was too low to detect measurable scattering. The simplest interpretation of this observation is the lack of an interaction between the mucin and the various PEGs, at least to a degree that induces a structural perturbation in the mucin. The same observations were made for all pHs examined, viz., pH 2, 7, and 9 (Figure S7 in the Supporting Information presents as exemplar the pH 2 data). Similarly, there is no change in the (relative) viscosity of the mucin solutions upon the addition of the PEG (Figure S8 in the Supporting Information).

The addition of 0.5 wt % PAMAM dendrimers (amino-terminated G2.0 and G4.0, carboxylic acid terminated G3.5 and G5.5) to 5 wt % mucin solutions did induce changes in the mucin scattering, as exemplified in Figure 3, indicating an
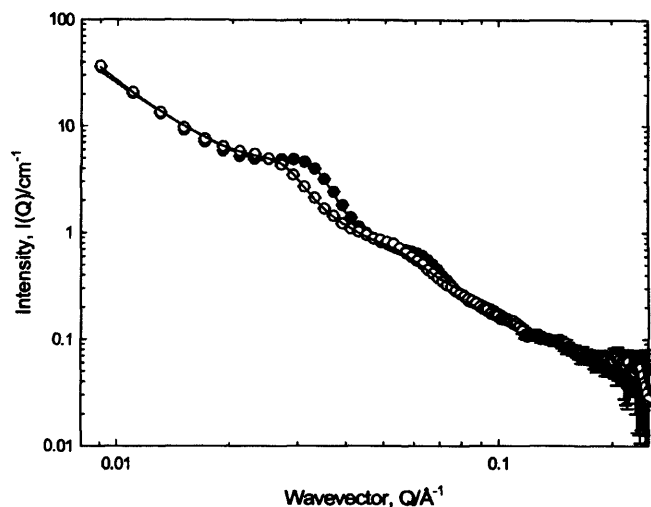
Figure 3. Scattering from 5 wt % mucin in the absence (closed circles) and in the presence of 0.5 wt % PAMAM dendrimer G2.0 (open circles) at 37 °C, pH 7. The lines correspond to the fits to the model described in the text.
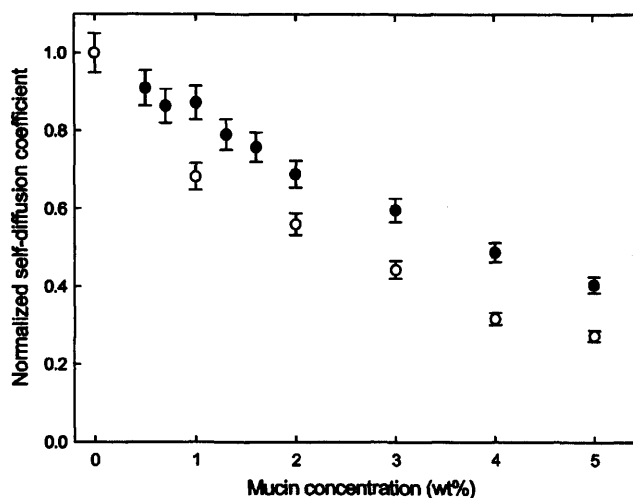

Figure 4. Normalized self-diffusion coefficients of 0.5 wt % PEG10K g mol⁻¹ (closed circles) and PEG100K g mol⁻¹ (open circles) in mucin solutions at 37 °C, pH 7.

interaction between these polymers and mucin. These changes were pH-dependent. Any contribution to the scattering from the PAMAM has been ignored because there was no measurable scattering in the absence of the mucin. The scattering from 0.5 wt % G2.0 (and G4.0) in 5 wt % mucin did not show any major change from the 5 wt % mucin scattering for pHs 2 and 9 (Figure S9 in the Supporting Information presents the pH 9 data), whereas a perturbation was observed at pH 7, Figure 3. Similar trends were observed in the viscosity behavior (Figures S10 and S11 in the Supporting Information).

The most obvious change is the shift of the maxima to lower Q. This indicates that the separation of the structures giving rise to these features has increased. Analogous behavior was observed for PAMAM G4.0.

In the case of the half-generation dendrimers, G3.5 (Figure S12a,b,c in the Supporting Information) and G5.5 (data not presented), a similar modulation of the scattering was observed but with three notable differences: (i) the change in scattering exhibited a rather different pH profile, viz., there was no change induced by the dendrimer at pH 2, but perturbations were evident at pH 7, which become more pronounced at pH 9; (ii) the peaks moved in the opposite direction, that is, toward higher Q values, indicating a decreasing separation of scatterers; and (iii) there appears to be slight drop in scattering intensity in the presence of the dendrimer, which increases with the strength of the interaction (no such change was observed in the G2.0 and G4.0 cases). Analogous behavior was observed for PAMAM G5.5. "Signature" pH effects were also observed when b-PEI2K (Figure S13 in the Supporting Information) was added to the 5 wt % mucin solutions (the changes in the perturbations in the scattering were much more pronounced that the PAMAM G2.0 and G4.0 dendrimer cases): no change in scattering at pH 2 but a much larger difference in scattering at pH 7. The presence of b-PEI25K caused flocculation of the mucin solutions; therefore, this system was not further studied but serves to underline the importance of the relative signs and magnitudes of the respective charge in these systems.

PGSE-NMR Study on Mucin Solutions in the Presence of Probe Polymers. The diffusion of a series of probe polymers (at fixed polymer concentration, 0.5 wt %) in a range of mucin solutions (0 < [mucin] < 5 wt %) has been examined at 37 °C. All polymers showed a decrease in the diffusion rate with increasing mucin concentration. Therefore, it is important to separate the effects of any specific interactions (e.g., binding) from that arising as a result of simple obstruction, namely, that the probe polymers have to diffuse around the mucin and there is the concomitant increase in diffusion path length. Additionally, there is the complication that the probe polymers are inherently of different molecular weights, and this will also affect their absolute diffusion rates.

Figure 4 presents representative normalized self-diffusion coefficients of *l*-PEG10K and *l*-PEG100K in mucin solutions, these being normalized to the measured self-diffusion coefficient of the PEG in free solution, that is, when [mucin] = 0 wt %. The diffusion of both *l*-PEG10K and *l*-PEG100K decreases with increasing mucin concentration because for [mucin] = 0, $D_s^{(10K)}$ > $D_s^{(100K)}$ by a factor of 3.5 (Figure S14 in the Supporting Information), which is consistent with the 10× decrease in molecular weight. The normalized diffusion data should at least to a first approximation remove the inherent effect of molecular weight and permit a comparison of the retardation induced by the mucin.

The (normalized) diffusion of 0.5 wt % PAMAM G2.0 and G4.0 shows a complex dependence on [mucin] and pH (Figure 5) in a fashion reminiscent of the characteristic profile observed in the SANS experiment. In particular, the data revealed a higher diffusion rate in mucin solutions at pH 9 (Figure 5) when compared with the diffusion of these probe polymers in mucin at pH 7 (Figure 5), suggesting that the same complex pH-dependent interaction between the dendrimers and the mucin is observable in the diffusion data. Analogous behavior was observed for G3.5 and G5.5. Furthermore, the diffusion of b-PEI2K was strongly retarded in mucin, interpreted as a very strong interaction between the dendrimer and the mucin. A manifestation of this strength of interaction was the short "shelf-life" of b-PEI25K/mucin samples, which phase separated after just a few hours.

A wider family of polymers has been examined by PGSE-NMR than has been possible by SANS, including dextrin, but over a more focused pH range. The conclusions of this larger study are presented in the bar-chart representation of Figure 6, where the normalized self-diffusion coefficients have been tabulated at one representative mucin concentration, 3 wt %.
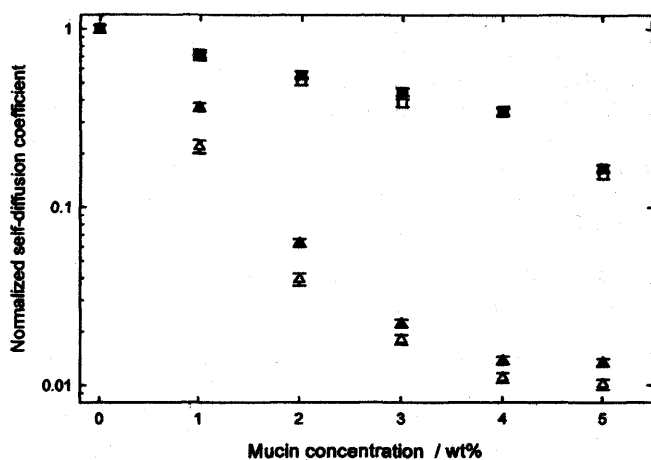
Figure 5. Normalized self-diffusion coefficients of 0.5 wt % PAMAM dendrimer G2.0 (open symbols) and G4.0 (filled symbols) at pH 9 (squares) and pH 7 (circles) in mucin solutions and 37 °C.
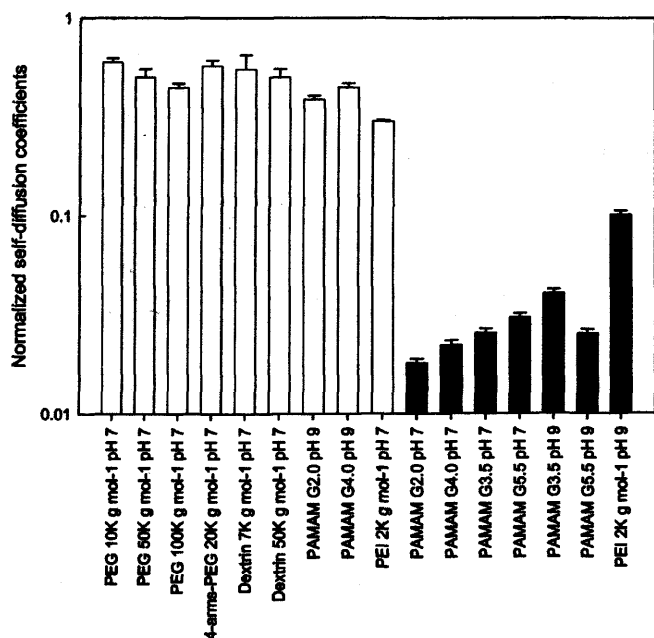

Figure 6. Bar chart of the normalized self-diffusion coefficients of all probe polymers in aqueous 3 wt % mucin solutions. The unshaded bars correspond to those systems for which SANS confirmed the lack of an interaction whereas the shaded bars correspond to interacting systems.

Discussion

For all polymer—mucin samples explored, the SANS and PGSE-NMR experiments gave complementary insight into the interaction of the probe polymer with the mucin. The nonionic polymers (dextrin 7K, dextrin 50K, *l*-PEG10K, *l*-PEG50K, *l*-PEG100K, 4-arms-PEG20K) displayed a behavior consistent with there being no interaction with the mucin; there was no change in the scattering profile, and one may therefore conclude that the moderate retardation in the diffusion arises simply because of the obstruction effect. There is the obvious molecular weight dependence to consider when discussing the absolute diffusion rates, but the normalized diffusion rates suggest no specific molecular-weight-dependent interaction with mucin. A similar study by Lafitte et al.[19,20] on the effect of PGM on the diffusion of PEG as a function of pH, ionic strength, and temperature demonstrated that pH imparted a stronger impact

on the PEG diffusion rate compared with that due to ionic strength and temperature, reflecting the underlying changes in mucin network homogeneity and viscosity. Furthermore, Lai et al.[21] found from their particle-tracking measurements that the diffusion of nanoparticles through mucin showed a complex dependence on particle size, but those particles coated with low-molecular-weight PEG diffused through mucus only slightly slower (×4—6) than in pure water. The same group[22] later showed that higher molecular weight PEGs led to mucoadhesion, highlighting the complexity of studying these systems, but would be consistent with the observation here of the slightly reduced normalized diffusion coefficient for the PEG 100K g mol⁻¹ sample compared with the PEG 10K g mol⁻¹ one.

The PAMAM dendrimers experienced a significant retardation in their diffusion within the mucin solutions (sometimes close to an order of magnitude) but under conditions where the PAMAM and mucin bore opposite charge. Concomitantly, there was a movement of the peak in the SANS data. Changing the pH to reverse the charge on either mucin or probe polymer "turned off" the interaction. The mechanism of interaction appears, therefore, to be driven by electrostatic interactions.

For the amino-terminated PAMAMs (G2.0 and G4.0) at pH 7, the amine groups are largely protonated (positively charged), whereas the mucin glycoprotein is deprotonated and negatively charged (via the carboxylic acid groups of the protein backbone ($pK_a \approx 3.9$ to 4.1) and the side groups of sialic acid ($pK_a \approx 2.6$), sulfated glucosamine, and galactoamines ($pK_a \approx 1$)), leading to the observed strong electrostatic interaction. The peak in the scattering moves to lower Q values, indicating that the separation of the scattering centers has increased. It is hypothesized that the PAMAM binds electrostatically to the oppositely charged mucin monosaccharide side chains, driving an expansion of the glyscoylated spacer, thus pushing the globules further apart. At pH 2, the amine groups are completely protonated (+ve charged), but the mucin is also partially positively charged (IEP = 2 to 3), and accordingly, no interaction is observed.

In contrast, for the half-generation PAMAMs (G3.5 and G5.5) at pH 7, the terminating carboxylic acid groups are already moderately deprotonated (i.e., negatively charged), and whereas the mucin is also negatively charged, surprisingly an interaction is still observed. This interaction becomes more pronounced at pH 9, that is, where the negative charge on the mucin is further increased. (No interaction is seen at pH 2.) Now, the peak in the SANS pattern has moved to higher Q, indicating that the separation of the globules has decreased. Clearly, a different mechanism is operating in the full- and half-generation PAMAMs. The origin of this interaction is most likely to be hydrogen bonds between the charged carboxylic acid groups on the PAMAM and the sugar residues on the monosaccharide side chains, leading to a collapse of the glysocylated spacer as the PAMAM induces bridging between adjacent saccharide structures.

Conclusions

The structure of aqueous probe polymer—mucin solutions has been explored by SANS, viscosity, and pulsed-gradient spin—echo NMR (PGSE-NMR). The SANS data provide a simple measure of the occurrence and nature of any interaction between the probe polymer and the mucin. The diffusion and viscosity data provide complementary insight into these systems. The scattering data were found to be most appropriately analyzed by a model describing the mucin as a dispersion of polydisperse spherical scatterers with a typical size of ~10 nm distributed throughout a polymeric matrix. Nonionic polymers such as

l-PEG10K and *l*-PEG100K did not interact with the mucin and caused no change in the bulk viscosity of the mucin/PEG solution but suffered a moderate retardation in their diffusion through the mucin. A pH-dependent interaction was found for a series of PAMAM dendrimers and PEI, exposing a strong electrostatic interaction. This study has shown that it is possible to distinguish and separate the effects of specific interactions between the probe polymer and mucin from simple obstruction effects. These conclusions should direct the choice of polymer structure to be adopted when designing polymer-based delivery systems for the delivery through such mucin-rich environments.

Supporting Information Available. Additional small-angle neutron scattering, viscosity, and NMR data (as referred to in the text). This material is available free of charge via the Internet at http://pubs.acs.org.

References and Notes

(1) Vicent, M. J.; Ringsdorf, H.; Duncan, R. *Adv. Drug Delivery Rev.* **2009**, *61*, 1117–1120.

(2) Sanders, N.; Rudolph, C.; Braeckmans, K.; De Smedt, S. C.; Demeester, J. *Adv. Drug Delivery Rev.* **2009**, *61*, 115–127.

(3) Bansil, R.; Turner, B. S. *Curr. Opin. Colloid Interface Sci.* **2006**, *11*, 164–170.

(4) Raynal, B. D. E.; Hardingham, T. E.; Sheehan, J. K.; Thornton, D. J. *J. Biol. Chem.* **2003**, *278*, 28703–28710.

(5) Hong, Z. N.; Chasan, B.; Bansil, R.; Turner, B. S.; Bhaskar, K. R.; Afdhal, N. H. *Biomacromolecules* **2005**, *6*, 3458–3466.

(6) Adikwu, M. U. *Bio. Pharm. Bull.* **2005**, *28*, 1801–1804.

(7) Hannig, M.; Herzog, S.; Willigeroth, S. F.; Zimehl, R. *Colloid Polym. Sci.* **2001**, *279*, 479–483.

(8) Glantz, P. O. J.; Arnebrant, T.; Nylander, T.; Baier, R. E. *Acta Odontol. Scand.* **1999**, *57*, 238–241.

(9) Jay, G. D.; Haberstroh, K.; Cha, C. J. *J. Biomed. Mater. Res.* **1998**, *40*, 414–418.

(10) Di Cola, E.; Yakubov, G. E.; Waigh, T. A. *Biomacromolecules* **2008**, *9*, 3216–3222.

(11) Griffiths, P. C.; Cheung, A. Y. F.; Davies, J. A.; Paul, A.; Tipples, C. N.; Winnington, A. L. *Magn. Reson. Chem.* **2002**, *40*, S40–S50.

(12) Stilbs, P.; Paulsen, K.; Griffiths, P. C. *J. Phys. Chem.* **1996**, *100*, 8180–8189.

(13) Papagiannopoulos, A.; Fernyhough, C. M.; Waigh, T. A.; Radulescu, A. *Macro. Chem. Phys.* **2008**, *209*, 2475–2486.

(14) Yakubov, G. E.; Papagiannopoulos, A.; Rat, E.; Easton, R. L.; Waigh, T. A. *Biomacromolecules* **2007**, *8*, 3467–3477.

(15) Yakubov, G. E.; Papagiannopoulos, A.; Rat, E.; Waigh, T. A. *Biomacromolecules* **2007**, *8*, 3791–3799.

(16) Waigh, T. A.; Papagiannopoulos, A.; Voice, A.; Bansil, R.; Unwin, A. P.; Dewhurst, C. D.; Turner, B.; Afdhal, N. *Langmuir* **2002**, *18*, 7188–7195.

(17) Carlstedt, I.; Sheehan, J. K. *Biorheology* **1984**, *21*, 225–233.

(18) Cao, X. X.; Bansil, R.; Bhaskar, K. R.; Turner, B. S.; Lamont, J. T.; Niu, N.; Afdhal, N. H. *Biophys. J.* **1999**, *76*, 1250–1258.

(19) Lafitte, G.; Soderman, O.; Thuresson, K.; Davies, J. *Biopolymers* **2007**, *86*, 165–175.

(20) Lafitte, G.; Thuresson, K.; Soderman, O. *J. Pharm. Sci.* **2007**, *96*, 258–263.

(21) Lai, S. K.; O'Hanlon, D. E.; Harrold, S.; Man, S. T.; Wang, Y. Y.; Cone, R.; Hanes, J. *Proc. Natl. Acad. Sci. U.S.A.* **2007**, *104*, 1482–1487.

(22) Wang, Y. Y.; Lai, S. K.; Suk, J. S.; Pace, A.; Cone, R.; Hanes, J. *Angew. Chem., Int. Ed.* **2008**, *47*, 9726–9729.

BM9009667